WORKSHOP PROGRAM AND ABSTRACTS

LPI Contribution No. 1280

Workshop on

DUST IN PLANETARY SYSTEMS

September 26–30, 2005

Kaua‘i, Hawai‘i

Sponsored by
National Aeronautics and Space Administration
European Space Agency
Lunar and Planetary Institute
Hawai‘i Institute of Geophysics and Planetology, University of Hawai‘i at Manoa

Conveners
Donald E. Brownlee,
University of Washington, Seattle
Eberhard Grün,
Max-Planck-Institute for Nuclear Physics and University of Hawai‘i at Manoa

Lunar and Planetary Institute 3600 Bay Area Boulevard Houston TX 77058-1113

LPI Contribution No. 1280

Compiled in 2005 by
LUNAR AND PLANETARY INSTITUTE

The Institute is operated by the Universities Space Research Association under Agreement No. NCC5-679 issued through the Solar System Exploration Division of the National Aeronautics and Space Administration.

Abstracts in this volume may be cited as

Author A. B. (2005) Title of abstract. In *Workshop on Dust in Planetary Systems*, p. XX. LPI Contribution No. 1280, Lunar and Planetary Institute, Houston.

This volume is distributed by

ORDER DEPARTMENT
Lunar and Planetary Institute
3600 Bay Area Boulevard
Houston TX 77058-1113, USA
Phone: 281-486-2172
Fax: 281-486-2186
E-mail: order@lpi.usra.edu

Mail orders requestors will be invoiced for the cost of shipping and handling.

ISSN No. 0161-5297

PREFACE

This volume contains abstracts that have been accepted for presentation at the Workshop on Dust in Planetary Systems, September 26–30, 2005, Kaua‘i, Hawai‘i.

Administration and publications support for this meeting were provided by the staff of the Publications and Program Services Department at the Lunar and Planetary Institute.

CONTENTS

PROGRAM

Monday, September 26, 2005
DEEP IMPACT
STARDUST
8:30 a.m. Ginger Room

Chairs: S. F. Green
C. M. Lisse

Brownlee D. E. *
Welcome

Lisse C. M. * **[Invited, 40 minutes]**
Deep Impact and Comet 9P/Tempel 1: From Evolved Surface to Interior Primeval Dust **[#4105]**

Brownlee D. E. * **[Invited, 40 minutes]**
Wild 2 Observations by Stardust **[#4090]**

Break [30 minutes]

Green S. F. * McBride N. Colwell M. T. S. H. McDonnell J. A. M. Tuzzolino A. J. Economou T. E. Clark B. C. Sekanina Z. Tsou P. Brownlee D. E. **[Invited, 40 minutes]**
Stardust Wild 2 Dust Measurements **[#4035]**

Tsou P. * Brownlee D. E. Hörz F. Flynn G. Keller L. McKeegan K. Sandford S. A. Zolensky M. E.
Dust Samples from Comet Wild 2 and Interstellar Stream **[#4101]**

11:30–1:00 Lunch, Naupaka Terrace

Monday, September 26, 2005
ASTEROID SAMPLE RETURN
LABORATORY DUST ANALYSES
1:00 p.m. Ginger Room

Chairs: J. P. Bradley
S. Sasaki

Fujiwara A. Kawaguchi J. Sasaki S. * Hayabusa Team **[Invited, 40 minutes]**
HAYABUSA Mission to Asteroid Itokawa: In-Situ Observation and Sample Return **[#4024]**

Jenniskens P. * Wercinski P. Wright M. Olejniczak J. Raiche G. Kontinos D. Schilling E. Rossano G. Russell R. W. Taylor M. Stenbaek-Nielsen H. Mcharg G. Spalding R. L. Sandquist K. Hatton J. Abe S. Rairden R. ReVelle D. O. Gural P. Hladiuk D. Hildebrand A. Rietmeijer F.
Hyperseed MAC: An Airborne and Ground-based Campaign to Monitor the Stardust Sample Return Capsule Reentry on 2006 January 15 **[#4030]**

Stephan T. * Leitner J. Hörz F.
TOF-SIMS Analysis of Residues from Allende Projectiles Shot onto Aluminum Foil — A Stardust Dress Rehearsal **[#4034]**

Flynn G. J. * Keller L. P. Sutton S. R.
Element Hosts in Anhydrous IDPs: A Test of Nebula Condensation Models **[#4011]**

Joswiak D. J. * Brownlee D. E. Pepin R. O. Schlutter D. J.
Mineralogy and Densities of Cometary and Asteroidal IDPs Collected in the Stratosphere **[#4106]**

Break [30 minutes]

Bradley J. P. * **[Invited, 40 minutes]**
A Revolution in the Nano-Scale Characterization of IDPs and Other Primitive Meteoritic Materials **[#4093]**

Ishii H. A. * Luening K. Brennan S. Pianetta P. Matrajt G. Bradley J. P.
Synchrotron X-Ray Fluorescence Analysis of Dust Particles **[#4079]**

Aléon J. * Duprat J. Robert F. Hutcheon I. D. Weber P. K. Toppani A. Derenne S.
Extreme Oxygen Isotope Ratios in Meteoritic Dust Grains — A Record of Irradiation in Dust-forming Regions of the Protosolar Nebula? **[#4081]**

Ferrini G. * Baratta G. A. Rotundi A. Palumbo M. E. Colangeli L. Palomba E.
Combined Micro-IR and Micro-Raman Measurements on Stratospheric IDPs **[#4043]**

Matrajt G. * Guan Y. Leshin L. Taylor S. Genge M. Joswiak D. Brownlee D.
Oxygen Isotope Measurements of Bulk Unmelted Antarctic Micrometeorites **[#4060]**

Tuesday, September 27, 2005
COMETARY DUST
8:30 a.m. Ginger Room

Chairs: H. U. Keller
W. T. Reach

Reach W. T. * **[Invited, 40 minutes]**
Cometary Debris Trails: Relics of the Disintegration of Short-Period Comets **[#4104]**

Agarwal J. * Boehnhardt H. Mueller M Grün E. T.
Dust Properties in the Trail of Comet 67P/Churyumov-Gerasimenko **[#4042]**

Jewitt D. * Matthews H. Andrews S.
Dust in Comets Observed at Submillimeter Wavelengths **[#4007]**

Clark B. C. *
Compositional Streaming and Particle Fragmentation at Comets 1P/Halley and 81P/Wild 2 **[#4016]**

Break [30 minutes]

Keller H. U. * Skorov Yu. V. Markelov G. N.
Dust Production and Nucleus Evolution **[#4039]**

Gustafson B. Å. S. * Espy A. J.
Scattering by "Bird's-Nest"-type Material and Large Dust Aggregates: Microwave Analogue Measurements **[#4098]**

Lauretta D. S. * Brown R. H. Schmidt B. Moores J.
Hydrogen Isotopic Fractionation and the Role of Dust During Sublimation from Cometary Ice **[#4067]**

Jäckel A. * Altwegg K. Wurz P. Balsiger H. Arijs E. Berthelier J. J. Fuselier S. Gliem F. Gombosi T. Korth A. Rème H.
ROSINA'S First Measurements from Space and Anticipated Analyses at Comet Churyumov-Gerasimenko **[#4045]**

11:30–1:00 Lunch, Naupaka Terrace

Tuesday, September 27, 2005
INTERPLANETARY DUST COMPLEX
DUST PROCESSES AND PROPERTIES
1:00 p.m. Ginger Room

Chairs: A. C. Levasseur-Regourd
M. V. Sykes

Sykes M. V. * **[Invited, 40 minutes]**
Constructing the Zodiacal Cloud **[#4091]**

Ipatov S. I. * Mather J. C.
Migration of Dust Particles to the Terrestrial Planets **[#4049]**

Madsen G. J. * Reynolds R. J. Ipatov S. I. Kutyrev A. S. Mather J. C. Moseley S. H.
New Observations of the Kinematics of the Zodiacal Dust Cloud **[#4072]**

Altobelli N. * Roy M. Kempf S. Srama R. Moragas-Klostermeyer G. Grün E.
Interplanetary Dust Between Jupiter and Saturn: Preliminary Results from the Cassini Cosmic Dust Analyzer **[#4048]**

Sasaki S. * Igenbergs E. Ohashi H. Münzenmayer R. Naumann W. Senger R. Fischer F. Fujiwara A. Grün E. Nogami K. Mann I. Svedhem H.
Summary of Observation of Interplanetary and Interstellar Dust by Mars Dust Counter on Board NOZOMI **[#4023]**

Mocker A. *
TOF Spectrometry of Hyper-Velocity Dust Impacts and Laser Ionization **[#4020]**

Wurm G. * Krauss O.
The Fundamental Role of Photophoresis for Dust in Planetary Systems **[#4006]**

Break [30 minutes]

Levasseur-Regourd A. C. * Lasue J.
Approaching Interplanetary Dust Physical Properties, from Light Scattering and Thermal Observations and Simulations **[#4099]**

Mukai T. * Okada Y.
Optical Properties of Large Aggregates **[#4036]**

Durda D. D. * Flynn G. J. Sandel L. E. Strait M. M.
Size-Frequency Distributions of Dust-size Debris from the Impact Disruption of Chondritic Meteorites **[#4056]**

Kehoe T. J. J. * Dermott S. F.
The Effect of Inter-Particle Collisions on the Dynamical Evolution of Asteroidal Dust and the Structure of the Zodiacal Cloud **[#4083]**

Asphaug E. * Agnor C. Williams Q.
Dust Production During Planetary Collisions Large and Small **[#4103]**

Matney M. J. *
Adventures in Gravitational Focusing **[#4080]**

Tuesday, September 27, 2005
POSTER SESSION:
PLANETARY, INTERPLANETARY, AND
INTERSTELLAR DUST OBSERVATIONS
7:00 p.m. Pakalana Room

Krüger H. Moissl R. Hamilton D. P. Grün E.
Galileo In-Situ Dust Measurements in Jupiter's Gossamer Rings **[#4021]**

Flandes A. Krüger H.
CIR Modulation of Jupiter Dust Stream Detection **[#4092]**

Juhasz A. Horányi M.
The E Ring of Saturn: Models Versus Observations **[#4015]**

Cooke W. J. McNamara H. A.
A Search for Meteor Shower Signatures in the LDEF IDE Data **[#4025]**

Kurth W. S. Averkamp T. F. Gurnett D. A. Wang Z. Z.
Cassini RPWS Observations of Dust Impacts in Saturn's E-ring **[#4074]**

Martínez-Gómez E. Durand-Manterola H. Pérez de Tejada H.
Dynamics of the Dust Grains in the Saturn's Rings **[#4009]**

Hillier J. K. McBride N. Green S. F.
Modelling Ion Behaviour in the Cassini Cosmic Dust Analyser **[#4087]**

Stubbs T. J. Vondrak R. R. Farrell W. M.
Impact of Lunar Dust on Space Exploration **[#4075]**

Dikarev V. Grün E. Baggaley W. J. Galligan D. P. Jehn R. Landgraf M.
Upgrade of Meteoroid Model to Predict Fluxes on Spacecraft in the Solar System and Near Earth **[#4037]**

Frisch P. C.
Tentative Identification of Interstellar Dust Towards the Heliosphere Nose **[#4096]**

Sternovsky Z. Horányi M. Amyx K. Robertson S. Bano G. Grün E. Srama R. Auer S.
Development of the Large Area Mass Analyzer **[#4017]**

Srama R. Rachev M. Helfert S. Kempf S. Moragas-Klostermeyer G. Mocker A. Postberg F. Grün E.
A New Large Area TOF Mass Spectrometer **[#4076]**

Srama R. Srowig A. Helfert S. Kempf S. Moragas-Klostermeyer G. Auer S. Harris D. Grün E.
Trajectory Sensor for Sub-Micron Sized Dust **[#4051]**

Tuesday, September 27, 2005
POSTER SESSION: COMETARY DUST OBSERVATIONS
7:00 p.m. Pakalana Room

Ootsubo T. Sugita S. Kadono T. Honda M. Miyata T. Sako S. Sakon I. Fujiwara H. Fujiyoshi T. Yamashita T. Takato N. Fuse T. SUBARU/COMICS Deep Impact Team
Mid-Infrared Observation of the Collision Between Deep Impact Projectile and Comet 9P/Tempel 1 with SUBARU/COMICS **[#4053]**

Kissel J. Krueger F. R. Silen J.
Analysis of Cosmic Dust by the 'Cometary and Interstellar Dust Analyser' (CIDA) Onboard the Stardust Spacecraft **[#4050]**

Miura N. Ishiguro M. Sarugaku Y. Usui F. Ueno M.
A CCD Search for the Dust Trail of Draconid Parent Comet 21P/Giacobini-Zinner **[#4095]**

Sarugaku Y. Ishiguro M. Miura N. Usui F. Ueno M.
Optical Observations of the Comet 2P/Encke Dust Trail **[#4094]**

Kissel J. Höfner H. Haerendel G. Czempiel S. Eibl J. Henkel H. Koch A. Glasmachers A. Torkar K. Rüdenauer F. Steiger W. Krueger F. R. Jessberger E. K. Stephan T. Gruen E. Thomas R. Langevin Y. von Hoerner H. Silen J. Rynö J. Genzer M. Hornung K. Schulz R. Hilchenbach M. Fischer H. Krüger H. Tubiana C. Thirkell L. Varmuza K. COSIMA Team
COSIMA: a High Resolution Time-of-Flight Secondary Ion Mass Spectrometer for Cometary Dust Particles on Its Way to Comet 67P/Churyumov-Gerasimenkov **[#4038]**

Goreva J. S. Lauretta D. S.
Developments in Thermal Analysis of Labile Trace Elements in Carbonaceous Chondrites **[#4085]**

Graham G. A. Bradley J. P. Dai Z. R. Kearsley A. T. Bernas M. Snead C.
Great Expectations — Dust Recovered from Aerogel **[#4089]**

Taylor S. Matrajt G. Lever J. H. Joswiak D. J. Brownlee D. E.
Size Distribution of Antarctic Micrometeorites **[#4014]**

Zolensky M. E.
Large Samples of Chondritic Interplanetary Dust Particles in Chondritic Meteorites **[#4066]**

Johnson N. M. Nuth J. A. III
Crystalline Silicate Formation and Comets **[#4082]**

Wednesday, September 28, 2005
INTERSTELLAR DUST WITHIN THE SOLAR SYSTEM
METEORS
8:30 a.m. Ginger Room

Chairs: M. D. Campbell-Brown
W. J. Baggaley

Altobelli N. * Grün E. Kempf S. Krüger H. Landgraf M. Srama R. **[Invited, 40 minutes]**
In-Situ Spacecraft Monitoring of the Interstellar Dust Stream in the Inner Solar System **[#4027]**

Baggaley W. J * **[Invited, 40 minutes]**
Interstellar Meteors **[#4033]**

Brown P. * Weryk R. J.
Interstellar Meteoroids Detected by the Canadian Meteor Orbit Radar **[#4031]**

Break [30 minutes]

Campbell-Brown M. D. * Brown P. G. **[Invited, 40 minutes]**
The Meteoroid Environment: Shower and Sporadic Meteors **[#4040]**

Jenniskens P. *
Meteor Showers from Broken Comets **[#4032]**

Meeting adjourns for the day. No lunch will be provided.

Thursday, September 29, 2005
PRESOLAR GRAINS
DUST PROCESSES
8:30 a.m. Ginger Room

Chairs: A. L. Graps
S. Messenger

Messenger S. * **[Invited, 40 minutes]**
The Nature and Histories of Presolar Dust Grains **[#4086]**

Krauss O. * Wurm G.
Experimental Determination of the Radiation Pressure Forces on an Individual Dust Particle **[#4010]**

Abbas M. M. * Tankosic D. Craven P. D. Spann J. F. LeClair A. West E. A. Taylor L. Hoover R.
Measurements of Photoelectric Yield and Physical Properties of Individual Lunar Dust Grains **[#4054]**

Colwell J. E. * Horányi M. Robertson S. Wheeler P.
Behavior of Charged Dust in Plasma and Photoelectron Sheaths **[#4008]**

Graps A. L. * Green S. F. McBride N. M. McDonnell J. A. M. Drolshagen G. Svedhem H. Bunte K. D.
GEO Debris and Interplanetary Dust: Fluxes and Charging Behavior **[#4041]**

Break [30 minutes]

Auer S. *
Computed Electrical Charges of Dust Particles with Highly Irregular Shapes **[#4018]**

Stubbs T. J. * Halekas J. S. Farrell W. M. Vondrak R. R.
Lunar Surface Charging: A Global Perspective Using Lunar Prospector Data **[#4070]**

Vondrak R. R. Stubbs T. J. * Farrell W. M.
A Dynamic Fountain Model for Dust in the Lunar Exosphere **[#4071]**

11:30–1:00 Lunch, Naupaka Terrace

Thursday, September 29, 2005
PLANETARY DUST
1:00 p.m. Ginger Room

Chairs: M. Horanyi
R. Srama

Srama R. * Burton M. Helfert S. Kempf S. Moragas-Klostermeyer G. Mocker A. Postberg F. Roy M. CDA Science Team Grün E. **[Invited, 40 minutes]**
Cassini Saturn Dust Measurements **[#4073]**

Roy M. * Burton M. Moragas Klostermeyer G. Srama R. Kempf S. Helfert S.
The Cassini Spacecraft at Saturn: An Overview of Science and Science Operations **[#4026]**

McBride N. * Hillier J. K. Green S. F. Schwanethal J. P. McDonnell J. A. M. Srama R. Kempf S. Postberg F. Grün E.
Cassini Cosmic Dust Analyser: Composition of Dust at Saturn **[#4047]**

Helfert S. *
Ring Plane Crossings with the Cassini CDA Instrument: Saturation Analysis and Deadtime Correction **[#4057]**

Moragas-Klostermeyer G. * Srama R. Kempf S. Helfert S. Roy M. Burton M. Altobelli N. Dikarev V. Krüger H. Grün E.
Generated Dust Impact Charge Measurements by Cassini's Dust Instrument, CDA **[#4064]**

Break [30 minutes]

Horányi M. * **[Invited, 40 minutes]**
Dusty Plasma Effects in Planetary Rings **[#4001]**

Economou T. E. * Tuzzolino A. J.
New Data from Stardust and Cassini Missions Obtained by DFMI and HRD Instruments **[#4097]**

Spahn F. * Albers N. Dikarev V. Economu T. Grün E. Hoerning M. Kempf S. Krivov A. V. Makuch M. Schmidt J. Seiss M. Srama R. Sremcevic M.
E Ring Sources — Cassini Flybys with Enceladus **[#4059]**

Wang Z. Z. * Gurnett D. A. Averkamp T. F. Persoon A. M. Kurth W. S.
Characteristics of Dust Particles Observed by Cassini at Saturn's Ring Plane Crossings **[#4065]**

Kempf S. * Srama R. Horányi M. Burton M. Grün E.
Interaction of Saturnian Dust Streams with the Solar Wind **[#4052]**

Showalter M. R. * Burns J. A. de Pater I. Hamilton D. P. Lissauer J. J. Verbanac G.
Updates on the Dusty Rings of Jupiter, Uranus and Neptune **[#4061]**

Friday, September 30, 2005
DUST MEASUREMENTS OF METEOROIDS
FUTURE MISSIONS
8:30 a.m. Ginger Room

Chairs: E. Grün
T. V. Johnson

Krüger H. * Linkert G. Linkert D. Anweiler B. Grün E. Ulysses Dust Science Team
Dust Stream Measurements from Ulysses' Distant Jupiter Encounter **[#4022]**

Johnson T. V. *
Thoughts on Small Body Exploration History and Prospects **[#4055]**

Ueno M. * Ishiguro M. Usui F. Nakamura R. Ootsubo T. Miura N. Sarugaku Y. Kwon S. M. Hong S. S. Mukai T.
WIZARD — A New Observation System of the Zodiacal Light **[#4100]**

Tsou P. * Giovane F. Corsaro R. Liou J. C.
A Large Area Cosmic Dust Collector on the International Space Station **[#4102]**

Liou J.-C. * Giovane F. Corsaro R. Tsou P. Stansbery E.
Characterizing the Near-Earth Cosmic Dust and Orbital Debris Environment with LAD-C **[#4028]**

Corsaro R. * Liou J.-C. Giovane F. Tsou P.
Continuous Large-Area Micrometeoroid Flux Measuring Instrument **[#4029]**

Break [30 minutes]

Grün E. * Srama R. Helfert S. Kempf S. Moragas-Klostermeyer G. Rachev M. Srowig A. Auer S. Horányi M. Sternovsky Z. Harris D.
Prospects of a Dust Astronomy Mission **[#4058]**

Auer S. *
Development of an Ultra-Low Noise Charge-Sensitive Amplifier for Cosmic Dust Particles **[#4019]**

Carpenter J. D. * Stevenson T. J. Fraser G. W. Kearsley A.
Nanometre Scale Films as Dust Detectors **[#4005]**

Dominguez G. D. Westphal A. J. * Jones S. M. Phillips M. L. F. Schrier M.
Calorimetric Aerogel Performance at Interstellar Dust Velocities **[#4077]**

11:30–1:00 Lunch, Naupaka Terrace

Friday, September 30, 2005
DUST DISKS
1:00 p.m. Ginger Room

Chairs: A. V. Krivov
A. Moro-Martin

Moro-Martín A. * Malhotra R. Wolf S. **[Invited, 40 minutes]**
Signatures of Planets in Debris Disks **[#4004]**

Su K. Y. L. * Rieke G. H. Stansberry J. A. Stapelfeldt K. R. Werner M. W. Trilling D. E. Hines D. C. Marengo M. Megeath S. T. Fazio G. G. Van Cleve J.
Spitzer's View on Resolved Debris Disks – Vega, Fomalhaut and β Pictoris **[#4063]**

Toppani A. * Robert F. Libourel G. de Donato P. Barrès O. d'Hendecourt L. Ghanbaja J.
Experimental Condensation of Silicate Gases: Application to the Formation of Dust in Circumstellar Environments **[#4088]**

Johnson N. M. * Nuth J. A. III
Organic Synthesis on Dust: Implications for Protostellar Systems **[#4062]**

Li A. *
Polycyclic Aromatic Hydrocarbon Molecules in Protoplanetary and Debris Disks **[#4069]**

Break [30 minutes]

Krivov A. V. * **[Invited, 40 minutes]**
Physics of Debris Disks **[#4084]**

Gurnett D. A. * Wang Z. Z. Persoon A. M. Kurth W. S.
Dust Particles Detected in the Outer Solar System by Voyager 1 and 2 **[#4068]**

Measurements of Photoelectric Yield and Physical Properties of Individual Lunar Dust Grains

M. M. Abbas[1], D. Tankosic[2,] P. D. Craven[1], J. F. Spann[1], A. LeClair[2], E. A. West[1], L. Taylor[3], and R. Hoover[1]
[1] NASA-Marshall Space Flight Center, Huntsville, AL 35812
[2]University of Alabama in Huntsville, Huntsville, AL 35899
[3]University of Tennessee, Knoxville, TN, 37996

ABSTRACT

Micron size dust grains levitated and transported on the lunar surface constitute a major problem for the robotic and human habitat missions for the Moon. It is well known since the Apollo missions that the lunar surface is covered with a thick layer of micron/sub-micron size dust grains. Transient dust clouds over the lunar horizon were observed by experiments during the Apollo 17 mission. Theoretical models suggest that the dust grains on the lunar surface are charged by the solar UV radiation as well as the solar wind. Even without any physical activity, the dust grains are levitated by electrostatic fields and transported away from the surface in the near vacuum environment of the Moon. The current dust charging and the levitation models, however, do not fully explain the observed phenomena. Since the abundance of dust on the Moon's surface with its observed adhesive characteristics is believed to have a severe impact on the human habitat and the lifetime and operations of a variety of equipment, it is necessary to investigate the phenomena and the charging properties of the lunar dust in order to develop appropriate mitigating strategies.

We will present results of some recent laboratory experiments on individual micron/sub-micron size dust grains levitated in electrodynamic balance in simulated space environments. The experiments involve photoelectric emission measurements of individual micron size lunar dust grains illuminated with UV radiation in the 120-160 nm wavelength range. The photoelectric yields are required to determine the charging properties of lunar dust illuminated by solar UV radiation. We will present some recent results of laboratory measurement of the photoelectric yields and the physical properties of individual micron size dust grains from the Apollo and Luna-24 sample returns as well as the JSC-1 lunar simulants.

DUST PROPERTIES IN THE TRAIL OF COMET 67P/CHURYUMOV-GERASIMENKO. J. Agarwal[1], H. Boehnhardt[2], M. Mueller[3] and E. T. Gruen[1,4]. [1]MPI-K, Saupfercheckweg 1, 69117 Heidelberg, Germany, jessica.agarwal@mpi-hd.mpg.de; [2]MPS, Max-Planck-Straße 2, 37191 Katlenburg-Lindau, Germany; [3]EDS at ESA/ESOC, Robert-Bosch-Str. 5, 64293 Darmstadt, Germany; [4]HIGP, University of Hawaii, 1680 East West Road POST 512c, Honolulu, HI 96822, USA.

Introduction: We report first results concerning the dust abundance and size distribution in the trail of comet 67P/Churyumov-Gerasimenko. The study is based on optical imaging data obtained in April 2004 with the Wide Field Imager (WFI) at the MPG/ESO 2.2m telescope in La Silla (Chile). For comparison we simulate images using a model with parameters derived from the observed emission history of the comet. By fitting the simulated intensity distribution to the observed one, we infer on the dust size distribution and column density. 67P/Churyumov-Gerasimenko is the target of ESA's Rosetta mission which will pass through the trail region during its approach to the nucleus in 2013.

Comet trails: Large (mm-sized) dust particles are emitted by comets at small heliocentric distances and with low relative velocities (several m/s). Since the strength of solar radiation pressure is weak compared to the gravity of the Sun, such particles move on trajectories similar to that of their parent comet. They concentrate along its orbit and appear to the observer as a long, line-shaped structure, the comet's dust trail. The emission of large dust particles is the principal mechanism by which a comet loses refractory mass to the interplanetary dust environment [1]. Trails of eight short-period comets were first observed with IRAS in 1983 [2,3], one of them being 67P/Churyumov-Gerasimenko.

Trail imaging: Comet trails are best observed when separated from smaller-sized dust grains. The latter are emitted with greater relative velocities and subject to stronger radiation pressure, hence they disperse in space on timescales of weeks to months from their release and their presence is not expected in the vicinity of an inactive comet far from the Sun. The WFI image (Fig. 1) was taken when 67P/Churyumov-Gerasimenko was at a heliocentric distance of 4.7 AU and we can confirm that no coma or young tail containing small particles is present in the image.

Trail modelling: We use a semi-analytical, generalised Finson-Probstein[4,5] model to produce simulated images of the dust trail [6]. For the time-dependent gas and dust production rates, we use observed values compiled from the literature, and the dust emission speed is computed using a hydrodynamic coma model [7]. The dust size distribution is the parameter we try to optimise by fitting the simulated image to the observed one. We find that using the size distribution derived in [8] from the VEGA2 measurements near comet 1P/Halley, is not optimal to reproduce the observed data and that a flatter size distribution is probably more appropriate.

References: [1] Sykes M.V. and Walker R.G. (1992) *Icarus, 95,* 180-210. [2] Sykes M.V. et al. (1986) *Science, 232,* 1115-1117. [3] Sykes M.V. et al. (1986) *Adv. Sp. Res., 6,* 67-78. [4] Finson M.L. and Probstein R.F. (1968a) *ApJ, 154,* 327-352. [5] Finson M.L. and Probstein R.F. (1968b) *ApJ, 154,* 353-380. [6] Agarwal J. et al. (2005) *Adv. Sp. Res, in press.* [7] Landgraf M. et al. (1999) *Planet. Space Sci., 47,* 1029-1050. [8] Divine N. and Newburn R.L. (1987) *A&A, 187,* 867-872.

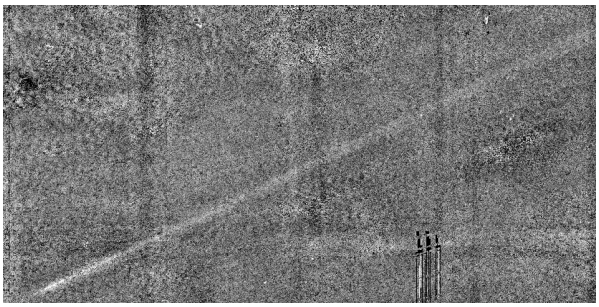

Fig. 1 - The trail of 67P/Churyumov-Gerasimenko in April 2004, observed with WFI at ESO/MPG 2.2m, La Silla. The image dimension corresponds to about 1 degree in mean anomaly and the nucleus is in the lower left corner, in the region which with the employed grey-scale range is saturated. The comet was at a heliocentric distance of 4.7 AU, and 3.7 AU from Earth.

EXTREME OXYGEN ISOTOPE RATIOS IN METEORITIC DUST GRAINS — A RECORD OF IRRADIATION IN DUST-FORMING REGIONS OF THE PROTOSOLAR NEBULA? Aléon J.[1,2], Duprat J.[3], Robert F.[4], Hutcheon I. D.[2], Weber, P. K.[2], Toppani A.[2] and Derenne S.[5]. [1]CRPG-CNRS, 15 rue Notre Dame des Pauvres, 54501 Vandoeuvre-les-Nancy, France (aleon@crpg.cnrs-nancy.fr), [2]LLNL, Livermore, CA 94550, USA, [3]CSNSM, Bat 104, 91405 Orsay campus, France, [4]LEME-MNHN, 61 rue Buffon 75005 Paris, France, [5]LCBOP-ENSCP, 11 rue Pierre et Marie Curie 75231 Paris, France.

Introduction: Large isotopic anomalies in minute meteoritic and cometary grains are commonly attributed to the survival of interstellar dust grains formed in previous generations of stars [1]. In this study, we mapped large oxygen isotope anomalies associated with unusual dust grains embedded in an organic residue from the carbonaceous chondrites Orgueil and Murchison.

Samples and analytical techniques: O isotopes were mapped at high mass resolving power by IMS 1270 ion microprobe at CRPG, Nancy using a 1 µm lateral resolution in insoluble organic matter from Orgueil and Murchison. Grains with isotopic anomalies were subsequently mapped for Si isotopes with 2 µm lateral resolution to increase the sensitivity and anlayzed by scanning electron microscopy (SEM). Residual grains were selected for (1) Mg isotope analysis by NanoSIMS at Lawrence Livermore National Laboratory (LLNL) with 200 nm lateral resolution, (2) N isotope analysis by IMS 1270 ion microprobe in CRPG, Nancy with 1 µm lateral resolution and (3) focussed ion beam sectioning followed by transmission electron microscopy (TEM) performed at LLNL.

Results: 36 grains with large excesses of ^{17}O and ^{18}O were discovered in the IOM from Murchison, while none were found in IOM from Orgueil. $^{17}O/^{16}O$ and $^{18}O/^{16}O$ ratios of these grains reach the largest values ever measured in solar system materials : 7.7×10^{-2} and 1.2×10^{-1}, respectively. By contrast with typical presolar grains which show the scatter expected from the contribution of multiple stellar sources, all Murchison grains lie on a single mixing line between the most extreme value and the bulk solar system value [2]. Given the yield of IOM extraction and the relative surface area analyzed, the grains account for ~1 ppm of Murchison, a concentration comparable with that of presolar oxide grains [1]. The abundance of similar grains is less than 40 ppb in Orgueil. In contrast to O, no deviations from solar system values were found for N, Mg or Si (uncertainties: 10 ‰ on Si isotopes, 20 ‰ on Mg isotopes, a factor 2 on N isotopes). The upper limit on the initial $^{26}Al/^{27}Al$ inferred from Mg isotopes is 4.8×10^{-4}. SEM imaging and energy dispersive spectroscopy revealed that the grains are facetted with Si and O being the only major constituents, suggesting that the grains could be silica. Preliminary TEM results suggest that the grains are amorphous silica.

Discussion: Large excesses of both ^{17}O and ^{18}O associated with normal Si and Mg isotopic compositions cannot be explained by conventional stellar nucleosynthesis models. Similar O isotopic ratios have been observed only once in our galaxy, in HR4049, an unusual post-asymptotic giant branch star [3]. If the Murchison grains originated in such a star, the fact that all O-isotope values lie along a single mixing line indicates the young solar system may have encountered a single unusual star responsible for the injection of these grains. However we note that this hypothesis is in contradiction with (1) the absence of anomalous grains in Orgueil, a meteorite rich in presolar grains, (2) the absence of large amounts of ^{26}Al in the grains, and (3) the absence of refractory oxide grains with similar compositions [1].

The observed compositions are successfully reproduced by irradiating a gas of solar composition by particles with the characteristics of ^{3}He-rich impulsive solar flares, followed by condensation and selective chemical trapping of anomalous O (O*). Such a condensation reaction could be $SiO + O^* \rightarrow SiO_2$. In this model the absence of Si isotope anomalies is explained by the dilution in the solar gas of the intermediate species, SiO. This may also be the case for Mg and Al. Any species trapped mechanically in the grains, such as the inert gas N_2, would also have the composition of the bulk solar gas. We propose that the isolation of O* followed by condensation could have taken place in energetic protosolar outflows. Protostellar outflows are commonly enriched in SiO [4], possibly allowing condensation of SiO_2. The discovery of these grains thus suggests that large isotopic anomalies could be produced within the young solar system and record highly energetic processes during an active phase of the young Sun.

References: [1] Clayton D.D. and Nittler L.R. (2004) *ARAA* 42, 39-78. [2] Aléon J. et al. (2005) *Nature* in press. [3] Cami J. and Yamamura I. (2001) *A&A* 367, L1-L4. [4] Nisini B. et al. (2002) *A&A* 395, L25-L28.

In-Situ Spacecraft Monitoring of the Interstellar Dust Stream in the Inner Solar System

N. Altobelli[1], E.Grün[2], S.Kempf[3], H.Krüger[4], M.Landgraf[5], R.Srama[6]

[1]NASA/JPL 4800 Oak Grove Drive CA-91101 Pasadena USA, nicolas.altobelli@jpl.nasa.gov,
[2]MPIK, Saupfercheckweg 1, 69117 Heidelberg, Germany/HIGP, University of Hawaii, Honolulu, USA, Eberhard.gruen@mpi-hd.mpg.de
[3]MPIK, Saupfercheckweg 1, 69117 Heidelberg, Germany, sascha.kempf@mpi-hd.mpg.de
[4]MPS, 37191 Katlenburg-Lindau, Germany, krueger@mps.mpg.de
[5]ESA/ESOC, 64293 Darmstadt, Germany, markus.landgraf@esa.int
[6]MPIK, Saupfercheckweg 1, 69117 Heidelberg, Germany, ralf.srama@mpi-hd.mpg.de

The Solar System motion relative to the surrounding interstellar medium results in a wind of gas and dust particles blowing onto the boundary region of the heliosphere. Evidence was found in 1993 by the dust detector on-board the *Ulysses* spacecraft that a collimated stream of interstellar dust (ISD) grains on hyperbolic trajectory penetrates deeply into the Solar System [Grün et al., 1993]. The downstream flux direction is compatible with the interstellar helium flux [Baguhl et al., 1995] and the bulk of its mass distribution is around 10^{-16}kg [Landgraf et al., 2000]. In-situ observation of ISD grains is of strong astrophysical interest and allows us to retrieve crucial information on individual grains which is not accessible by astronomical observations.

Over the past decade, study of the ISD flux alteration under the influence of the heliospheric environment provided important clues to the physical properties of individual ISD grains. Dynamics of ISD grains is ruled mainly by three perturbating accelerations: the Sun's gravitation (involving the grain mass), the radiation pressure (involving the grain's surface optical properties) and the Lorenz perturbation resulting from the coupling of charged grains (according to their charge-to-mass ratio) with the interplanetary magnetic field (IMF). The relative strength of these perturbations is also dependent upon the location in the Solar System and is reflected by the ISD flux alteration. Therefore, to better constrain the grain properties, it is highly desirable to determine the ISD flux value at many different locations in the Solar System. The *Ulysses* spacecraft measurements were performed between 2.5 and 5 AU. We analyze dust data sets retrieved by the interplanetary probes *Helios*, *Galileo*, and *Cassini*, extending the heliocentric distance range of the ISD observations down to 0.3 AU.

The ISD data presented here have been obtained on orbit segments where a discrimination between ISD and the interplanetary dust particles (IDPs) background was possible. The identification scheme used for this analysis involves geometrical criteria and criteria based on the comparison of the impact energy. A careful selection of the orbit segments is required: the impact energy of ISD grains is higher when the spacecraft is moving toward the ISD downstream direction, while the impact energy of IDPs on bound orbit is constrained by their orbital elements and mass distribution, evaluated from an interplanetary dust flux model.

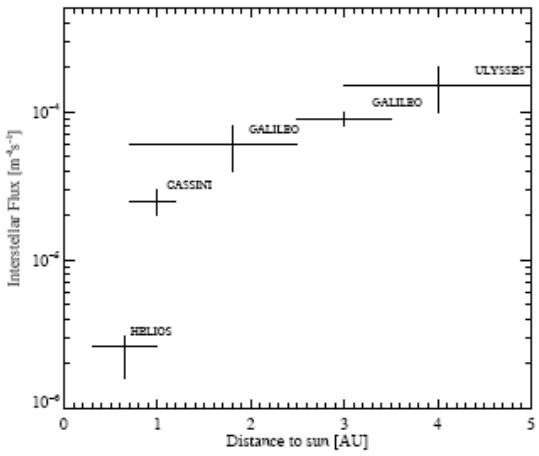

Figure 1: Plot showing the values of the ISD flux calculated with the data presented in this work, as function of the heliocentric distance

We first applied our identification scheme to the *Cassini* dust data during the interplanetary cruise phase when the spacecraft was located between Venus and the Earth. An ISD flux of about $2.5 \cdot 10^{-5} m^{-2} s^{-1}$ was detected. The energy of the ISD impactors was compatible with typical grain masses of about $3 \cdot 10^{-16}$ kg, as derived from the analysis of the *Ulysses* ISD data [Landgraf et al., 2000]. The analysis of the *Galileo* data between the orbits of Venus and Mars confirmed the presence of ISD at close heliocentric distances. About 115 ISD impactors were identified amongst 435 dust impact events between December 31st, 1989 and December 31st, 1993. Finally, the *Helios* dust data (235 impactors) obtained between December 1974 and

January, 1980 were also analyzed for ISD. A weak but significant ISD flux of about $2.6 \pm 0.3 \cdot 10^{-6}$ $m^{-2}s^{-1}$ was detected down to 0.3 AU (see Fig. 1). Interestingly, the *Helios* ISD data suggest larger grains (micrometer size) than detected with the other instruments (sub-micrometer size).

The decrease of the ISD flux at close heliocentric distances can be explained by the radiation pressure filtering effect. Zones of avoidance are shaped by the solar radiation, inside which ISD grains smaller than a certain size can not penetrate [Landgraf, 2000]. Our ISD flux measurements show a good agreement with the theoretical boundary locations of the avoidance zones, assuming for the dust grain surface optical properties the astronomical silicates model [Gustafson, 1994]. On the other hand, the spatial density of big ISD grains is enhanced by gravitation focusing at close heliocentric distances. Thus, the closer to the Sun, the bigger the low-mass cut off of ISD grains. This picture is supported by the excess of big ISD grains found in the *Helios* ISD data.

Furthermore, clues to the elemental composition of the ISD grains detected were found by the *Helios*time-of-flight mass spectrometer, indicating that individual grains are a varying mixture of various mineral and carbonaceous compounds.

References

[Baguhl et al., 1995] Baguhl, M., Grün, E., Hamilton, D. P., Linkert, G., Riemann, R., and Staubach, P. (1995). The flux of interstellar dust observed by Ulysses and Galileo. *SpaceSci.Rev.*, 72:471–476.

[Grün et al., 1993] Grün, E., Zook, H., Baguhl, M., Balogh, A., Bame, S., Fechtig, H., Forsyth, R., Hanner, M., Horanyi, M., Kissel, J., Lindblad, B.-A., Linkert, D., Linkert, G., Mann, I., McDonnel, J., Morfill, G., Phillips, J., Polanskey, C., Schwehm, G., Siddique, N., Staubach, P., Svestka, J., and Taylor, A. (1993). Discovery of Jovian dust streams and interstellar grains by the Ulysses spacecraft. *Nature*, 362:428– 430.

[Gustafson, 1994] Gustafson, B. (1994). Physics of zodiacal dust. *Ann.Rev.EarthPlanet.Sci.*, 22:553–595.

[Landgraf, 2000] Landgraf, M. (2000). Modeling the motion and distribution of interstellar dust inside the heliosphere. *J.Geophys.Res.*, 105:10303–10316.

[Landgraf et al., 2000] Landgraf, M., Baggaley, W. J., Grün, E., Krüger, H., and Linkert, G. (2000). Aspects of the mass distribution of interstellar dust grains in the solar system from in situ measurements. *J.Geophys.Res.*, 105:10343– 10352.

Interplanetary dust between Jupiter and Saturn: preliminary results from the Cassini Cosmic Dust Analyzer. N. Altobelli (1) and M. Roy (2), S.Kempf (3), R.Srama (4), Georg Moragas-Klostermeier (5), E. Grün (6). (1)NASA/JPL 4800 Oak Grove Drive CA-91101 Pasadena USA nicolas.altobelli@jpl.nasa.gov, (2)NASA/JPL 4800 Oak Grove Drive CA-91101 Pasadena USA mou.roy@jpl.nasa.gov, (3)MPIK, Saupfercheckweg 1, 69117 Heidelberg, Germany sascha.kempf@mpi-hd.mpg.de, (4) MPIK, Saupfercheckweg 1, 69117 Heidelberg, Germany ralf.srama@mpi-hd.mpg.de, (5)MPIK, Saupfercheckweg 1, 69117 Heidelberg, Germany moragas@mpi-hd.mpg.de, (6) MPIK, Saupfercheckweg 1, 69117 Heidelberg, Germany/ HIGP university of Hawaii, Honolulu, USA eberhard.gruen@mpi-hd.mpg.de.

Introduction: We report in this work the preliminary analysis of the Cosmic Dust Analyzer (CDA) data, obtained when the Cassini spacecraft was between Jupiter and Saturn. The data cover the time period between the Jupiter fly-by and the Saturn orbit insertion (SOI).

Previous analysis: Until the Cassini mission, the only in situ dust detectors ever flown in this region were the Pioneer 10 and Pioneer 11 dust experiments. A nearly constant flux of interplanetary dust (IDP) about 10^-6/m^2/s was derived from the Pioneer instruments data outside the orbit of Jupiter [2]. Owing to the sensitivity of these instruments, only big particles (larger than 10 μm for Pioneer 10 and larger than 25 μm for Pioneer 11) could be detected. Three dust sources accounting for the measured flux beyond 5 AU were identified, involving short-period Oort cloud comets (retrograde particles with low inclination), short-period Jupiter-family comets (low eccentricities and inclinations) and Edgeworth-Kuiper belt objects (low eccentricities and inclinations) [4].

Preliminary results and goals of this work: The CDA is a more sensitive instruments and allows the detection of smaller grains. In particular, streams of high-velocity submicrometre-sized dust particles, originating from both Jupiter and Saturn [1,3] are detected far away from their source and contribute significantly to the data set. However, bigger IDPs on bound low-inclined orbits have been detected as well. A preliminary analysis suggests both prograde and retrograde trajectories for these grains. As Cassini was located downstream to the interstellar dust (ISD) flux, no ISD grains can be detected on this part of the Cassini trajectory since this would require the instrument pointing to be directed toward the Sun (forbidden configuration). The IDP flux values measured are compared with the values derived from the Pioneer IDP data. Furthermore, deriving the flux value in the vicinity of Saturn provides a lower estimate of the IDP contamination onto the Saturn dust rings.

References:

[1] Grün, E., Zook, H., Baguhl, M., Balogh, A., Bame, S., Fechtig, H., Forsyth R., Hanner, M., Horanyi, M., Kissel, J., Lindblad, B.-A., Linkert, D., Linkert, G., Mann, I., McDonnel, J., Morfill, G., Phillips, J., Polanskey, C., Schwehm, G., Siddique, N., Staubach, P., Svestka, J., and Taylor, A. (1993). *Discovery of Jovian dust streams and interstellar grains by the Ulysses spacecraft.* Nature 362, 428-430.

[2] Humes, D.~H. (1980). *Results of Pioneer 10 and 11 meteoroid experiments – Interplanetary and near-Saturn.* JGR 85, 5841-5852.

[3] Kempf, S., Srama, R., Horanyi, M., Burton, M., Helfert, S., Moragas-Klostermeyer, G., Roy, M., and Grün, E. (2005). *High-velocity streams of dust originating from Saturn.* Nature 433, 289-291.

[4] Landgraf, M., Liou, J.-C., Zook, H.~A., and Grün, E. (2002). *Origins of Solar System Dust beyond Jupiter.* Astron. Journal 123, 2857-2861.

DUST PRODUCTION DURING PLANETARY COLLISIONS LARGE AND SMALL. E. Asphaug, C. Agnor and Q. Williams, IGPP Center for Origin, Dynamics & Evolution of Planets, Earth Sciences Dept. University of California, Santa Cruz CA 95064, asphaug@pmc.ucsc.edu

Introduction: Dust production in planetary systems has often been proposed to be the result of high strain rate fragmentation events, as asteroids and comets grind one another down to smaller and smaller sizes. But it is also possible to produce copious dust, particularly in young planetary systems, through pressure-release phreatic eruptions, as large planetary embryos rip each other to shreds, unloading 100's of kbars of pressure during late stage accretion.

Having recently demonstrated that planetary collisions are seldom accretionary [1; see Fig. 1], we find that disruptive tides and gravitational torques may do much of the work of planetary evolution. The focus here is predominantly upon the smaller of the encountering bodies – the "impactor" – which is frequently *not* accreted in a collision, and whose material is severely disrupted and in many cases pulled off of its central body (see Fig. 2), in events not dissimilar from the tidal break-up of comet Shoemaker-Levy 9. These planet-scale volumes of unloaded material are proposed as copious sources for dust production in early planetary systems. The character of this dust is predicted to be volcanic in origin and highly outgassed.

Meteoritics and Impacts: Impacts are typically understood as shock-related phenomena, based on laboratory comparison and our understanding of impact cratering. But shock physics fares poorly, in many instances, in explaining asteroid and meteorite genesis. Mixing by shock acceleration should leave few un-shocked products. Melting and thermal processing by impact are inefficient on small bodies [2] since material shocked to high temperature escapes their weak gravity. Melts, melt residues, welded agglomerates and hydrous and gas-rich phases are abundant among meteorites, leading to an array of diverse puzzles. Also puzzling is the relative abundance of stony-irons [~2-3% of all falls), when unambiguous mantle meteorites are rare [reviewed in 3 and refs therein]. Where are these mantle rocks, when so many irons and stony-irons were excavated from the deepest mantles and cores?

A possible solution is that mantle rock, when ripped from a parent planet, becomes dust in a single event related to gravitational unloading from hydrostatic equilibrium over the encounter timescale.

Fragmentation by Elastic Unloading: Consider a cold elastic planet, unloading by tidal stress during a gravitational timescale $\tau_{grav} \sim (G\rho)^{-1/2}$. If release rates are high, one can apply a dynamic fragmentation model [4] to evaluate the expected fragment size. Consider a Weibull distribution of active flaws per unit volume $n(\varepsilon) = k\varepsilon^m$, where $\varepsilon = \sigma/E$, σ is the flaw activation stress, and E the elastic modulus. Fragment size decreases with strain rate $\dot{\varepsilon}$. If the characteristic mantle stress $\sigma \approx G\rho^2 a^2$ unloads uniformly over τ_{grav}, then the characteristic strain rate $\dot{\varepsilon} = G^{3/2}\rho^{5/2}a^2/E$ gives mean fragment size $L \approx 6 c_g \alpha^{-1/m+3} \dot{\varepsilon}^{-m/m+3}/(m+2)$, where c_g is the crack growth velocity and $\alpha = 8\pi c_g^3 k/[(m+1)(m+2)(m+3)]$. Here a is the disrupted body's radius. Fragment size decreases with almost the square of disrupted planet size, since $m > \sim 6$ for most geologic materials. A 500 km diameter basalt sphere ($k = 4 \cdot 10^{29}$ cm^{-3}, $m = 9$) cracks into ~200 m fragments if unloaded over τ_{grav}, and a 1000 km sphere cracks into ~70 m fragments. Instant rubble piles result if these fragments do not disperse; families of sub-km asteroids form otherwise, thereafter comminuting to smaller sizes.

Fragmentation During Viscous Response: Viscous deformation is indicated when $\tau_{grav} < \tau_{maxwell}$, and this is the more likely scenario for accreting embryos where accretional heating and short half-life radionuclide decay kept them hot for millions of years. Viscosity decreases with $e^{-1/T}$, where T is temperature. For power-law creep, $\dot{\varepsilon} = A\sigma^n$, about the

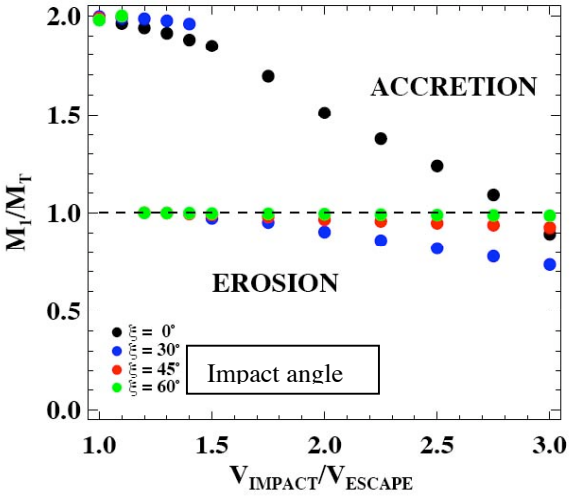

Fig. 1 Many planetary collisions result in net mass loss, not mass accretion (from [1])

square of the applied stress (n~3 for cold ice and dry quartzite). As a guide, models of early-Earth convection assume mid-mantle viscosities ~10^9 poise [5], and η~10^9-10^{13} poise is used [6] to model Io's present asthenosphere. Dissolved H_2O expected in primitive mantles further lowers the viscosity, especially if exsolved during unloading (see below). Once tidal deformation begins, pressure unloading ensues, and this triggers partial melting and possible H_2O exsolution, lowering the viscosity and leading to efficient melt segregation and possible outgassing.

Tidal disruption requires significant deformational strain, let's say $\varepsilon_{def} \approx 10$, accruing over a few times τ_{grav}. The maximum viscosity $\eta_{\lim}$ allowing this deformation is approximately the stress that must be unloaded, $\sigma \approx G\rho^2 R^2$, divided by the required strain rate, $\dot{\varepsilon} \approx \varepsilon_{def} / \tau_{grav}$. This gives the result

$$\eta_{\lim} \approx \varepsilon_{def}^{-1} \sqrt{G} \rho^{3/2} a^2$$

Strains ε_{def}>10 can occur if $\eta < \eta_{\lim} \sim 10^{12} a_{km}2$ poise (g cm^{-1}s^{-1}), where $a_{km} = a/(1000\text{ km})$.

Young planetary embryos are thus expected to be particularly vulnerable to viscous disruptive deformation. Once they cool, they still fail but by brittle fragmentation as described earlier, which as shown by Jeffreys will occur to grazing interlopers larger than about 200 km diameter [7].

These analyses describe mechanisms separately from impact shock, which further contributes to disruption, mass loss, and dust production.

Gravitational Unloading: A planet suffering a grazing (non-impacting) encounter at close to v_{esc} with a planet ten times its mass unloads its interior pressure by about half. This unloading might trigger degassing and dust production as the material unloads from an existing high-pressure hydrostatic state. The energy per unit mass during decompression is $\int dP/\rho$, which for constant density (e.g. up to the onset of vaporization) is $\sim P/\rho \approx G\rho r^2$ ~ $2 \cdot 10^{10}$ erg g^{-1} for the base of a Mars-sized planet's mantle. The effect of this energetic release is very dependent on the equation of state. The fragments of comet Shoemaker-Levy 9 were very active, producing copious dust, probably owing to sudden exposure (large dP) of a pristine interior. A disrupted planetary embryo unloads from pressures millions of times greater, and if rich in mantle volatiles might erupt [e.g. 8].

Mass Fractionation: Without even touching the target, the planet above loses its outer mantle and crust, some in the form of a disk or satellite swarm. Impacting non-accretionary encounters have even more severe tidal effects, as will be discussed in the

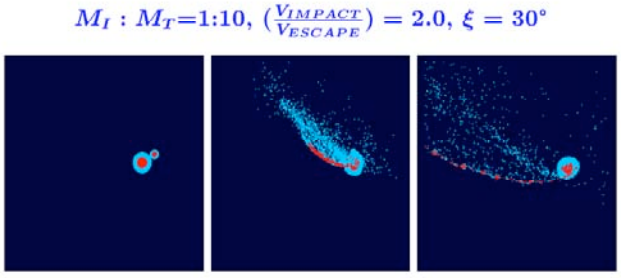

About half of impacts between planetary embryos in the late stage of accretion do not result in mass merger. What happens to the debris? (From [1])

talk. The atmosphere is lost, as tidal deformation is greatest for the lowest density layers (demonstrated by the stretching-out of the dust-rich comae of comet SL9. Much of these outer materials drain down onto the larger planet, increasing the volatile and atmophile inventory of the larger body at the expense of the smaller. As tidal collisions are much more common than accretionary collisions, embryo volatile inventory will evolve to vary inversely with mass.

Degassing: Extreme thermodynamical transitions raise the possibility of planetary degassing. The limited solubility of water in silicate liquids at low pressures can leave the shallow mantle of a primitive embryo relatively dry, down to a pressure of about 6 kbar, whereas deeper mantle can retain abundant water. As the planet unloads, the deep mantle crosses the water solubility pressure, so the question is whether there is adequate time for gas to segregate.

Dust Production: In the case of material stripped off of the host planet – in the manner of Shoemaker-Levy 9 but at much larger scales – the issue is less subtle. Transitioning from deep mantle pressures to almost complete unloading, over the course of hours, results in intense fragmentation, explosive degassing, and highly efficient dust production.

REFERENCES

[1] Agnor, C. & Asphaug, E., Ap. J. 613, L157-L160 (2004).

[2] Keil, K. et al. MAPS 32, 349-363 (1997).

[3] Burbine, T. H., Meibom, A. & Binzel, R. P. (1996). Meteoritics 31, 607-620.

[4] Grady, D. E. & Kipp, M. E. (1980). Int. J. Rock Mech. Min. Sci. Geomech. Abstr. 17, 147-157.

[5] Walzer, U. et al.; Tectonophysics 384, 55-90..

[6] Tackley et al, Icarus 149, 79-93 (2001)

[7] Jeffreys, H. (1947). MNRAS 107, 260-272

[8] Wilson et al., MAPS 34, 541-557 (1999)

DEVELOPMENT OF AN ULTRA-LOW NOISE CHARGE-SENSITIVE AMPLIFIER FOR COSMIC DUST PARTICLES

S. Auer (dusty789@shentel.net)

A new amplifier is being developed for the Dust Trajectory Detector of the Dust Telescope project. It shall enable us to measure the trajectories of dust particles with charges as low as 10^-16C (600 electrons) with an accuracy of 1° in direction and 1% in speed. Particular emphasis is placed on new methods of resetting the amplifier to prevent its saturation when currents of solar wind electrons or of photoelectrons from are charging the sensing electrodes.

COMPUTED ELECTRICAL CHARGES OF DUST PARTICLES WITH HIGHLY IRREGULAR SHAPES

S. Auer (dusty789@shentel.net)

The electrical charges of highly irregular particles were computed. It turns out that long needles and snowflake-like particles assumed charges as high as 30 times the charge of a spherical particle having the same volume and surface potential. This ratio influences the derivation of a particle's mass from its charge.

INTERSTELLAR METEORS. W.J Baggaley, Physics and Astronomy Department, University of Canterbury, PB 4800, Christchurch, New Zealand. jack.baggaley@canterbury.ac.nz.

Interstellar dust particles larger than about 1μm (4.10^{-12} g) can penetrate freely into the inner solar system where, in the event of Earth impact, they can be accessed by detecting the plasma and excited species created when the particles ablate in the Earth's atmosphere. The ablation process and current experimental techniques available for plasma detection mean that the particle size regime accessible from ground-based sensing is much larger than can be sampled from spacecraft. However, the much larger collecting area provided by the atmosphere in the meteor mode results in comparable detection statistics for the two techniques.

The value of this Earth based probing of interstellar dust lies in the ability to provide quality dynamical characteristics: the velocity information allows the tracking of pre-solar system encounter trajectories.

This paper provides an overview of experimental techniques and the attempts to map the galactic sources of interstellar dust.

A REVOLUTION IN THE NANO-SCALE CHARACTERIZATION OF IDPs AND OTHER PRIMITIVE METEORITIC MATERIALS. John P. Bradley, [1]Institute of Geophysics and Planetary Physics, Lawrence Livermore National Laboratory, Livermore CA , 94550 <jbradley@igpp.ucllnl.org>

Introduction: In the past five years a suite of new instruments have enabled materials scientists to significantly advance the state-of-the-art in the analysis of nano-materials. These instruments include the Focused Ion Beam (FIB), nanoSIMS and an emerging generation of analytical scanning transmission electron microscope known generically as the SuperSTEM. We are developing an integrated approach to the microanalysis of IDPs and meteorites, using FIB, SuperSTEM, (and nanoSIMS), with the goal of expanding the science yield that can be obtained from a single sample. FIB is a key bridging technology that enables production of samples that can be interchanged between FIB, nanoSIMS and STEM environments.

The FIB utilizes a gallium ion beam within an SEM environment to harvest electron transparent sections and site-specific samples with sub-micrometer-scale spatial resolution. The biggest impact of FIB in meteoritics has been the almost routine recovery of isotopically anomalous "hot spots" from ion microprobe mounts, precipitating a flood of highly specific new data about the mineralogy and even optical properties of presolar grains [e.g. 1-3].

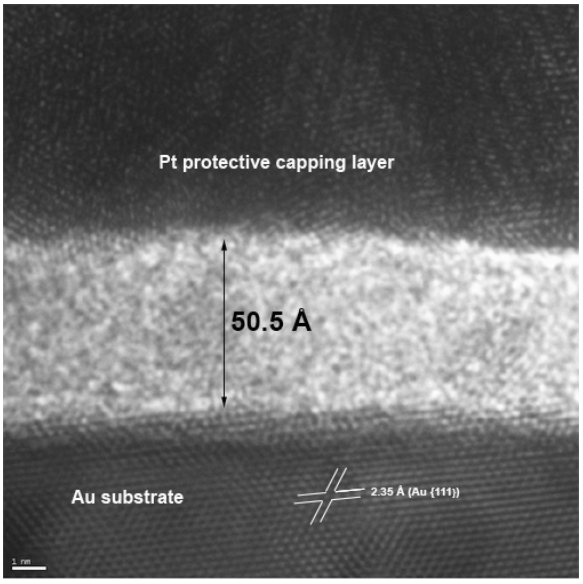

Figure 1: *High-resolution lattice-fringe image of a solar-wind implanted Au substrate (lower) from the Genesis mission. The surface is coated with a contamination layer 50.5 Å thick. The Pt protective capping layer (upper) was applied during FIB specimen preparation. Scale bar measures 1 nm.*

FIB is proving useful in other critical areas of planetary materials analysis. Figure 1 shows a brightfield image of what is suspected to be a siloxane-based contaminant stain on the surface of a gold solar-wind collection substrate from the Genesis spacecraft. Measurements of the thickness of this layer using surface sensitive techniques yielded conflicting results ranging from 50 Å to 160 Å. Accurate measurement of the stain thickness may be a prerequisite to meaningful analyses of the isotopic compositions of the some of the implanted solar wind elements. Figure 1 establishes that the stain is 50 Å thick, at least in this region of the gold foil.

Significant new developments in analytical transmission electron microscopy include high-resolution electron energy-loss spectroscopy, optical spectroscopy and nanometer-scale compositional mapping. Figure 2 shows a 200 keV zero-loss peak obtained using a Tecnai™ F20 monochromated STEM recently installed at Lawrence Livermore National Laboratory (LLNL). The 0.07 eV energy resolution at a one second exposure is due to a higher stability high-voltage source, a monochromator and a high-resolution energy filter. This performance record for energy-loss spectroscopy opens a whole new level of chemical analysis at the nanometer scale by probing bonding states, bandgap and valence band

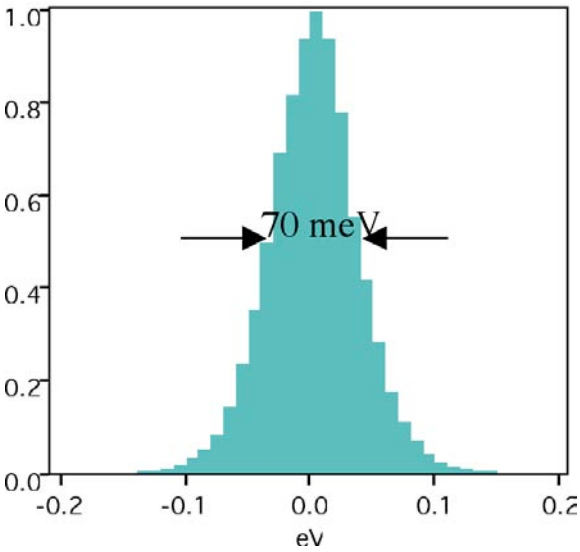

Figure 2: *Electron energy-loss zero-loss peak obtained using a 200 keV monochromated transmission electron microscope.*

transitions of known and unknown materials. The overall spatial resolution is an order of magnitude better than synchrotron XANES and it is complimentary to that technique.

With improved energy resolution the width of the zero-loss peak is reduced, opening up a spectral region that contains a wealth of new information. For example, it is now possible to perform optical spectroscopy in the near-infrared, visible and UV spectral regions with nanometer-scale spatial resolution. Using this new capability, a spectral match to the astronomical 2175 Å extinction feature was recently observed within IDPs using EELS (Fig. 3) [4].

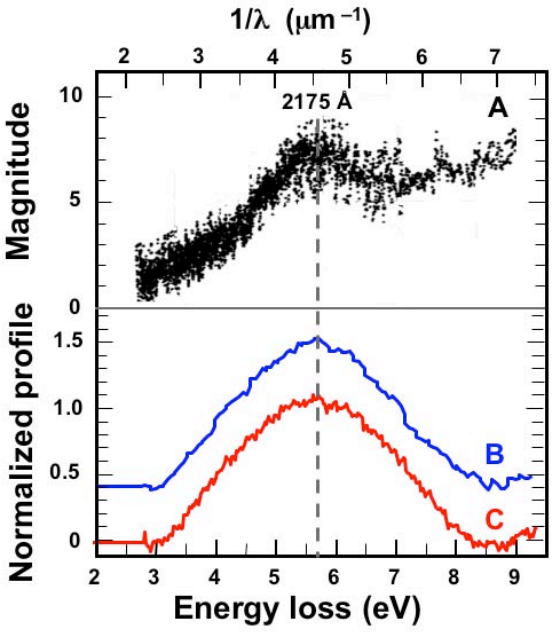

Figure 3: *The astronomical 2175 Å UV extinction feature (A) compared with EELS UV spectra from IDPs (B & C). From Bradley et al., 2005* [4] *).*

Figure 4 shows the near-infrared, visible and UV region of an energy-loss spectrum of Acid Fuchsin obtained using the monochromated STEM at LLNL. (Acid Fuchsin is a common sodium salt histological stain used for staining cytoplasm and collagen). The spectrum was acquired using gun deceleration lens mode, a 1 mm spectrometer aperture, 0.01 eV/pixel dispersion and 1 second acquisition. Specimen thickness is 0.74x the inelastic mean free path. Zero-loss energy resolution is 0.18 eV FWHM on the specimen. The visible electron energy-loss absorption spectrum is due to electron optical transitions corresponding to exciting the molecular orbitals of the valence electrons, giving rise to the emission of photons in the visible region of the spectrum. A UV absorption peak at 5.9 eV (λ~210 nm) is clearly visible (as it is in the optical spectrum of Acid Fuchsin).

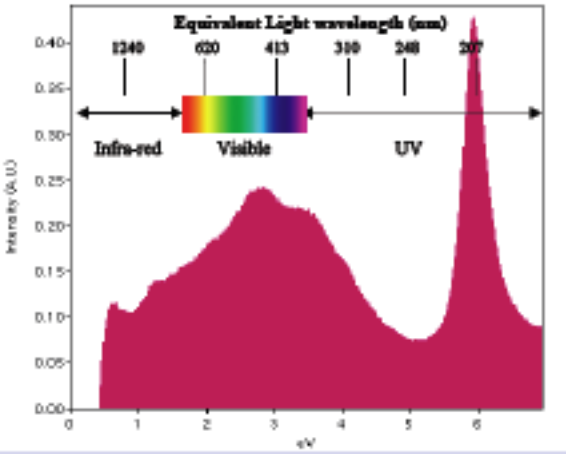

Figure 4: *Near-infrared, visible and UV region of an energy-loss spectrum of Acid Fuchsin obtained using the monochromated STEM at LLNL (data courtesy of M.Barfels, (Gatan Inc) and Z. Dai (LLNL)).*

References: [1] Stroud R. M. and Bernatowicz T. J. (2005) *LPS XXXVI*, Abs# 2010. [2] Floss C. F. et al. (1997) *Meteoritics & Planet. Sci., 32*, A74. [3] Yada, T. et al., (2005) *LPS XXXVI*, Abs #1227. [4] Bradley J. P. et al. (2005) *Science 307*, 244-247.

Acknowledgements: This work was performed in part under the auspices of the U.S. Department of Energy, NNSA by the University of California and Lawrence Livermore National Laboratory under contract No. W-7405-Eng-48. This work was also performed as part of the Bay Area Particle Analysis Consortium (BayPAC). Supported by NASA grant NNH04AB491.

INTERSTELLAR METEOROIDS DETECTED BY THE CANADIAN METEOR ORBIT RADAR. P. Brown[1], R.J. Weryk[1], [1]Department of Physics and Astronomy, University of Western Ontario, London, ON, N6A 3K7

Introduction: The number density of very large (>50 μm) interstellar grains is largely unknown [1]. Such large interstellar particles (ISPs) are of interest as they could contain a significant mass fraction of the solids in interstellar space [2]. Larger grains also have their original trajectories less affected by Lorentz and gas drag forces in the interstellar medium in addition to having longer lifetimes against catastrophic collisions. As a result, it is more probable that the specific origin for a given large ISP (such as ejecta from AGB or T Tauri systems and debris disks around young main sequence stars) can be established, assuming individual grain trajectories and velocities are known prior to detection. Such large ISPs should be able to penetrate deeply into the solar system without being stopped by the interplanetary magnetic field [3] and could potentially be detected at the Earth. Detection of large ISPs at the Earth has already been claimed based on data from the Advanced Meteor Orbit Radar (AMOR) operating in New Zealand [4].

Equipment: The Canadian Meteor Orbit Radar (CMOR) has been in routine operation since 2002 near 43N, 81W. This 6 kW interferometric automated radar operates at 29.85 MHz and records atmospheric trajectories and velocities for ~2500 meteoroids per day [5], [6]. The typical meteoroid mass detected by CMOR is near 10 μg, corresponding to particle sizes of order 100 μm. The beam coverage for CMOR is essentially all-sky, with 3 dB sensitivity contours located 60 degrees from the zenith. CMOR has a typical atmospheric collecting area of 200-300 km^2 for a given radiant direction. Meteoroid velocity is computed based on time-of-flight measurements made at two outlying stations; typical errors have previously been found to be of order 10% of the measured speed. Simulations [6] imply this error should be reducible by a factor of 2 – 3, suggesting further optimization of the existing signal analysis algorithms are warranted. Path orientation is dependent on both accurate measurement of the time-of-flight delays (t_1-t_0 and t_2-t_0 as in the figure) between different specular points along the trail as measured at the outlying stations (relative to the main station) and interferometric determination of echo location from the main radar station. Typical interferometric errors for high signal:noise ratio echoes are of order one degree.

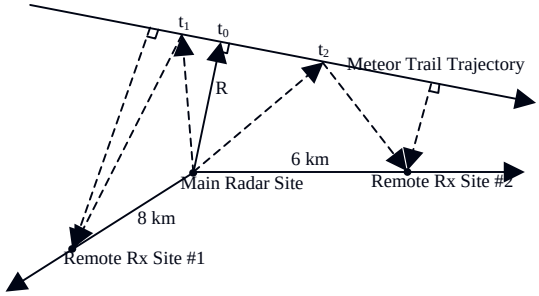

Figure 1.

Analysis and Results: A preliminary examination of potential very large ISPs detected by CMOR [7] produced only a handful (40) of possible detections from our initial population of more than 10^6 orbits. The primary limitation of this earlier work was a 2σ selection criterion, i.e. only echoes whose heliocentric orbits were more than 2σ above the hyperbolic threshold were examined. In practice, this produced a cutoff for events with heliocentric speeds greater than 55 km/s at the Earth. Here we extend this earlier analysis to the 1σ case and examine the large number of hyperbolic meteoroids having heliocentric velocities below 48 km/s at 1 AU. We have further improved our time-of-flight detection algorithm producing higher precision velocity measurements. We will present results of this investigation examining the fraction of unbound orbits at the 1σ level as a function of ecliptic coordinates to establish the nature of the hyperbolic meteoroids (solar system or possible true interstellar). Earlier results from the AMOR system have also suggested a discrete southern hemisphere interstellar meteoroid stream source [4] at smaller masses than CMOR detects. We will similarly examine northern hemisphere data to search for such discrete sources at the larger particle sizes detected by CMOR.

References: [1] Gruen E. and Landgraf, M. (2000) *JGR, 105*, 10291–10297. [2] Frisch et al. (1999) ApJ., *525*, 492-516. [3] Landgraf, M. et al.. (2003) *JGR, 108*, LIS 7-1 [4] Baggaley, W.J. (2000) *JGR, 105*, 10353-10361. [5] Webster, A.R. et al. (2004) Atmos. Chem. Phys. Discuss., 4, 1181-1201. [6] Jones, J. et al. (2005) Planet. Sp. Sci., 53, 413-421. [7] Weryk, R.J. and Brown, P. (2005), Earth, Moon and Planets, accepted.

WILD 2 OBSERVATIONS BY STARDUST D. E. Brownlee, Department of Astronomy 351580, University of Washington, Seattle, WA, 98915 (brownlee@astro.washington.edu)

Introduction: The Stardust comet sample return mission successfully made a close flyby of comet Wild 2 on January 2, 2004. The flyby provided a close-up view of a 4.5 km diameter Jupiter family comet that is an active source of interplanetary dust. The mission provides both detailed information on ejected particles as well as information on the way in which comets eject particulates. During the flyby the spacecraft passed 234 km from the surface and onboard meteoroid sensors indicated that the fluence of impacting particles exceeded the primary mission goal for collection of more than 500 particles with diameters >15μm. In addition to meeting this goal, Stardust also made dust flux measurements with its acoustic and PVDF impact sensors (DFMI - Dust Flux Monitor Instrument), it measured mass spectra of impacting particles with its mass spectrometer (CIDA - Cometary and Interstellar Dust Analyzer) and took high resolution images with its optical navigation camera, an instrument whose primary function was to provide navigation data.

Dust measurements: The results from the dust impact and mass spectrometry measurements are reported elsewhere [1-4] and will also be elaborated in other presentations at this meeting.

Dust collection and analysis: The DFMI data indicate that thousands of analyzable particles impacted the Stardust's collector. About 85% of these particles were collected in low density silica aerogel designed to capture comet dust particles at the encounter speed of 6.1 km/s. About 15 % of the particles impacted aluminum foil that covered the aerogel support grid. The craters in foil can be analyzed for projectile residue and they can be used to directly determine the particle size distribution. The crater size distribution can be compared with the DFMA results and can also be used to calibrate the aerogel impacts.

When the collected samples are returned to Earth on January 15, 2006, a small portion of the particles will be studied during a 6 month preliminary analysis period by an international team of researchers. The primary goals of this initial investigation will be A) general characterization of the nature and state of preservation of the samples to provide information for the allocation and most efficient analysis of the samples, B) determine if the Wild 2 samples are similar or distinct from known types of material found in meteorites and interplanetary dust, and C) estimate the ratio of pre-solar to nebular components using criteria that are currently used for meteorites and IDPs.

Encounter images: The flyby occurred on the sunward side on the comet and the camera took 72 images over a full range of phase angles, providing stereo images of the entire sunlit hemisphere. The closest images have a scale of 14 m/pixel and the exposures were toggled between 10 ms and 100 ms, providing excellent images of the nucleus as well as the much fainter dust jets. A spectacular result from the imaging was the large number of highly collimated dust jets [5]. Due to the strong angular dependence of scattering, the jets were best seen at low phase angles. It was expected that one or two jets would be observed but 22 were detected. The high collimation of the Wild 2 jets is similar to those seen on Borrelly and, as suggested for Borrelly [6], their surface vents may be supersonic. The large number of jets, their small source regions, and the fact that almost the entire surface of Wild 2 is covered with depressions, suggests that the jets are short lived and occur, at various times, over most of the nucleus surface. The small size of the jet sources presumably produces an environment where weak aggregate comet particles can be comminuted by collisions that result from shear and differential acceleration. During the flyby, it appears that the majority of the jets originated from equatorial regions of the slightly oblate body. No jets were seen to originate from the sunlit polar region, perhaps an indication that this heated region has been, at least temporarily, depleted in volatiles in near-surface regions. Wild 2 had two jets emanating from the dark side implying that the sources of these regions remain active for an appreciable fraction of the spin period.

The surface of Wild 2 is appreciably different from the four other cometary nuclei that have be imaged- Halley, Borrelly and Temple 1. Temple appears to be covered with impact craters and presumably retains a significant of its surface that was exposed in the Kuiper belt. The remarkably complex and rough surface of Wild 2 is different from the other three comets, probably because of prolonged evolution in the inner solar system. [1] Green S. F., et al (2004) JGR 109, 12, E12S04. [2] Clark B. C. et al. JGR 109, 12, E12S.03. [3] Tuzzolino A. J., et al. (2004) Science 304, 1776-1780. [4] Kissel, J(2004) Science 304, 1774-1776. [5] Sekanina Z., (2004) Science 304, 1769-1774. [6] Yelle, R.V. (2004) Icarus 167, 30-36.

AN INTERNAL WATER OCEAN ON LARGE EARLY EDGEWORTH-KUIPER OBJECTS AND OBSERVATIONAL PROPERTIES OF SOME COMETS V. V. Busarev, Sternberg State Astronomical Institute, Moscow University, Universitetskij pr., 13, Moscow 119992, Russian Federation, e-mail: busarev@sai.msu.ru

We have shown a possibility of a water ocean formation in the early Edgeworth-Kuiper objects (EKOs) [1]. A study of the most reliable data on matter content of the known comets, interplanetary dust particles, carbonaceous chondrites and utilization of the model distributions of the physico-chemical parameters of the matter in the solar proto-planetary disk allows to estimate an initial content of the short-lived Al^{26} radionuclide in EKOs materials. A thermal balance calculation for the large bodies (R>100 km) shows that the quantity of heat discharged due to Al^{26} decay in some first millions of years of their existence was sufficient to fully melt the water ice being in up to 30% proportion of their mass. An additional mechanism of EKOs' material heating up was probably a process of heat discharge under intensive collisional events in the mentioned and subsequent time. From analytical estimations [1] we have found that the water ocean might have been in a liquid state (at temperatures ~3-7°C) in EKOs' interiors for ~10^7 yr before complete freezing. This time was enough for the silicate fully sedimentation and serpentinisation, the silicate core formation (up to 0.5-0.6R of the bodies) and for the dissolution or floating of the main part of organics to the upper water boundary [2]. The proposed model of EKOs' initial thermal evolution agrees well with available observational data on the bodies. Additionally, it makes possible to predict the physico-chemical properties of some new comets or to explain those of the known.

The comets could come from Kuiper belt as debris of differentiated EKOs (e. g., [3]) and may be distinguished by a large content of organic matter or dust as compared to the other comets. However, some of them are probably among observed dusty comets such as 21P Giacobini-Zinner, C/1987 P1 Bradfield, C/1988 A1 Liller and so on (e. g., [4]).

References: [1] Busarev V. V. et al. (2003) *EM&P, 92*, 345-357). [2] Busarev V. V. et al. (2005) *LPSC 36th*, abs. #1074. [3] Ipatov S. I., Mather J. C. (2003) *EM&P, 92*, 89-98. [4] Kiselev et al. (2000), P&SS, 48, 1005-1009.

THE METEOROID ENVIRONMENT: SHOWER AND SPORADIC METEORS. M. D. Campbell-Brown[1] and P. G. Brown[2], [1]University of Western Ontario, Department of Physics and Astronomy, London ON N6A 3K7, Canada, Margaret.Campbell@uwo.ca, [2] University of Western Ontario, Department of Physics and Astronomy, London ON N6A 3K7, Canada, pbrown@uwo.ca.

Introduction: Interplanetary particles larger than 10^{-13} kg (3 μm) create significant light and ionization when colliding with the atmosphere of the Earth. This provides a way to study the larger component of the interplanetary dust complex, since the collecting area of the Earth's atmosphere is large and the meteors resulting from these impacts are easily recorded with optical cameras and radars. Particles in this size range are generally too large to be captured in dust detectors, and are almost impossible to detect remotely. Meteoroids are generally divided into two broad categories: shower meteors, which come from narrow radiants and occur over a limited range of the Earth's orbit every year, and sporadic meteors, which are always active and come from diffuse radiants. Recent advances in observing technology, particularly in automated data analysis, have produced great advances in the understanding of meteoroid distribution at 1 AU.

Shower meteors: Many meteor showers have been linked with a parent object, most often a comet, though a few are linked with asteroids. The meteoroids generally have a very similar orbit to their parent body, and are thought to be relatively recent (<10 000 years) ejecta from the parent. Debris which is older loses coherence due to planetary perturbations and becomes part of the dust background. Their speeds and radiants are very similar, and tracing back their orbits can reveal the parent body. The recent rise in the discovery rate for near-Earth asteroids has also led to a resurgence in the investigation of potential asteroid – meteoroid stream associations (as in the case of the Quadrantids [1]). Recently, even the ejection age of streams has become constrained (extensively modeled for the Leonids [2]). This is now making it possible to use meteoroid stream activity as a proxy to constrain dust ejection models from comets, measure older active periods and past orbital behaviour of comets. Major showers, such as the Geminids, can nearly double the meteoroid flux at the Earth during their peaks; minor showers may only be visible after carefully subtracting the background activity. Some showers return year after year with similar activity levels; others may show outbursts in some years and even disappear in others. The major nighttime showers have been extensively studied with optical methods, but minor showers and daytime showers are much less understood. Maximum shower activity, averaged over five years of radar data from the Canadian Meteor Orbit Radar (CMOR) in Tavistock, Ontario, Canada), is shown in Figure 1, with the major showers marked.

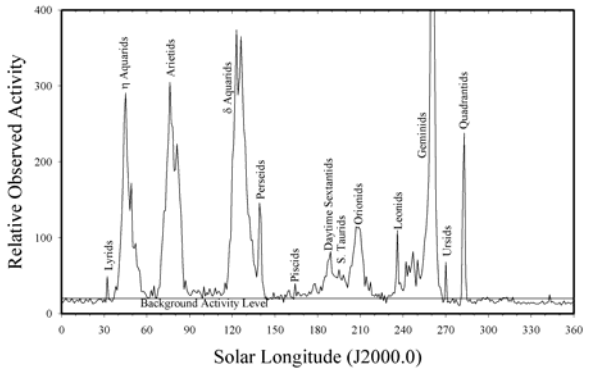

Figure 1. Maximum shower activity per degree of solar longitude; the data represents the average of five years of radar data

Sporadic meteors: Sporadic meteors are, by definition, those that do not belong to a recognized shower. They come from a few broad radiants which have constant positions relative to the sun. The most active sources are the helion and antihelion sources, which are centered near the solar and antisolar points; these and the apex source were first found by Hawkins [3], in a radio survey. The fastest sporadic meteors are associated with the apex source, which may be divided into a northern and a southern component, centered on the direction of the Earth's motion. The remainder of the sporadic meteors are concentrated approximately 60 degrees above and below the ecliptic, in the direction of the Earth's motion: these are the north and south toroidal sources (see [4] and [5]). Recent meteor patrol radar observations show the position and annual variation of these sources with unprecedented accuracy, and agree well with previous observations of the variation of the helion and antihelion sources [6]. A sample of CMOR sporadic data is shown in Figure 2, for April 10, 2004. The plot is in heliocentric coordinates, with the apex at the origin and the sun at +90 degrees. Sporadic meteors appear to have a longer dynamical history after separation from their parent body than shower meteors, but most appear to originate from short-period comets. Orbits of sporadic meteors have been studied extensively using radar [7]. Sporadic meteors are by far the dominant component of the meteoroid flux at the Earth, and become more dominant at smaller sizes. Because of the diffuse nature of the sporadic sources, they have been much less studied than shower meteors.

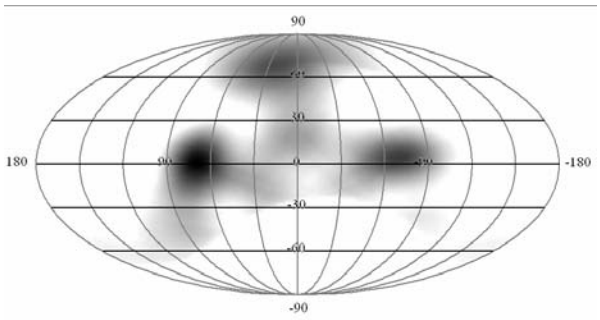

Figure 2: Heliocentric plot of sporadic radiants for April 10, 2004, as seen by CMOR, using an image resolution of 15 degrees. The apex of the Earth's way is at the origin, and the sun at +90 degrees. The north toroidal, north apex, helion and antihelion sources are clearly visible.

References:

[1] Jenniskens P., Marsden B.G., 2003, IAU Circ. 8252, 2.
[2] Lyytinen E.J., van Flandern T., 2000, EM&P 82, 149.
[3] Hawkins G. S., 1956, MNRAS 116, 92—104.
[4] Elford W. G., Hawkins G. S., 1964, Smithsonian. Astrophys. Obs. research rept no. 9.
[5] Jones J., Brown P., 1993, MNRAS 265, 524—532.
[6] Poole L.M.G., 1997, MNRAS 290, 245—259.
[7] Galligan D.P., Baggaley W.J., 2005, MNRAS 359, 551—560.

NANOMETRE SCALE FILMS AS DUST DETECTORS. J. D. Carpenter[1], T. J. Stevenson[2], G. W. Fraser[3] and A. Kearsley[4], [1,2,3]Space Research Centre, Department of Physics and Astronomy, University of Leicester, University Road, Leicester, LE1 7RH, UK, [1]jdc13@star.le.ac.uk, [2]tst@star.le.ac.uk, [3]gwf@star.le.ac.uk, [2]Natural History Museum, Cromwell Road, London, SW7 5BD, UK, A.Kearsley@nhm.ac.uk.

Introduction and Background: The exposure of 60nm thick aluminium films on the International Space Station (ISS) to assess the effects of the ISS environment on filmed microchannel plate (MCP) optics for the LOBSTER-ISS X-ray telescope [1] has resulted in the serendipitous discovery of nanometre scale dust and debris impactors. The inferred flux of this combined population is approximately $6m^{-2}s^{-1}$ [2]. These aluminium films are supported by the array of 12.5μm diameter MCP microchannels, which have a sensitivity almost two orders of magnitude greater than previously exposed foil experiments and are sensitive to impacts by dust particles with diameters of tens of nanometres.

New Impact Site Analyses: Since the discovery of this new population, work has been ongoing to analyse detailed impact morphologies on the films [3] and to determine the composition of the remaining trace residues through a combination of energy dispersive X-ray spectroscopy (EDXS) and secondary ion mass spectroscopy (SIMS). Such analyses can be used to refine impactor size estimates, sepatate different impactor populations and differentiate between natural dust and man-made debris impacts.

Future Passive Detector Exposures: Future thin film exposures, using films of varying thicknesses and pointing directions, and with an optimised location on the ISS are required, as the original ISS exposure was not optimised as a dust detection experiment. The exposed film surfaces need not be large. Analysis of the ISS exposed films indicates approximately one impact per minute for a $1cm^2$ surface area assuming that the density of impact features observed on the previously exposed films is characteristic of the flux in this size regime and is not dominated by a single event.

Development of an Active Detector: Such passive experiments are limited to retrievable samples in low Earth orbit. This environment is not ideal, particularly for the detection of very small particles, which are, in general, dominated by debris [4]. We are developing an active detector based on the thin film technology and utilising solid state detector readout solutions. Such a detector will use off the shelf devices, will be small, low in mass and suitable as an add-on to any spacecraft. It could therefore provide detailed data on nanonmetre scale dust populations throughout the Solar System.

References:

[1] Fraser, G. W. and 30 other authors (2002) *Proc. SPIE*, 4497, 115-126.

[2] Carpenter J. D., Stevenson T. S., Fraser G. W., Lapington J. S., Brandt D. (2005) *JGR., 110,* E05013, doi:10.1029/2004JE002392.

[3] Carpenter J. D., Fraser G. W., Stevenson T. J. (2005) *Proc. 4th European conference on Space Debris,* Darmstadt, Germany, In press.

[4] McDonnell J. A. M. (2001) in "Interplanetary Dust", edited by E. Grun, 163-261, Springer, London and Berlin.

COMPOSITIONAL STREAMING AND PARTICLE FRAGMENTATION AT COMETS 1P/HALLEY AND 81P/WILD 2. B.C. Clark, Lockheed Martin, POB 179, MS S-8000, Denver, CO 80201. benton.c.clark@LMCO.com

Introduction: The flyby of comet Wild 2 by the Stardust spacecraft revealed strong particle number density heterogeneities in the coma, while the Halley flyby missions showed that the particles in that cometary coma exhibit not only a great range in physical size, but also a range of compositions, including mixed particles and several apparent varieties of organic-rich materials. In this study, advantage is taken of the data from the Particle Impact Analyzer (PIA) on the Giotto spacecraft to provide a new classification of particle compositions in the coma of comet Halley. The time sequences of specific classes of particles are reexamined to evaluate potential additional evidence for spatial concentrations reflecting fragmentation and/or unique source regions, and compared with a model developed to characterize fragmentation patterns in the coma of Wild 2.

Data: Over 3000 TOS-MS spectra were obtained for elemental composition of Halley particulates by the PIA instrument. Each was time-tagged to an accuracy of 118 ms, corresponding to a distance traveled of 8 km. Over 9000 particles were analyzed for size by the Dust Flux Monitor Instrument (DFMI) on the Stardust mission, with a time resolution of 100 ms, or a spatial resolution element of 0.6 km. In both cases, the spacecraft flyby velocity was sufficiently higher than the cometocentric dust outflow speeds that the flux measurement can be interpreted directly in terms of number density of particle concentration. However, for PIA data not all events were transmitted.

Approach: Dust flux measurements in the Wild 2 coma have been recently analyzed in terms of a fragmentation model [1] and fragmentation interpretations [1, 2, 3]. Cluster sizes have been estimated from the model in terms of cluster radius and minimum mass content [1]. Similar metrics are now applied to apparent clusters in selected portions of the Halley coma, based upon specific compositional classes as determined from the PIA analyses. The classification scheme adopted here [4] utilizes a key element decision tree, with simple branching, building upon the initial compositional groups identified previously from PIA and PUMA data [5, 6, 1]. The first major branch in the trunk is for C, with immediate yes/no criteria for Si on both the C and no-C branches. These may be loosely interpreted as mineral and organic branches, and the four subsequent branches lead to silicates, non-silicate minerals (e.g., sulfides, oxides), organics, and Mixed particles containing C, Si, Mg and O (presumably, both carbonaceous and silicate matter). Subsequent branches result in 23 distinct classifications. Certain classifications can degenerate into other classes if one peak is missing, as can be the case for minor elements. Most of the classes are robust to criteria which provide independent methods of assessing their uniqueness.

Results: Although the statistical significance is marginal, it is found for example that Mixed particle encounter frequency is highly variable on the 3 s timescale (200 km), with evidence for 5 to 8 major apparent clustering's over a distance of 14,000 km in the coma. Even for this single particle class, variations in counts are significantly deviant from any simple Poisson distribution and the inverse-square law with distance from the nucleus is not strictly followed.

Numerous possible clusters are examined, for a range of grouped and ungrouped classes of particles. In many cases, there is correspondence in occurrence rate between members of different classifications, indicating a conglomerate source region, whether on the cometary surface or released as a large aggregate. In some cases, however, there is evidence of disparity between the classes of particles, with one or more members predominant and one or more members sparse. Correlations between types may be indicative of intrinsic associations of different types of cometary constituents, or possible undetected degeneracy's in the classification scheme.

Applications: The "ground truth" that the analyses of samples returned by Stardust should be helpful in refining the PIA and PUMA results, and relating the compositions of those portions of the two comae, Halley and Wild 2.

The refined analyses of these Halley results will be the only method available for ascertaining the similarities and differences in the compositional makeup of the particulate populations of comets Halley and Wild 2. In view of the loss of the CONTOUR comparative cometology mission, these data assume special significance.

References: [1] Clark et al. (2004), *JGR 109 : E12S03.* [2] Green et al. (2004), *JGR 109 : E12S43.* [3] Sekanina et al., *Science (2004) 304 : 1769-74.* [4] B.C. Clark and L. W. Mason (1991), Giotto/PIA Data Set, internally published. [5] Clark et al. (1987) *Astron. Astrophys. 187: 779-784.* [6] Fomenkova et al. (1994) *GCA., 58,* 4503-4512.

BEHAVIOR OF CHARGED DUST IN PLASMA AND PHOTOELECTRON SHEATHS. J. E. Colwell[1] , M. Horányi[1], S. Robertson[2], and P. Wheeler[2], [1]Laboratory for Atmospheric and Space Physics, University of Colorado, Boulder CO 80309-0392, josh.colwell@lasp.colorado.edu, [2]Dept. of Physics, University of Colorado, Boulder CO 80309.

Introduction: Dust particles in the regoliths of planetary satellites, asteroids, and ring particles can become charged due to photoemission from solar ultraviolet photons, solar wind currents, and in some case magnetospheric electrons. These currents produce a plasma sheath over the nighttime surface and a photoelectron layer over the daytime surface. Lunar electrostatic dust dynamics have been proposed for several observed dust phenomena [1-6]. Similar phenomena may play a role in the spokes of Saturn's rings [7, 8] and in the formation of smooth deposits in the floors of some craters on the asteroid Eros as observed by the NEAR-Shoemaker spacecraft [9].

Observations: Observations from the lunar surface by several of the Surveyor landers revealed a horizon glow over the western horizon shortly after sunset [3, 4, Figure 1].

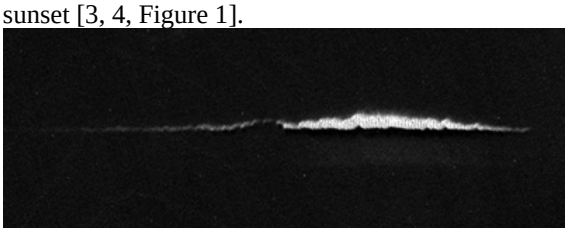

Figure 1: Observation of the Western horizon by the Surveyor 7 spacecraft shortly after sunset showing horizon glow. The glow is sunlight scattered by dust particles launched off the lunar surface by electrostatic forces.

The Lunar Ejecta and Meteorites Experiment (LEAM) detected increased signals near sunset and sunrise that have been interpreted as lunar dust particles moving over the surface [1, 2]. An analysis of the geometry of these images and the calculated levitation heights and trajectories for charged dust suggest that these observed dust particles are tens to hundreds of meters above the lunar surface. While they may be levitating or partially suspended, this may not be required to explain the observations of lunar horizon glow and the impacts detected by LEAM.

The NEAR-Shoemaker spacecraft observed smooth flat deposits, called ponds, in the floors of medium-sized craters. Observations are consistent with these deposits consisting of dust particles though they cannot rule out cm-sized particles. These ponds are in topographic lows that are therefore also regions of changing illumination and shadowing over the course of an Eros day. In addition, regolith (possibly dusty) aprons were observed adjacent to some large boulders and ejecta blocks on the surface of the asteroid.

Simulations: We simulate the trajectories of charged dust particles lifted off a dusty regolith, including gravitational and electrostatic forces as well as time-dependent charging of the grains. These simulations show a tendency for dust to accumulate in shadowed regions, suggesting that this charged dust transport may play a role in the dust deposits seen in craters and adjacent to large boulders on Eros. Particles in some conditions may be stably levitated over the surface with the electric force balancing gravity. We find that the typical stable levitation heights are much higher than previously assumed for most particles small enough to be levitated (Figure 2). Dust responsible for the lunar horizon glow (Figure 1) may be tens or hundreds of meters above the surface, rather than hovering at the Debye scale height of ~ 1 m above the surface.

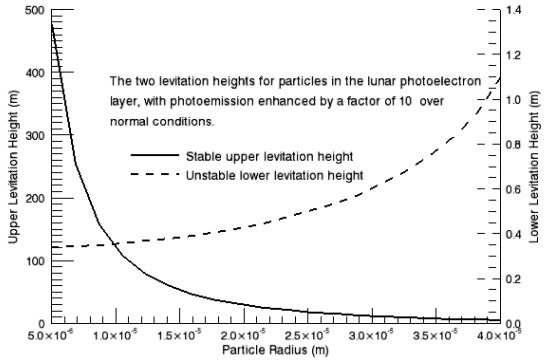

Figure 2: Calculated levitation heights for charged dust in the lunar photoelectron layer. The stable levitation height (solid line) is tens of meters for all particles except those close to the largest particle that can be suspended by the electric field.

On Eros we find levitation possible for particles smaller than 1 μm at heights of tens to hundreds of meters. Whether particles levitate or not, there is a net transport of dust into shadowed regions where there is no surface photoemission and therefore no vertical electric field to counter gravity. The

timescale for dust transport on Eros through this mechanism is short enough to explain the Eros crater dust deposits, though the simulations do not reproduce the smooth distribution of dust in detail. Other processes such as impact-induced seismic shaking likely also play an important role.

Experiments: We have performed experiments on levitation and transport of charged dust in a plasma sheath as well as charging of dust in a photoelectron sheath. In experiments where a small region of dust on a surface is exposed to a plasma, non-conducting dust particles, such as lunar and Martian regolith simulants, spread horizontally when placed on a conducting surface. This spreading is due to the dust particles charging to a potential that is significantly different from that of the conducting surface. This generates an electric field with a horizontal component that transports the dust away from the initial pile. Conducting dust on a conducting surface, on the other hand, remains at the same potential as the surface and no transport is observed. Experiments where the dust is placed on a sloped surface produce the expected transport of dust down the gradient in gravitational potential energy.

Summary: Observational evidence from several surfaces in the solar system points to charged dust particles lifting off the surface. Electrostatic effects can facilitate the transport of dust down gravity gradients and into regions of different electrical properties, such as different surface materials or shadowed regions. Terminator crossings are associated with increased dust activity on the lunar surface, but dust observed above the lunar horizon travels to much higher altitudes than previously estimated.

References: [1] Berg, O. E., E. F. Richardson, J. W. Rhee, and S. Auer (1974) *GRL, 1*, 289-290. [2] Berg, O. E., H. Wolf, and J. Rhee (1976) *Interplanetary Dust and Zodiacal Light* (Springer-Verlag), 233-237. [3] Rennilson, J. J., and D. R. Criswell (1974) *Moon, 10*, 121-142. [4] McCoy, J. E., and D. R. Criswell (1973), *LPSC, 5*, 496-497. [5] Zook, H. A., and J. E. McCoy (1991), *GRL, 18*, 2117-2120. [6] Zook, H. A., A. E. Potter, and B. L. Cooper (1995), *LPSC, 26*, 1577-1578. [7] Goertz, C. K. (1989) *Rev. Geophys., 27*, 271-292.. [8] Nitter, T., O. Havnes, and F. Melandsø (1998) *JGR, 103*, 6605-6620. [9] Colwell, J. E., A. A. S. Gulbis, M. Horányi, S. Robertson (2005), *Icarus, 175*, 159-169.

A SEARCH FOR METEOR SHOWER SIGNATURES IN THE LDEF IDE DATA. W. J. Cooke[1] and H. A. McNamara[2], [1]Meteoroid Environment Office, Mail Code EV13, Marshall Space Flight Center, AL 35812 USA, william.j.cooke@nasa.gov, [2]Meteoroid Environment Office, Mail Code EV13, Marshall Space Flight Center, AL 35812 USA, heather.a.mcnamara@nasa.gov

Introduction: For 346 days after the deployment of the LDEF satellite on April 7, 1984, the tape recorder belonging to the Interplanetary Dust Experiment (IDE) stored information on over 15,000 impacts made by submicron and larger-size particles on its metal oxide silicon (MOS) detectors . These detectors were mounted on trays facing in six orthogonal directions - LDEF ram and trailing edge, the poles of the LDEF orbit (north and south), and radially inward (towards the Earth) and outward (towards space). The 13.1 second time resolution provided by the IDE electronics, combined with the high sensitivity of the MOS detectors and large collecting area (~ 1 sq. m) of the experiment, conclusively showed that the small particle environment at the LDEF altitude of 480 km was highly time-variable, with particle fluxes spanning over four orders of magnitude.

A large number of the 15,000 impacts recorded by IDE occurred in groups, which were of two types - the *spikes*, single, isolated events of high intensity and the *multiple orbit event sequences* (MOES), which were series of events separated in time by integer multiples of the LDEF orbital period. Even though the spikes were generally more intense, the MOES could be quite long-lived, some lasting for many days.

A previous paper by Cooke et al. [1] attributed the MOES to impacts by man-made debris particles in orbits intersecting that of LDEF. The 20 day longevity of one of these events – termed the *May Swarm* – led to the suggestion that the debris particles must be constantly replenished by their source, as the orbits of micron sized particles will rapidly decay under the influence of radiation pressure and other non-gravitational forces, entering Earth's atmosphere after only a few revolutions.

However, the date of onset of the May Swarm (May 22) and the long duration of this event may indicate a possible correlation with the annual Arietid meteor shower, which peaks around June 8. As this seemed to hold the promise of a less "artificial" explanation than a satellite or rocket body continuously "dribbling" debris , it was decided to take a fresh look at parts of the IDE data set in an attempt to detect meteor showers within the impact record.

Analysis: Three major annual showers – the daytime Arietids, the Perseids, and the Geminids were chosen for the initial search. A subset of the data, the impact record for the IDE space facing tray was extracted, as this set of detectors should sample the meteorid environment with little contamination from orbital debris. The number of impacts on the tray facing radially down, towards Earth, was too small to be useful, as it was shielded by the Earth.

There was no shower signature detected for the Geminids; no impacts on the space tray occurred while it was exposed to the shower radiant. However, the Perseids showed a remarkably strong signature – 18 impacts on the 1 μm detectors occurred over the shower duration while the tray was exposed to the radiant, with only one occurring when it was not. Figure 1 shows the impact record, binned in 1 day intervals, for the 1 μm space-facing detectors from July 17 to August 24; Note the concentration of impacts about day 225 – August 11, near the time of the traditional Perseid peak.

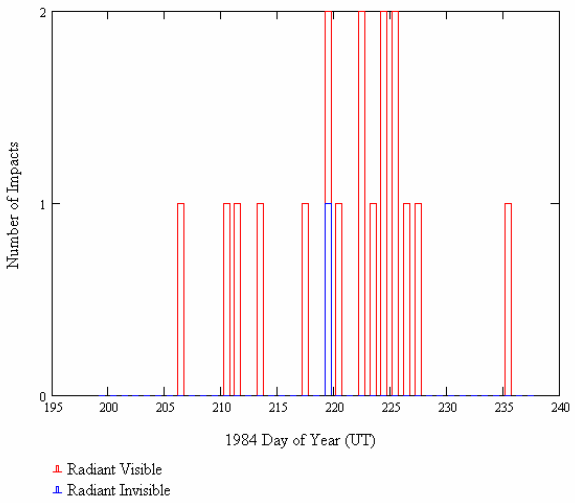

Figure 1. Impacts on IDE space facing 1 μm detectors from July 17 to August 24, 1984.

There is also a strong impact signature during the daytime Arietids (May 22 – July 8). However, the fact that this radiant is close to the Sun, being imbedded in the sporadic Helion source, and also the high likelihood that IDE observed significant numbers of β meteroids [2], make it difficult, if not impossible, to attribute any of these impacts to the Arietids with confidence.

Searches for other showers (Eta Aquarids and Orionids) were also conducted. The results of these, and

more details of the analyses will be presented, along with an examination of the possible causes for the "May Swarm."

References:

[1] Cooke W. J. et al. (1995) *LDEF 3rd Post-Retrieval Symposium*, 361-371.

[2] Cooke W. J. et al. *Advances in Space Research, 13*, 119-122.

CONTINUOUS LARGE-AREA MICROMETEOROID FLUX MEASURING INSTRUMENT. R. Corsaro[1], J.-C. Liou[2], F. Giovane[1], and P. Tsou[3], ([1]Naval Research Laboratory, Washington D. C. 20375, Corsaro@NRL.Navy.mil, [2]ESCG/ERC at NASA JSC, [3]NASA Jet Propulsion Laboratory).

Introduction: An instrument capable of continuously measuring the flux of micrometeoroids is described in this paper. The instrument can be utilized in interplanetary space or on planetary or satellite surfaces for future solar system exploration missions.

Heritage: Funded by NASA Planetary Instrument Definition and Development (PIDD) Program, an instrument was developed combining a conventional aerogel particle collector with a new acoustic system for detecting the time of each particle's arrival. This latter system, called PINDROP (Particle Impact Noise Detection and Ranging On autonomous Platforms) uses piezoelectric strain sensors to detect the time and location of each particle impact [1]. In addition, the signal rise time and the waveform of the signal can be used to estimate the impact speed. Knowing the time and speed of impact, combined with direction information from the particle track in the aerogel (measured on retrieval), permits a possible determination of the orbit of the impactor. A dynamical link from the collected sample to its parent object may be established. This highly successful instrument development effort has led to a 10 square meter system currently under development called LAD-C (Large Area Debris Collector), which is scheduled for deployment on the ISS in 2007 [2].

The PINDROP acoustic detection system component can also be used without aerogel in cases where retrieval is not practical. On man-made structures, the sensors can be applied directly to hard surfaces as well as thin fabric to form a large sensing array. This has been demonstrated in laboratory tests on various materials including, for example, the outer layer of a conventional thermal blanket. Using telemetry, the instrument then can continuously monitor particle impact flux, as well as platform noise for diagnostic purposes.

The previous systems have many applications, particularly on near-Earth satellites and platforms. However they have some limitations for interplanetary applications. In particular, when used to monitor infrequent large particles, the large arrays required will involve using a very large number of sensors. Additionally the sensors have temperature limitations that make them unsuitable in very warm environments.

New Capability: A variation on this instrument has been proposed for a large-area solar sail deployment. It consists of thin sail-like polymer film supported by a frame containing associated surface motion detectors. Micro-particles impacting the film generate surface vibrations that can be detected by displacement sensors located near the supports.

The impacting particle generates surface motion in the film predominately at the normal modes of the structure. As such, it behaves much like a drum. This has two benefits: the motions induced are relatively large due to the modal response of the surface, and only a few sensors are required to monitor this motion. Because of the relatively low frequency of these responses, the entire surface can be monitored with relatively few sensors.

Status: The optimum sensor type to detect film vibrations caused by particle impacts has been determined to be a surface-normal fiber optic displacement sensor. Sensors of this type developed for other applications at NRL have very high sensitivity to displacement (nominally 1 Angstrom), operate over a wide range of temperatures (to 1000°C) and are relatively insensitive to radiation.

The feasibility of this system was demonstrated using a hypervelocity impact range at NASA JSC [3]. A fiber optic displacement sensor was attached to the frame supporting a test section of a film (intended for a solar sail), and the motion of the film was monitored during an impact with a hypervelocity particle. The strong vibrations induced in the film following impact were easily detected by this sensor.

Applications: Potential applications for this instrument include (1) characterization of particle environment near and on the surfaces of the Moon, Mars, and other planets or satellites and (2) monitoring impacts on large-scale structures for future exploration missions. For example, the condition of a sail-like film can be continuously monitored since the modal frequencies depend on tension. Hence the device is a low-cost low-mass addition to any sail-like structure, such as the proposed Solar Sail platform.

References:

[1] New Scientist, (28 Aug 2004, page 20) (staff writer) [2] R. Corsaro, F. Giovane, P. Tsou, J.-C. Liou, D., Buzasi, B. Gustafson, (2004) *Orbital Debris Quarterly News* Vol. 8, Issue 3, 3-4. [3] J.-C. Liou, E. Christiansen, R. Corsaro, F. Giovane, and E. Stansbery (2005) *Orbital Debris Quarterly News*, Vol. 9, Issue 1, 6-7..

UPGRADE OF METEOROID MODEL TO PREDICT FLUXES ON SPACECRAFT IN THE SOLAR SYSTEM AND NEAR EARTH. V. Dikarev[1,2], E. Grűn[1,3], W. J. Baggaley[4], D. P. Galligan[4,5], R. Jehn[6], M. Landgraf[6], [1]Max-Planck-Institut fűr Kernphysik, Heidelberg, Germany, [2]Astronomical Institute of St. Petersburg University, Russia, [3]Hawaii Institute of Geophysics and Planetology, University of Hawaii, USA, [4]University of Canterbury at Christchurch, New Zealand, [5]Currently at Defence Technology Agency, Devenport, New Zealand, [6]ESA/ESOC, Darmstadt, Germany.

We present some aspects of the new interplanetary meteoroid model developed to predict fluxes on spacecraft in the Solar system and near Earth. The model is distinguished from the previous work due to the new data incorporated, new design of the meteoroid populations whose orbital distributions are now constructed using approximate theories of the orbital evolution, and an outstanding quality of fit to observations. With the new experience from modeling the interplanetary dust cloud on the large scale, we come up with some recommendations for the future development of scientific and engineering models of meteoroid environment.

CALORIMETRIC AEROGEL PERFORMANCE AT INTERSTELLAR DUST VELOCITIES. G. D. Dominguez[1], A. J. Westphal[1], S. M. Jones[2], M. L. F. Phillips[3] and M. Schrier[3], [1]Space Sciences Laboratory, U. C. Berkeley, Berkeley, CA 94720-7450, [2]Jet Propulsion Laboratory, Pasadena, CA 91109, [3]Pleasanton Ridge Research Corporation, 27468 Hayward Blvd, Hayward, CA 94542

Introduction: No contemporary interstellar dust particles have ever been identified and analyzed in the laboratory. The Stardust mission will return a few dozen small (~1 micron) interstellar dust grains in January 2006. Identification of these grains will be a major challenge, and is the focus of the Stardust@home project [1]. Analytical techniques available to study such small grains exist but are limited.

A large collecting power, of order several m^2-years, is required to collect large (several micron) interstellar dust grains[2]. Such a large array can probably be deployed most easily in low-earth orbit (LEO), but the ubiquitous orbital debris in LEO would present an huge background that would probably preclude the identification of IS dust using ordinary silicate aerogels.

We have recently developed a robust, monolithic, fluorescent "calorimetric" aerogel. The aerogel is silica doped with Gd and Tb, and is ordinarily not fluorescent. When heated the aerogel undergoes a permanent phase transformation to a brightly fluorescent phase. This phase transformation occurs even with the very brief thermal pulse associated with the capture of a hypervelocity particle. We have previously demonstrated that the integrated fluorescence intensity (S) is a function of the kinetic energy of the captured hypervelocity particle[2]. Such an aerogel could be used to collect orbital debris and extraterrestrial hypervelocity dust grains in low-earth orbit, and simultaneously passively record the kinetic energy of each hypervelocity impact. Since it is passive and requires no power or telemetry, an instrument composed of calorimetric aerogel would be intrinsically low-risk. It is also extremely simple --- all of the sophistication of the instrument is in the post-recovery terrestrial laboratory. Such a collector could also be used to capture and identify for the first time thousands of contemporary interstellar dust grains in LEO, and, depending on the collecting power, many large IS dust grains.

Calibration: Until recently, all of the calibrations of this calorimetric aerogel have been done at relatively low velocities (<6 km sec^{-1}) and with glass beads (ρ=2500 kg m^{-3}). Here we report measurements of the detector response at much larger velocities, characteristic of the speeds of the interstellar dust that is continuously streaming into the Solar System from the local interstellar medium. The detector was exposed to 10-12 and 18-22 km sec^{-1} latex spheres (r~0.375 and 0.8 μm) using the 2 MV Van-de-Graaff accelerator in Heidelberg. We subsequently examined the calorimetric aerogel using a standard UV microscope at the Biological Imaging Facilities in Berkeley and found that there were fluorescent impact features in the exposed aerogel samples (Fig. 1). These fluorescent impact craters were then imaged and the integrated fluorescence signal was determined using techniques similar to those used in [2]. The dispersion in the signal for these particles corresponds to a velocity resolution of ~20%, similar to that of previous calibrations.

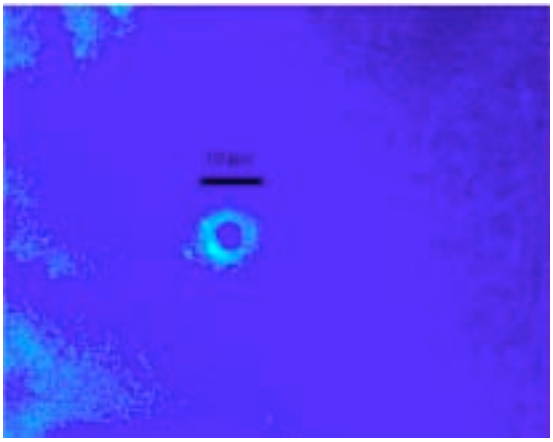

Figure 1. Fluorescence image of latex sphere (r=0.375 - 0.8 microns) with impact velocity equal to 10-12 km/s. This image was taken at 20x magnification. The contrast has been enhanced for clarity.

We have previously found that the response of this calorimetric aerogel can be described by a function of the form $S=Ar^a v^b$ with a=2.16 and b=1.8 [3]. These values imply that the calorimetric aerogel responds to the kinetic energy loss of the projectile near the surface of the aerogel. The results of our experiments with latex spheres with v> 10 km sec^{-1} suggest that the response of the calorimetric aerogel is fundamentally different at higher velocities. This is evident in Fig. 2 where the response of our shots at Heidelberg is compared to the response of the lower velocity shots (v<6 km sec^{-1}). To directly compare

the two data sets, a correction factor was applied to the Heidelberg data to account for differences in magnification and lamp intensity between the two data sets. That the response is significantly higher than a naïve extrapolation from lower velocities predicts, suggests that the size threshold for interstellar particles could be quite small.

The Heidelberg data show that the response of calorimetric aerogel continues to increase as a function of velocity. Because the size of latex spheres at higher velocities (18-22 km sec $^{-1}$) was smaller (r~0.3 μm) than those at 10-12 km sec $^{-1}$ (r~0.8 μm), this effect is even more dramatic than it appears in Fig. 2. Future work with latex spheres velocities will be needed in order to determine the detailed response function of this calorimetric aerogel to hypervelocity dust with v>10 km km sec $^{-1}$.

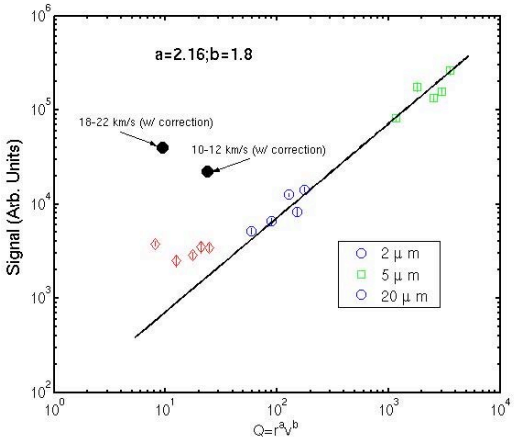

Figure 2. Combined response function of calorimetric aerogel to both glass and latex spheres (black dots).

References: [1] Westphal, A. J. et al. (2005) *LPS XXXVI*, Abstract #1908. [2] Dominguez, G., Westphal, A. J., Phillips, M. L. F., and Jones, S. M., (2003) Astrophys. J. 592, 631. [3] Dominguez, G. D. et al. (2005) in press; Dominguez, G. D., PhD Thesis, U. C. Berkeley (2005).

Additional Information: This work was supported by the NASA PIDDP program. We are grateful to Ralf Srama and Anna Mocker-Ahlreep for their generous support at Heidelberg.

SIZE-FREQUENCY DISTRIBUTIONS OF DUST-SIZE DEBRIS FROM THE IMPACT DISRUPTION OF CHONDRITIC METEORITES. D. D. Durda[1], G. J. Flynn[2], L. E. Sandel[3], and M. M. Strait[3]. [1]Southwest Research Institute, 1050 Walnut Street Suite 400 Boulder CO 80302 durda@boulder.swri.edu, [2] SUNY-Plattsburgh Plattsburgh NY 12901, [3]Alma College Alma MI 48801.

Introduction: In order to understand the collisional evolution of asteroids and interplanetary dust and to accurately model the infrared signature of small particles in our own Solar System and in other young planetary systems, we must address the fundamental problem of better understanding dust production from primary impact disruption events covering a wide range of sizes. At present, however, we understand well the size frequency distributions (SFDs) for collision fragments within only a couple orders of magnitude of the size scale of the original target body; for impact disruption events at all size scales we still know next to nothing (and in many cases identically nothing) about the primary production of fragments many orders of magnitude smaller than the original target body size. Thus, existing modeling results in these areas have tremendous uncertainties.

Laboratory-scale impact experiments can provide direct know edge of the SFDs of dust-size debris produced directly from the impact disruption of ~5-cm scale meteorite targets, roughly the size scale of the immediate parent bodies of zodiacal dust particles. Here, we report results of a set of impact disruption experiments involving chondritic meteorite samples, conducted at the NASA Ames Vertical Gun Range (AVGR). Preliminary results from these experiments were reported previously in [1].

Impact Experiments: Chondrite meteorites were impacted by small aluminum projectiles at speeds of about 5 km/s in order to examine the production of dust particles and the mechanics of fracture of real meteoritic materials under the impact regimes that presently exist in the main asteroid belt. The ~5 cm-scale targets were each suspended at the center of the AVGR impact chamber and surrounded with four passive dust 'detectors' consisting of thin aluminum foils (~7- and 13-μm thick, mounted in 35mm slide mounts, and 51-μm thick, taped across larger cutouts in the detector foam core backing) and rectangular blocks of aerogel (with dimensions of ~2×2×3 cm). Figure 1 shows one of the detectors in detail and in place in the impact chamber near one of the meteorite targets. The foils were thin enough that high-speed particles would penetrate, providing a size distribution of ejecta; particles captured intact in the aerogel were analyzed *in situ* for chemical composition [2,3]. Large fragments were collected from the chamber and weighed. The impacts were recorded by 500 fps video.

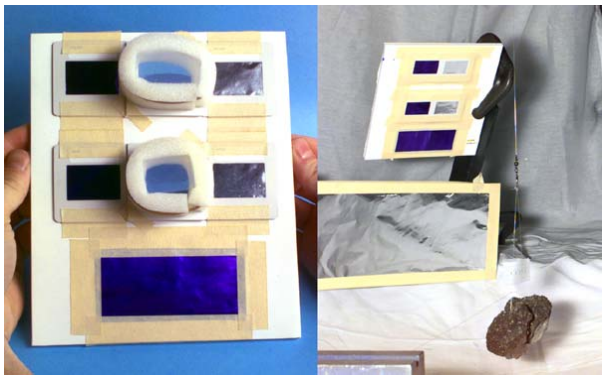

Figure 1. Passive particle detectors used in AVGR impact experiments to capture and measure the properties of dust-size debris. (Left) Detail showing the arrangement of foils and aerogel in a typical detector layout. ~7-, 13-, and 51-μm thick foils are set along the top, middle, and bottom rows, respectively, with blocks of aerogel set in foam holders between the foils. (Right) typical deployment of a detector near a meteorite target within the AVGR impact chamber.

Foil Hole Data: The foil hole sizes were measured via two independent methods. To cover the entire area of a particular foil (equal to the window size of a standard 35mm slide mount), the foil was scanned with Nikon slide scanners at 2700 dpi and at 4000 dpi. The resulting 3894×2592 pixel and 4000×5888 pixel images have a resolution of ~9.4 and ~6.3 μm/pixel, respectively. Figure 2 shows an example of one of the slide scanner foil images. Smaller, sample areas of some foils were surveyed with a microscope/video setup at a resolution of ~1.6 μm/pixel. The hole size distributions from the resulting scanner and microscope images were determined by analysis with the software package ImageJ from NIH.

Preliminary Results: Analysis of the foil image data is still underway. Results presented in [1], however, are illustrative of the more complete data sets that will be used to extend the SFDs of the fragments from the disruption of the meteorite samples down to dust-size particles.

As an example, Fig. 3 shows the size distribution of holes from the 7-μm thick foil from detector 3 of shot 011015 (the target for this shot was a 248.0 g sample of NWA620, an unclassified ordinary chondrite; the projectile was a ¼-in aluminum sphere impacting at 5.59 km/s), which was mounted 48 cm from

the target, roughly 240° in azimuth from the direction of the incoming projectile. The holes appear to represent comparatively low-speed ejecta and tend to lie at the bottom of stretched impact depressions in the foil (holes observed in other foils from other shots clearly resulted from high-speed particles, being cleanly punched and displaying surrounding, raised rims). The scanner image for this foil was tightly focused and the distributions measured from the scanner and microscope data are very similar.

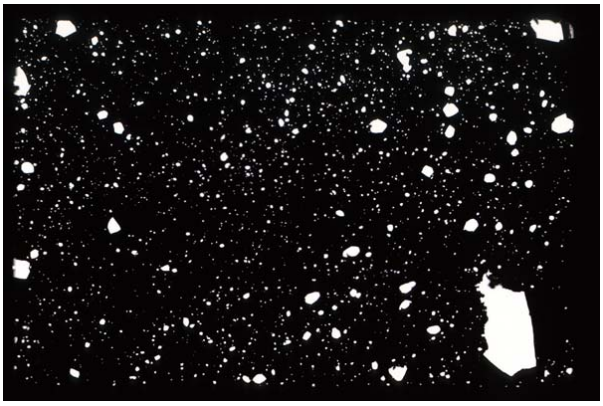

Figure 2. Slide scanner image of a 7-μm thick foil from detector 3 of shot 011015. The image resolution is 2700 dpi.

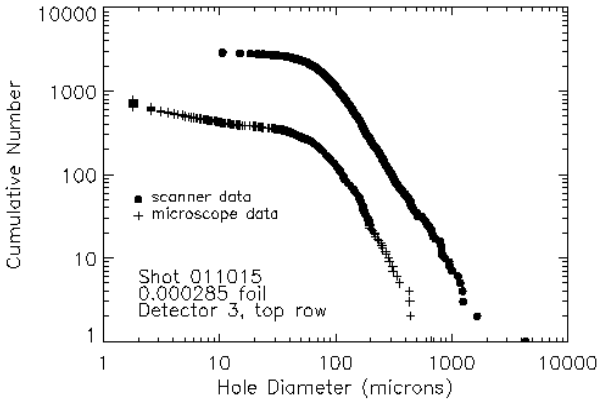

Figure 3. Size distribution of 'low-speed' holes from a 7-μm thick foil from detector 3 foil of shot 011015.

Similar data from the other foils from this and the other shots will be combined to extend the mass frequency distributions of mm- to cm-scale fragments down to dust-size particles. The foil/aerogel detectors were arranged to provide a broad sampling of the dust flux through area surrounding the meteorite targets; when properly normalized to the full 4π steradians surrounding the targets, the dust SFDs will provide very useful knowledge of the primary fragment SFDs to much smaller sizes than is conventionally measured in laboratory impact experiments.

References: [1] Durda D. D., Flynn G. J., Hart S. D., and Asphaug E. (2002) *LPS, XXXII*, abstract #1535. [2] Flynn G. J and Durda D. D. (2004) *Planet. Space Sci.*, **52**, 1129-1140. [3] Flynn G. J. et al. (1996) *LPS, XXVII*, 369.

NEW DUST DATA FROM STARDUST AND CASSINI MISSIONS OBTAINED BY DFMI AND HRD INSTRUMENTS. T. E. Economou, A.J. Tuzzolino, Laboratory for Astrophysics and Space Research, University of Chicago, Chicago, IL.60637.

Introduction: On January 3, 2004 the STARDUST spacecraft encounterd 81P/Wild-2 comet, performed in-situ investigation on the comet and collected cometary dust particles to bring back to Earth. On July 4, 2004 the Cassini spacecraft entered into Saturn orbit and started a multiyear study of Saturn, its satellites and its rings. The Dust Flux Monitor Instrument (DFMI) on the STARDUST mission and the High Rate Detector (HRD) on the Cassini mission, both from the University of Chicago, returned important information about the dust particle mass distribution and dust fluxes from 81P/Wild-2 comet and during multiple Saturn ring crossings.

DFMI Dust Results from 81P/Wild-2 Comet: The DFMI instrument which is based on two different technologies, has two PVDF sensors, each one with four different mass thresholds, and two acoustic counters, each one with two mass thresholds. From the data on the 12 mass thresholds, we were able to determine the cometary dust particle mass distribution in the mass regime from 10^{-14} to 10^{-6} kg [1]. The dust fux was determined throughout the flyby of the comet 81P/Wild-2 and found to be very non-uniform. The DFMI has encountered several regions of intense swarms of particles or dust clouds only a few hundred meters across. Figure 1 shows the fine time scale of dust particles distribution of one of such jet streams.

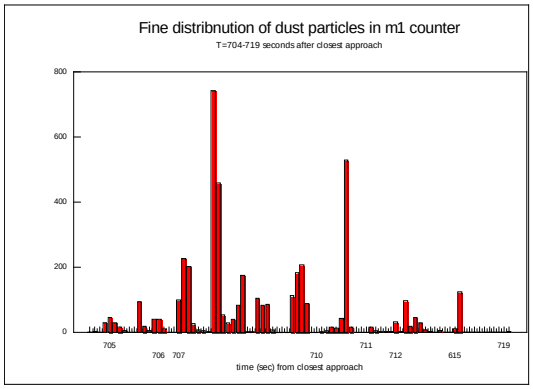

Fig. 1 showing the fine time distribution of dust particles as measured by m1 PVDF counter of the DFMI instrument during the flyby of 81P/Wild-2 comet.

The spikelike distribution of dust particle impacts was unexpected and different from previous experience. It was concluded that jets emanating from isolated emission centers on the nucleus is the primary source of the cometary activity. The characteristics of the coma structure can be easily explained by fragmentation of the fragile material coming out from the nucleus when it is subjected to several forces acting upon it [2]. Although several characteristics of the 81P/wild-2 coma differ from other comet observations and different coma models, by modifying various parameters in models, the DFMI data could be interpreted by such models [3].

HRD Dust Results from the Saturn Rings Crossings: The HRD is part of the CDA instrument on the Cassini mission and its overall objective is to obtain quantitative measurements of particle flux and mass distribution throughout the Saturn ring system, when the counting rate was expected to be very high to saturate the Dust Analyzer of the CDA instrument. The particle mass range covered by the HRD ranges from 10^{-12} to about 10^{-7} g for differential and cumulative flux measurements and $>10^{-7}$ g for cumulative flux measurements. The HRD is capable of handling counting rates up to 10^4 impacts per second with very little dead time. The time resolution of the HRD is programmable and ranges from 1 s down to 0.1 s in the encounter mode.

Although the HRD was ON during most of the time since launch, it has seen very little activity during the entire cruise period. There are no dust data during theSaturn Orbit Insersion (SOI) because the CDA power was OFF during that period. However, the HRD has seen increase dust activity every time there was an E-ring crossing.

Especially significant activity was so far observed during the encounters with Encelladus satellite on days 2005_048 and 2005_068. Figure 2 is showing the cumulative and differential spectra during the 2005_048 crossing for M1 and m1 counters and Figure 2 is showing similar activity for the M2 and m2 counters. It is worthy to notice that the frequency of the mpacts on all counters is not uniform and shows discontinuity. From Figure 4 it can be seen that the lighter particles on m1 preceed the heavier particles on M2 at the beginning of the encounter and lag in time at the end of the encounter. That would indicate the the heavier par-

ticles are concentrated in a less space volume within the dust torus. Enceloadus seems to be one the dust particles sources for the E ring.

References:

[1] A. J. Tuzzolino, T. E. Economou, B. C. Clark, P. Tsou, D.E. Brownlee, S. F. Green, J.A.M. McDonnell, N. McBride, M. T.S.H. Colwell, Dust Measurements in the Coma of the Comet 81P/Wild 2 by the Dust Flux Monitor Instrument, SCIENCE VOL. 304 18 June 2004, pp 1776-1780.

[2] B. C. Clark, S. F. Green , T. E. Economou, S. A. Sandford, M. E. Zolensky, N. McBride, D. E. Brownlee, Release and Fragmentation of aggregates to produce heterogeneous, lumpy coma streams, J. Geoph. Res. Vol.109, E12S03, doi:10.1029/ 2004JE002319, 2004.

[3] Z. Sekanina, D. E. Brownlee, T. E. Economou, A. Tuzzolino, S. F. Green, Modeling the Nucleus and Jeets of Comet 81P/Wild 2 Based on the Stardust Encounter Data, VOL. 304 18 June 2004, pp 1769-1774.

[4] R. Srama, et al., The Cassini Cosmic Dust Analyzer, Space Science Reviews **114**, 465-518, 2004.

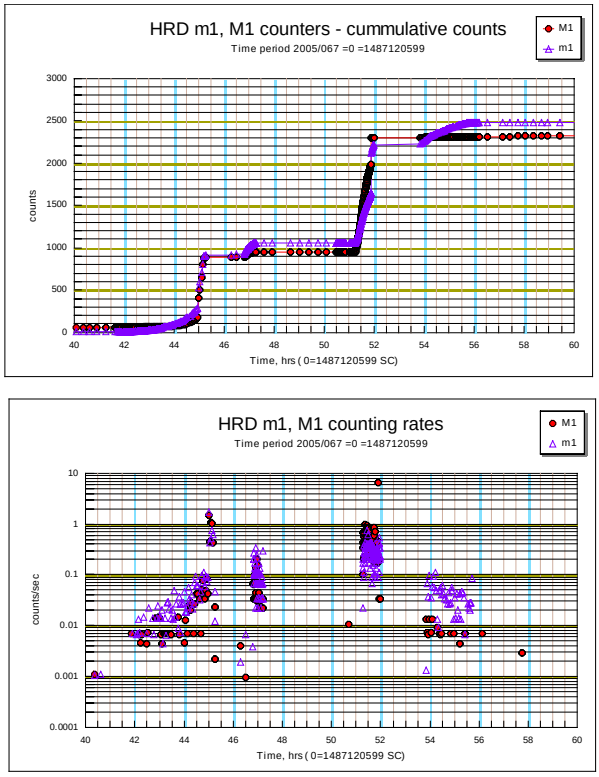

Fig.2 HRD data taken with M1 and m1 counters during Enceladus encounter on day 2005_048. On top the cumulative counts are showing, on bottom, the corresponding differential rates.

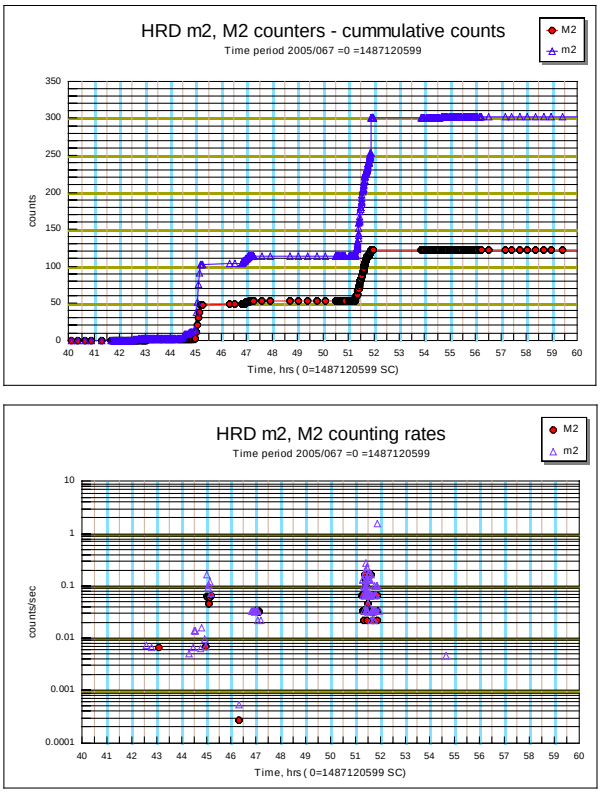

Fig.3 HRD data taken with M2 and m2 counters during Enceladus encounter on day 2005_048. On top the cumulative counts are showing, on bottom, the corresponding differential rates.

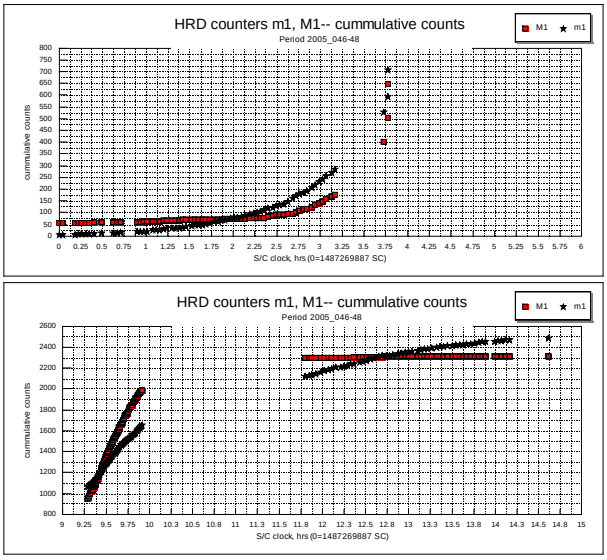

Fig.4 HRD data taken with M1 and m1 counters during Enceladus encounter on day 2005_048. On top the cumulative counts at the start of the encounter are showing, while on bottom, the corresponding cumulative counts at the end of the encounter are shown.

COMBINED MICRO-IR AND MICRO-RAMAN MEASUREMENTS ON STRATOSPHERIC IDPs. G. Ferrini[1], G. A. Baratta[2], A. Rotundi[3], M. E. Palumbo[2], L. Colangeli[1], E. Palomba[4], [1]INAF-Osservatorio Astronomico di Capodimonte, Via Moiariello, 16 - Napoli (Italy), gferrini@na.astro.it, [2]INAF-Osservatorio Astrofisico di Catania, Via Santa Sofia 78, 95123 Catania (Italy), [3]Università Parthenope, Via A. De Gasperi, 5 -Napoli (Italy), [4]INAF-Istituto di Fisica dello Spazio Interplanetario, Via del Fosso del Cavaliere 100, 00133 Roma (Italy) .

Introduction: Interplanetary Dust Particles (IDPs) provide a unique opportunity to study extraterrestrial materials in laboratory. IDPs are known to have high carbon content: 1-47 wt%, on average 2-3 times higher than that found in carbonaceous chondrites [1]. TEM studies have identified amorphous, turbostratic and poorly graphitised carbons in IDPs [2,3], other studies found organic carbons [Flynn et al, 2004, GCA. An apparent correlation between vescicular carbon and magnetite rims suggests volatiles loss during atmospheric entry flash heating [4]. The property of the carbonaceous unit in IDPs remain poorly defined [5]. Raman studies have shown that many IDPs exhibit the characteristic amorphous carbon feature. Different degrees of order could be indicative of different irradiation doses by solar wind particles and fast solar protons, suffered by IDPs in the interplanetary medium before collection in the Earth stratosphere [6].

In preparation to the STARDUST sample analyses, we performed combined micro-IR / micro-Raman measurements, supported by a FESEM investigation, on five stratospheric IDPs. We provide the IR spectral characterization of these IDPs and some new insight on the evolution of the amorphous carbon phase in IDPs The specific aim was to investigate on the potentiality of the synergry between these techniques in the identification of mineral phases other than silicates (e.g. oxides).

Experimental: Five stratospheric IDPs (L2021C13, -C20, -D9, -D12, -F17) were allocated to our laboratory by the NASA-JSC Astromaterials Curation Center (ACC). All analyses we performed on bulk grains placed on Special Sample Holders (SSHs) were non destructive [7]. We especially designed these SSHs because IDPs directly placed on them at the NASA ACC could be shipped to our laboratory where without sample manipulation the IDPs could be used for micro-IR, micro Raman and FESEM analyses

Micro-IR analyse. Micro-IR spectra have been acquired in the range 4000-600 cm^{-1} at a spectral resolution of 4 cm^{-1}, with an infrared microscope attached to a FTIR interferometer (Mod. Bruker-Equinox 55). For each particle we acquired six spectra of 6000 scans, in order to optimize the S/N ratio. The average of the six spectra was considered.

Micro-Raman analyses.. Raman microscopy was performed with a confocal microscope (by DILOR) adapted on a triplemate spectrometer (by SPEX) with a CCD detector. The objectives used gives a laser spot size on the sample of 2 µm. The laser power (Ar^+, 514.5 nm) on the sample was kept below 2 mW. No laser-induced thermal modification was detected for the IDPs studied in this work.

Results and Discussion: Micro-IR spectra of IDPs are shown in Fig. 1. The spectral classes have been assessed for IDPs -D9 and -D12 (Tab. 1). Infrared spectra of the other particles do not fall into any of the major IR spectral classes of IDPs. The results for these IDPs show the presence of oxides and sulphides in the grain mineralogy consistent with the NASA-JSC preliminary chemical EDS analyses. For particles -C13 and -F17 the IR features at about 800 cm^{-1} suggest the presence of iron oxides. The -C20 particle will require additional IR analyses to confirm the presence of iron sulphide.

L2021 -	Texture	Size (µm)	IR-class	Raman
D9	aggregate very porous	12	Ol+Py	Maghemite[1] (+Hematite[2])
D12	aggregate very porous	10x8	LLS	α-Carbon
C13	aggregate low porosity	12x10	FeO	α-Carbon (+Maghemite)
C20	spherical compact	14	FeO - FeS	Magnetite[3]
F17	cluster compact	10	FeO	Maghemite (+ Magnetite)

Table 1: IR-class* (Ol = Olivine, Py = Pyroxene, LLS = Layer Lattice Silicates) and other mineral phases (FeO = Fe-oxide-rich; FeS = Fe-sulfide-rich); Raman spectroscopy (mineral phases, (1)= γ-Fe_2O_3 [maghémite] (2)= α-Fe_2O_3, [hematite](3) = Fe_3O_4[magnetite]. *The IDP IR classification is from [8].

IDPs Raman spectra are displayed in Fig. 2. Only two of the considered IDPs (-C13, -D12) exhibit the D (Disorder) and G (graphitic) band typical of amorphous carbon (α-carbon) with intermediate degree of order. All the other IDPs exhibit the Raman

signatures typical of different forms of iron oxides (Fe_2O_3 and Fe_3O_4).

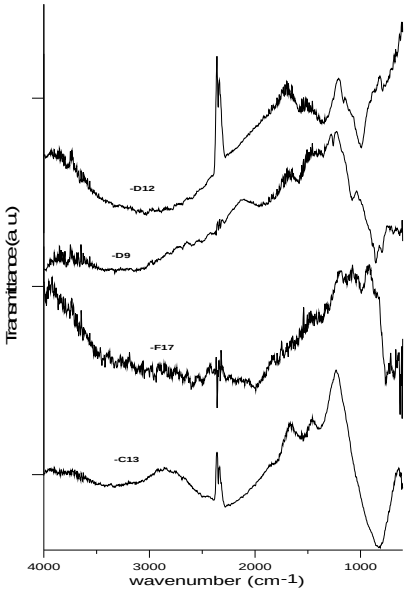

Figure 1: Micro-IR Spectra.

The Raman measurements confirm the results of micro-IR analyses and support the preliminary hypothesis on the –C20 IR characterization. The Raman bands peaking at 350, 503 and around 700 cm^{-1} typical of maghémite (γ-Fe_2O_3) [9] are present in -F17. Also the broad and poor resolved feature near 1420 cm^{-1} can be attributed to maghémite [9,10]. Maghémite signatures are visible also in the -D9 spectrum in which the additional weak bands at 224 and 292 cm^{-1} are characteristic of hematite (α-Fe_2O_3). The main bands of magnetite (Fe_3O_4) falling at 667, 545 and 305 cm^{-1} [9] are evident in the -C20 spectra. Magnetite features are also present in -F17 as indicated by its most prominent band at 667 cm^{-1}. The presence of maghémite and magnetite could indicate a severe flash heating of the particles during atmospheric entry. The formation of magnetite nanocrystals on Mg,Fe-silicate grains and magnetite or maghémite rims are due to pyrometamorphism [5, 11].

Amorphous carbon: Raman spectroscopy is a powerful tool of investigation for the study of the structure of the carbonaceous phases in IDPs [12]. Sensitive parameters are peak position, width (FWHM, Full Width at Half Maximum) and relative intensity of G and D bands. The spread in the degree of order disorder observed by Raman spectroscopy in IDPs, could be indicative of a different residence time (dose suffered) in the interplanetary medium before collection in the Earth's atmosphere [6]. The effects of

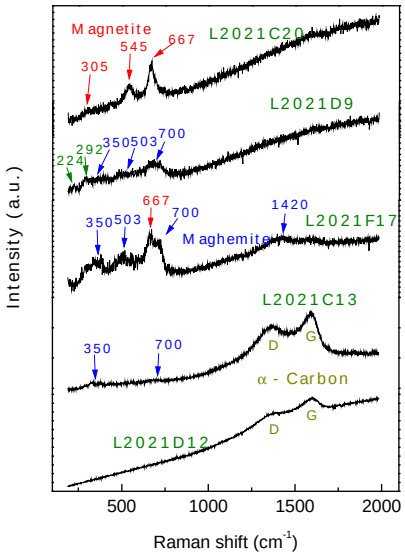

Figure 2: IDPs Raman spectra

pyrometamorphism in IDPs during atmospheric entry, can not be ruled out as a contributing factor of the measured degree of order/disorder of the carbon. Thus the indigenous structure and irradiation history of amorphous carbon in IDPs could be partially overprinted.

Conclusion: We were able to detect combination of carbon/Fe-oxides/Fe-sulfides performing combined micro-Raman and micro-IR investigations on same IDP thanks to the SSH. Same combined investigations will be applied to the Stardust grains mounted on SSHs. We will be able to detect in these particles the possible presence of the combination of Fe-oxides, Fe-sulfides and carbons that will be a diagnostic assemblage for rapid thermal heating. In particular, detecting maghémite will be strong proof of a flash-heating origin, thus it will be possible to drive conclusions on possible thermal effects due to aerogel impact.

References: [1] Keller L.P. *et al.* (1993) *AIP Conf. Proc. 310*, 159–172. [2] Rietmeijer F.J.M. and Mackinnon I.D.R. (1985) *Nature*, *315*, 733-736 .[3] Rietmeijer F.J.M. (1992) *Geochim. Cosmochim. Acta*; *56*, 1665-11671. [4] Keller L.P. et al. (1996) *LPS XXYIII*, Abstract #659. [5] Rietmeijer F.J.M. (1998) in Papike J.J., Eds., *Revs. Mineral. 36*, 2-1-2-95. [6] Baratta G.A. et al. (2004) *JRS, 35,* 487-496. [7] Palomba E. et al. (2001) *M&PS, 36,* A156. [8] Sandford, S.A. and Walker R.M (19985) ApJ, 291, 838-851. [9] Balasubramaniam R. et al. (2003) *Current Science, 11,* 1546-1555. [10] Sousa M.H. et al. (2000) *JRS, 31,* 185-191. [11] Rietmeijer (2004) *M&PS,* 39, 1869-1887. [12] Wopenka B. (1988) *E&PSL, 88,* 221–231.

CIR MODULATION OF JUPITER DUST STREAM DETECTION

A. Flandes[1] and H Krüger
[1]Instituto de Geofisica (UNAM) xytrahx@yahoo.com.mx

During late 2003 and early 2004, Ulysses approached Jupiter (~0.8 AU at its closest distance) and detected 24 new dust streams. The tiny positively charged dust grains (~10nm) in the streams are pushed away from Jupiter by its co-rotational electric field, accelerating them to very high speeds (>200 km/s). Once outside the Jovian magnetosphere, dust grains are under the influence of the interplanetary magnetic field and some characteristics of this field are observable on the streams. Dust streams seem to be correlated to the solar *Co-rotating Interacting Regions* (CIR). On the whole, there seems to be a previous CIR for every set of streams. The duration of the set of steams matches roughly the duration of the CIRs, indicating a confinement of the dust stream particles in the compressed regions of the interplanetary plasma. On the other hand, most dust stream peaks and the precedent CIR peaks seem to be separated by an interval roughly similar to the time needed by a dust particle to travel from the source to the spacecraft's detector.

ELEMENT HOSTS IN ANHYDROUS IDPS: A TEST OF NEBULA CONDENSATION MODELS.. G. J. Flynn[1], L. P. Keller[2], and S. R. Sutton[3], [1]Dept. of Physics, SUNY-Plattsburgh, Plattsburgh NY 12901, USA. george.flynn@plattsburgh.edu. [2]NASA Johnson Space Center, Houston, TX 77058. [3]Dept of Geophysical Sciences and CARS, The University of Chicago, Chicago, IL 60637.

Introduction: Many anhydrous interplanetary dust particles (IDPs) are the most pristine samples of primitive Solar System dust that are currently available for laboratory analysis. Because these primitive, anhydrous IDPs show little or no evidence that they have experienced either thermal or aqueous alteration since their formation, they preserve materials that formed in the early Solar Nebula as well as presolar materials. Thus, we can test the applicability of equilibrium nebula condensation models to our Solar System by comparing the host mineral of each element with the host that is predicted by the nebula condensation models.

Samples: We have mapped the spatial distribution of most of the elements from K to Zn in ultramicrotome sections, each ~100 nm thick, in 3 primitive, anhydrous IDPs – L2011*B2, L2010B10, and L2009*F3, all of which are fragments of cluster IDPs. We employed a zone plate focused X-Ray Microprobe (XRM) at Sector 2 of the Advanced Photon Source (APS) at the Argonne National Laboratory to perform the element mapping. This XRM has ~150 nm spatial resolution, which is sufficient to resolve individual mineral grains in most of the anhydrous IDPs.

Results: Each element was found to be localized within each IDP, with some hot-spots being sub-micron is size.

K Results. L2011*B2 is a cluster fragment that contains a relatively high K concentration. The K is spatially correlated with the silicate in this particle (see Fig. 1). Nebula condensation models indicate that K should condense at ~1000 K into K-feldspar [1, 2]. However, Transmission Electron Microscope (TEM) examination of other ultramicrotome sections of this fragment indicate that the silicate in L2011*B2 is pyroxene, rather than feldspar.

S Results, Small S hot-spots were detected in each IDP. Most of the S is concentrated in Fe-sulfides, consistent with the prediction of nebula condensation models that S should condense at ~650 K into Fe-sulfide [1, 2].

Zn Results, The Zn is concentrated into small hot spots, which are collocated with S. However, the Fe K-alpha peak is significantly higher than the Zn K-alpha peak in the spectrum of the Zn hot-spot, indicating that the Zn host is either a Zn-rich Fe-sulfide, or Fe- and Zn-sulfides are intermixed on a size scale that is small compared to the analysis spot. The nebula condensation models generally include the thermodynamic properties of only pure Zn-sulfide, and predict that Zn should condense at ~660 K into Zn-sulfide [1, 2].

Cu Results: The Cu is concentrated into hot spots, which are collocated with S. The equilibrium nebula condensation models predict Cu condenses at ~1040 K into a metal [1, 2].

Cr Results: The Cr is concentrated into hot spots (see Fig. 2), which are collocated with Si, Ca, and Fe (see Fig. 3) indicating the Cr-host is an Fe-silicate. In most nebula condensation models, Cr condenses into Fe-metal, which alters to Fe-Cr oxide (a Cr-spinel) as the nebula cools further.

Ca, Ti, Cr, Mn, and Ni Results, We also observed hot-spots of Ca, Ti, Cr, Mn, and Ni in the element maps. The host minerals of each of these elements will be determined by TEM, and compared to the predictions of the equilibrium nebula condensation models.

Conclusions: High spatial resolution chemical mapping of the most primitive IDPs provides a way to test nebula condensation models. The results of this project should provide important information on the minerals whose thermodynamic properties should be included in future models.

References: [1] Grossman, L. 1972, *Geoch. Cosmochim. Acta*, **36**, 597-619. [2] Grossman, L. and Larimer, J. W. 1974, *Reviews of Geophys. and Space Physics*, **12**, 71-101.

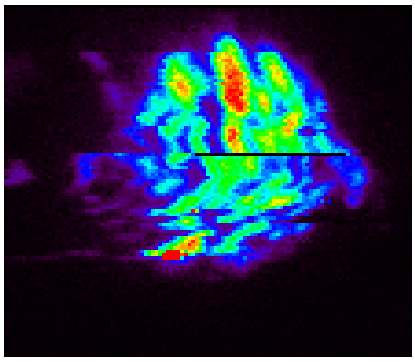

Figure 1: K map of L2011*B2. Bright areas are highest concentration. The K-rich areas are also high in Si.

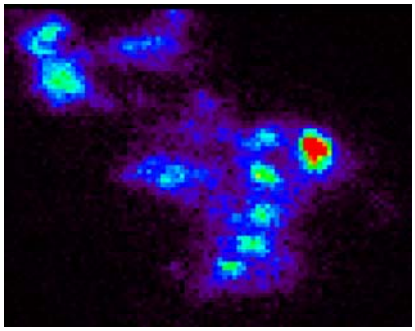

Figure 2: Cr map of L2009*F3.

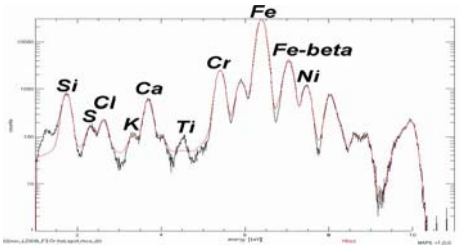

Figure 3: X-ray fluorescence spectrum of Cr hot-spot in L2009*F3.

TENTATIVE IDENTIFICATION OF INTERSTELLAR DUST TOWARDS THE HELIOSPHERE NOSE. P. C. Frisch. Department of Astronomy and Astrophysics, University of Chicago, 5640 South Ellis Ave., Chicago, Il 60637, U.S.A.

Optical polarization data from Tinbergen (1982), which show the weak polarization of light for stars within 35 pc of the Sun, are reinterpreted to show an origin consistent with the entrainment of the polarizing grains in the outer heliosheath. The original data indicated that a small patch of polarizing dust grains are present within ~35 pc of the Sun near the galactic center region. It is shown here that both the region of maximum polarization and polarization position angle suggest an origin associated with small grain entrainment in the interstellar magnetic field draped over the heliosphere. The region with best grain alignment as measured by correlated position angels, ecliptic longitude $\lambda = 281° \rightarrow 330°$, is offset by over 20° from the upwind direction. The region showing maximum polarization is centered near $\lambda = 295°$, $\beta = 0°$ (ecliptic coordinates), compared to the heliosphere nose direction $\lambda = 259°$, $\beta = +5°$. The polarization strength anticorrelates with ecliptic latitude in this region. These properties are consistent if the polarization is caused by small interstellar grains, radii <1 micron, aligned by the interstellar magnetic field draped aroudn the heliosheath. If this interpretation is correct, these trapped interstellar dust grains provide a means of monitoring the outer heliosheath over the solar cycle, and may possibly contaminate the cosmic microwave background.

HAYABUSA MISSION TO ASTEROID ITOKAWA: IN-SITU OBSERVATION AND SAMPLE RETURN.
A. Fujiwara[1], J. Kawaguchi[1], S. Sasaki[2], & Hayabusa Team, [1]ISAS/JAXA (The Institute of Space and Astronautical Science of Japan Aerospace Exploration Agency) 3-1-1 Yoshinodai, Sagamihara, 229-8510, JAPAN (fujiwara@planeta.sci.isas.ac.jp), [2] National Astronomical Observatory of Japan, 2-12 Hoshigaoka, Mizusawa, 023-0861, JAPAN (sho@miz.nao.ac.jp).

Introduction:
Recent direct observations of asteroids by spacecrafts are revealing their various interesting characteristics which cannot be obtained either from ground-based observations or meteorite studies. However, identification of the real material species constituting asteroids and their corresponding meteorite analogs are still ambiguous. Space weathering process makes it difficult to identify the real material, and there is still a great gap between the remote sensing data (from the ground and/or from spacecrafts) and the local microscopic data from meteorites. Surface of many asteroids may be covered with fine regolith materials which would be different from usual meteorite specimen. Sample return missions from asteroids are indispensable to solve these problems. HAYABUSA (MUSES-C) spacecraft which was launched on May 9th 2003 is the first attempt on the sample return from an asteroid. Here outline of the mission is described with special emphasis on its science.

Outline of mission:
HAYABUSA is an engineering spacecraft to develop technologies required for future missions such as electric propulsion, autonomous navigation, sampling, and reentry technique [1]. The spacecraft is three-axis stabilized, its dry weight is 380kg, and the total weight including chemical fuel and Xe propellant is 510kg. The target asteroid is Itokawa (1998 SF36) among Apollo group of near-earth asteroids. Properties of the target asteroid were extensively studied [2-4]. The orbital elements are a= 1.324AU, e=0.279, q=0.955AU, Q=1.693AU, and i=1.713deg. From radar observations, diameter is estimated to be approximately 600m x 300m. Rotation period is 12.1 hours and the rotational axis is supposed to be almost perpendicular to the ecliptic plane. The provisional spectral type is S and corresponding meteoritic type is considered to be LL ordinary chondrite [4].

On May 9, 2003. HAYABUSA was launched successfully by an M-V rocket from Kagoshima Space Center. It made a fly-by with the earth in May 2004 and was transferred to the orbit toward the target asteroid. by gravity assist. HAYABUSA approach Itokawa in September 2005. It hovers above the asteroid surface at the sunlit side at altitude of about 7km. From this home position, HAYABUSA will perform global mapping of the asteroid. Rotation period of Itokawa is 12.1 hours. Although HAYABUSA spends most of time near the home position, it will also approach the terminator side of the asteroid. On the basis of information obtained from remote sensing observation, sampling points are determined from the viewpoint of the safety of the spacecraft and the scientific interest. In early November 2005, HAYABUSA will descend to the asteroid surface to make sampling of the surface material. After the descent to altitude about 20m by LIDAR, HAYABUSA will deploy a target marker for the touchdown and a small robotic rover called MINERVA. The target marker is used as the artificial target to be referred for the descent. The MINERVA hops on the asteroid surface by the reaction of the two torquers installed in it. Sampling of asteroid material is carried out by shooting a small projectile onto the asteroid surface and catching the ejected material. Just after the contact of the sampling device with the asteroid surface, HAYABUSA will start rising back to the home position. Sampling will be carried out from two different locations on the asteroid surface.

The spacecraft will leave the asteroid Itokawa (hovering position) in December 2005, and after cruising under the operation of the ion engine it will approach the earth in June 2007. The reentry capsule separated from the spacecraft plunges into the earth atmosphere at velocity 12km/s directly from the interplanetary orbit. After sufficient deceleration in the earth atmosphere a parachute is deployed and the front ablator shield is removed off to avoid the additional heat invasion into the sample canister. The landing site is scheduled to be Woomera desert in Australia.

Scientific instruments:
Scientific instruments on board are a CCD imaging camera (AMICA) with 8 filters of wavelength bands similaer to the ECAS system and polarizers, a near-infrared spectrometer (NIRS), a light detection and ranging device (LIDAR) using a YAG pulse laser emitter and a Si-APD receiver, and a CCD X-ray fluorescence spectrometer (XRS) (see Table 1). Under corporation with NASA, several instruments involve co-investigators from U.S.

Primary objective of AMICA and LIDAR is for navigation, but they play important roles to obtain topographical data of the asteroid surface. Ranging data by LIDAR provides the information of the asteroid gravity and mass. Coupled with the asteroid shape data, Itokawa's density will be estimated. Spatial resolution of the asteroid surface by the AMICA is less than 10 m at the home position. Search for satellites and dust particles around Itokawa will be also conducted by AMICA. NIRS is an InGaAs 64 pixel linear array detector, and the wavelength covered is 0.85-2.10 micron. NIRS will provide valuable data on surface mineralogy of Itokawa and ongoing space weathering process. XRS has energy resolution 100eV at 1.5keV, and can detect Fe, Na, Mg, Al, Si, and S. All these instruments are installed on the base panel of the spacecraft. The MINERVA has three miniature cameras to obtain stereoscopic images and different focal lengths images of the asteroid surface and landscape. It also has six platinum thermometers and they measure the surface temperature.

The sampling device is also installed on the base panel. Its main part is the funnel-type tube called a horn of length 1m and diameter 20cm. Immediately after sensing the contact of the bottom of the horn with the asteroid surface the projectile of mass 5g made of tantalum is shot at velocity 300m/s and asteroidal fragments are ejected. The sample through passing the horn is caught by the canister attached on the top of the horn. Microgravity experiments confirmed that this shooting method can collect either rocky or regolith materials on the surface. Total amount of the sample will be expected to be about 1g [5]. The spacecraft lifts off the asteroid surface with the aid of chemical thrusters within a few second after the contact to avoid the damage by the contact of the tumbling main body with the asteroid surface. The samples from two different locations are separately enclosed in the small canister rooms and the canister is transferred into the reentry capsule mounted on the side panel of the spacecraft. The canister is sealed by double O-rings and the sample is separated from the outside environment.

Sample analysis:

The asteroid sample in the canister retrieved in Australia is transferred to a curation facility at ISAS/JAXA. After fundamental characterization some portion of the samples is separated and distributed for the initial analysis. The initial analysis will be carried out on the scheduled program in several facilities in Japan by the MASPET team consisting of Japanese, US, and Australian scientists during about one year. In the following detailed analysis phase, the samples will be distributed to the researchers all over the world on the basis of AO.

Conclusion:

HAYABUSA is the first sample return mission from an asteroid. During its rendezvous phase with the target asteroid Itokawa, HAYABUSA will provide first detailed image of topographic feature of an asteroid of diameter less than 1km, and be able to answer whether regolith exists or not on such a small body and whether the body is monolithic or not. It will also able to find mineralogical and chemical inhomogeneity with sufficient spatial resolution, if it exists. The remote sensing instruments (AMICA, NIRS, XRS) boarded on the spacecraft will provide global, but in various spatial scale, mineralogical and elemental abundance data along with the topographical data from AMICA, LIDAR, and MINERVA cameras. The returned sample will provide the detailed and abundant chemical, mineralogical, and physical information of the asteroid surface in the finest scale, which enables to make direct comparison with meteorite data. These data will be used to establish a strong link between the asteroids of S-type spectra obtained by ground-based observation and material properties obtained from meteorite research

References: [1] Kawaguchi, J et al. (2003) *Acta Astronautica, 52,* 117–123. [2] Ohba, Y. et al. (2003) *Earth Planets Spac,e55,* 341-347. [3] Ishiguro, M. et al (2003)*Publ. Astron. Soc. Japan 55,* 691–699. [4] Binzel, R. et al. (2001) *Meteorit.Olanet. Sci. 31,* 1167 [5] Yano, H. et al. (2002) *Proc. ACM 2002(ESA SP500),* 103-106.

Table 1
Instruments and sciences on HAYABUSA mission

Instrument/Theme	Team Leader	
AMICA	J. Saito	ISAS/JAXA
NIRS	M. Abe	ISAS/JAXA
LIDAR	T. Mukai	Kobe U.
XRS	M. Kato	ISAS/JAXA
MINERVA		
(Technology)	T. Yoshimitsu	ISAS/JAXA
(Science)	S. Sasaki	NAOJ
Astrodynamics	M. Yoshikawa	ISAS/JAXA
Sample Analysis	T. Yamamoto	Hokkaido U.
	(formerly I. Kushiro	JAMSTEC)

ISAS Project Manager	J. Kawaguchi
ISAS Project Scientist	A. Fujiwara
NASA Project Scientist	D. Yeomans

THE PARENT BODIES OF MICROMETEORITES. M. J. Genge, Impact and Astromaterials Research Centre (IARC), Imperial College London & The Natural History Museum, Exhibition Road, London SW7 2AZ, UK. Email: m.genge@imperial.ac.uk.

Introduction: Micrometeorites (MMs) are that fraction of the Earth's extraterrestrial dust flux that survives atmospheric entry to be recovered from the Earth's surface. Large numbers of MMs have been collected from Antarctic ice [1] and provide an important sample of dust present in the Zodiacal cloud at 1 AU for direct study in the laboratory using micro-analysis.

The capture mechanics of dust by the Earth favours those interplanetary dust particles with low geocentric velocities and low ecliptic latitudes at 1 AU and thus asteroidal sources with the lowest inclinations and eccentricities are likely to make the largest contributions. Low geocentric velocity dust is also more likely to survive atmospheric entry without significant heating to be recovered at the surface of the Earth [e.g. 2,3].

The current study presents mineralogical, textural and compositional data on 730 micrometeorites recovered from Antarctic ice that allows the parent body affinities of these materials to be tested. It is argued on the basis of the distribution of particle types that MMs are derived predominately from four main genetic groups of parent body of which three have close affinities to chondritic meteorites and the fourth may be closely related to cometary materials, albeit with what are currently considered definitively asteroidal characteristics.

Samples and Methods: The MMs described in this study are 50-400 μm in size and were collected from Antarctic blue ice near Cap Prudhomme. Analytical and separation techniques are described in Genge et al., [4].

The Relative Abundances of MM Types: Micrometeorites can be split into two main groups on the basis of the degree of heating during atmospheric entry: (1) unmelted particles and (2) melted and partially melted particles. This study focuses on unmelted particles that preserve sufficient mineralogical and textural features to allow their parent body affinities to be assessed. This approach, however, introduces a bias towards those particles comprised principally of high temperature components.

Unmelted MMs include two main particle types: (1) fine-grained MMs (fgMMs), with sub-micron grain-sizes, and textural and compositional affinities to the hydrated matrices of carbonaceous chondrites and (2) coarse-grained MMs (cgMMs), which are dominated by pyroxene, olivine and glass, and usually have igneous textures.

Fine-grained MMs can be sub-divided into three gradational classes on the basis of texture and mineralogy. (a) C1 particles consist of low porosity matrix comprised of phyllosilicates (clay minerals) or their dehydration products with few anhydrous silicates. The matrices of C1 particles show little spatial variation in Fe-content over scales of 10-100 μm similar to CI1 chondrites [5] and implies extensive elemental mobility during aqueous alteration and high water to rock ratios. (b) C2 particles are dominated by low porosity matrix consisting of phyllosilicates (or their thermal decomposition products). The matrices of C2 particles show up to 10 wt% variation in Fe content over 10-100 μm and include much higher abundances of anhydrous silicates including Fe-rich pyroxenes, which are sensitive to aqueous alteration. The mineralogies and textures of C2 particles are broadly similar to those of CM2 chondrites [5] and suggest limited elemental mobility and lower water to rock ratios than C1 particles. (c) C3 particles consist of high porosity matrices (up to 50% by volume) dominated by micron-sized olivine and pyroxene grains. These are, however, a diverse group of particles and many contain variable amounts of interstitial phyllosilicate (or dehydration product). The matrices of C3 particles show little variatiation in Fe content over 10-100 μm scales and contain relatively abundant isolated (>4 μm) pyroxene and olivines grains. The presence of phyllosilicate and framboidal magnetite within C3 particles suggests they have experienced a degree of aqueous alteration, however, their high porosities indicate this was less than C1 or C2 particles. C3 particles have no direct meteorite equivalents.

Coarse-grained MMs are a group of particles dominated by pyroxene, olivine and glass that have broadly similar mineralogies, compostions and textures to chondrules found within chondritic meteorites. The principal evidence that cgMMs represent fragments of chondrules is: (1) the majority of cgMMs fall into either reduced, oxidized or radiating pyroxene groups similar to chondrules, (2) the grain-sizes of cgMMs is <50 μm and not consistent with most achondritic (igneous differentiated meteorites), and (3) cgMMs often have unequilibrated mineral assemblages indicating non-equilibrium crystallization. To date only a single

cgMM has been identified that is demonstrably achondritic [6].

Composite MMs consisting of fine-grained and coarse-grained portions are highly significant since these indicate that cgMMs sample small igneous objects which were embedded in C2 fine-grained matrix [7]. These composite MMs are dominated (>70%) by reduced igneous objects suggesting a close affinity to CM2 chondrites that are dominated by reduced (Type I) chondrules. The overall abundance of composite MMs (which sample the chondrule/matrix interface) to cgMMs (which are interior fragments of chondrules) suggests an average chondrule diameter of ~1600 μm larger than in any meteorite group [8].

The abundance of cgMM also suggests differences from CM2 chondrites. Chondrules comprise ~15% by volume of CM2's and yet the abundance of cgMMs is approximately equal to that of fgMMs. Furthermore CM2 chondrules are dominated by Type I (reduced chondrules) [5] and yet ~40% of cgMMs are oxidized (Type II) materials. These data suggest that a significant proportion of cgMMs are derived from a chondrule-dominated source containing abundant Type II chondrules. This source would, therefore, have affinities to ordinary chondrites [5]. Chromium and Mn contents of olivines from some cgMM support this hypothesis since they fall in the range of those of ordinary chondrites. The occurrence of glass in the majority of cgMMs furthermore indicates an unequilibrated source.

Although cgMMs usually preserve glass indicating no significant metamorphism or aqueous alteration, several fgMMs contain either unusually high abundances of euhedral enstatite and/or forsterite within a fine-grained matrix or have spatial variations in Fe-content within their fine-grained matrix suggesting these contain pseudomorphs of pre-existing euhedral crystals. Similar textures are observed within intensely aqueously altered CM2 chondrites such as Cold Bokkeveld and are hydrated chondrules [5].

Discussion: The relative abundances of unmelted MM types suggest there are four main parental sources: (1) a C1 asteroidal source, which has experienced intense aqueous alteration, (2) a C2 asteroidal source containing chondrules that has experienced less aqueous alteration, (3) a C3 source that has experienced little compaction and minor aqueous alteration, and (4) a chondrule-dominated unequilibrated source.

Although three of these sources have affinities to CI1, CM2/CR2 and ordinary chondrites their mineralogies and textures differ in detail. Transmission electron microscope studies of fgMMs indicate that the clay mineral smectite dominates MM matrices [9, 10, 11] whilst serpentine or serpentine-smectite interlayed clay minerals dominate CI1 and CM2 chondrite matrix [5]. Pyroxene is also the most abundant anhydrous silicate found amongst MMs, whilst olivine dominates within most of the chondritic meteorite groups. These differences indicate that chondritic meteorites and MMs sample different asteroidal parent bodies.

The discrete oxygen isotope abundances of chondritic meteorite groups are often considered as evidence that these are not derived from a single heteorogeneous parent body [5]. A recent study of the oxygen isotope systematics of MMs likewise indicates a wide range of values, however, these are also not consistent with those of meteorites [12].

The presence of highly porous C3 particles is anomalous. These materials have some affinities with the matrices of CR2 chondrites since these also contain framboidal magnetite, include areas that are relatively porous and have experienced a low degree of aqueous alteration. They are also broadly similar to hydrated interplanetary dust particles. The discovery of isotopically anomalous presolar silicates within MMs, CR2 matrix and IDPs [13, 14] may suggest a genetic link between all three groups of materials. The occurrence of an oxidized (Type II) chondrule fragment within one C3 particle in the current study, however, implies that the materials have an asteroidal source, albeit one that may be transitional to comets.

Implications: The results of this study indicate that MMs are derived from at least 4 principal types of parent body, all of which are likely to be asteroids but differ from those of meteorites. Athough it is impossible to determine at present whether meteorite parent bodies are sampled by MMs, it is clear that meteorites do not sample parent bodies representative of the predominant sources of MMs. It is clear that meteorites and/or MMs are a highly biased sample of the main asteroid belt.

References:[1] Maurette M. M. et al., (1991) *Nature*, 351, 44-47. [2] Kortenkamp S. J. & Dermott S. F. (1998) *Icarus*, 135, 469-495. [3] Nesvorny D. et al., (2004) *Astrophys. J.*,591, 486-497. [4] Genge M. J. et al. (1997) *GCA,61*, 5149–5162. [5] Brearley A. J. & Jones A. P. (1998) *Reviews in Min*, 36, 1-191. [6] Gounelle et al. (2005) *Science*, in press. [7] Genge M. J. (2005) *MAPS* (Feb delayed). [8] Genge M. J. (2004) 35th *LPSC*, abs 1102. [9] Nakamura T. et al., (2001) GCA, 65(23), 4385-4397. [10] Noguchi T. et al. (2002) *EPSL*, 202(2), 229-246. [11] Genge M. J. et al. (2001) 32nd *LPSC*, abs. 1546. [12] Matrajt et al. (2005) *This conference*. [13] Yada T. et al. (2005) 36th *LPSC*, abstract 1227. [14] Kobayashi S. et al., (2005) 36th *LPSC*, abstract 1931.

DEVELOPMENTS IN THERMAL ANALYSIS OF LABILE TRACE ELEMENTS IN CARBONACEOUS CHONDRITES.

Julia S. Goreva and Dante S. Lauretta, University of Arizona, Lunar and Planetary Laboratory, Tucson

Introduction and technique. Abundances and isotopic compositions of the labile chalcophile and siderophile elements (in order of increasing condensation temperature – Hg, Cd, Tl, In, Bi, Pb, S, Te Se Zn Sn, Ge, Sb, Ga, Na, Ag, As, Au, Fe) in primitive materials reflect low temperature gas-solid interactions in the early solar system. Most of these volatile, non-ice-forming elements are predicted to initially condense as a trace element in the bulk metal phase; others are transferred during metal sulfurization [1, 2]. Because of their high volatility and their mobility in aqueous systems, these elements may be excellent indicators of the low-temperature, thermal and hydrological processes experienced by primitive chondritic meteorites and cometary particles.

Here we present results using new, thermal-analysis (TA-) ICP-MS technique. By coupling a home-built inductively heated programmable furnace with a high-resolution ICPMS, we are able to simultaneously measure the thermal release profiles of elements from small samples. This technique is essentially an advanced thermogravimetry method. Isotopically pure ^{200}Hg spike solution supplied into the furnace from cold-vapor generator is used to optimize the system performance and as an internal standard during heating experiments.

A series of heating experiments were performed on a suite of CI, CM, CV, and CO carbonaceous chondrites. Small aliquots of the meteorite powders were heated from room temperature to 1100 °C under an inert Ar atmosphere. For the external quality control of the bulk chemical abundance of the trace elements of interest we have use certified standard reference materials JG-1 Granodiorite and JB-2 Basalt as well as the Allende meteorite reference sample. Acid dissolution of both heated and pristine aliquots of standards used as a control on the amount of liberated material.These experiments allow us to determine the bulk abundances of labile elements, and their distribution among different (mostly S-bearing phases).

Results. Typical element release profiles during the heating experiments for different carbonaceous chondrite classes are plotted in Fig.1.

CI chondrites (Orgueil) releases detectable quantities of S over the entire temperature range with distinct maxima at 250, 500, and 650 °C (Fig. 1a). Low amounts of As and Sb are liberated. Significant quantities of Se, Cd, Te, and Hg are detected with correlated maxima in S, Se, and Te release profiles at 250 and 500 °C. The release of S, As, Se, Cd, and Te reach maxima at 650 °C.

CM chondrites continuously release S at temperature greater than 100 °C. There are maxima in the S-release profiles at 300°C and 600 °C (Fig. 1b). They release small amounts of As above 700 °C with maxima at 400 °C. Selenium is released continuously from the CM chondrites at temperatures above 200 °C with maxima at 400 °C. There are maxima in the Cd-release between 700 and 800°C. Antimony and Te are released at low levels throughout the entire duration of the experiments. There are sharp peaks in the Te-release at 725 °C.

CV chondrites release significantly less S compared to the CM chondrites There are two maxima in the S-release profile from Allende (CV) and Grosnaja (CV) at 320 and 420 °C. Continuous S release occurs above 500 °C. Sulfur release from Mokoia (CV) begins at 200 °C with a maxima at 500 °C. Vigarano (CV, Fig. 1c) is distinctly different. The majority of S is released at 400 °C and continues to release throughout the experiment. The maxima in the S release profiles from Allende (CV), Mokoia (CV), and Grosnaja (CV) correlates with ones in the As and Se profiles. The maxima in the Vigarano (CV) S-release profile is perfectly correlated with those in the As, Se, and Te profiles. There are peaks in the Cd release profiles from Allende, Mokoia, and Vigarano between 675 - 700 °C.

CO chondrites do not release detectable amounts of S below 500 °C (Fig. 1d). The release of As, Se, Cd, Sb, and Te reach maxima between 300 and 400 °C from Kainsaz (CO). The release pattern from Ornans (CO) is distinctly different. Very little material is liberated below 800 °C. The release of S and Se is correlated. Isna (CO) releases Se, Sb, and Hg at low T and has a S-release pattern that is similar to Kainsaz. It releases Sb between 350 and 550 °C. The peak release for Cd and Te occurs above 900 °C.

Interpretation and application to Stardust. There is a low-temperature S-bearing phase in the CI, CM, and CV carbonaceous chondrites, which is absent in the CO chondrites. These results place constraints on the origin and thermal history of volatile elements in these meteorites. The bulk abundances are the result of condensation processes in the solar nebula. Subsequent alteration on the

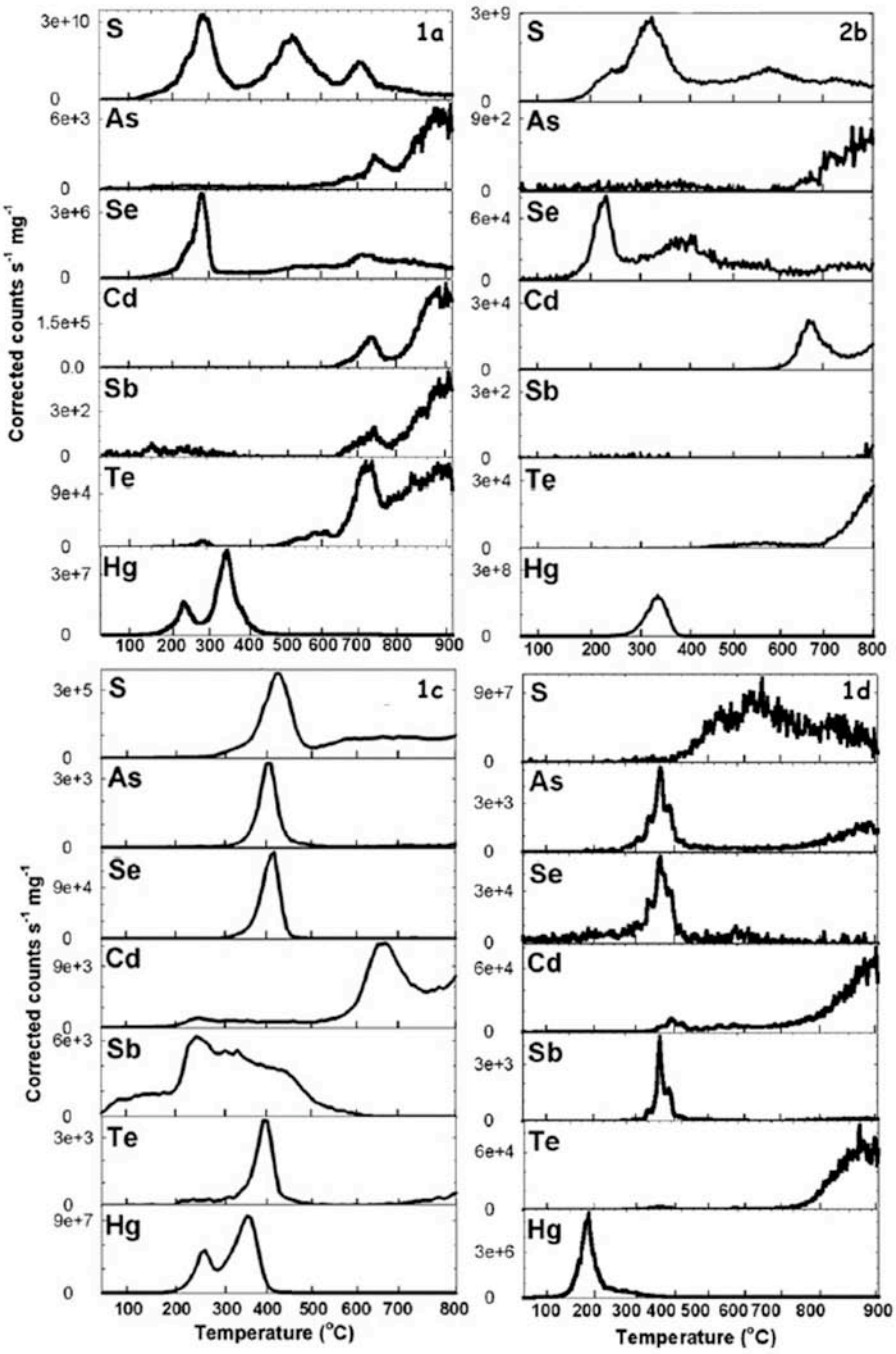

Figure 1. Thermal release profiles for 1a Orgueil (CI), 1b Murchison (CM), 1c Vigarano (CV) and Kainsaz CO)

meteorite parent bodies likely redistributed the trace elements into low-temperature phases. This redistribution had a significant effect on the rate and extent of volatile loss during thermal metamorphism.

Since the amount of the material required for analyses is very small and techniques is non-destructible with respect to silicates and metals, it can be applied to Stardust particles prior to other chemical and isotopic analyses. Moreover, labile elements are excellent indicators of the heating and volatile loss experienced by Stardust samples as they passed through the aerogel. Investigation of the volatile abundances along the particle tracks may help to determine the order in which different trace elements were released and a degree of heating.

Ref. [1] Lauretta et al. (2002) *LPSC, XXXIII*, 1602. [2] Lodders and Fegley (1998) *The Planetary Scientist's Companion, Oxford*

GREAT EXPECTATIONS – DUST RECOVERED FROM AEROGEL. G. A. Graham[1], J. P. Bradley[1], Z. R. Dai[1], A. T. Kearsley[2], M. Bernas[3] and C. Snead[4], [1]Institute of Geophysics & Planetary Physics, Lawrence Livermore National Laboratory, CA 94551, USA (graham42@llnl.gov), [2]Mineralogy Department, The Natural History Museum, London SW7 5BD, UK, [3]Applications Laboratory, FEI Company, OR 97124, USA, [4]Space Sciences Laboratory, University of California at Berkeley, CA 94720, USA.

Introduction: Cometary dust particles captured during the flyby of comet 81P/Wild-2 by NASA's Stardust spacecraft will be returned to Earth in January 2006 [1-2]. One of the fundamental questions to be answered in the preliminary examination is whether the captured particles are similar to the current materials studied in the laboratory, i.e. interplanetary dust particles (IDPs). From detailed IDP studies it is assumed that anhydrous particles are from cometary bodies [3] and hydrous particles are from asteoridal bodies [4].

Although the stratospheric collection of IDPs results in the capture of material in a near-pristine state, significant heating is extensive in all particles [5]. This is in stark contrast to Stardust, where the cometary particles have embedded into the low-density silica aerogel collectors at ~6.1 km s^{-1}. Previous studies have shown that hypervelocity impact (HVI) capture of dust can result in fragmentation, thermal and shock alteration [6] even when the substrate is a low density material [7].

In the build-up to Stardust, several laboratory studies have accelerated analogue projectiles (e.g. single mineral grains and meteorite fragments) into aerogel targets at encounter velocities to investigate the effects of HVI capture [8-9]. In addition to these laboratory materials, NASA's Orbital Debris Collection (ODC) experiment exposed 0.63 m^2 of 0.02g cm^{-3} silica aerogel on the Mir space station for 18 months [10]. Recent studies of impacts extracted from ODC aerogel tiles have focused on in-situ mapping [11-12]. While these studies highlight the degree of fragmentation, they only enable the acquisition of bulk chemical or elemental data so it is not possible to directly observe structural or mineralogical alteration that would be comparable to IDPs. In this study we report on the composition of individual particles extracted from the terminal point of impacts.

Methods: The particles were isolated from the bulk aerogel using glass micro-needles. The particles were subsequently mounted onto standard SEM pin-stubs using carbon adhesive tabs.

Preliminary SEM/EDX Screening. A JEOL 5900 LV SEM fitted with an Oxford Inca EDX system was used to confirm extraterrestrial origin. The particles were then subjected to X-ray mapping to identify the location of molten aerogel which adheres to the surface of the particle during the HVI capture.

FIB Lift-out. Electron transparent sections of the terminal particles were produced using focused ion beam (FIB) milling in an FEI DB237 FIB/FESEM tool fitted with STEM and EDAX Genesis EDS detectors [13].

TEM Analysis. A CM300 Field Emission Gun Transmission Electron Microscope (FEGTEM) fitted with an Oxford X-ray energy dispersive spectrometer was used to characterize the FIB sections.

Results & Discussion: Any particle collector exposed in low-Earth-orbit will also contain impacts generated by artificial orbital debris. As a result, all of the particles used in this study were from the so-called "chondritic swarm" impacts [10]. Preliminary secondary electron imaging in the SEM showed that all of the particles had the characteristic molten aerogel coating on the surface of the grains (Figure 1). This has been seen on all previously studied ODC particles [10] and in particles extracted from laboratory impacts [9]. This molten aerogel is essentially a fusion layer most likely formed during the initial collision between the whole particle and the substrate. A significant benefit of using FIB microscopy to prepare the electron transparent sections (~100 nm) is that precise sections can be made that are nearly free of the molten aerogel which would have contaminated any detailed mineralogical or chemical analyses.

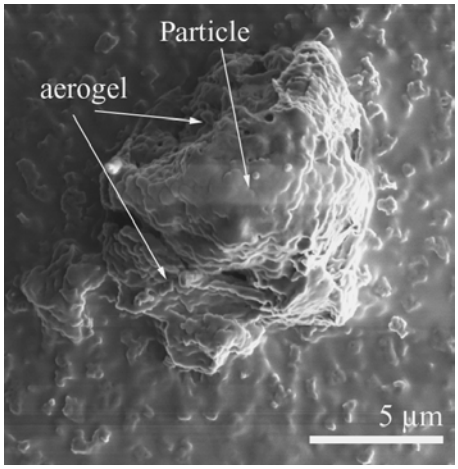

Fig.1: Secondary electron image of a terminal particle extracted from aerogel. The particle diameter is ~7 µm.

Figure 2 shows a 30 kV SEM-STEM bright-field image of one of the terminal particles. Unlike the previous study of the chondritic swarm particles [10] the section does not show extensive evidence of aerogel penetrating into the bulk particle. Detailed TEM investigation of the particle section identified the major mineral component to be serpentine with additional minor phases including spinel. This is a different mineral assemblage to that originally identified in the chondritic swarm particles where the major phase was olivine [10]. However as the swarm particles are proposed to have been generated by a grazing impact of a larger chondritic mass on the space station, it is not unreasonable that the composition of the particles captured is varied. In addition to the characterization of the mineralogy of the terminal particle, the TEM study revealed that extensive thermal alteration had occurred to the rim of the particle evident by the amorphous material and the vesicular texture. It can be argued from the observations made on ODC particles that they are not analogues of Stardust particles as the HVI speeds of capture were in excess of 10 km s^{-1} compared to 6.1 km s^{-1}. Therefore higher degrees of alteration could be expected. However, the observations made on the ODC particles are similar to those seen in recent laboratory impact simulations at ~2-6 km s^{-1} where vesicular and amorphous material was observed at the rims of the mineral grains while the cores were relatively pristine [9,15].

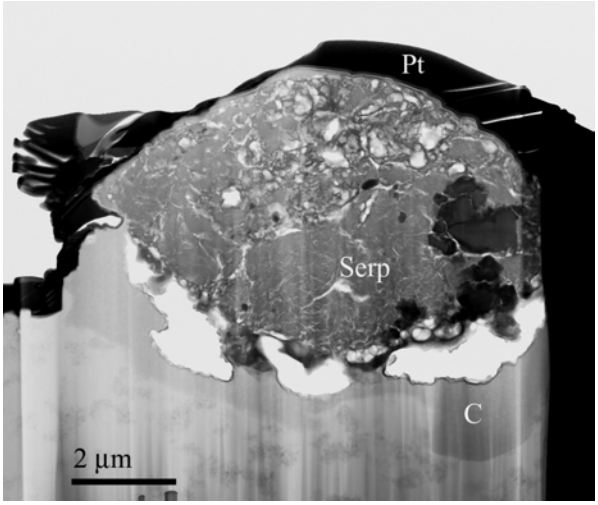

Fig.2: 30 kV SEM-STEM bright-field image of the terminal particle FIB section.

Both theoretical modeling [14] and synchrotron x-ray mapping studies of ODC impacts [11-12] suggest a high degree of fragmentation will be observed in Stardust impacts. As a consequence, it can be argued that the terminal particles will only represent the most robust grains. However both in this study and the previous study of extraterrestrial terminal grains extracted from the ODC tiles [10], the compositions have been found to be polymineralic.

Conclusions: The terminal particles showed clear evidence of vesiculation and alteration of mineralogy at the rims; however, in at least one of the particles, the core appeared relatively unaltered. Therefore, while it is likely that Stardust particles will have undergone degrees of alteration during capture, at least some of the material within the particles will be in a relatively pristine state. So while it is likely that Stardust particles will not be as pristine in nature as IDPs there will still be significant unaltered material to investigate and compare with the current meteoritic collections.

References: [1] Brownlee D. E. et al. (2004) *Science, 304,* 1764-1769. [2] Tuzzolino A. J. et al. (2004) *Science, 304,* 1776-1780. [3] Bradley J. P. and Brownlee D. E. (1986) *Science*, 231, 1542-1544. [4] Bradley J. P. and Brownlee D. E. (1991) *Science,* 251, 549-552. [5] Bradley J. P. (2005) *Pers. Comm*. [6] Graham G. A. et al. (2001) *IJIE*, 26, 263-274. [7] Burchell M. J. et al. (1999) PSS, 47, 189-204. [8] Burchell M. J. et al. (2001) *MAPS*, 36, 209-221. [9] Okudaira K. et al. (2004) *ASR*, 34, 2299-2304. [10] Hörz F. et al. (2000) *Icarus*, 147, 559-579. [11] Borg J. et al. (2004) *LPS XXXV*, Abstract #1580. [12] Ishii H. A. et al. (2004) *LPS XXXVI*, Abstract #1387. [13] Graham G. A. et al. (2004) *LPS XXXV*, Abstract #2044. [14] Okudaira K. et al. (2005) *LPS XXXVI*, Abstract #1832. [15] Anderson W. W. and Ahrens T.J. (1994) *JGR*, 99, 2063-2071.

Acknowledgement: This work was in part performed under the auspices of the U.S. Department of Energy, National Nuclear Security Administration by the University of California and Lawrence Livermore National Laboratory under contract No.W-7405-Eng-48. This work was performed as part of the Bay Area Particle Analysis Consortium (BayPAC). GAG, JB and ZRD are supported by NASA grant NNH04AB49I and CS is supported by NASA grant NAG5-119. F. Hörz (NASA JSC) is thanked for the supplying the ODC tiles used in this study.

GEO DEBRIS AND INTERPLANETARY DUST: FLUXES AND CHARGING BEHAVIOR. A. L. Graps[1], S. F. Green[2], N. M. McBride[2], J. A. M. McDonnell[3], G. Drolshagen[4], H. Svedhem[4], K. D. Bunte[5]
[1]Institute of the Physics of Interplanetary Space (IFSI), CNR-ARTOV, Via del Fosso del Cavaliere 100, 00133 Rome, Italy. Amara.Graps@ifsi.rm.cnr.it, [2]The Open University, UK, [3]Unispace Kent, UK, [4]ESTEC, The Netherlands, [5] eta_max space, Germany

Introduction: A population of cosmic dust mixed with a population of man-made debris exists within the Earth's magnetosphere. Measurements of these provide the data samples for studies of the interplanetary dust particles that travel through our magnetosphere from the outside, and for studies of the local byproducts of our space endeavours. Even though instruments to detect natural meteoroids and space debris particles have been flown in Low Earth Orbits (LEO) and on interplanetary missions, very little information on the particle environment for Earth orbits above about 600 km altitude have been available. In particular, knowledge about particles smaller than 1 m in the geostationary (GEO) region was largely unknown before GORID [1]. In September 1996, a dust/debris detector: GORID, was launched into GEO as a piggyback instrument on the Russian Express-2 telecommunications spacecraft. The instrument began its normal operation in April 1997 and ended its mission in July 2002. The goal of this work was to use GORID's particle data to identify and separate the space debris from the interplanetary dust particles (IDPs) in GEO, to more finely determine the instrument's measurement characteristics and to derive impact fluxes. Here we present results of that study.

Clustering: Very large variations in daily event rates led to the identification of clusters of events, some of which re-occurred on consecutive days at the same local time [1,2]. They were interpreted as clouds of aluminium oxide debris resulting from the firing of solid rocket motors. Clustering of events is therefore indicative of a debris source and provides a selection criteria for statistical separation of the debris and IP populations. The mean rate for science events is 1.83 day^{-1} corresponding to an interval of 0.55 d. The distribution of times between events shows a bimodal distribution with one component peaking at about the expected "random" rate and the other with very much shorter times, indicating clustering. The limit of cluster membership is consequently defined at 0.05 days.

The temporal and charge distributions: Debris are concentrated near midnight local time except during summer. In early summer, clustered events are concentrated near 5 am, just at the time when beta-meteoroids may be expected to be detected. The GORID pointing geometry implies preferential detection of debris after recent crossing of the equatorial plane in the magnetotail. This may be because debris are physically constrained to this region or because some process in the magnetosphere, such as a charging mechanism, makes them more detectable. One possible mechanism leading to the clustered events is electrostatic fragmentation of the slag particles, after passing through the current sheet.

The detection rate and fluxes: The detection rate of interplanetary events is 0.54 d^{-1} and debris events is 2.46 d^{-1}. The fluxes of interplanetary particles are reasonably close to the well-defined model prediction, allowing for the impact speed uncertainty. The mean fluxes are 1.35×10^{-4} m^{-2} s^{-1} for IP and 6.1×10^{-4} m^{-2} s^{-1} for debris at the detection threshold of $Q_i = 1.3 \times 10^{-13}$ C. The flux of space debris detected by GORID appears to be higher than in LEO although the results are sensitive to the assumed speeds.

References:

[1] Drolshagen, G., Svedhem, H., Grün, E., Grafodatsky, O., and Prokopiev, U. (1998). "Microparticles in the Geostationary Orbit (GORID Experiment)", COSPAR 98, B0.2 – 0014. [2] Svedhem, H., Drolshagen, G. Grün, E. Grafodatsky, O. and Prokopiev, U. (2000). "New results from in-situ measurements of cosmic dust – Data from the GORID experiment", Adv. Space Res. 25, 309-314.

STARDUST WILD 2 DUST MEASUREMENTS. S. F. Green[1], N. McBride[1], M. T. S. H. Colwell[1], J. A. M. McDonnell[1], A. J. Tuzzolino[2], T. E. Economou[2], B. C. Clark[3], Z. Sekanina[4], P. Tsou[4], D. E. Brownlee[5], [1]PSSRI, The Open University, Walton Hall, Milton Keynes, MK7 6AA, UK, s.f.green@open.ac.uk, [2]Laboratory for Astrophysics and Space Research, Enrico Fermi Institute, University of Chicago, 933 East 56th St, Chicago Ill 60637, USA, [3]Jet Propulsion Laboratory, California Institute of Technology, 4800 Oak Grove Drive, Pasadena CA 91109, USA, [4]Lockheed Martin Astronautics, P.O. Box 179, MS-B0560, Denver, CO 80201, USA, [5]Astronomy Department, University of Washington, bx 351580, Seattle, WA 98195, USA.

Introduction: The Stardust Dust Flux Monitor Instrument (DFMI) detected almost 9000 dust impacts over a broad mass range of 10^{-14} to 10^{-6} kg during the 236 km flyby of comet 81P/Wild 2 on 2 January 2004. Cometary dust particles, trapped in the volatile ices of the nucleus since their formation, contain information on the conditions in the pre-solar nebula, its precursor interstellar cloud and nucleosynthetic processes in the stars from which their constituent grains originally formed. The primary objective of Stardust is to capture these samples intact and return them to the Earth for in-depth microanalysis [1]. These dust grains are the source of a major component of interplanetary dust and large (sub-mm and larger) grains are observed in cometary dust trails forming relatively long lasting meteoroid streams, which gradually dissipate into the zodiacal dust complex. Micron sized (and somewhat smaller) grains can be swept out of the inner solar system by solar radiation pressure. The contribution of comets to the total interplanetary dust complex, and the subsequent dynamics of the individual grains, are critically dependent on the dust mass (or size) distribution. Furthermore, the dust-to-gas ratio in cometary nuclei provides constraints on the conditions in the region in which it formed. DFMI provided time resolved dust fluxes and mass distributions in the inner coma of comet Wild 2 at the highest resolution yet obtained.

DFMI: The DFMI [2] combines small area but high sensitivity PVDF (polyvinylidene fluoride) sensors with two piezoelectric acoustic sensors, mounted on the first two layers of the spacecraft Whipple dust shield, to measure the flux of larger particles. The PVDF sensors each had four mass channels with thresholds from 10^{-14} kg (particle radius ~ 3 μm) to 10^{-7} kg. The front shield acoustic sensor could detect particles of mass larger than 3×10^{-11} kg (~50 μm diameter), while the second sensor detected penetrating particles of mass > 2×10^{-7} (~ 1 mm diameter).

The objectives of the Stardust Dust Flux Monitor Instrument (DFMI) were to:

1) Measure the interplanetary dust flux,
2) Determine particle fluxes during the 81P/Wild 2 flyby,
3) Determine the particle mass distribution in the coma of 81P/Wild 2,
4) Provide the context for the collected dust samples,
5) Monitor the dust environment at P/Wild 2 for spacecraft health and interpretation of anomalies.

Although an unidentified noise source prevented interplanetary cruise measurements, the instrument worked flawlessly throughout its 30 minutes of operation in the inner coma of comet Wild 2.

DFMI Encounter measurements: The first dust detections were made by the front shield acoustic sensor, 264 s before closest approach (at a cometocentric distance r = 1630 km). The event rate gradually increased up to closest approach and then decayed afterwards with a second period of high activity between +620 s (r = 3810 km) and +720 s (r = 4420 km). The last detected particle was at +922 s at a cometocentric distance of r = 5650 km [3].

The spatial distribution of dust was highly non-uniform, with short duration bursts of impacts implying localized spatial density changes of orders of magnitude on scales of less than a km [3]. Long exposure images of the comet reveal large numbers of jets projected nearly around the entire perimeter of the nucleus, many of which appear to be highly collimated, with angular sizes of a few degrees [4].

The overall mass distribution in the inner coma is dominated by the largest grains, with an average cumulative mass distribution index of $\alpha = 0.75 \pm 0.05$ (where the number of particles of mass m or larger, $N(m) \propto m^{-\alpha}$). However, the mass distribution was also highly variable during the flyby and almost 80% of the detected impacts occurred during the second period of high activity, ~4000 km from the nucleus, where small grains dominated, with $\alpha = 1.13 \pm 0.2$ [5].

Jets and Fragmentation: The detection rates are characterized by structure on timescales of seconds ('swarms' with spatial scales of 10s of km) and fractions of a second ('bursts' with spatial scales of less than 1 km) [3].

The swarms have dimensions consistent with the jets seen in the Stardust NAVCAM images. Many of the swarms can be correlated with the positions of jets [6] although definitive solutions are not possible due to lack of knowledge of the nucleus rotation rate and grain terminal velocities.

The enormous variations in dust spatial density over distances of a few hundred metres, which characterize the bursts, cannot be explained by grain dynamics within the coma, particularly as they occur outside the innermost coma, where gas drag is no longer the dominant force. Particle fragmentation provides the only viable explanation [3],[5],[7]. The bursts result from the passage of Stardust through expanding dust clouds resulting from extended fragmentation. The second period of high activity results from outgassing and/or fragmentation of a large (10s of metres diameter) boulder [6].

The interpretation of this highly structured coma as due to a combination of jets and particle fragmentation has been received with some skepticism. The evidence will be reviewed and common criticisms refuted. Comparisons with results from The P/Halley and P/Grigg-Skjellerup flybys indicate that the same processes occurred in both comets for which in-situ dust data are available and therefore may be common in comets in general.

References:

[1] Brownlee D. E. et al (2003) *JGR, 108,* SRD-1, 1-12. [2] Tuzzolino A. J. et al. (2003) *JGR, 108,* SRD-5, 1-24. [3] Tuzzolino A. J. et al. (2004) *Science*, *304*, 1776-1780. [4] Brownlee D. E. et al (2004) *Science 304*, 1764-1769. [5] Green S. F. et al. (2004) *JGR, 109,* E12SO4, 1-13. [6] Sekanina Z. et al. (2004) *Science*, *304*, 1769-1774. [7] Clark B. C. et al. (2004) *JGR*, *109*, E12SO3, 1-13.

PROSPECTS OF DUST A ASTRONOMY MISSION. E. Grün[1,2], R. Srama[1], S. Helfert[1], S. Kempf[1], G. Moragas-Klostermeyer[1], M. Rachev[1], A. Srowig[1], S. Auer[3], M. Horanyi[4], Z. Sternovsky[4], and D. Harris[2], [1]MPI-K, Heidelberg, Germany, [2]HIGP, Honolulu, USA, [3]A&M Assoc., Basye, USA, [4]LASP, Boulder, USA

Dust particles, like photons, carry information from remote sites in space and time. From knowledge of the dust particles' birthplace and their bulk properties, we can learn about the remote environment out of which the particles were formed. This approach is called "Dust Astronomy" which is carried out by means of a dust telescope on a Dust Observatory in space.

There are different types of dust particles in interplanetary space: dust from comets and asteroids and interstellar grains traversing the solar system. The most obvious sources of interplanetary dust are comets which move on highly excentric orbits through the solar sytem. A significant fraction of meteors and dust grains in the zodiacal cloud have their origin in the asteroid belt. Their orbits have low inclinations and low eccentricities which allows for a distinction from fresh cometary dust which moves on highly eccentric orbits.

Galactic dust grains passing through the planetary system have been positively identified at Jupiter's distance by the dust detector onboard the Ulysses spacecraft. Analysis of data obtained within and beyond the Earth orbit by different spacecraft (Helios, Galileo, and Cassini) show that a significant amount of ISD is at our reach. The motion of interstellar grains through the solar system is parallel to the flow of neutral interstellar hydrogen and helium gas, both traveling at a speed of 26 km/s.

So far, a clear identification of the origin of cosmic dust near Earth was not possible. Especially, the origin of Interplanetary Dust Particles (IDPs) collected in the Earth's stratosphere and extracted from Antarctic ice is still unclear. These are the only cosmic dust grains which are currently accessible for laboratory analysis. By simultaneously measuring in-situ the particles' trajectories in space and their chemical composition we will distinguish interstellar from cometary and asteroidal dust grains and obtain important cosmochemical information.

In interplanetary space the expected impact rate on dust detectors at 1 AU is low, e.g. an impact detector of 0.1 m^2 sensitive area records only about 1 particle of 10^{-13} g (0.2 μm radius) per day and 1 particle of 10^{-10} g (2 μm radius) per two weeks, respectively. Therefore, a dust telescope needs to have at least 0.1 m^2 sensitive area.

Any meteoroid in interplanetary space is electrically charged. Because of the predominance of the photoelectric effect in interplanetary space, meteoroids are usually charged at a potential U of about +5 Volts. In near-Earth environment (LEO) the low energy plasma prevails leading to dust grain potentials of about -0.5 V whereas in the highly variable high energy plasma regime at geostationary distance dust potentials from -30 V to +3 V are expected. It was Cassini's CDA [1] instrument that for the first time reliably identified this dust charge ($\geq 10^{-15}$ C corresponding to ~ 2 μm radius) in interplanetary space [2]. From the signal the speed and impact direction was determined.

Compositional analyses of cometary dust have been achieved by the dust mass analyzers, PIA and PUMA on board spaceprobes to comet Halley [3]. The instruments employed a time-of-flight mass spectrometer in order to obtain the elemental composition of the plasma generated upon impact of cometary dust particles onto the sensor. A mass resolution of $M/\Delta M > 100$ was achieved by the use of a reflectron that provided energy focusing. Because of the very high dust fluxes expected near the comet only a very small sensitive area of 5 cm^2 was necessary to obtain thousands high resolution dust mass spectra. The data collected by PIA/PUMA demonstrate that each individual event detected contains a wealth of scientific information.

The Stardust spacecraft carrying the Cometary and Interstellar Dust Analyzer instrument, CIDA, flew by comet Wild 2 in 2004. CIDA, too, is an impact mass analyzer employing a reflectron stage in order to provide high resolution ($M/\Delta M > 100$) mass spectra. The sensitive area of this instrument is 90 cm^2. CIDA provided compositional analyses of a few tens of cometary [4] and of presumably interstellar grains [5]. Krueger et al. conclude that the main constituents of interstellar grains are organic with a high oxygen and low nitrogen content.

Based on experience with current space dust instruments a novel dust telescope is being developed. It is optimized for (1) large area (0.1 to 1 m^2) impact detection and trajectory analysis of submicron-sized and larger dust grains, (2) the determination of physical properties of sub micron sized grains, such as flux, mass, speed, electrical charge, and (3) high resolution chemical analysis ($M/\Delta M \geq 100$) of cosmic dust. A plasma monitor supports the dust charge measurements.

A dust telescope is a combination of a dust trajectory sensor (Fig. 1) together with an analyzer for the

chemical composition of dust particles in space. Dust particles' trajectories are determined by the measurement of the electric signals that are induced when a charged grain flies through a position sensitive electrode system. The objective of the trajectory sensor is to measure dust charges in the range 10^{-16} to 10^{-13} C and dust speeds in the range 6 to 100 km/s. First tests with a laboratory set-up have been performed and demonstrate the expected performance. An ASIC charge sensitive amplifier and an ASIC transient recorder has been developed with a RMS noise of about 1.5 10^{-17} C.

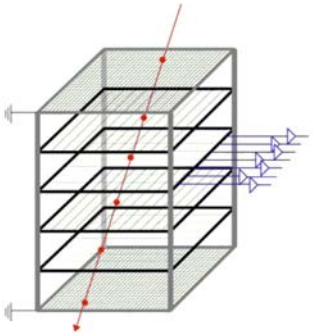

Fig. 1 Schematics of the Dust Trajectory Sensor

The dust chemical analyzers (Fig. 2) has sufficient mass resolution in order to resolve ions with atomic mass numbers up to 100. The annular impact area of the mass analyzer will be more than 0.1 m^2. The mass spectrometer consists of the target area with an acceleration grid and the single-stage reflectron consisting of two grids and the central ion detector. An ion detector of 50 to 110 mm radius is necessary to collect all generated ions. A lab model has been constructed and first dust accelerator show that a mass resolution of $M/\Delta M > 150$ can be obtained for impacts onto the target.

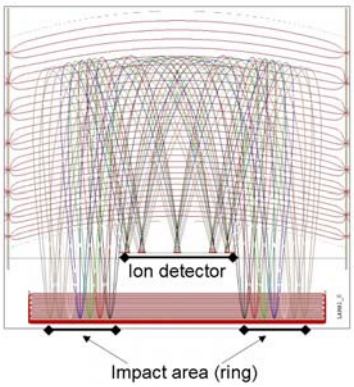

Fig. 2 Schematics of the Large-Area Mass Analyzer showing ion trajectories from different impact positions and equal potential lines.

A Dust Astronomy Mission named Cosmic DUNE is being proposed. It establishes the next logical step beyond NASA's Stardust mission, with four major advancements in cosmic dust research: (1) Analysis of the elemental and isotopic composition of individual cosmic dust grains, (2) determination of the size distribution of interstellar dust, (3) characterization of the interstellar dust flow through the planetary system, and (4) analysis of interplanetary dust of cometary and asteroidal origin.

The mission scenario and measurements requirements has been studied using the small European ConeXpress platform with solar electric propulsion for transport to an halo orbit around L2. ConeXpress is three axis stabilized and provides a pointing accuracy better than the 1°. The power demand of the instruments is largely covered by the electrical power provided by the solar arrays. The first half of the mission consists in reaching the Moon in order to prepare for a Moon flyby that, in turn, deflects the spacecraft into an orbit around the L2 point. The second half of the mission scenario consists in a Moon flyby, preparing the insertion of the spacecraft into a Halo orbit around L2.

Cosmic DUNE is well suited to investigate the micro meteoroid environment in interplanetary space or in the near-Earth environment. For the first time, this instrument will allow us the in-situ analysis of the properties of micron sized particles together with the identification of its source. Cosmic DUNE will prepare the way for effective collection in near-Earth space of interstellar and interplanetary dust for subsequent return to Earth and analysis in laboratories.

[1] Srama, R., et al., 2004b, ESA-SP 543, 73-78. [2] Kempf, S., et al., 2004, Icarus, 171, 317-335. [3] Kissel, et al., 1986, Nature 321, 336-338. [4] Kissel, J., Krueger, F.R., Silen, J., Clark, B.C., Science, 304, 1774-1776, 2004. [5] Krueger F. R. et al., Rapid Comm. Mass Spectrom. 18, 103 (2004).

DUST PARTICLES DETECTED IN THE OUTER SOLAR SYSTEM BY VOYAGER 1 AND 2.

D. A. Gurnett, Z. Z. Wang, A. M. Persoon, and W. S. Kurth (University of Iowa, Dept. of Physics and Astronomy, Iowa City, IA 52242, USA; donald-gurnett@uiowa.edu)

In this paper we report PWS observation of dust impacts detected in the outer solar system by the Voyager 1 and 2 plasma wave instruments. During the Voyager 1 and 2 flybys of the outer planets, it was discovered that the plasma wave (PWS) instrument could detect small micron-sized particles striking the spacecraft. When a small particle strikes the spacecraft at a high velocity, the particle is instantly vaporized and heated to a very high temperature, typically 10^4 K, or more. At this high temperature a substantial fraction of the gas is ionized. As the resulting plasma cloud sweeps over the PWS electric antenna, it produces a voltage pulse on the antenna. By counting the number of pulses per unit time, the impact rate can be determined.

An example of a dust impact detected by Voyager 2 at a heliocentric radial distance of 53.62 AU (Astronomical Units) is shown in Figure 1. Typically the voltage pulse detected on the antenna consists of an abrupt step with a rise time of a few tens of microseconds followed by complicated recovery waveform lasting several milliseconds.

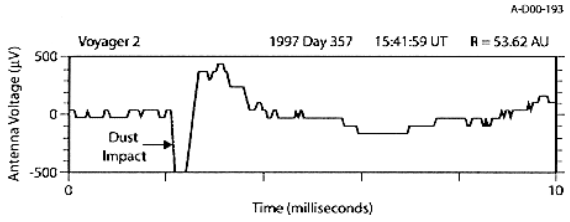

Figure 1. A dust impact detected by the Voyager 1 plasma wave instrument at a heliocentric radial distance of 53.62 AU.

The waveforms detected in interplanetary space are very similar to the waveforms detected at the Saturn ring plane crossings, which are believed to be due to micron-sized particles. After eliminating dust impacts detected during the flybys of the outer planets, the impact rates detected by Voyagers 1 and 2 are found to be nearly constant, approximately 4 impacts per hour for Voyager 1, and 5 impacts per hour for Voyager 2, after correcting for the observation duty cycle. Plots of the impact rates detected by Voyagers 1 and 2 are shown in Figures 2 and 3, respectively.

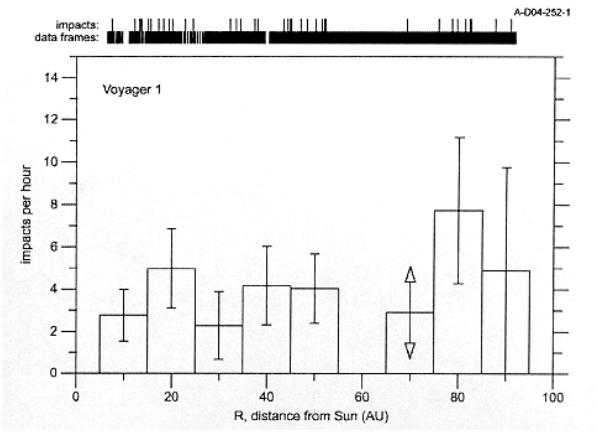

Figure 2. The dust impact rate detected by the plasma wave instrument on Voyager 1

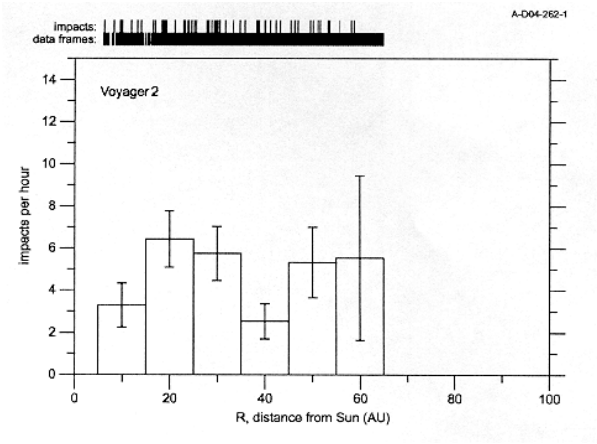

Figure 3. The dust impact rate detected by the plasma wave instrument on Voyager 2.

The impact rates shown in Figures 2 and 3 appear to be completely independent of the heliocentric radial distance of the spacecraft. Voyager 1 is currently at a heliocentric radial distance of 96.1 AU, and Voyager 2 is at 77.0 AU. Because of a failure of the wideband receiver on Voyager 2, the ability to measure dust impacts on that spacecraft ended at a distance of about 64 AU. The impact rates also do not depend on ecliptic latitude or longitude, although the date coverage for these two parameters is much more limited than for heliocentric radial distance.

If we assume that the spacecraft is effectively sweeping up the particles, we can make a rough estimate of the number density of the impacting particles by using the formula n = R/UA, where R is the impact rate, A is the cross-sectional area of the spacecraft, and U is the heliocentric speed of the spacecraft. Using A = 1.66 m^2, which is our best estimate of the effective area of the spacecraft for detecting dust impacts, and U = 18 km s^{-1}, which is a typical spacecraft velocity, the average number density works out to be about 4 x 10^{-8} m^3. The mass of the impacting particles is more difficult to estimate, but is believed to be on the order of 10^{-10} to 10^{-11}g (i.e., in the micron size range), mainly because the impacts have waveforms very similar to those observed near Saturn's ring plane which are thought to be due to micron-sized particles. The absence of significant latitudinal or radial gradients suggests that the particles probably do not originate from planetary rings, moons, or asteroids. Most likely they are of interstellar origin, or possibly from objects orbiting the Sun at great distances, such as comets. Dust originating from Kuiper belt objects, which are confined relatively close to the ecliptic plane, can probably be ruled out because the impact rate does not show any dependence on distance above or below the ecliptic plane out to at least z = 50 AU. We have also looked for evidence of dust streams, such as might be related to comet trails, and none were found. The time interval between impacts has a good fit to a Poisson distribution, indicating a purely random distribution.

SCATTERING BY "BIRD'S-NEST" –TYPE MATERIAL AND LARGE DUST AGGREGATES: MICROWAVE ANALOGUE MEASUREMENTS. B. Å. S. Gustafson[1] and A. J. Espy[1], [1]Department of Astronomy, University of Florida, Gainesville, Florida 32611, USA.

Introduction: Planetesimals in the outer parts of the solar system, beyond the ice-line, are now known as comet nuclei and Kuiperbelt objects. These are believed by many to preserve solids that predate the solar system, solids that formerly were interstellar grains[1]. These grains brought the matter that the solar system is made of to the solar nebula and are our solar system's link to the stars that predates it. Evidence for how these grains grow into aggregates (ballistic or cluster-cluster, randomly oriented or aligned, with volatile solids preserved or evaporated, etc…) is possibly still preserved in the very morphology of comet nuclei and Kuiperbelt objects on the scale of tens to hundreds of micron. This structure may be exposed in dusty comet comae and dust tails as sunlight strikes grains shed by comet nuclei or it may be exposed as objects collide creating what has become known as dust bands in the Zodiacal cloud.

Objective: Our long-term objective is to extract statistically significant information on this structure from bodies across the Kuiperbelt, among comets and primitive type asteroids. A step along the way is the search for optical properties that differentiate between relevant particle morphologies and might be observable. Work on extraction of scattering properties by complex grains with morphologies similar to the "Bird's-Nest" structure[2] has long been part of theoretical and experimental efforts in our group at the University of Florida and by several other researchers. Earlier work has however been confined either to smaller grains, simpler structures, or both. This limitation to theoretical works is because the complexity of the scattering body and most severely affects large structures. Experimental works using optical light is limited by control over the experiment while the size of the analogue models used in experiments scaled to microwave frequencies usually is the limitation. This was a formal limitation in the famous microwave laboratories built by Greenberg et al. in New England respectively Giese et al. in Germany. This limitation was overcome in the present microwave laboratory at the University of Florida due primarily to the antenna design. However the challenge to build large models involving thousands or tens of thousands of individual particles was not previously overcome.

Results: We will present results for aggregates of spheres where each sphere represents a grain grown by condensation in the outflow from red giant stars or from supernovae. These oldest of solids are believed to be amorphous refractories with amorphous organic refractory mantles and therefore to grow at equal rates in all directions. This should lead to equidimensional growths of size in the 0.1 micron range that we represent by spheres. These can be homogeneous since the refractive index of both core and mantle is believed to be in the 1.7 to 1.8 range in real part and to have an imaginary part in the 0.01 range or less[3]. This means that although the chemical composition is different in the core and mantle, the optical properties of the core and mantle materials are the same to within the range of uncertainties and may thus be represented by a single analogue material that has the appropriate refractive index at the laboratory set of frequencies. We represent the classical size interstellar grains by sets of two or three spheres since they are known to be elongated with 2:1 to 3:1 aspect ratios. This property of grain elongation (and alignment) is evident from interstellar polarization, a linear polarization in extinction. Ices with inclusions of smaller grains are believed to form a second mantle on dust in the molecular clouds and the nebulae from which planetary systems form. These dirty ice mantles played an important role in determining the packing in grain aggregates that formed in the outer parts of the solar system where the ice mantles survive nebula heating from contraction. Analogue models of ice-less aggregates containing a few thousand spheres have been built by first joining spheres in sets of two or three and then by stacking these together in a manner that simulates ballistic aggregation taking the ice mantle into account. These have then been joined together to form successively larger models. This means that we simulate aggregates that once grow from grains that had ice mantles. The ice later sublimated as the material heated up causing the release of the dust aggregates and surely caused many aggregates to break into pieces. The ice sublimating away is believed to leave behind the low packing aggregates with approximately 90% void that we have simulated in our models. These are larger although in many ways similar to earlier "Bird's-Nest" models but we emphasize that since these are break-up products, they are not likely to retain the overall fractal dimension character that is so well established a characteristic of growing aggregates. The models we made are therefore of approximately equal packing throughout. Some aggregates however, have multiple centers with denser packing corresponding to the central parts of aggregates that formerly existed as separate aggre-

gates (Figure 1). The growth process we simulate has these formerly separate aggregates colliding and sticking together in a cluster-cluster aggregation process.

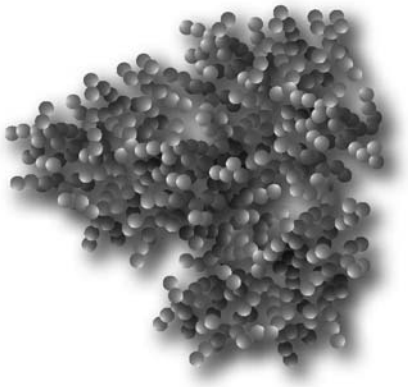

Figure 1) Sample aggregate based on irregular grain distribution and the packing of the refractory materials of 10% in an ensemble whose morphology or structure depends strongly on the scale and the corresponding growth regime

The aggregates are similar to the original "Bird-Nest" structures by Greenberg and Gustafson[2] in that they have approximately 10% packing (90% void). The major differences from the earlier model are in the size of the aggregates and the fact that there are multiple centers of higher packing density corresponding to aggregates grown in a ballistic process and then as cluster-cluster aggregation. The aggregates simulate parts of a large body (comet nucleus or Kuiper belt object) that has broken off and therefore has no low packing outer parts or protruding linear growths. The mass depends on the linear dimension cubed and therefore has a whole rather than fractal dimension. These aggregates are also not fractals since their structure is scale dependent. There are specific growth regimes that dominate depending on the scale. Condensation occurs on the 0.1 micron scale and below, ballistic aggregation on the scale of a few microns and cluster-cluster aggregation on larger scales.

We find that polarization, color and angular brightness distributions all depend on the specific packing but uniqueness is a more difficult issue. We discuss ways in which scattering properties might be used to recognize the specific structures we have modeled. Specifically we address how this might be used to recognize if the parent body generating the observed dust had differentiated by the time of the dust release. If the parent body is fund not to be differentiated, we like to know on what scale cluster-cluster aggregation took place.

Acknowledgements: The authors gratefully acknowledge Mr. Michael Pavel for his assistance in the laboratory. This work is supported by NASA through its Planetary Atmospheres Program.

References: 1) Grün, Gustafson, Dermott, and Fechtig, Eds., "Interplanetary Dust", Springer Verlag, pp. 509-567, (2001).
2) Greenberg, J.M., and B.Å.S. Gustafson, "A Comet Fragment Model for Zodiacal Light Particles", *Astron. Astrophys.*, **93,** pp. 35-42 (1981).
3) Gustafson B.Å.S., J.M. Greenberg, L. Kolokolova, R. Stognienko, and Y.-l. Xu. "Scattering Theory and Laboratory Simulations", in "Interplanetary Dust", (Grün, Gustafson, Dermott, and Fechtig, Eds.) Springer Verlag, pp. 509-567, (2001).

Ring Plane Crossings with the Cassini CDA Instrument: Saturation Analysis and Deadtime Correction.

S. Helfert[1] [1]Max-Planck-Institut für Kernphysik, Saupfercheckweg 1, 69117 Heidelberg, Germany. Stefan.Helfert@mpi-hd.mpg.de

CDA Instrument: The Cosmic Dust Analyzer[1] onboard Cassini comprises two distinct instruments: the Dust Analyzer (DA) and the High Rate Detector (HRD). The HRD is capable of counting thousands of impacts per second on its PVDF foils, whereas the DA instrument was designed to process about one impact event per second. The DA event processing consists of recording up to 2000 digital values for each of the 4 entrance channels and the Time-of-Flight mass spectrometer, computing key parameters, counting and classifying the event and filtering, compressing, and storing the raw data until delivery to the spacecraft Solid State Recorder.

Sensitivity: Early cruise measurements and the Jupiter Flyby already demonstrated that the sensitivity of the DA instrument exceeded the design criteria. The detection of Saturnian stream particles already at a distance of 1100 R_S was an additional result. Inside the saturnian system, during Ring Plane Crossings, the DA instrument is in saturation for prolonged periods of time. During these hour-long periods the DA is analyzing only a fraction of the incoming particles, so no count rates can be derived. Due to the high mass threshold of the HRD instrument, HRD cannot fill in the count rates for the dust environment that CDA is exposed to.

Instrument Dead Time Variation: One of the design criteria for the DA instrument was that the dead time between measurements should be within a one-second range and be independent of the processing complexity for the previous recorded event. To accomplish this, the dead time calculation was tied to a slow (8 Hz) periodic interrupt. Due to the discrete effects of this design, the variation of the dead time is of the order of 125 ms. To improve analysis of the DA count rates also during saturation phases, the dead time algorithm is upgraded in the current development Flight Software version. In this new version the DA dead time and the time between the opening of the measurement channels and the event trigger (live time) are measured and stored on a millisecond basis.

Laboratory Results: First ground test results from implementing this modification will be presented. A preliminary dead time correction for previous saturation phases will be demonstrated.

Enhancing Dead Time Correction: The lab tests and on-board data collected during saturation phases in Ring Plane Crossings in 2006 will be used for enhancement of the Dead Time correction for the rate[2]:

$$r_{corr} = \frac{r}{1 - r \cdot \tau}$$

Summary: Measuring, storing, and downlinking the instrument dead and live times in higher resolution should lead to accurate number density values even in periods of saturation.

References:

[1] Srama, R. et al.(2004) *Space Science Reviews 114, 465-518*, The Cassini Cosmic Dust Analyzer.

[2] Horanyi, M., Grün, E. (2005) private comm.

MODELLING ION BEHAVIOUR IN THE CASSINI COSMIC DUST ANALYSER. Jon K. Hillier[1], N. McBride[1] and S. F. Green[1].
[1]Planetary and Space Sciences Research Institute, The Open University, Milton Keynes, MK7 6AA, UK, j.k.hillier@open.ac.uk.

Interpreting the time of flight (TOF) mass spectra produced by the Cosmic Dust Analyser (CDA) on the Cassini spacecraft requires accurately identifying which ion species contribute to which spectral peaks. The relationship $t = a\sqrt{m}+b$ (t: time, a:stretch parameter relating to instrument field strengths, m:ion mass and b:zeropoint offset), usually used for calibrating TOF mass spectra is complicated in the CDA as the instrument does not perform any ion energy discrimination (such as that obtained by using a reflectron). The resulting spread in ion energies (and hence arrival times) tends to broaden and/or merge individual peaks, with plasma shielding, ion trajectory path length differences and field strength changes further affecting the spectra.

Hypervelocity dust impacts using a Van de Graaff generator to accelerate dust in the laboratory can be used to investigate the plasma (and spectra) produced by particles with a limited range of compositions, masses and velocities but this approach is unable to recreate the range of impact characteristics observed by CDA *in-situ*.

In this paper we present initial results from spectral modelling using the CDACAD numerical simulation software. This software uses the velocity verlet algorithm to simulate ion trajectories within the CDA instrument, allowing spectra to be created from impact plasmas of arbitrary composition with arbitrary initial velocity distributions. All of the CDA channels are simulated, at instrument-accurate sampling rates, allowing not only spectra to be recreated but also an estimation of ion losses to other parts of the instrument to be made. We present simulated fits to a variety of different types of flight spectra and comment on the implications for the impact plasma conditions.

SUBARU/COMICS OBSERVATIONS OF COMETARY DUST AND DUST AROUND YOUNG STARS

M. Honda[1] and COMICS team, [1]Institute for Space and Astronautical Science / JAXA (3-1-1 Yoshinodai, Sagamihara, Kanagawa, 229-8510, Japan; hondamt@ir.isas.jaxa.jp) .

Introduction: Crystalline silicate which is often found toward dust in Oort cloud comets (OCs) is supposed as a probe of thermal history of silicate dust. Since silicate dust in the interstellar matter (starting material) is completely amorphous [1], presence of crystalline silicate dust in OCs indicate that initially amorphous silicate dust must have experienced heating process which resulted in silicate dust crystallization. To understand when and how dust processing occurred at the early stage of solar-system / exo-planetary system formation, we investigated properties of dust around young stars (especially low-mass young stars which is similar to our Sun). Furthermore, to investigate how efficiently radial mixing have occured in the solar-nebula, we observed dust from Edgeworth-Kuiper Belt comets (EKBCs) which may be formed at more distant region than OCs.

Observations: We made mid-infrared low-resolution spectroscopic observations (R~250) of cometary dust and dust around young stars using the mid-infrared instruments COMICS [2,3] on 8.2m Subaru Telescope. We also made imaging observations at 8.8μm and 12.4μm to estimate absolute flux. Observations of standard stars for flux calibration and atmospheric absorption correction are also made before and/or after observation of the target.

Results: A 10μm silicate emission feature is frequently seen toward low-mass young stars and also toward EKBCs with signatures of not only amorphous silicate but also crystalline silicate. We derived fraction of crystalline silicate by fitting the model spectrum to the observed spectrum. Based on our analysis, we found following things. 1) Crystalline silicate dust around young stars seems to be formed at very early stage of star formation (~1 Myr or earlier). 2) Crystalline silicate is also found toward cometary dust from EKBCs, indicating that radial transportation of crystalline silicate dust toward outer solar nebula is very efficient.

References: [1] Kemper, F. et al. (2004) *ApJ, 609* , 826. [2] Kataza H. et al. (2000) *SPIE, 4008*, 1144. [3] Okamoto Y. J. et al. (2003) *SPIE, 4841*, 169.

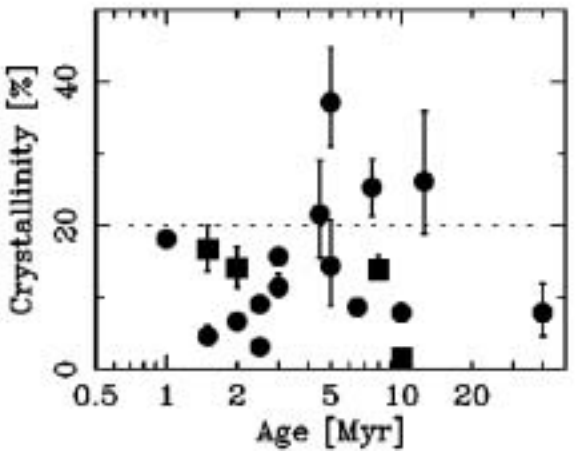

Figure 1: Fraction of crystalline silicate dust derived from model fitting to the silicate feature in 10 μm spectra of T Tauri stars against stellar age. Stellar age is estimated by comparison with theoretical evolutionary tracks in HR diagrams (Siess et al. 2000). Even at very young stage (~1 Myr) about ~20% of silicate dust appear in the form of crystalline silicate indicating that crystalline silicate formation occurs at the very early stage.

Dust Plasma Interactions in Planetary Rings

Mihály Horányi

Laboratory for Atmospheric and Space Physics, and Department of Physics, University of Colorado, Boulder, Colorado 80309-0392, USA

Planetary rings are our best examples of environments where dusty plasma effects can establish the size and spatial distributions of small grains. Simultaneously, dust often influences the composition, density and temperature of the plasma surrounding it. The dynamics of charged dust particles can be surprisingly complex and fundamentally different from the well understood limits of gravitationally dominated motions of neutral particles, or the adiabatic motion of electrons and ions in electromagnetic fields that dominate gravity [1].

This talk will focus on recent Cassini observations at Saturn that are best explained by theories describing the effects of the magnetospheric fields and plasmas on the rings. We will compare the theoretical model predictions with in situ and remote sensing observations of the E-ring. We also discuss the physics describing the formation of the `spokes' and their apparent lack to date in the Cassini images.

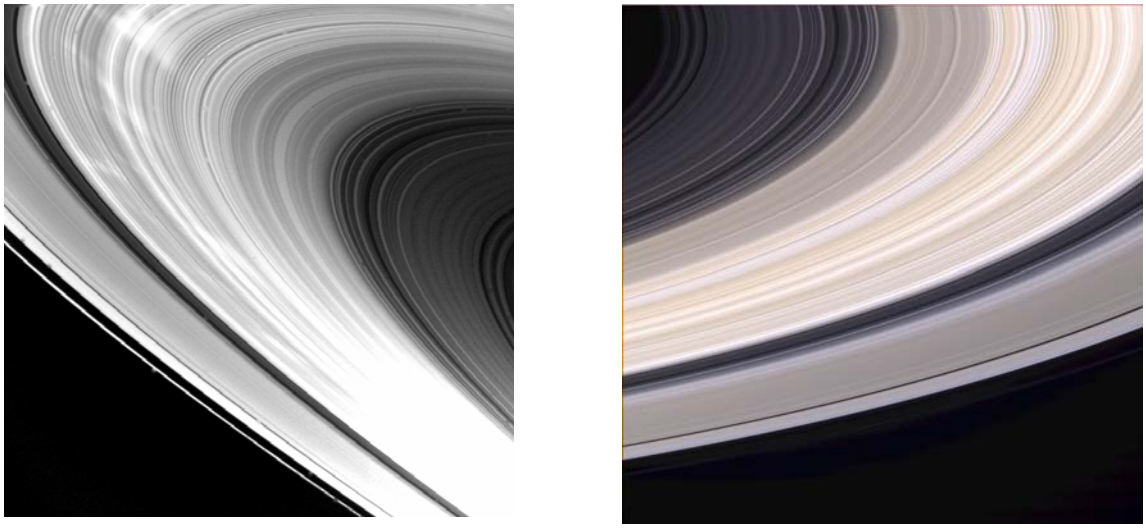

Fig.1 Images of Saturn's main rings taken by the Voyager (left) and Cassini (right) spacecraft. Voyager observed bright radial features that intermittently appeared above the rings. Cassini did not find these during its first year in orbit around Saturn.

[1] M. Horányi, T. W. Hartquist, O. Havnes, D. A. Mendis and G. E. Morfill, Dusty Plasma Effects in Saturn's Magnetosphere, Reviews of Geophysics, 42, RG4002, 2004

MIGRATION OF DUST PARTICLES TO THE TERRESTRIAL PLANETS. S. I. Ipatov, *University of Maryland, USA (siipatov@mail333.com)*, J. C. Mather, *NASA/GSFC, Greenbelt, MD, USA*.

Introduction: There are a lot of papers on migration of dust (see references in [1-2]). In contrast to papers by other scientists, we study the orbital evolution of dust particles for a wider range of masses of asteroidal and cometary particles and consider also migration of dust particles produced by comets 10P and 39P.

Model: We integrated [1-2] the orbital evolution of about 12,000 asteroidal, cometary, and trans-Neptunian dust particles under the gravitational influence of planets, the Poynting-Robertson drag, radiation pressure, and solar wind drag, varying the values of the ratio β between the radiation pressure force and the gravitational force from $\leq$0.0004 to 0.4 (for silicates, such values correspond to particle diameters between $\geq$1000 and 1 microns). The considered cometary particles started from comets 2P, 10P, and 39P. A few hundred of particles were considered in each run. In our runs orbital elements were stored with a step of d_t of $\leq$20 yr for asteroidal and cometary particles and 100 yr for trans-Neptunian particles. The planets were assumed to be material points; however, using orbital elements obtained with a step d_t, we calculated the mean collision probability of a particle with the planet during the particle lifetime P=P_Σ/N, where P_Σ is the probability for all N considered particles. The relative error per integration step less than 10^{-8} was adopted. The integration continued until all of the particles either collided with the Sun or reached 2000 AU from the Sun.

Collision probabilities of dust particles with planets: The probability P of a collision of an asteroidal dust particle with the Earth was found [2] to have a maximum ($\sim$0.001-0.02) at 0.002$\leq\beta\leq$0.01, i.e., at diameters of particles $d\sim$100 μm. This is in accordance with cratering records in the lunar soil and also with particles record on the panels of the Long Duration Exposure Facility, which showed that the mass distribution of dust particles encountering Earth peaks at d=200 μm. At β>0.01 collision probabilities of asteroidal particles with the terrestrial planets decreased with growing β. For Venus these probabilities didn't differ much from those for Earth, whereas for Mars they were by an order of magnitude smaller at $\beta\geq$0.01 compared to Earth, and nearly similar to those for Earth at $\beta\sim$0.0004-0.001.

Collision probability P of a particle started from Comet 10P with a terrestrial planet sometimes differed by a factor of several from that for an asteroidal particle of the same size. In turn, for Comet 2P dust debris, the P values were found usually smaller than for asteroidal and 10P particles: for Earth at 0.002$\leq\beta\leq$0.01, P was by an order of magnitude smaller for 2P particles than for asteroid particles. For 2P particles at some β, P is by a factor of 2 or 4 greater for Venus than for Earth.

For trans-Neptunian and 39P particles, maximum values of the probability of collisions with the Sun (0.2-0.3) were reached at 0.05$\leq\beta\leq$0.1. For $\beta\geq$0.05, the fraction of trans-Neptunian particles collided with the Sun was less than that of asteroidal particles by a factor of 4-6.

Probabilities of collisions of trans-Neptunian particles with Earth and Venus at 0.01$\leq\beta\leq$0.2 were $\sim(0.3-4)\cdot10^{-4}$ and were usually less than those for asteroidal particles by a factor of less than 4. The ratio of values of time T during which a particle has perihelion less than 1 AU for asteroidal particles to the values of T for trans-Neptunian particles was about 3-7 at $\beta\geq$0.1 and about 20 at β=0.05. The mean values e_m and i_m of eccentricities and inclinations at distance R=1 AU from the Sun were mainly greater for trans-Neptunian particles than those for asteroidal particles. Nevertheless, the ratio P/T was greater for trans-Neptunian particles. It may be caused by that perihelia or aphelia of migrating trans-Neptunian particles more often were close to the orbit of the Earth, or the fraction of Earth-crossing trans-Neptunian particles with small e and i was greater (though e_m and i_m were greater) than for asteroidal particles.

Probabilities P_E of collisions of trans-Neptunian and 39P dust particles with the Earth were usually smaller by a factor of several or more than those for asteroidal and 10P particles of the same size. At β=0.0001 one 39P particle moved in an Earth-crossing orbit located inside Jupiter's orbit for 6 millions of years, and the values of P and T for this run were much greater than those for other 39P runs. For 39P particles greater than 1000 μm, one need to consider many thousands of particles in order to get reliable statistics because for such runs the probability of a collision of one particle with the terrestrial planets can be greater than the total probability of collisions of thousands other particles. Comet 39P is located outside Jupiter's orbit ($a\approx$7 AU), and studies of the orbital evolution of dust particles produced by this comet help to better understand migration of trans-Neptunian particles to the terrestrial planets at small β. At 0.01$\leq\beta\leq$0.2 the values of P_E for trans-Neptunian dust particles were similar to those for 39P particles ($\sim10^{-4}$), but the times in Earth-crossing orbits for trans-Neptunian particles were smaller by a factor of several than those for 39P particles. Due to

a small fraction of large (>1000 μm) particles that can move in Earth-crossing orbits for a long time, it may be possible that the probability of a collision of such trans-Neptunian particle with the Earth can be of the same order of magnitude as that for d<50 μm, but much more runs are needed for accurate estimates.

Interstellar particles can be effective in destruction of trans-Neptunian dust particles through collisions, especially with grains between 9 μm and 50 μm, as it is argued in [3]. Larger particles may survive because interstellar grains are too small to destroy them in a single impact. Since the total mass of the trans-Neptunian belt exceeds that of the asteroid belt by more than two orders of magnitude, and the derived in our model mean residence times ratio in orbits with perihelion distance q<1 AU for asteroid and trans-Neptunian particles is less than 20 at $\beta\geq$0.05, then for $d\sim$1-10 μm the fraction of trans-Neptunian dust of the overall dust population can be significant even at R<3 AU.

Distribution of migrating dust particles: Based on our runs, we studied [2] the distribution of spatial density n_s (i.e., the number of particles per unit of volume) near ecliptic over distance R from the Sun. For asteroidal particles, n_s quickly decreases with an increase of R. So asteroidal dust particles cannot explain the constant spatial density of dust particles at $R\sim$3-18 AU. At such distances, many of the dust particles could have come from the trans-Neptunian belt and from comets. In our runs at $\beta\geq$0.05, spatial density n_s of trans-Neptunian particles near ecliptic at R=1 AU was greater than at R>1 AU. At 0.1$\leq\beta\leq$0.4 and 2<R<45 AU (at β=0.05 for 11<R<50 AU) for trans-Neptunian particles, n_s varied with R by less than a factor of 4, but at R=5 AU it was smaller by at least a factor of 2 than at 15 AU.

Velocities of dust particles: Ipatov et al. [4-5] studied how the solar spectrum is changed by scattering by dust particles. Positions of particles were taken from the runs of migration of dust particles. For each such stored position, we calculated many ($\sim10^2$-10^4 depending on a run) different positions of a particle and the Earth during the period P_{rev} of revolution of the particle around the Sun, considering that orbital elements do not vary during P_{rev}. Three different scattering functions were considered [2]. For each considered position, we calculated velocities of a dust particle relative to the Sun and the Earth and used these velocities and the scattering function for construction of the solar spectrum received at the Earth after been scattering by different particles located at some beam (line of sight) from the Earth. The direction of the beam is characterized by elongation ϵ and inclination i. Particles in the cone of 2° around this direction were considered. In each run, particles of the same size (at the same β) and the same source (i.e., asteroidal) were studied. Ipatov et al. [5] and Madsen et al. [6] compared the rotation curves, i.e., plots of velocities of Mg I line (at zero inclination) versus elongations ε (measured eastward from the Sun), with the observational plots obtained by Reynolds et al. [7]. The rotation curves obtained for different considered scattering functions were similar for 30°<ε<330°, the difference was greater for more close direction to the Sun. The difference between different plots for different sources of dust was maximum at ε between 90° and 120°. In our opinion, the main conclusion of the comparison of such curves is that asteroidal dust doesn't dominate in the zodiacal light and a lot of zodiacal dust particles were produced by high eccentricity comets (such as comet 2P Encke). Significant contribution of cometary dust was considered by several other authors. For example, based on cratering rates from an ensemble of Earth- and Lunar-orbiting satellites, Zook [8] estimated that the cometary contribution to the near-Earth flux of particles is ~75%.

Conclusions: Probabilities of collisions of migrating asteroidal and cometary dust particles with the terrestrial planets during the lifetimes of these particles were maximum at diameter $d\sim$100 μm, which is in accordance with the analysis of microcraters.

Cometary dust particles (produced both inside and outside Jupiter's orbit) are needed to explain the constant spatial density of dust particles at 3-18 AU. The spatial density of migrating trans-Neptunian particles near Jupiter's orbit is smaller by a factor of several than that beyond Saturn's orbit. Only a small fraction of asteroidal particles can get outside Jupiter's orbit.

Comparison of velocities of particles obtained in our runs with the results of observations also show that only asteroidal dust particles cannot explain these observations, and particles produced by high-eccentricity comets (such as Comet Encke) are needed for such explanation.

Several our recent papers are presented on astro-ph.

References: [1] Ipatov S. I., Mather J. C., and Taylor P. (2004) *Annals of the New York Acad. of Sciences, 1017*, 66-80. [2] Ipatov S. I. and Mather J. C. (2005) *Advances in Space Research*, in press. [3] Liou J.-C., Zook H. A., Dermott S. F. (1996) *Icarus, 124*, 429-440. [4] Ipatov S. I. et al. (2005) *LPSC XXXV*, abstract #1266. [5] Ipatov S. I. et al. (2005) *BAAS*, late abstracts of AAS 206 Meeting, #449, in press. [6] Madsen G. J. et al. (2005) *this abstract book*. [7] Reynolds R. J., Madsen G. J., Moseley S. H. (2004) *Astrophys. J., 612*, 1206-1213. [8] Zook H. A. (2001) in: Peucker-Ehrenbrink, B. and Schmitz, B. (Eds.) *Accretion of extraterrestrial matter throughout Earth's history*, Kluwer, New York, 75-92.

SYNCHROTRON X-RAY FLUORESCENCE ANALYSIS OF DUST PARTICLES. H. A. Ishii[1], K. Luening[2], S. Brennan[2], P. Pianetta[2], G. Matrajt[3] and J. P. Bradley[1], [1]Institute for Geophysics and Planetary Physics, Lawrence Livermore National Laboratory, Livermore, CA 94550, USA (hope.ishii@llnl.gov), [2]Stanford Synchrotron Radiation Laboratory, Stanford Linear Accelerator Center, Stanford, CA 94025, USA (brennan@stanford.edu), [3]Department of Astronomy, University of Washington, Seattle, WA 98195.

Introduction: Synchrotron x-ray fluorescence (SXRF) studies carried out on a microprobe endstation allow non-destructive analysis of both major and trace element abundances in particles only microns in size. The technique has been applied to IDPs captured in the stratosphere to study atmospheric entry effects such as stratospheric contamination and frictional heating [1, 2]. SXRF will also be applied to the analysis of samples from NASA's Stardust mission [3] returning to Earth in January of 2006 with cometary dust particles captured in silica aerogel collectors during its flyby of the comet Wild-2. For Stardust particles, as for IDPs, trace element analysis of volatiles may provide an indication of the degree of thermal processing during capture in the aerogel collectors. Assuming negligible processing, trace elements can be used to study petrogenetic relationships between Stardust particles and other known extraterrestrial materials. In general, analysis of trace element abundances in extraterrestrial materials is highly relevant because variations in concentration patterns of these elements may act as signatures for origin and conditions of formation of the carrier mineral phases [4].

A number of challenges must be overcome for trace element studies by SXRF: sample preparation, contamination, choice of sample mount, potential for sample damage in the x-ray beam and positional stability of the beam on the sample. IDP SXRF studies to date offer only limited discussion of experimental setup and analytical limitations. We discuss here the experimental requirements for obtaining high quality SXRF data on small particles for trace element analysis and our progress in achieving this goal.

Experimental Methods: We collected SXRF data from several chondritic porous IDPs on a scanning fluorescence microprobe endstation currently being commissioned on Beamline 6-2 at the Stanford Synchrotron Radiation Laboratory (SSRL). The final focus is provided by a Kirkpatrick-Baez mirror pair capable of focusing monochromatic x-rays into a micron-sized spot. The current non-optimized photon flux for a ~3 μm spot is ~$5x10^8$ photons/s, and the x-ray energy range extends past the Br K absorption edge. We have previously demonstrated SXRF mapping of major elements at low and high spatial resolutions [5]. For this early trace element work during endstation commissioning, there was unusual beam motion at the source, and we used a ~10 μm spot size to encompass entire IDP particles and sections. In future work, we will combine trace element mapping with TEM imaging and EDS analysis as discussed below.

Experimental Requirements and Results: To obtain the best quality SXRF data on small particles, we want no sample damage and high sample stability with no extraneous fluorescence to obscure peaks of interest and reduce signal-to-noise ratios.

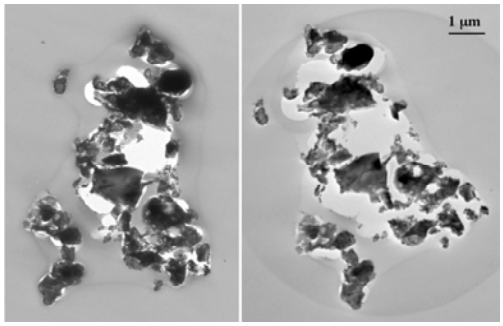

Fig. 1: Evidence of ozone damage without a He environment: Bright field TEM images of a 200 nm section of IDP W7154I1 before (left) and after (right) 7 hours of x-ray irradiation.

Damage to the sample by x-rays. In an initial estimation of particle heating in the beam, a microthermocouple (35 micron welded bead) showed a rise of only 0.5°C before stabilizing in temperature in the x-ray beam. In addition, a 200 nm thick TEM section of a chondritic porous IDP was scanned in the x-ray beam for 7 hours with a 3 μm spot. TEM analysis before and after x-ray irradiation showed no evidence of structural or chemical changes due to heating in the x-ray beam. (Sample heating will be reevaluated with the final optimized photon flux.) There is clear evidence of attack by ozone formed by x-rays interacting with air. Ozone etches the sample, especially organics like the embedding epoxy, particularly near voids (Figure 1). We subsequently employed a He "shower", a gentle flow of He over the sample and most of the beam path to the detector to eliminate ozone damage by excluding air. This has the important advantage of greatly reducing the Ar fluorescence and improving detection of low Z elements such as Na, Al and Mg.

Sample mounting. Mounting is a critical challenge for particle sizes on the order of 10 μm. We require excellent positional stability since sample motion, due to mechanical or thermal instability, results in the x-ray beam wandering on the sample or off the sample completely. We collected spectra from two forms of samples: thin sections and whole IDPs.

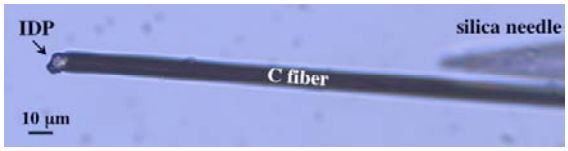

Fig. 2: An IDP (L2005AN6) mounted atop a C fiber attached to a silica needle (tip visible in background).

For bulk analysis of whole, intact IDPs, a 10 μm diameter C fiber was glued to the end of a 1 mm diameter silica needle leaving 100-200 μm of fiber extending from the end of the needle. Each IDP was mounted by micromanipulator on the end of the C fiber with a tiny amount of partially-cured embedding epoxy (Figure 2). These mounts proved highly stable and presented the particle to the x-rays free of any substrate. For whole IDPs, 13.5 keV incident x-rays accessed trace elements up to Br. Figure 3 shows the SXRF spectrum (unprocessed) of a mounted IDP.

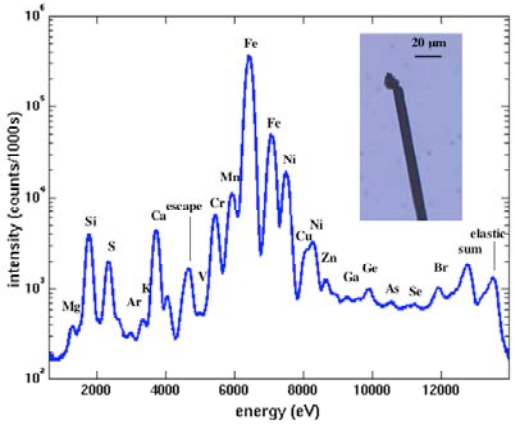

Fig. 3: SXRF spectrum from a whole chondritic porous IDP L2005AN5 mounted on a C fiber.

Microtomed particle thin sections allow correlation of SXRF and TEM data. In this way, local trace element abundances in particles can be correlated with local mineralogy to gain insight into particle origins and processing. IDP sections were precision-centered in 400 μm aperture Cu TEM grids on C/Formvar substrates using a method developed in the cosmic dust lab at U. of Washington (Brownlee). To avoid exciting fluorescence from the grid, spectra from thin sections were collected ~200 eV below the Cu K edge at 8780 eV. Due to overlap of the Cu Kα resonant Raman scattering peak (~940 eV below the incident energy) with Fe or Ni, Cu is a poor grid material even at energies below the Cu K edge. To access higher-Z trace elements in thin sections, future studies will be carried out using low-Z (C, Be) grids. Figure 4 shows a microtomed thin section in a Cu TEM aperture grid and its SXRF spectrum (collected in He). Knowledge of trace element contaminants in mounting media is critical. The Na and Cl peaks in Figure 4, for example, are likely due to salt in the epoxy, and the Cu shoulder on the Ni peak in Figure 3 is not associated with the particle.

We have made much progress in attaining high quality SXRF spectra from small particles. Sample damage in the beam is being assessed and addressed. C fiber mounts are well-suited to whole IDP studies, and appropriate TEM grids have been identified for thin section studies. Spectra obtained show excellent signal-to-noise, and we are in the process of analyzing them for quantitative results.

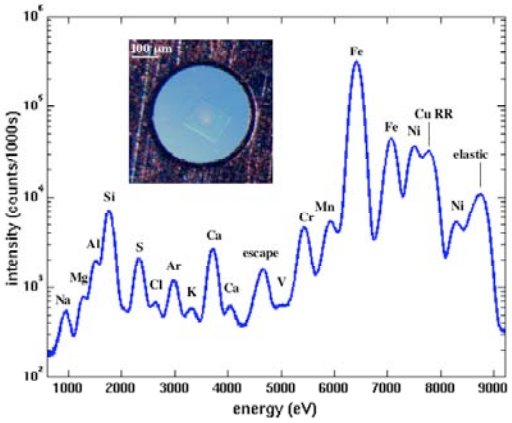

Fig. 4: SXRF spectrum from a microtomed thin section of IDP W7154I1, 200 nm thick, mounted in a TEM aperture grid. Epoxy discoloration in the inset optical image is due to prior TEM analysis rather than x-ray exposure.

References: [1] Flynn G. J. et al. (1996) *LPS XXVII*, 367-368. [2] Kehm K. et al. (2002) *MAPS, 37*, 1323. [3] Brownlee, D. E. et al. (2003) *JGR, 108*, SRD 1-15. [4] Kashiv, Y. et al. (2001) *LPS XXXII*, Abstract #2192. [5] Ishii, H. A. et al. (2005) *LPS XXXVI*, Abstract #1393.

Acknowledgements: This work was performed in part under the auspices of the U.S. Department of Energy, NNSA by the Lawrence Livermore National Laboratory under contract No. W-7405-Eng-48 and in part at the Stanford Synchrotron Radiation Laboratory, a national user facility operated by Stanford University on behalf of the U.S. Department of Energy, Office of Basic Energy Sciences. This work was performed as part of the Bay Area Particle Analysis Consortium (BayPAC) and was supported by NASA Grant NNH04AB49I. We thank Z. Dai for valuable assistance with TEM.

ROSINA'S FIRST MEASUREMENTS FROM SPACE AND ANTICIPATED ANALYSES AT COMET CHURYUMOV-GERASIMENKO. A. Jäckel[1], K. Altwegg[1], P. Wurz[1], H. Balsiger[1], E. Arijs[2], J. J. Berthelier[3], S. Fuselier[4], F. Gliem[5], T. Gombosi[6], A. Korth[7], and H. Rème[8], [1]Physikalisches Institut, Universität Bern, Sidlerstr. 5, CH-3012 Bern (jaeckel@phim.unibe.ch), [2]Belgisch Instituut voor Ruimte-Aeronomie, B-1180 Brussel, [3]Institute Pierre Simon Laplace, F-94107 St.-Maur-des-Fossés, [4]Lockheed Martin Advanced Technology Center, Palo Alto, CA 94304, USA, [5]University of Michigan, Space Physics Research Laboratory, Ann Arbor, MI 48109, USA, [6]Max-Planck-Institut für Sonnensystemforschung, D-37191 Katlenburg-Lindau, [7]Centre d'Etude Spatiale des Rayonnements, F-31028 Toulouse.

Introduction: The Rosetta Orbiter Spectrometer for Ion and Neutral Analysis (ROSINA) is an orbiter payload instrument onboard the ROSETTA spacecraft that was successfully launched in March 2004 by the European Space Agency. The ROSINA instrument package is designed to determine the elemental, isotopic, and molecular composition of the atmosphere of comet 67P/Churyumov-Gerasimenko.

ROSINA Characteristics: The instrument package ROSINA consists of two mass spectrometers and one pressure sensor. The mass spectrometers are the Double Focussing Mass Spectrometer (DFMS) and the Reflectron Time-Of-Flight mass spectrometer (RTOF) that are both designed to analyze cometary neutral gases and cometary ions. The third sensor, the COmetary Pressure Sensor (COPS), consists of a pressure gauge assembly. These three sensors will measure the neutral gas and the ion composition in the cometary environment as a function of the heliocentric distance to the comet [1]. The Data Processing Unit (DPU) controls all three sensors and is fully redundant. The characteristic features of the three sensors are described in more detail below:

DFMS. The DFMS is a very compact state of the art high-resolution double-focussing mass spectrometer [2] realized in the Nier-Johnson configuration [3]. The sensor weights 16 kg and the power consumption averages 22 W. The DFMS is a high resolution mass spectrometer with a large dynamic range and good sensitivity. It covers a mass range of 12-140 amu/e and has a mass resolution of $m/\Delta m > 3000$ at the 1% peak height which corresponds to > 7000 at the 50% level. This allows separation of, e.g., ^{13}C and ^{12}CH. With an integration time of typically one second the recording of a whole mass spectrum measured with the Channel Electron Multiplier (CEM) detector from 12 to 140 amu/e takes approximately two hours. The mass resolution of the DFMS is high enough to measure interesting isotopic ratios of, e.g., the two nitrogen isotopes ($^{14}N^+$, $^{15}N^+$). This is of great importance in order to determine and explain the anomalous nitrogen isotopic ratios in comets.

RTOF. The RTOF is characterized by an extended mass range from 1 up to > 300 amu/e in order to identify organic material, e.g., polyaromatic hydrocarbons. The sensor weights 15 kg and consumes about 30 W. The high sensitivity of the RTOF sensor is essential with respect to the pressure range that is expected when Churyumov-Gerasimenko is at 3 AU where measurements are activated. The expected water production rates at perihelion, during peak activity, and at 3 AU at comet Churyumov-Gerasimenko are given in table 1.

Tab. 1: Expected water production rate and the corresponding pressure at 2 km from the nucleus for comet Churyumov-Gerasimenko [4].

Heliocentric distance	$Q(H_2O)$ [s^{-1}]	H_2O density [cm^{-3}] @ 2 km	Pressure [mbar]
Perihelion (1.3 AU)	4.1×10^{27}	2.0×10^{11}	6.0×10^{-6}
Peak activity	1.0×10^{28}	8.0×10^{11}	2.5×10^{-5}
3 AU	1.0×10^{23}	1.0×10^{7}	1.0×10^{-10}

An advantage of the RTOF sensor is that a full mass spectrum of the entire mass range (1-300 amu/e) that is only limited by the signal accumulation memory is recorded within 100 µs. The mass resolution in the triple reflection mode is $m/\Delta m > 4500$ at the 50% peak height. DFMS and RTOF complement one another.

COPS. The COPS weights 1.7 kg and consumes 7 W. It consists of two ionization gauges to determine the gas dynamics of the comet. One gauge is a nude hot filament extractor type Bayard Alpert ionization gauge [5]. It measures the total particle density with a nitrogen sensitivity of about 20 $mbar^{-1}$ at 100 µA. The other gauge, a closed ionization gauge, with its opening facing towards the comet, measures the molecular flow from the comet. Combining the results from both gauges and the known spacecraft orientation relative to the nucleus of the comet, the velocity and the density of the cometary gas can be calculated. In addition, this sensor serves as a safety instrument for Rosetta in case of pressure increases.

Anticipated Analyses: During the increasing activity of the comet from aphelion to perihelion more and more cometary material like dust particles as well as ice will evaporate. The evaporation products can easily be measured by the ROSINA mass spectrometers. Together with other instruments onboard Rosetta that are specialized on dust measurements it will be possible to determine the dust composition due to the capability of ROSINA to measure in an extended mass range (> 300 amu/e) with a high sensitivity and a large dynamic range. Therefore, the two ROSINA mass spectrometers support the dust analyses performed by the dust specialized instruments.

Conclusions: The ROSINA instrument package was designed to measure relevant elemental, isotopic, and molecular abundances from the onset of activity through perihelion. It will easily cope with the activity of Churyumov-Gerasimenko at 4 AU as well as at perihelion. Finally, it will analyze the composition of the volatile material over a large mass range with a large dynamic range, and it will significantly contribute to our understanding of the dynamics of this comet.

References: [1] Balsiger H. et al. (2001) *ESA SP-1165*. [2] Mattauch J. and Herzog R. (1934) *Z. Physik, 89,* 786. [3] Johnson E. G. and Nier A. O. (1953) *Phys. Rev., 91,* 10-17. [4] Schleicher D. G. and Millis R. L. (2003) DPS 35th Meeting, oral presentation, 30.06. [5] Redhead R. A. (1966) *J. Vac. Sci. Technol., 13,* 173-180.

METEOR SHOWERS FROM BROKEN COMETS. P. Jenniskens, SETI Institute (515 N. Whisman Rd., Mountain View, CA 94043; pjenniskens@mail.arc.nasa.gov).

Introduction: When Whipple [1] discovered a mechanism to accelerate meteoroids by the drag of water vapor in1951, the old idea of meteor showers originating from comet breakup went into remission. Even though comets were frequently observed to break, there was no strong evidence that the meteoroids generated in these discrete and relatively rare events accounted for our meteor showers on Earth. Now, recent minor planet discoveries have recovered remnants of those breakups in some of our strongest showers.

The giant comet hypothesis: Active Jupiter Family Comets are known to frequently break and shed a series of 10-m to 1000-m sized fragments [2]. Examples are the 1832 breakup of 3D/Biela and the 1995 breakup of 73P/Schwassmann-Wachmann 3. Both comets used to, or will in the future, pass by Earth orbit. During those fragmentations, meteoroids are created that can lead to temporary meteor showers on Earth when the resulting dust trails are steered in Earth path. If the amount of dust is substantial, fragmentations can even lead to annual showers when the streams evolve into elongated structures that cross Earth's path.

The idea that the fragmentation of comets is a source of meteoroids causing meteor showers on Earth was first proposed following the 1872 and 1885 Andromedid storms, which followed the breakup of lost comet 3D/Biela in 1832, and the continued fragmentation of the comet observed in the returns of 1846 and 1852 [3]. At the time, comets were seen by many as a flying sand bank, dust grains orbiting each other and held together by their mutual gravity [4] and there was no clear distinction between a comet ensemble and individual meteoroids.

In recent years, the products of fragmentations are known to be comets in their own right, possibly creating new meteoroid streams by water vapor drag. Nuclear fragments in orbits with other orbital period than the parent comet were implicated in the periodic returns of the Lyrids [5], which we now know are due to periodic perturbations by Jupiter, which steer a continuous trail of dust in Earth's path instead. Another example of comet fragmentation implicated as the source of a meteor shower is the Giant Comet Hypothesis for the origin of the Taurid complex [6]. While in my opinion the Taurid shower is indeed likely the product of comet fragmentation, most of the implicated minor bodies have been proven to be unrelated asteroids, instead.

Fragments of broken comets in meteoroid streams: In 1983, Fred Whipple discovered a minor planet 3200 Phaethon among the meteoroid stream responsible for the Geminid shower [7]. The reflectance properties of the minor planet (taxonomic type B) make the nature of this object as an extinct comet nucleus uncertain, but only because of the small perihelion distance. The surface of the minor planet and the properties of the meteoroids are altered from repetitive heating by the Sun. It has since been shown that the Geminids appear to have been created close to perihelion, more typical of comet ejection than asteroidal collisions [8].

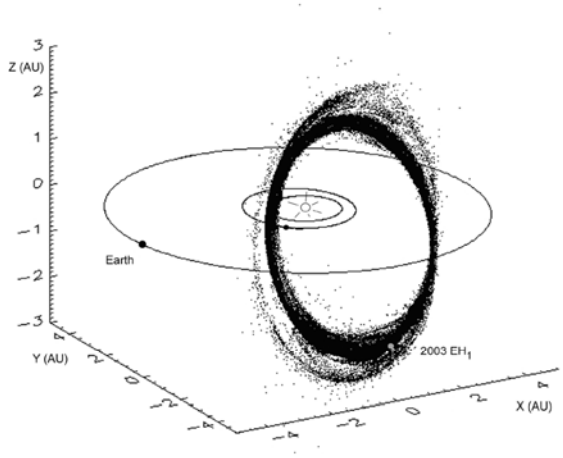

Fig. 1: 2003 EH_1 and the Quadrantid meteoroid stream, in a model by Jerémié Vaubaillon.

In 2003, I identified a minor planet 2003 EH_1 in the high-inclination orbit of the Quadrantids [9]. This is a massive stream, containing a thousand times more mass than typically ejected by an active Jupiter Family Comet. The minor planet passes outside of Earth orbit, but the stream evolves rapidly due to perturbations of Jupiter at aphelion (and at the ascending node). Accurate measurements of meteoroid orbits imply that the stream is not older than 500 years and must have formed in a short period of time. The comet C/1490 Y_1, seen in early 1491, may have been the manifestation of that breakup [10].

Now, a second such minor planet has been recognized, 2003 WY_{25}, which traces back to comet D/1819 W1 (Blanpain) [11]. The comet orbit is not known well and the comet was lost after the 1819 sighting,. However, 2003 WY_{25} has angular elements

within 0.2º from those of Blanpain at that time, and is therefore most likely a fragment of a breakup that must have occurred in the 18th or early 19th century, most likely just before the return of 1819.

We demonstrated that the dust generated in a breakup in 1819 would have wandered in Earth's path in 1951 and 1956, and could have been responsible for the strong 1956 Phoenicid outburst. The trail has not been in Earth's path since (at least not when Earth was at the node). Hence, the 1956 Phoenicids were likely the debris from the breakup of comet Blanpain in or shortly before 1819 [11].

More recently, the Marsden group of sunskirting comets was found to have a short orbital period [12], which implies that whatever was responsible for this large family of comet fragments is also responsible for the Daytime Arietids. The associated delta-Aquariids are then also formed after the breakup of a comet of that same group, albeit further evolved along a Kozai cycle.

In summary, the meteor showers that are likely from the fragmentation of comets rather than from Whipple-type ejection by water vapor drag are the Quadrantids, Daytime Arietids, delta-Aquariids, Andromedids, Phoenicids, and Geminids, and probably also the Capricornids, kappa-Cygnids, and Taurids, representing most of our annual showers.

Comet fragmentation: One of the more interesting results from comparing mass estimates of the comet fragments and the meteoroid streams of these Jupiter-Family-Comet parents is that the streams represent a mass no more than that of a single fragment [11]. In contrast, the disruption of long-period comet C/1999 S4 (Linear) was thought to have created as much as 200 times more mass than the sum of fragments combined [13]. Hence, the fragmentations in question are not necessary wholescale, but could pertain to the release of just a small number of cometesimals from their parent comet, in the process brightening the comet by a few magnitudes from the release of fine dust and gas.

The cause of those fragmentations remains unknown, but the impact of large meteoroids has been implicated as a mechanism to trigger such events [14]. While containing a relatively small amount of kinetic energy, such impacts may heat trapped subterranean gasses that can lead to sufficient pressure buildup to gently break off cometesimals.

The Deep Impact probe hit 9P/Tempel 1 in terrain dotted by impact craters that had clearly weathered similar events in the past. The approach images did not immediately show the breaking off of a fragment.

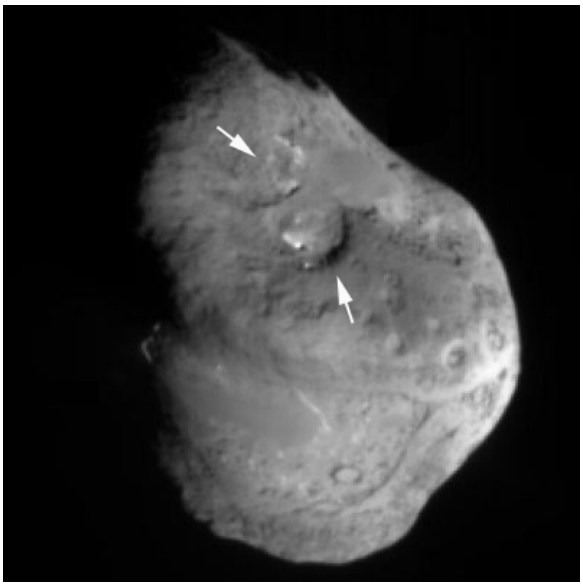

Fig. 2: Deep Impact target 9P/tempel-1. Arrows mark areas that might be the scars from recent fragmentation. Photo: NASA/JPL/Deep Impact.

However, the surface of comet 9P/Tempel 1 (Fig. 2) shows some areas with steep ridges that containing spots of high albedo terrain. Instead of impact craters, these structures could be the site of such fragmentation. In the case of 9P/Tempel 1, at least two 0.5-km sized fragments may have been lost from the comet. Other terrain is smooth, without much albedo variation, at the bottom of larger bowl-shaped depressions. That flat terrain likely resulted from dust fallen back to the comet that accumulated at the bottom of the bowls. It is not clear, at present, if that debris could have been created during the disruption, or was the result of normal Whipple-type ejection of meteoroids by the drag of water vapor instead.

References: [1] Whipple, F.L. (1951) *ApJ* 113, 464. [2] Sekanina, Z. (1997) AA 318, L5. [3] Olivier C.P. (1925) *Meteors*, Williams & Wilkins Co., Baltimore. [4] Lyttleton, R.A. (1948) MNRAS 108, 465. [5] Arter, T.R., Williams, I.P. (1995) *MNRAS* 277, 1087. [6] Clube, S.V.M., Napier, W.M. (1984) MNRAS 211, 953. [7] Whipple, F.L. (1983) IAUC 3881, 1. [8] Gustafson, B. Å. S. (1989) AA 225, 533. [9] Jenniskens, P. (2003) IAUC 8252 (Dec. 08). [10] Jenniskens, P. (2004) AJ 127, 3018. [11] Jenniskns, P., Lyytinen E. (2005) AJ (Sept., in press). [12] Marsden, B.G. (2004) MPEC 2004-X73. [13] Altenhoff, W.J., *et al.* (2002) AA 391, 353. [14] Babadzhanov, P.B., Wu, Z., Williams, I.P., Hughes, D.W. (1991) MNRAS 253, 69.

HYPERSEED MAC: AN AIRBORNE AND GROUND-BASED CAMPAIGN TO MONITOR THE STARDUST SAMPLE RETURN CAPSULE REENTRY ON 2006 JANUARY 15. P. Jenniskens,[1] P. Wercinski, M. Wright, J. Olejniczak, G. Raiche, D. Kontinos, and E Schilling,[2] G. Rossano and R.W. Russell, [3] M. Taylor, [4] H. Stenbaek-Nielsen, [5] G. Mcharg, [6] R. L. Spalding and K. Sandquist, [7] J. Hatton, [8] S. Abe,[9] R. Rairden, [10] D.O. ReVelle, [11] P. Gural, [12] D. Hladiuk and A. Hildebrand,[13] and F. Rietmeijer.[14] [1]SETI Institute (515 N. Whisman Rd., Mountain View, CA 94043; pjenniskens@mail.arc.nasa.gov), [2]NASA Ames Research Center, [3]The Aerospace Corporation, [4]Utah State University, [5]University of Alaska Fairbanks, [6]USAF Academy, [7]Sandia National Laboratories, [8]ESTEC/ESA, [9]Kobe University, [10]Lockheed Martin, [11]Los Alamos National Laboratories, [12]S.A.I.C., [13]University of Calgary, Canada. [14]University of New Mexico Albuquerque.

Introduction: The reentry of the Stardust Sample Return Capsule on 2006 January 16 is the fastest entry of a NASA space craft in NASA history and the first > 11 km/s since the Apollo era. The hypervelocity entry of a sample return capsule is an artificial meteor with flow conditions similar to natural asteroids for studies of the shock emissions and ablation process, without the confusion of fragmentation and the obscuring emissions from the ablated meteoric metals of natural fireballs. The entry is also a real-life test of key risk drivers for future Thermal Protection System (TPS) design: the amount of radiative heat flux and the response of the TPS.

The Stardust SRC entry: Stardust will be a night time reentry which permits intensified spotting cameras with a large field of view. The star background will provide a coordinate frame. We will now also have central access to the latest trajectory files from the Stardust mission navigators.

Stardust will enter Earth's atmosphere at a shallow angle of 8.2º, spin at 15 rates per minute, and experience a surface heat rate of about 1200 W/m^2. The peak deceleration in Earth's atmosphere will be 34 g. The phenolic impregnated carbon ablator (PICA) heat shield will bear the brunt of the entry.

Fig. 1: Genesis SRC entry.

Results from the Genesis SRC Entry campaign: The Stardust SRC entry follows the return of the Genesis SRC at the Utah Test and Training Range (U.T.T.R.) on September 8, 2004. That entry was observed in a first Hyperseed MAC mission, during which broadband optical emissions and infrasound signatures were detected. The anticipated emissions were calculated from a flow and radiation model, and were expected to be dominated by blackbody emission, but with measurable signatures from the shock wave [1]. The observations were only partially successful, because the spectrograph and imagers that needed to be aimed at the meteor did not acquire the object in the daytime sky due to a simple, yet significant, error in the instrument pointing simulation. Staring cameras did detect the bright SRC, as did ground-based infrasound detectors at Wendover and a handheld video camera. The results from the observations show that the surface-averaged brightness temperature was close to that predicted [2]. The infrasound signal was only a factor of two different from that calculated based on Apollo data [3].

The Genesis SRC was larger than the Stardust SRC (1.52m compared to 0.811m), but arrived at lower speed (11.0 km/s versus 12.9 km/s @ 135 km). Stardust's kinetic energy will be 1/4 that of Genesis, making the reentry 1.4 magnitudes fainter, but the higher speed will induce more intense shock emissions. Preliminary calculations show that the emission lines should stand significantly above the continuum emission from the hot surface area. The peak brightness (from a distance of 100 km) will be about -5 magnitude panchromatic and brighter at red and near-infrared wavelengths.

Hyperseed MAC: We will report on how results from the Genesis Hyperseed MAC mission help guide the ongoing efforts to bring together a second airborne mission using NASA's DC-8 Airborne Laboratory. This will enable a large team of researchers to view the entry above clouds and in a low-water-vapor line-of-sight. This airborne mission will be supported by ground-based observations.

References: [1] Jenniskens P., *et al.* (2005) *EMP (in press).* [2] Jenniskens P., *et al.* (1997) *AIAA Reno meeting. (submitted).* [3] ReVelle D.O., Edwards W., Sandoval T.D. (2005) *Met. & Planet. Sci. (in press).*

Additional Information: More information will be provided at the website http://reentry.arc.nasa.gov while the campaign unfolds.

DUST IN COMETS OBSERVED AT SUBMILLIMETER WAVELENGTHS

D. Jewitt[1], H. Matthews, S. Andrews
[1]Institute for Astronomy, University of Hawai'i, HI 96822; jewitt@hawaii.edu

The dust size distribution in comets is such that, while small particles dominate the scattering cross-section, it is the large particles which dominate the mass. Historically, most studies of cometary dust employed optical wavelength data and so were most sensitive to micron-sized particles in the cometary coma. This lead to dramatic under-estimates of the mass production rates in cometary dust and to unreasonably small values of the cometary dust/gas ratio.

The use of infrared and, more recently, submillimeter wavelength observations (Figure 1) has changed our appreciation of the number and role of large particles in comets. Large cometary particles are analogues of the dust sensed remotely from thermal excesses in the circumstellar disks of other stars: indeed, the cometary dust assemblage may be thought of as a frozen sample of dust from the Sun's own accretion disk. In this talk we will discuss the long-wavelength data available for comets, much of it acquired in a long-term program conducted at the James Clerk Maxwell Telescope. We will discuss implications for the mass loss rates and relate the cometary dust to precursor material in the accretion disk of the Sun.

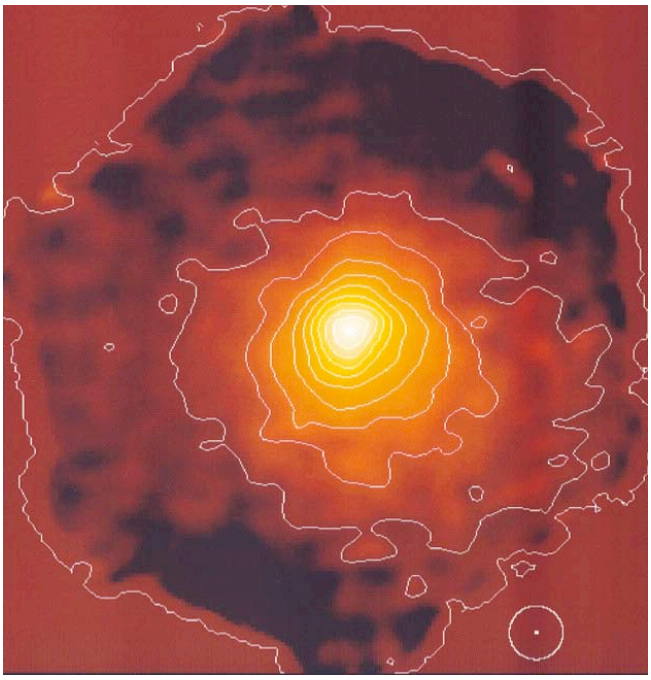

Figure 1

Image of C/Hale-Bopp taken at 850 μm with the SCUBA bolometer array. Field of view is 155" (160,000 km). The circle shows the 15" angular resolution of JCMT at this wavelength. Dust mass loss rate inferred from this image was near 1000 tonnes/second.

ORGANIC SYNTHESIS ON DUST: IMPLICATIONS FOR PROTOSTELLAR SYSTEMS. N. M. Johnson[1,2] and J. A. Nuth III[1]. [1]Astrochemistry Lab, NASA's Goddard Space Flight Center, Greenbelt, MD 20763 (njohnson@lepvax.gsfc.nasa.gov). [2]NAS/NRC Resident Research Associate.

Introduction: Hydrogen (H_2), nitrogen (N_2) and carbon monoxide are the most abundant molecular constituents in astrophysical environments, including protostellar nebulae. Although some organic molecules may be produced on very long timescales by the irradiation of ices formed on the cold surfaces of interstellar grains [1], pre-solar organics could be swamped by the efficient conversion of nebular H_2, N_2 and CO to simple organic materials. We carried out experiments that demonstrate that almost any surface can serve as a 'mediator' for this conversion process.

Surface-Mediated Chemistry: While it is unknown what exact process or combination of processes produced organics that are found in meteorites or are detected in comets and nebulas, one particular method that forms organics are Fischer-Tropsch type (FTT) reactions. Fischer-Tropsch type synthesis produces complex hydrocarbons by hydrogenating carbon monoxide via surface mediated reactions. The products of these reactions have been well-studied using 'natural' catalysts [2] and calculations of the efficiency of FTT synthesis in the Solar Nebula suggest that these types of reactions could make significant contributions to the composition of material near three AU [3]. We use FTT synthesis to coat Fe-silicate and Mg-silicate amorphous grains with organic material to simulate the chemistry in the early Solar Nebula. These coatings were found to be composed of macromolecular organic phases [4]. Previous work also showed that as the grains became coated, Haber-Bosch type reactions took place resulting in nitrogen-bearing organics [5].

We discuss the differences/similarities of the produced organics (solid and gas phase) and their production rates using either amorphous Mg- silicate grains or amorphous Fe- silicate grains as the starting material.

Experiments: We circulate CO, N_2, and H_2 gas through Fe- or Mg- amorphous silicate grains that are maintained at a specific temperature. The gases are passed through an FTIR spectrometer and are measured to monitor the reaction progress. Each cycle begins with 75 torr N_2, 75 torr CO, and 550 torr H_2 before the grains are brought to temperature (i.e., 400 or 500°C). After the gas has circulated for a predetermined amount of time, the heating element is turned off and the gas is pumped away. We repeat this process approximately fifteen times.

In addition to real time gas measurements using FTIR, we periodically collect a gas sample for additional analysis using a cold trap and a solvent (e.g., high purity acetonitrile). We analyze the 'trapped' gas sample using GCMS. Solid samples are analyzed using FTIR, GCMS (including pyrolysis) and potentially by NMR spectroscopy. Extraction techniques are also used to analyze the organic coatings.

Discussion: These experiments show that these types of reactions are an effective process to produce complex hydrocarbons. In the future, we will subject the reacted samples to thermal annealing and/or hydration to determine how these processes affect the deposited organic layers. These secondary processes would mimic what may have occurred on meteorite parent bodies and ideally give insight into the history of meteoritic organics. Overall, organics generated in this manner could represent the carbonaceous material incorporated in comets and meteorites.

Dust grains falling into a protostellar system would provide the surfaces that promote the reaction of H_2, N_2 and CO into both volatile organics and a macromolecular coating that continues to promote the formation of organic materials. Although the reaction is most efficient in the innermost regions of the nebula this does not pose significant problems as the reaction products as well as the coated grains can migrate back out to the far reaches of the nebula, thus seeding the entire nebula with the organic building blocks of life.

Acknowledgements: We thank M. Martin, J. Dworkin, G. Cody, and C. Alexander for their support.

References: [1] Gerakines, P. A. et al. 2004 *Icarus* 170:202-213. [2] Hayatsu R. and Anders E. 1981. *Topics in Current Chemistry* 99:1-37. [3] Kress M. E. and Tielens A. G. G. M. 2001. *Meteoritics & Planetary Science* 36:75-91. [4] Johnson N. M. et al. 2004. Abstract #1876. 35th Lunar & Planetary Science Conference. [5] Hill H. G. M and Nuth J. A. 2003. *Astrobiology* 3:291-304.

CRYSTALLINE SILICATE FORMATION AND COMETS. N. M. Johnson[1,2] and J. A. Nuth III[1]. [1]Astrochemistry Lab, NASA-Goddard Space Flight Center, Greenbelt, MD 20763 (njohnson@lepvax.gsfc.nasa.gov). [2]NAS/NRC Resident Research Associate.

Introduction: A traditional view of the early solar nebula and planet formation involves the outer edges being cold and wet and the interior regions remaining hot and dry. While this generalization is a gross over-simplification, it does give a nutshell idea of the early solar nebula. However, the problem with this view is that as more data is acquired, this simple model is no longer sufficient to explain all the observations. We focus on the existence of crystalline silicates in comets [e.g., 1,2]. In the traditional view, comets form by accumulating materials that formed at low temperatures and are stable in the 'comet-feeding-zone' at the outer edges. Such a zone would include gases and a variety of ices but not crystalline silicates. Crystalline silicates must form in the presence of high temperature and/or energy from shocks. There are a couple of places where these conditions could be met: the hotter, denser inner solar nebula or by shocks [3]. These two conditions are not mutually exclusive. Nuth [4] previously contended that amorphous silicates were annealed within the inner regions of the Solar Nebula and were later transported out beyond the snowline via nebular winds and ultimately incorporated into comets. This idea of outward transport is not without merit as Boss [5] shows that materials could move both inward and outward in the nebula. Others have also argued that outward transport is viable [e.g., 6]. Chondrules and CAIs have been proposed to form in the hottest inner regions of the nebula. If there was indeed outward migration, the Stardust mission will give direct evidence of this outward movement if it collects samples containing CAIs, for example. Shocks in the outer nebula can also anneal amorphous grains, and probably do, but the question is, "Can we determine if there is a dominant process or can either process be ruled out?"

We suggest that there is a direct and definitive observational test to distinguish between the relative importance of the two models for the origin of crystalline grains in comets: namely the presence or absence of crystalline iron-bearing silicates in the cometary grain population. This argument is presented in more detail in Nuth and Johnson [7] and in our poster at this workshop.

References: [1] Crovisier J. et al. (1997) *Science, 275,* 1904-1907. [2] Wooden, D. H. et al. (2004) *ApJ,* 612, L77-L80. [3] Harker, D. E. and Desch, S. J. (2002) *ApJ,* 565, L109-L112. [4] Nuth, J. A. (1999) *LPSCXXX*, 1726. [5] Boss, A. P. (2004) *ApJ*, 616, 1265-1277. [6] Prinn, R. G. (1990) *ApJ*, 348, 725-729. [7] Nuth, J. A. and Johnson, N. M. (2005) *Icarus*, submitted.

Thoughts on Small Body Exploration History and Prospects

T. V. Johnson
Jet Propulsion Laboratory, California Institute of Technology, Pasadena, CA 91109

Developing a viable program of small body (comets, asteroids, dust) space exploration has been difficult. The project landscape of the last thirty years or so is littered with the remains of proposed small body missions which never made it to the budget phase or were canceled (from Halley-Temple 2 to CRAF). The only early major successes were the ESA Giotto mission and the Soviet Vega missions, dedicated to Halley flybys. Following the Halley missions the NASA space science program had many proposals for small body missions of varying degrees of ambition but had little success in selling a major thrust in small body exploration, despite numerous advisory committee recommendations. Major progress in small body exploration has come about primarily by shifting the focus from large, dedicated missions to an approach combining use of existing assets (e.g. Galileo, Cassini), the Discovery mission line, and technology development through the New Millennium program. The result has been a greatly increased level of knowledge about these intriguing classes of objects and their environments: Galileo flybys of Gaspra and Ida (plus Dactyl), interplanetary dust observations on Galileo, ESA's Ulysses, and Cassini, the NEAR mission to Eros (flyby of Mathilde), DS1's encounter with Borrelly (plus demonstration of ion drive), the Stardust encounter with Wild 2 and upcoming sample return, the selection of DAWN to study main belt asteroids Vesta and Ceres, and the recent spectacular Deep Impact success. ESA has also pursued the major, cornerstone approach with the launch of Rosetta. What of the future? Continued use of the current strategy will undoubtedly increase our sampling and knowledge of small bodies, but the very success of the last two decades has resulted in the community's development of science objectives for the future (most recently through the NRC's decadal survey) which may only be achievable with larger more complex and costly missions, including sample return. This work was done at the Jet Propulsion Laboratory, California Institute of Technology under a contract from NASA.

Mineralogy and Densities of Cometary and Asteroidal IDPs Collected in the Stratosphere. [1]D. J. Joswiak, [1]D E. Brownlee, [2]R. O. Pepin and [2]D.J. Schlutter. [1]Dept. of Astronomy, 351580, University of Washington, Seattle, WA 98195, [2]Dept. of Physics, University of Minnesota, Minneapolis, MN 55455. e-mail: joswiak@astro.washington.edu

Introduction: IDPs collected in the stratosphere comprise astromaterials from both cometary and asteroidal sources [1]. Of primary interest are cometary IDPs as these particles are the only physical samples of comets available for study in the laboratory. IR spectroscopic measurements of comets taken during spacecraft flybys along with laboratory analyses of anhydrous IDPs indicate that comets are composed of complex mixtures of unequilibrated crystalline and noncrystalline materials including Fe-Mg-rich silicates, glasses, Fe sulfides, and organic compounds [2]. Since comets were formed at heliocentric distances of 5 – 50 AU in the solar nebula, these materials likely represent the first building blocks during solar system formation.

In a collaboration with the University of Minnesota, we have been conducting an ongoing investigation to determine which subset of IDPs collected from the stratosphere are likely to have originated from comets vs asteroids. We have compiled a database containing mass, density, ^{4}He abundance, atmospheric entry temperature, atmospheric entry velocity and mineralogy for IDPs that have likely cometary or asteroidal origins. Here we report on some of the results we have obtained on 32 stratospheric IDPs with an emphasis on the cometary IDPs.

Analytical Methods: Thirty two chondritic stratospheric IDPs ranging in size from 5 – 15 μm were systematically processed after removal and washing from six collector flags. Mass, density and bulk composition were measured for each IDP in the Cosmic Dust Lab at the University of Washington [3]. The particles were then embedded in either epoxy resin or sulfur and microtomed for mineralogical studies by TEM. Peak heating temperatures were measured at the University of Minnesota from the remaining particle in the potted butt by generating a stepped-He release curve [4]. The mineralogy of each IDP was obtained by detailed TEM/STEM/EDX investigations on microtomed sections using microanalytical EDX, SAED and high resolution imaging techniques.

Atmospheric Entry Velocities: The likely cometary or asteroidal origin for each IDP was determined using the temperature measured after 50% release of He with the atmospheric entry model of Love and Brownlee [5]. For the 32 IDPs measured, peak heating temperatures ranged from 505 – 1067 °C (Fig 1). Atmospheric entry velocities varied from 10.1 km/s to greater than 26 km/s (Fig 2). The IDPs were subdivided into low ($V \leq 14$ km/s), intermediate (14 km/s < $V < 18$ km/s) and high ($V \geq 18$ km/s) velocity groups. We believe that IDPs that fall in the low velocity group are likely have an asteroidal origin while those in the high velocity group are likely to have a cometary origin; we do not attempt to classify those in the intermediate velocity group.

Cometary IDPs ($V \geq 18$ km/s): Twelve IDPs have velocities consistent with a cometary origin (Fig 2); atmospheric entry temperatures range from 721 – 1016 °C. Measured densities range from 0.62 – 1.73 g/cm^3 with an average density of 1.03 g/cm^3 (Fig 3). Both non-crystalline and crystalline silicates including Mg-rich olivines, pyroxenes (enstatite, pigeonite, augite and diopside) and GEMS were observed in these IDPs (Table 1); grain sizes are typically 100 – 200 nm. Pyrrhotite, pentlandite, Fe-Mg-Al silicate glass (not GEMS), noncrystalline carbon, FeNi metal and occasional spinel and feldspar were also found. One IDP (U2070A-10A) with an entry speed of 20.3 km/s contained the hydrated minerals cronstedtite and saponite as major phases. A small amount of nearly pure forsterite was observed in this IDP as well.

Asteroidal IDPs ($V \leq 14$ km/s): Figure 2 shows that 4 of the 32 measured IDPs fall in the low velocity group. Atmospheric entry heating temperatures range from 505 – 1067 °C while IDP densities vary from 1.54 – 4.2 g/cm^3 with an average density of 3.3 g/cm^3(Figs 1 and 3). Three of the four IDPs are composed of the phyllosilicate minerals cronstedtite or saponite (Table 1). These minerals are generally poorly crystallized (this may be due to decomposition from atmospheric entry heating). Consistent chemical composition along with 0.71 nm or 1.0 – 1.4 nm lattice fringes were occasionally observed to confirm these phases. All contain minor quantities of pyroxenes. One IDP is phyllosilicate-free and composed of a mixture of grains typical of the cometary group – olivine, pyroxene and possibly GEMS. Pyrrhotite, pentlandite and Fe-Mg-Al silicate glass are also present in the asteroidal IDPs.

Discussion and Summary: Atmospheric entry velocities measured from 32 stratospheric IDPs indicate that 12 are probably comet dust while four likely have an asteroidal origin. Sixteen IDPs with intermediate velocities may have been derived from either source. Significant differences in density and mineralogy are evident between the cometary and asteroidal groups. The cometary IDPs have an average density of 1.03 g/cm^3 compared to 3.3 g/cm^3 for the asteroidal group. Mineralogically, the cometary IDPs do not contain phyllosilicate minerals (with one exception) but are composed of Mg-rich olivines, pyroxenes and glass, similar to materials observed by IR spectroscopic measurements taken by spacecraft from comets in the inner solar system [2]. Nearly identical mineralogy - crystalline Fo_{90}, crystalline clino+ortho pyroxenes (Mg/Fe+Mg≥0.9) amorphous olivine (Mg/Fe+Mg=0.5) and amorphous pyroxene (Mg/Fe+Mg=1.0) – was shown to comprise the best fit components to ISO SWS IR spectra taken from the ESA spacecraft of comet Hale-Bopp [6]. Hydrated

silicates could also be present at the 1% level or less. The minerals we observe in cometary IDPs are strikingly similar to those observed in comets.

References: [1] Joswiak, D.J., Brownlee, D. E., Pepin, R. O, and Schlutter, D.J., *LPSC XXXI*, 2000. [2] Hanner, M. S., in *Astromineralogy*, T.K. Henning ed., 171-188, 2003.. [3] Love, S. G., Joswiak, D. J. and Brownlee, D. E., *Icarus*, 111, 227-236, 1994. [4] Nier, A. O. and Schlutter, D. J., *Meteoritics* 28, 675-681, 1993. [5] Love, S. G. and Brownlee, D. E., *Icarus*, 89, 26-43, 1991. [6] Wooden, D. H. et al., *AJ*, 517, 1034-1058, 1 June 1999.

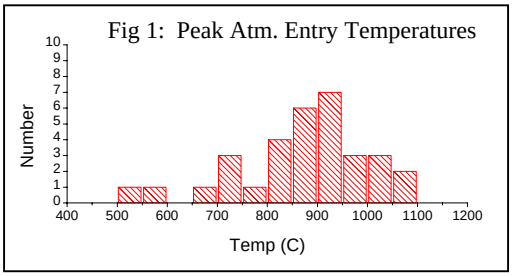

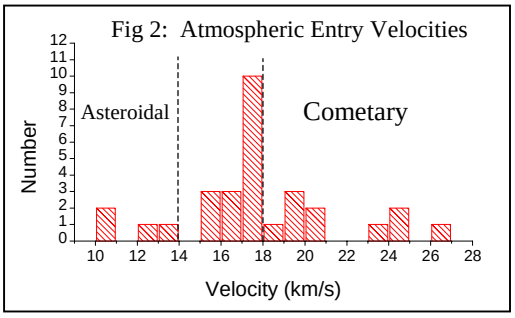

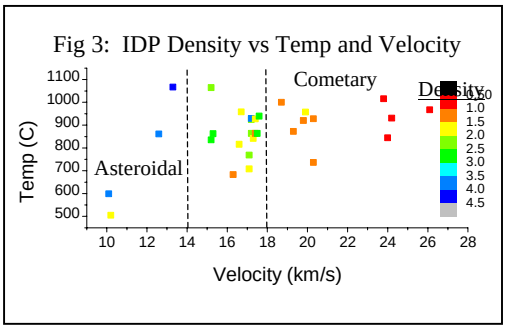

Figure Captions

Fig 1: Histogram showing measured atmospheric entry temperatures from 32 chondritic IDPs.

Fig 2: Histogram showing modeled atmospheric entry velocities from 32 choncritic IDPs. Four low speed IDPs ($V \leq 14$ km/s) are believed to have originated from asteroids while 12 high speed IDPs ($V \geq 18$ km/s) were likely derived from comets. Two IDPs with $V > 26$ km/s are not shown in the histogram.

Fig 3: IDP density as a function of atmospheric entry temperature and velocity. Cometary IDPs show lower overall density than asteroidal IDPs.

Table 1: Mineralogy in cometary and asteroidal IDPs

IDP	Vel (km/s)	Temp (°C)	Density (g/cm^3)	Olivine	Pyroxene	GEMS	Phyllo-silicates
			Cometary IDPs				
U2070A-4A	18.7	1000	1.29	$Fo_{80\text{-}84,\ 97}$	CEn_{99}, En_{99}, Aug	Yes	
U2012A-2G	19.3	872	1.13	$Fo_{88\text{-}93}$	En_{96}, Di?	Yes	
U2073B-8B	19.8	920	1.19	$Fo_{80\text{-}87,97}$	$En_{96\text{-}97}$	?	
U2-30C-4B	19.9	957	1.73				
U2012A-10G	20.3	736	1.00				
U2070A-10A	20.3	928	1.25	Fo_{99+}			Cron,Sap
U2073A-9A	23.8	1016	0.98	$Fo_{72\text{-}80,90}$	En_{93}, Ca-Px	?	
U2073A-7F	24.0	844	0.62	$Fo_{81\text{-}87,98}$	$En_{92,97}$; Pig	Yes?	
U2073B-2I	24.2	931	0.86	Fo_{95}	$En_{94,99}$; Aug, Pig	Yes	
U2073B-3C	26.1	967	0.88	Fo_{88}	CEn_{86}, Di, Pig	Yes	
U2012A-4J	>26	721	0.78				
U2073B-3A	>26	1009	0.70	$Fo_{77\text{-}78,\ 91}$	$En_{87,97}$; Di, Pig	Yes	
			Asteroidal IDPs				
U2012A-1G	10.1	599	3.68		Di		Sap?
U2012A-3G	10.2	505	1.54	$Fo_{65\text{-}67,87\text{-}97}$	En_{94}, Pig	Yes?	
U2012C-1B	12.6	861	3.64		En_{87}		Sap
U2073A-9F	13.3	1067	4.20	$Fo_{60\text{-}62}$	Aug		Cron?

Table 1: Entry velocities, measured stepped ^{4}He release temperatures, densities and partial mineralogy from cometary and asteroidal IDPs. Fo=forsterite, En=enstatite, CEn=clinoenstatite, Pig=pigeonite, Aug=augite, Di=diopside, Ca-Px=Ca pyroxene, Sap=saponite, Cron=cronstedtite.

THE E RING OF SATURN: MODELS VERSUS OBSERVATIONS. A. Juhasz[1] and M. Horanyi[2], [1]KFKI Research Institute for Particle and Nuclear Physics, Department of Space Physics, Budapest, Hungary, (juhasz@rmki.kfki.hu), [2]LASP University of Colorado, Boulder, Colorado, USA (Mihaly.Horanyi@colorado.edu).

A number of remote sensing and in situ observations of Saturn's E ring exist, including ground based and HST images taken during ring plane crossings, indirect observations of dust impacts measured by Voyager 1 and Pioneer 11 spacecraft, and the recent direct dust flux measurements by CDA onboard Cassini.

In this presentation we compare these observations with theoretical models that were developed to explain the dynamics and distribution of dust particles in the E ring [1,2,3,4,5,6,7].

Our earlier model [6] reproduced most remote sensing observations, including the color and the spatial distribution of the measured optical depth as function of distance from Saturn. We are now using a new fully 3D version of this code to follow the seasonal variations in the E ring [7], that is no longer assumed to remain azimuthally symmetric. We will report on the comparisons of the calculated in situ dust flux measurements with the CDA observations. Though the orbit-by-orbit comparisons remain difficult, the emerging global picture - based on multiple ring-plane crossings - can be used to adjust our model to optimize its predictive capability.

References: [1] Horanyi et al. (1992) *Icarus, 97*, 248-259. [2] Hamilton D.P. (1993) *Icarus, 101*, 244-264. [3] Hamilton D.P. and Burns J.A. (1994) *Science, 264*, 550-553. [4] Dikarev V.V. and Krivov A.V. (1998) *Solar System Research, 32*, 128-143. [5] Dikarev V.V. (1999) *Astron. Astrophys. 346*, 1011-1019. [6] Juhasz A. and Horanyi M. (2002) *JGR, 107*, 10.1029/2001JA000182. [7] Juhasz A. and Horanyi M. (2004) *GRL, 31*, L19703, 10.1029/2004GL020999.

THE EFFECT OF INTER-PARTICLE COLLISIONS ON THE DYNAMICAL EVOLUTION OF ASTEROIDAL DUST AND THE STRUCTURE OF THE ZODIACAL CLOUD. T. J. J. Kehoe[1] and S. F. Dermott[1], [1]Department of Astronomy, University of Florida, 211 Bryant Space Science Center, PO Box 112055, Gainesville, FL 32611-2055 (kehoe@astro.ufl.edu).

Introduction: Our approach to building detailed models of the zodiacal cloud is to utilize the results from numerical simulations of the dynamical behavior of its constituent dust particles. These dynamical models are then compared with observational data and refined.

Numerical Simulations: Due to computational constraints, our previous models of the zodiacal cloud [1] were limited to considering small particles, generally less than 100μm in diameter, that spiral rapidly into the Sun under the effect of Poynting-Robertson (P-R) drag [2]. Larger particles have correspondingly longer dynamical (i.e., P-R drag) lifetimes and hence require longer integration times. To enable a comprehensive numerical investigation of the orbital evolution of a realistic size distribution of particles in the zodiacal cloud has therefore required the application of a powerful new *N*-body code [3].

Moreover, we note that dust particles in the inner solar system with diameters of around 500μm have P-R drag lifetimes comparable to the timescale for the particle to be destroyed by inter-particle collisions [4], whereas the P-R drag lifetimes of particles much smaller than this are too short for them to be significantly affected by such collisions. To investigate the evolution of large dust particles has therefore required that, in addition to the previously modeled effects of radiation pressure, P-R drag, solar wind drag, and planetary perturbations, the effects of stochastic size changes due to particle fragmentation have also had to be incorporated into our numerical simulations of their orbital evolution. We have achieved this by employing a semi-analytic technique that combines the results of secular perturbation theory with numerical integrations using the *N*-body code discussed above.

Results: The orientation of the mean plane of symmetry of the zodiacal cloud is determined by the forced inclinations of the dust particles comprising the cloud together with their forced longitude of ascending nodes [5]. These forced elements are a function of semimajor axis, time, and the physical properties of the particles, such as size.

Figure 1 shows the forced inclinations as a function of semimajor axis for waves of 20-μm (green diamonds), 100-μm (red triangles), and 500-μm (blue squares) diameter dust particles. Each wave contained 1,000 particles that were released from the Veritas asteroid family at various epochs in the past so that they arrived at the semimajor axes indicated at the current epoch. The forced elements were calculated using the "particle on a circle" method [6]. Also shown (solid black line), is the forced inclination as a function of semimajor axis for a massless particle obtained using linear secular perturbation theory for the "zero-drag" case at the current epoch. The current inclination of Jupiter is shown as a dashed black line and the filled circle indicates the present location of the Veritas asteroid family. The figure clearly illustrates that as particle size increases, the forced inclinations of the dust particle waves tend towards the "zero-drag" secular solution, which is dominated by the effect of Jupiter in the region of the outer asteroid belt. Similar results were obtained in the case of the forced longitude of ascending nodes of the Veritas family particles, and for several other asteroidal sources investigated.

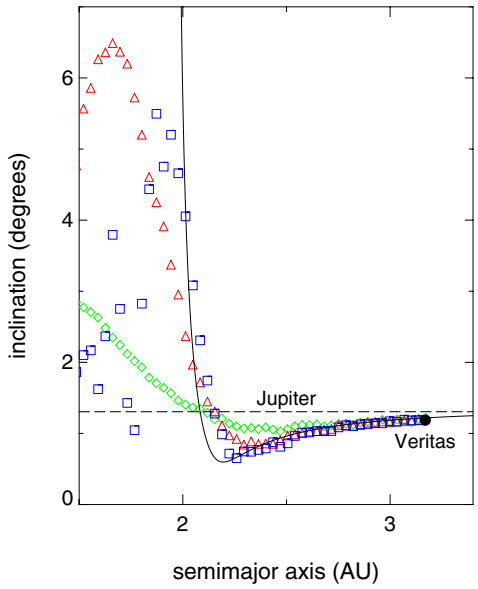

Figure 1

The forced inclinations as a function of semimajor axis for waves of 100-μm diameter dust particles are shown in Figure 2. These waves of particles were released from the Veritas asteroid family at various epochs in the past so that they arrived at the semimajor axes indicated when: (i) Jupiter's inclination was at its minimum value during its last secular oscillation (green diamonds), and (ii) at its maximum value (red triangles). The (i) green and (ii) red dashed lines indi-

cate the inclination of Jupiter at these two epochs. The solid black line again shows the forced inclination obtained using linear secular perturbation theory at the current epoch. The dotted and dashed black lines show the secular solution for a "zero-drag" massless particle when Jupiter's inclination was (i) at its minimum value and (ii) at its maximum value, respectively, during its last secular oscillation. At both these epochs, the forced inclinations of the dust particle waves continue to approximate the secular solutions, which are dominated by Jupiter in the outer asteroid belt.

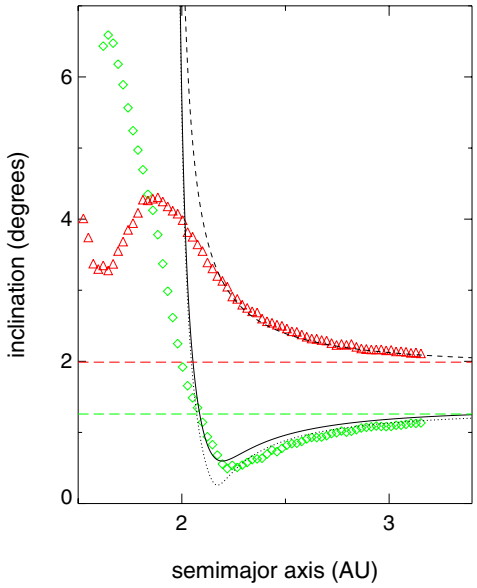

Figure 2

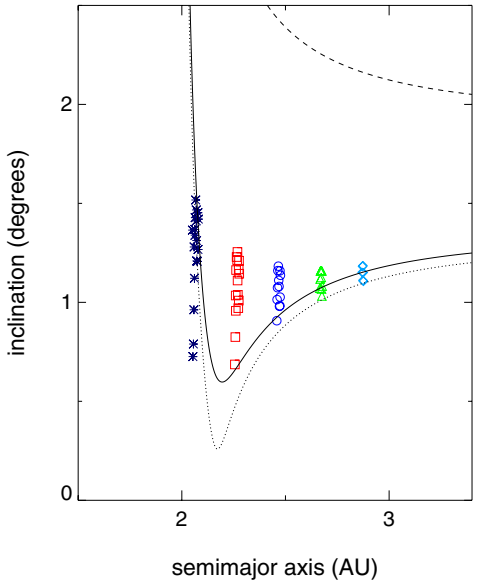

Figure 3

Figure 3 shows the forced inclinations as a function of semimajor axis for waves of collisionally evolved 20-μm diameter dust particles. The waves of particles were initially released as larger particles from the Veritas asteroid family 8.3Ma and fragmented at various epochs in the past so that they arrived at the semimajor axes indicated at the current epoch. The solid black line shows the forced inclination as a function of semimajor axis for a massless particle obtained using linear secular perturbation theory for the "zero-drag" case at the current epoch. The dotted and dashed black lines show the secular solution for a "zero-drag" massless particle when Jupiter's inclination was at its minimum value and its maximum value, respectively, during its last secular oscillation. The dispersion in the forced inclinations of the waves of 20-μm diameter particles at each semimajor axis arises because they were generated at different epochs in Jupiter's secular oscillation cycle.

Discussion: The orientation of the mean plane of symmetry of the zodiacal cloud outside 2AU is dominated by the effect of Jupiter as it evolves through its secular cycle. It is for this reason that we are able to observe the solar system dust bands discovered by IRAS [7]. The inner edge to the dust bands at 2AU results from the significant effect of secular resonances on particle orbits that disperses the dust band signal to the extent that it merges naturally into the flux from the background zodiacal cloud. The effect of interparticle collisions also introduces dispersion in the distribution of the forced elements of the particles as a result of the variation of Jupiter's orbital elements, and the "zero-drag" secular perturbation solution, over the course of a secular cycle. These new results contribute to a more accurate description of the orbital evolution of a realistic size distribution of zodiacal cloud particles and are now being employed to build detailed models of the solar system dust bands.

References: [1] Grogan K. et al. (2001) *Icarus, 152,* 251–267. [2] Wyatt S. P. Jr. and Whipple F. L. (1950) *ApJ, 111,* 134–141. [3] Kehoe T. J. J. et al. (2003) *AJ, 126,* 3108–3121. [4] Wyatt M. C. et al. (1999) *ApJ, 527,* 918–944. [5] Dermott S. F. et al. (2001) in *Interplanetary Dust,* edited by Grün E, Gustafson B. Å. S., Dermott S. F., and Fechtig H. [6] Dermott S. F. et al. (1992) in *Chaos, Resonance and Collective Dynamical Phenomena in the Solar System,* edited by Ferraz-Mello S. [7] Low F. J. et al. (1984) *ApJ, 278,* L19–L22.

Acknowledgments: This work was supported by NASA under Grant Nos. NAG5-11643 (PGG) and NAG5-13105 (ADP).

DUST PRODUCTION AND NUCLEUS EVOLUTION. H. U. Keller[1], Yu. V. Skorov[1,2], and G. N. Markelov[3], [1]Max-Planck-Institut für Sonnensystemforschung, 37191 Katlenburg-Lindau, Germany, [2]Keldysh Institute of Applied Mathematics, Miusskaya pl. 4, 125047 Moscow, Russia, [3]AOES, Haagse Schouwweg 6G, 2332 KG Leiden, The Netherlands.

Physical properties of comets like their density, porosity, and thermal conductivity are apparently determined by cometary evolution and history. These primordial differences affect the processes occurring when a comet is heated by the Sun. At the same time the release of volatiles influences the physical properties of the nucleus changing its porosity, e.g. forming a dust crust on the surface etc.

A complete physical description of the energy and mass transfer inside and outside the nucleus is a complicated problem. Due to the high porosity and the presence of transparent ice solar light can penetrate to a substantial depth leading to volume energy absorption in the uppermost porous layer of a cometary nucleus [1,2]. Note that the nucleus and the innermost coma of an active comet constitute a interacting physical system: both heat and mass are exchanged between the two regions, and their physical properties develop in close symbiosis. Therefore correct thermo physical modelling of a comet cannot be restricted to the nucleus itself - the whole system must be considered simultaneously [3,4]. This motivated us to a revision of the conventional model of a cometary nucleus. The following important aspects are now included: i) radiative energy transport in porous media; ii) energy transport by sublimation products; iii) heat and mass exchange between the nucleus and the innermost coma, iv) DSMC model of dust-gas flow in the innermost coma region [5].

We demonstrate that for a porous cometary nucleus vapour molecules escape from the non-isothermal upper sub-surface layer. High porosity leads to a significant decrease of the effective gas flux of volatiles and, as a result, the total dust production decreases. More of the absorbed energy is available to be transferred into the interior of the nucleus. The dependence of the gas production rate on the heliocentric distance is different for comets of different morphology of the uppermost surface layers (e.g. for the comets with surface or layer energy absorption). In the frame of kinetic DSMC model fields of density and velocity are calculated for the gas and for the dust. We show that the spatial structure of inner-most dust-gas coma is sensitive to the nucleus shape as well as to the variations of local gas production rates. In general, spatial structure of the innermost coma (both gas and dust) is a result of interactions of gas flows sublimated from different surface regions. We conclude that the nucleus shape as well as physical properties of nucleus play the major role in interpretation of innermost coma.

References:

[1] Skorov Yu. V. et al. (2001*) Icarus, 153*, 180. [2] Skorov Yu. V. et al. (2002) *Earth, Moon, and Planets, 90*, 293. [3] Davidsson B. J. R. and Skorov Yu. V. (2002) *Icarus, 56*, 223. [4] Davidsson B. J. R. and Skorov Yu. V. (2004) *Icarus, 168*, 163. [5] Skorov Yu. V., Markelov G. N., and Keller H. U. (2004) *Solar System Research, 38*, 455.

INTERACTION OF SATURNIAN DUST STREAMS WITH THE SOLAR WIND

S. Kempf[1], R. Srama[1], Mihaly Horányi[2], M. Burton[3], and E. Grün[1,4]

[1] MPI für Kernphysik, Saupfercheckweg 1, 69117 Heidelberg, Germany [2] Laboratory for Atmospheric and Space Physics, University of Colorado, Boulder, Colorado 80309, USA [3] Jet Propulsion Laboratory, Pasadena, California 91109, USA [4] Hawaii Institute of Geophysics and Planetology, University of Hawaii, 1680 East West Road, Honolulu 96822, USA

One of the major findings during the approach of the Cassini spacecraft to Saturn was the discovery of high velocity streams of nanometer-sized dust originating from the inner Saturnian system [4]. Until then, only the Jovian system was known to be a source of dust streams [1]. The dust stream phenomenon is of particular interest for a few reasons: (i) outside the planetary magnetosphere the stream particle dynamics is governed by the interaction with the solar wind plasma [2]; (ii) stream particles are the fastest solid bodies of the solar system known so far [6]; (iii) dust streams may transport material from areas which cannot be explored in-situ by space probes [4].

Numerical simulation by Zook et. al [6] proved that for the Jovian streams only grains of about 10 nm with speeds exceeding 200kms^{-1} reproduced the observations by Ulysses. Based on the impact signals caused by the Saturnian stream particles as well as by numerical simulations [3] those grains were found to have similar properties (radii ranging between 2 and 25 nm, speeds $\geq$ 100kms^{-1}). Furthermore, the simulations indicated that particles detected at large distances from Saturn most probably originated from the outskirts of Saturn's A ring. Surprisingly it was found that stream particles predominately consist of a silicon-bearing material[5] even though Saturn's rings are composed of water ice. This proposes that stream particles are rather the impurities of the icy ring material than the ring material themselves.

Here we report on results based on one year of continuous monitoring of Saturnian stream particles by the Cosmic Dust Analyser (CDA) on the Cassini spacecraft. All dust bursts detected within 150 Saturnian radii so far clearly coincided with the spacecraft's traversal through 'co-rotating interaction regions' (CIR) in the interplanetary magnetic field (IMF) – regions characterised by compressed plasma, increased solar wind speed, and enhanced magnetic field strength (Fig. 1). This finding together with our analysis demonstrates that the peculiar properties of dust streams can be explained by the interaction of the charged grains with the plasma inside the CIRs.

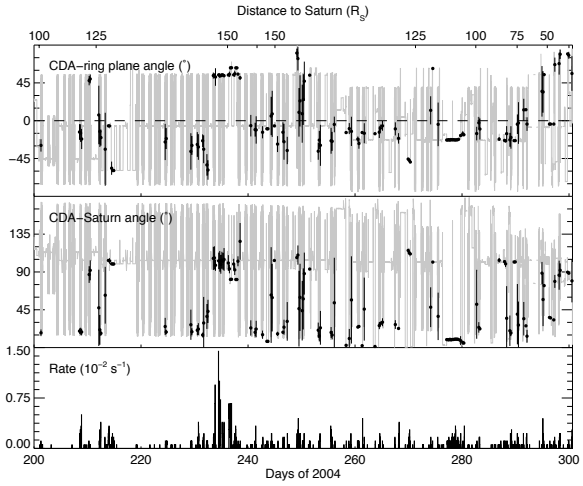

Figure 1: Impact rate and directionality of stream particles recorded during Cassini's first revolution around Saturn outside Titan's orbit spanning days 200 and 300 in 2004. The upper panel shows the angle between the CDA instrument normal and Saturn's ring plane, the middle panel indicates the angle between the CDA and the Cassini-Saturn line of sight. The mean angle is plotted whenever more than 2 impacts within 4 hours were registered; the attached bars indicate the 1-σ deviation from the mean angle. The gray solid line marks the evolution of the CDA normal due to the varying spacecraft orientation. The lowermost panel shows the stream particles impact rate. The pronounced impact bursts around day 210 and around day 235 of 2004 coincide with Cassini's traversal through co-rotating interaction regions in the solar wind. Note also that the directionality of the streams changed during these periods.

References

[1] E. Grün et al (1993) *Nature*, 362:428–430.
[2] D.P. Hamilton and J.A. Burns (1993) *Nature*, 364:695–699.
[3] S. Hsu and S. Kempf (2005) in prep.
[4] S. Kempf et al. (2005) *Nature*, 433:289–291.
[5] S. Kempf et al. (2005) *Science*, 307:1274–1276.
[6] H.A. Zook et al. (1996) *Science*, 274:1501–1503.

LUNAR SEISMIC DEVELOPMENT AND GAS-DUST STREAMS; GENESIS OF LIFE

Oleg B. Khavroshkin , Vladislav V. Tsyplakov,
Schmidt Institute of Physics of the Earth, RAS, B .Gruzinskay, 10,
Moscow, D-242, 123995 GSP-5 Russia, e-mail: khavole@ifz.ru

Review of Main Results of Lunar Seismic Development

Introduction: Results of previous research related to lunar seismicity (Nakamura Catalogue) and cosmogonic objects and processes are briefly outlined.

The Mapping of Impact Processes from Meteoroid Streams and Solar Wind on the Moon into Durations of Seismograms: Data of annual histograms (distributions) for durations of seismograms from exogenous acting on the Moon were analyzed. Peculiarities of these actions and their comparison with data of optic lunar events were taken into consideration. It has been found that dust-gas plasma of meteoroid streams and solar wind are modulated by Sun free oscillations. Histograms from meteoroid streams with intensity of 4-8 impact/days contain durations corresponding to periods of free lunar oscillations.

The Temporal Structure of Meteoroid Streams and Lunar Seismicity; the Peculiarities of Shape of Histogram Envelopes: The shapes of histogram envelopes for annual interval are changed from the Gauss curve to a more complicated one. It betokens the unsteady-state of seismic processes and, at times, their similarity to earthquake recurrence curves for regions of mines and/or to energy distribution for powerful solar bursts.

Simple Estimation for Non-gravity Effects on the Moon: Estimations of integral pressure on the Moon by solar wind (under undisturbed Sun and Sun burst) and gas-dust component of meteoroid streams have been made. Energy of these disturbances (under Sun bursts or its maximum stream density) is enough for initiation of free Moon oscillations and recording lunar seismic events.

Conclusions: The Moon is unique cosmogonic and astrophysical detector which can be realized by information of its own seismicity.

Manifestation of Gas-Dust Streams from Double Stars on Lunar Seismicity

Information content of the Nakamura`s Catalog of moonquakes is very rich: from solar-earth tides to clustering among the meteoroid streams [1,2]. The histograms from meteoroid-impact seismic data revealed the seismic wave responses of the Moon to solar oscillations and the action on the lunar surface by dust-gas plasma of meteoroid streams [3]. The time series of seismic events were generated as follows: on the ordinate axis the peak amplitudes of events in standard units, on abscissa axis - seismogram durations of the same moonquakes and subsequent time intervals between them were used [4]. Spectrum of the series of meteoroid streams disclosed time picks on orbital periods of some planets and their satellites and solar oscillations [4, 5]. The research of peculiarities of histogram envelopes [3] and comparative common analysis of solar bursts data and mass meteoroid distribution are confirmed [3, 4] and reveal Forbush`s effect for gas-dust plasma [6]. Hidden astrophysical periodicities of lunar seismicity were earlier obtained from analysis of time series [7] similar to series [4]. A part of results (picks) presents orbital periods of double stars nearest to the Solar system [7]. The path of results of [7] is presented in Table.

The first hypothesis for explanation of this result is existing gas-dust streams from binary stars near the solar system and their interaction with lunar surface; the second hypothesis is connected with the gravitation radiation from the same stars. Probably the first hypothesis is more real. First hypothesis for explanation of the Table results is existing gas-dust streams from binary stars near systems solar system and interacting with lunar surface; second is correlation them to the gravitational radiation from the same stars. We suppose that first hypothesis is more real.

Table

Characteristic of binary stars systems and picks of the lunar seismicity periodicity.

N Tabl 1	lunar periods, day	Name of system	Half period /period day	Masses of component solar unit.		distans parsec	Gravitation radiation. Gd/s
4	6.7	V380 Cyg	6.21	13.3	7.6	4168	10^{21}
		CV Vel	T=6.89	6.0	6.0	1047	
5	4.8	V356 Sgr	4.45	12.3	4.7	3090	10^{21}
6	3.5	CV Vel	3.44	6.0	6.0	1047	$2*10^{21}$
		h Aql	3.58			100	
7	2.25	UW Cma	2.20	43.5	32.5	8912	$5*10^{24}$
8	2.03	AG Per	T=2.029	4.5	4.5	660	
		α Vir	2.007	10.3	6.4	257	$3*10^{22}$
9	1.33	V906 Sco	1.393	3.5	2.8	251	
10	0.966	G Aql	0.975	6.8	5.4	549	$2*10^{23}$

11	0.666	Y Aql	0.651	7.5	6.9	275	$5*10^{23}$
12	0.543	IM Mon	0.595	8.4	5.6	724	$1*10^{24}$
14	0.323	VV U.Ma	0.343	2.1	0.5	512	$1*10^{22}$
		YY Eri	T=0.321	0.76	0.5	42	$1*10^{22}$
16	0.265	i Boo	0.268	1.35	0.68	12	$1*10^{23}$
20	0.160	SW Lac	0.160	0.97	0.82	74	$1*10^{23}$
21	0.142	j U.Mi	T=0.143			>100	
28	0.0751	j. U.Mi	0.0715				
29	0.0559	WZ Sge	T=0.0559	0.08	0.6	100	
34	0.0285	WZ Sge	0.0280	0.08	0.6	100	$4*10^{22}$

First hypothesis for explanation of the Table results is existing gas-dust streams from binary stars near systems solar system and interacting with lunar surface; second is correlation them to the gravitational radiation from the same stars. We suppose that first hypothesis is more real.

Genesis of Life

If the solar system is reached by the gas-dust streams from binary stars, then all bodes in space have particles of star dust on their surfaces and/or atmospheres. Solar system has made 8-10 revolutions around galactic center and thus captured dust from many thousands stars. As these stars caught in turn dust particles from other stars too then probably our solar system has mainly dust samples from all objects of our galaxy. The age of galaxy and old stars is approximately more than15 billion years and that of the Earth is only ~ 4,5 Gyr. Genesis of Life for the Earth has not more than 3 billion years. Thus comparative analysis of simple balance of these times shows that the genesis of Life for Earth is the result of galactic processes/objects and not of the solar system of course. After formation of the solar system all old and new captured dust particles are first accumulated in the Oort cloud and then they are carried by comets to planets. The modern state of the Earth exists for more than 3 billion years, so possibilities for appearing Life were always. These processes had happened a few times during this period of the Earth state. We must attach modern data of archaeology to confirm these results.

References

1. Sadeh D. Possible siderial period for the seismic lunar activity // Nature, 1972. Vol. 240, p.139
2. Oberst J. and Nakamura Y. A Search for Clustering among the Meteoroid Impacts Detected by the Apollo Lunar Seismic Network // ICARUS, Vol. 91, 315-325, 1991; Balazin M. and Zetzsche A. // PHYS.STAT.SOL., Vol.2, ,1962 1670-1674
3. Khavroshkin O.B. and Tsyplakov V.V. Meteoroid stream impacts on the Moon: Information of duration of the seismograms / In: Proceedings of the Conference METEOROID 2001, Swedish Institute of Space Physics, Kiruna, Sweden, 6-10 August 2001
4. Khavroshkin O.B. and Tsyplakov V.V., Temporal Structure of Meteoroid Streams and Lunar Seismicity according to Nakamura's Catalogue / In: Proceedings of the Conference METEOROID 2001, Swedish Institute of Space Physics, Kiruna, Sweden, 6-10 August 2001
5. O.B.Khavroshkin, V.V.Tsyplakov. Moon exogenous seismicity: meteoroid streams, micrometeorites and IDPs, Solar wind // Herald of the DGGGMS RAS: Electr. Sci.-Inf. J., 4(21)'2003
http://www.scgis.ru/russian/cp1251/h_dgggms/1-2003/scpub-3.pdf
6. O.B.Khavroshkin, V.V.Tsyplakov. Peculiarities of envelops of histograms of lunar impact seismogram durations / In: Geophysical research essays. Schmidt United Institute of Physics of the Earth Press, Moscow, 2003. 471 p., (in Russian).
M., ОИФЗ РАН, 2003, 471с.
7. O.B.Khavroshkin, V.V.Tsyplakov**.** Hidden astrophysical periodicities of lunar seismisity // Herald of the DGGGMS RAS: Electr. Sci.-Inf. J., 4(14)` 2000
http://www.scgis.ru/russian/cp1251/h_dgggms/4-2000/scpub-3.pdf

COSIMA: A High Resolution Time-of-Flight Secondary Ion Mass Spectrometer for Cometary Dust Particles on Its Way to Comet 67P/Churyumov-Gerasimenkov

J. Kissel[1], H. Höfner[2], G. Haerendel[2], S. Czempiel[2], J. Eibl[2], H. Henkel[3], A. Koch[3], A. Glasmachers[4], K. Torkar[5], F. Rüdenauer[6], W. Steiger[6], F. R. Krueger[7], E. K. Jessberger[8], T. Stephan[8], E. Grün[9], R. Thomas[10], Y. Langevin[11], H. von Hoerner[3], J. Silen[12], J. Rynö[12], M. Genzer[12], K. Hornung[13], R. Schulz[14] M. Hilchenbach[1], H. Fischer[1], H. Krüger[1], C. Tubiana[1], L. Thirkell[10], K. Varmuza[15] and the COSIMA team.

(1) MPI für Sonnensystemforschung, Max-Planck-Str. 2, D-37191 Katlenburg-Lindau; (2) MPI für extraterrestrische Physik, Giessenbachstr., D-85740 Garching; (3) von Hoerner und Sulger GmbH, Schlossplatz 8, D-68723 Schwetzingen (4) UNI/GH Wuppertal FB 13, Lehrstuhl f. Messtechnik, Fuhlrottstr. 10, D-42097 Wuppertal; (5) Inst. für Weltraumforschung, Infeldgasse 12, A-8010 Graz; (6) Inst. für Physik, Forschungszentrum Seibersdorf, A-2444 Seibersdorf; (7) Ingenieurbüro Krueger, Messeler Str. 24, D-64291 Darmstadt; (8) Inst. für Planetologie der Uni Münster, Wilhelm Klemm Str. 10, D-48149 Münster; (9) MPI für Kernphysik, Saupfercheckweg 1, D-69117 Heidelberg; (10) Laboratoire de Phys.& Chim. de L'Environment, 3 Av. De la Recherche, F-45071 Orléans; (11) Inst. D'Astrophysique, Bat.121, Faculté des Sciences d'Orsay, F-91405 Orsay; (12) Finnish Meteorological Inst., Department of Geophysics, Vuorikatu 15, SF-00101 Helsinki 101; (13) Universität der Bundeswehr LRT-7, Werner Heisenberg Weg 39, D-85577 Neubiberg; (14) ESA/ESTEC, NL-2200 AG Noordwijk; (15) Labor Chemometrie, Inst. für Verfahrenstechnik, Umwelttechnik und Techn. Biowissenschaften, TU Wien, A-1060 Wien

The **CO**metary **S**econdary **I**on **M**ass **A**nalyser (COSIMA) is a high-resolution time-of-flight (TOF) mass spectrometer system on board ESA's ROSETTA spacecraft flying to comet 67P/Churyumov-Gerasimenkov. COSIMA will collect cometary dust particles on metal black targets which are exposed to space. After target exposure dust particles with sizes $10\,\mu$m and bigger are identified on the target with an optical camera. An Indium ion beam is shot onto the particle surface and material from the particle is sputtered and ionised. The secondary ions are accelerated in an electric field and from the mass- and charge-dependent flight times of the ions a time-of-flight secondary ion mass spectrum (TOF-SIMS) is measured with a mass resolution of $m/\Delta m \approx 2000$ at $m = 100$. During commissioning in 2004 the COSIMA flight instrument performed according to specification. The first TOF-SIMS spectra in space in positive and negative ion modes were obtained from one of the instrument targets. COSIMA is now ready for the comet. The goal of the COSIMA investigation is the in-situ characterisation of the elemental, molecular, mineralogic and isotopic composition of dust particles in the coma of comet Churyumov-Gerasimenkov. Comets are remainders from the formation of the solar system and, therefore, analysis of cometary material can give important insights into the conditions of the first stages of planetary system formation and cometary evolution.

ANALYSIS OF COSMIC DUST BY THE 'COMETARY AND INTERSTELLAR DUST ANALYSER' (CIDA) ONBOARD THE STARDUST SPACECRAFT. J. Kissel[1], F. R. Krueger[2] and J. Silen[3], [1]Max-Planck-Institute for Aeronomy, D-37191 Katlenburg-Lindau, [2]Messeler Str. 24, D-64291 Darmstadt, [3]Finnish Meteorological Institute, Vuorikatu 24, SF-00101 Helsinki

The CIDA instrument on board the Stardust spacecraft is a time-of-flight mass spectrometer used to analyze ions formed when fast dust particles strike the instrument's target. The instrument has been calibrated with high speed dust particles at the Heidelberg dust accelerator. Laboratory work has been performed to better understand the ion formation processes of organic grains impacting at speeds of >15 km/s and to relate them to some other ion formation methods. On board Stardust spacecraft a series of positive and negative ion mass spectra from the impact of (apparently) interstellar and cometary dust particles has been collected since 1999. In the spectra of 45 presumably interstellar particles, quinone derivates were identified as constituents in the organic component. The 29 spectra obtained during the flyby of Comet 81P/Wild 2 on 2 January 2004 confirm the predominance of organic matter. In contrast to interstellar dust organic material in cometary dust seems to have lost most of its hydrogen and oxygen as water and carbon monoxide. These are now present in the comet as gas phases, whereas the dust is rich in nitrogen-containing species. Sulfur ions were detected in one spectrum, which suggests that sulfur species are important in cometary organics.

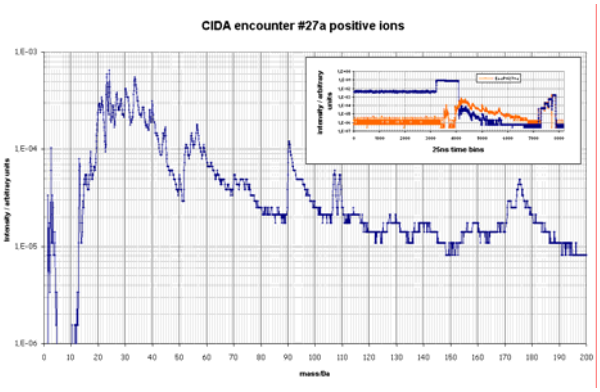

CIDA positive ion spectrum of a ~1 pg particle of mixed composition recorded during Wild 2 encounter. The spectrum is typical for nitrogen organic chemistry. The m/z = 107, 109 doublet is due to the Ag^+ from the target. The inset shows the raw data.

EXPERIMENTAL DETERMINATION OF THE RADIATION PRESSURE FORCES ON AN INDIVIDUAL DUST PARTICLE. O. Krauss and G. Wurm, Institute for Planetology, University of Münster, Wilhelm-Klemm-Str. 10, 48149 Münster, Germany, e-mail: okrauss@uni-muenster.de.

Introduction: As soon as the circumstellar disk of a forming planetary system gets optically thin submicron and micron-sized dust particles are subject to the radiation pressure of the central star. The influence of this force on the dust is then present throughout the further evolutionary stages of the system. Today, the dynamic evolution of cometary, asteroidal and also interstellar dust particles in the Solar System is influenced by the radiation pressure of the Sun [1].

The radiation pressure force is usually quantified by its ratio to the gravitational force of the star or the Sun, referred to as β. This value describes the balance between these two counteracting forces in radial direction. Radiation pressure can substantially reduce the lifetime of dust grains with high β values in the Solar System or a circumstellar disk. For spherical grains β usually reaches a maximum at particle sizes on the order of 100nm, depending on the dust material and on the properties of the star. For larger spheres β decreases rapidly.

However, the dust particles in a disk or in interplanetary space are, in general, irregularly shaped, they may have an aggregational structure or are more or less porous. The details of how these morphological features determine the radiation pressure experienced by a dust particle are not very well understood. Various calculations yield that fluffy aggregates do not show a strong decrease of β with increasing particle size [2, 3]. That means that 10µm aggregates of absorbing material can have a β value considerably larger than unity. The β values for non-spherical particles also become dependent on the orientation of the particle with respect to the incident radiation. Computational studies on spheroids [4] and cylinders [5] show a strong dependence of β on the orientation angle and the aspect ratio. Furthermore, irregularly shaped particles will have a radiation pressure force component that is perpendicular to the direction of irradiation, which is due to their asymmetrical light scattering. This transverse force component may reach several 10% of the radiation force in forward direction [4, 6, 7].

Experimental data on these features of radiation pressure that are related to the irregular shape or aggregational structure of dust particles is very rare.

Dynamic measurement of radiation pressure: We have developed a measurement technique that allows for measuring the radiation pressure forces on an isolated dust particle that is levitated in an electrodynamic trap [7, 8]. The particle is irradiated by an intense laser pulse, and its change in velocity is observed. During this process of measurement the electric fields of the trap are turned off, leaving the particle under free fall conditions without any external forces acting on it. By measuring the velocity difference of the particle and the energy density of the laser pulse the β value is obtained.

The effect is observed in two dimensions, which yields also the transverse component of the radiation pressure force. For a graphite aggregate as described below with a size of 17x7µm (largest x smallest extent) we measured a mean ratio of the transverse to the radial component of the radiation pressure force of 70% with a strong dependence on the orientation of the particle for each individual measurement [7].

Since the particle is recaptured by the trap after the measurement, a series of thousands of measurements can be performed with a single particle. Due to the wide tuning range of the applied laser source a radiation pressure spectroscopy from 220nm to 2500nm is possible.

Several techniques are currently being tested and implemented in order to charge an individual sample particle by UV or electron irradiation, put it into the trap, and retrieve it after the measurement non-destructively, which will make this method also applicable to IDP samples or particles obtained from sample return missions.

β values of graphite aggregates: First measurements applying the method described above were done with graphite aggregates in the 10µm size range. These particles consist of flake-like constituents of various sizes. The overall size of such an aggregate varies in different dimensions. Their most dominant morphological feature is that they are plates with a thickness of 100nm or less and a surface of several μm^2, which stick loosely together and are oriented in different directions. This results in a very high projected-area to mass ratio of these aggregates.

In the following we show data of about 600 measurements for a graphite aggregate of 17x6µm in size. In Fig 1 the obtained β values are plotted against the energy density of the laser pulse. Each data point is an average of 30 individual measurements using the same set of parameters.

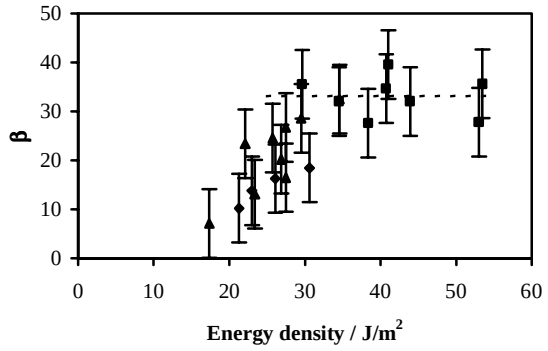

Fig 1. Measured β values as a function of laser pulse energy density for a 17x6µm graphite aggregate. The different symbols correspond to three different sets of measurements with the same particle performed on different days.

It can be seen that for energy densities larger than 30J/m^2 β reaches a constant value of about 33 (±4). Thus, above a certain threshold that is due to the experimental method the β value is independent of the laser energy density as expected. The rather high value of β is due to the typical structure of the graphite aggregates. Their large surface areas result in large cross sections for radiation pressure while at the same time the mass of these aggregates of loosely connected plates is very low.

In Fig 2 the β value of the same graphite particle is shown as a function of the wavelength in a region from 470nm to 630nm. Within the error the β value is constant. This is also expected in this small spectral range. In further experiments the wavelength range will be extended to the UV and the NIR, so that spectral features of the material or morphology-dependent resonances can be detected.

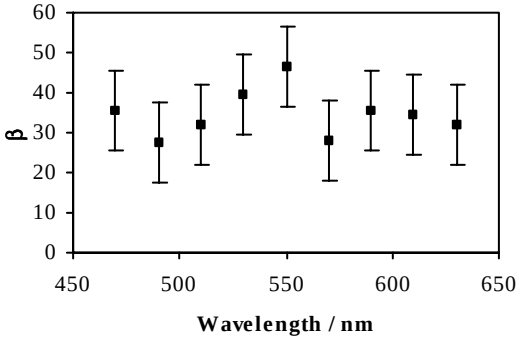

Fig 2. Measured β values as a function of the wavelength for the same graphite particle as in Fig 1.

Further studies are in progress to compare these results on graphite aggregates with other samples.

Acknowledgement: This work is funded by the Deutsche Forschungsgemeinschaft (DFG).

References: [1] Burns J.A. et al. (1979) *Icarus, 40*, 1-48. [2] Mukai T. et al. (1992) *A&A, 262*, 315-320. [3] Kimura H. et al. (2002) *Icarus*, *157*, 349-361. [4] Il'in V.B. and Voshchinnikov N.V. (1998) *A&S SS, 128*, 187-196. [5] Saklayen M.A. and Mukai T. (2004) *Earth Planets Space, 56*, 613-620. [6] Saija R. et al. (2005) *JQSRT, 94*, 163-179. [7] Krauß O. and Wurm G. (2004) *JQSRT, 89*, 179-189. [8] Krauß O. and Wurm G. (2004) *LPS XXXV*, Abstract #1526.

PHYSICS OF DEBRIS DISKS. Alexander V. Krivov[1], [1]Astrophysical Institute and University Observatory. Friedrich Schiller University, Schillergäßchen 2-3, 07745 Jena, Germany, krivov@astro.uni-jena.de.

Introduction: Debris disks are solar system-sized, optically thin, gas-poor dust disks around main-sequence (MS) stars. Their origin and status can easily be understood in the framework of the conventional planetary system formation scenario. Planetesimals, planetary embryos, and then planets form in a primordial protoplanetary disk around a star. A fraction of planetesimals – those that were neither used to make up planets nor ejected – survive this relatively rapid process (1-10 Myr). These left-overs begin to produce dust by mutual collisions and, possibly, comet-type activity [1,2], creating a tenuous debris disk. Being continuously replenished by small bodies, the disk can then persist over much of the star's lifetime.

Although only about a dozen of disks have been resolved so far at different spectral ranges from visual to sub-mm, many more images are expected from ongoing ground-based and space-based searches. Surveys reveal infrared excesses in spectra of hundreds of MS stars and show that at least 15% of MS stars may possess debris disks [3]. Ironically, the "debris disk of the Sun" (dust disk presumably encompassing the Kuiper belt, whose extensions, mass, and cross section area should by far supersede those of the zodiacal cloud) has not been observed yet, due to its extremely low optical depth, typical of Gyr-old systems such as the Sun.

Importance of debris disks stems not only from the fact that they must be a typical constituent of young and mature planetary systems. Due to large total cross section area, dust is much easier to observe than planets. On the other hand, dust distributions reflect distributions of the parent bodies, and are sensitive to presence of embedded perturbers. Hence debris disks can be used as indicators of directly invisible small body populations and tracers of alleged planets.

Interpretation of the rapidly growing bulk of observational data necessitates a major theoretical effort to understand the disk's physics and evolution. This review outlines main physical mechanisms acting in debris disks and their essential properties.

Unperturbed Debris Disks: Parent bodies steadily supply the disk with solids. Initially, most of the mass is released as larger meteoroids, which then undergo collisional grinding. Subsequent evolution of dust-sized particles (<1mm) is largely controlled by three players: stellar gravity, radiation pressure forces, and mutual collisions. Their relative importance depends primarily on the disk's optical depth τ which, in turn, is correlated with system's age.

Observations reveal a nearly linear decay of debris disks with time: τ reduces from ~10^{-2} for Myr-old stars to ~10^{-7} for Gyr-old ones. The phenomenon is naturally explained by collisional depletion of dust parent body populations [4,5]. In old systems with roughly $\tau<10^{-5}$, exemplified by the solar system's debris disk, the Poynting-Robertson (P-R) effect causes migration of smaller grains toward the primary star where they evaporate, while larger grains are typically lost to mutual collisions [6]. If $\tau>10^{-5}$ (all observable extrasolar disks), P-R drag is inefficient [7], as the collisional lifetimes are much shorter than the P-R times. In contrast to protoplanetary disks, collisions in debris disks are destructive and create smaller fragments. Removal of fine debris by stellar radiation pressure is a main loss "channel" of material in such systems. All loss mechanisms listed here imply grain lifetimes of <1Myr, showing that debris disks cannot be primordial.

At any time, a disk contains two distinct populations of dust: bigger grains that can stay in bound orbits around the star (α–meteoroids) and smaller ones that are placed by stronger radiation pressure in hyperbolic orbits, but are steadily replenished through collisional cascade (β–meteoroids). A boundary between the two populations can be estimated from the ratio of the radiation pressure to gravity [8] and lies typically at ~1μm, depending mainly on the mass and luminosity of the star and optical properties of grains, as well as on typical eccentricities of the dust parent bodies (Fig. 1).

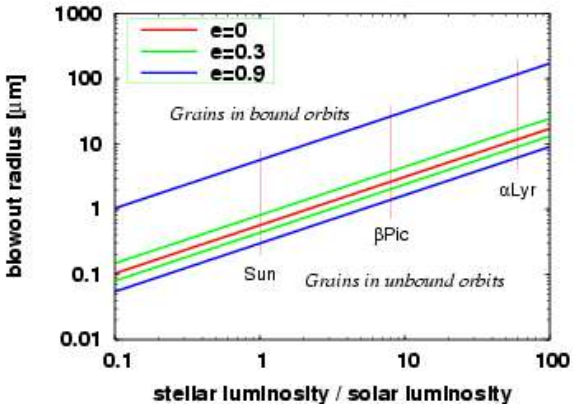

Fig.1. Grain radius that separates particles in bound and hyperbolic orbits, as function of star's luminosity (assuming dust bulk density of 2g/cm^3, a unit radiation pressure efficiency, and a standard mass-luminosity relation for MS stars). Different colors are for different typical eccentricities of parent bodies. Grains between two lines of the same color may be in both types of orbits.

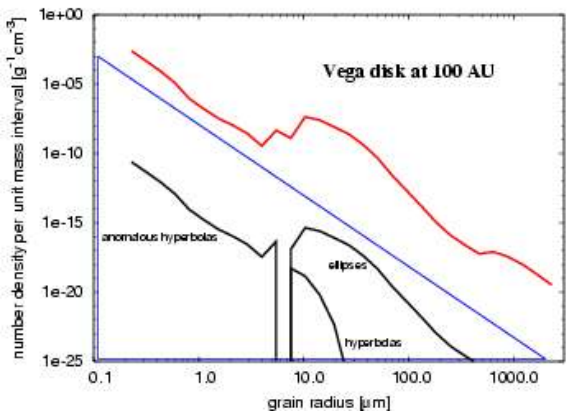

Fig.2. Size distribution in the Vega disk [model, ref. 9]. Triangular inset shows relative contributions to the number density made by grains in bound elliptic orbits, hyperbolic orbits and "anomalous" hyperbolas open outward from the star (orbits of smallest grains, for which radiation pressure exceeds gravity).

A typical size distribution of dust obtained by modeling of the α Lyr disk [9] in depicted in Fig. 2 [see ref. 7 for similar β Pic results]. The total cross section is dominated by particles with radii somewhat above the blowout limit. The entire two-population model provides a good fit to both spectrophotometric and polarimetric data [10].

Not only size distribution, but also spatial distribution of material in the disks must be determined by, and therefore hold the key to, sources, dynamics, and sinks of particles. As a consequence, there exists a principal possibility to constrain properties of the directly invisible small body populations through observations of dust.

Debris disks may contain some gas. In contrast to optically thick young disks around Herbig Ae/Be and T Tau stars, however, the gas density in debris disks is too low to affect the dust dynamics. It may be of some importance only in youngest systems, such as the 12Myr-old β Pic [11], but even this is questionable, because observations aiming to determine the amount of gas yield extremely controversial results [ref. 12 and discussion therein].

Debris Disks Perturbed by Planets: The dust distributions are further complicated by planets that can be embedded in the disk. Many authors studied nonresonant features in the disk arising from secular perturbations (warps and offsets) [13], resonant structures (clumps and voids) [14], and inner gaps resulting from close encounters of dust grains with an alleged planet [15]. All these structures can be directly observable, which offers an indirect method to search for extrasolar planets. Liou and Zook [16] have shown that, were the solar system observed from outside, the presence of at least Neptune and Jupiter could be obvious merely from the analysis of the images of the interplanetary dust disk. Similar research has been done for ε Eri [17], α PsA [18], and other systems. Substructure in the disks is, however, not necessarily produced by presumed planets and may also reflect their intrinsic clumpiness (recent collisions between the large planetesimals). Another problem is that catastrophic grain-grain collisions that may smear out the planet-induced structure already at moderate optical depths [19]. Nevertheless, observations of the fine structure together with dynamical simulations may help to pinpoint unseen planets, even with a moderate mass. These issues are addressed in detail by Moro-Martin (this volume).

Debris Disks as Sources of Interstellar Dust: Recently, radar detection of a stream of dust particles was reported [20], whose source has been identified with β Pic. Observed fluxes and velocities of stream particles are marginally compatible with scenario in which β Pic is a young planetary system that recently passed through an intensive clearance phase by at least one nascent Jupiter [21]. This has reinforced an old discussion [e.g. 22] of whether dust material ejected from debris disks make a perceptible contribution to interstellar dust. There are many reasons to expect that a significant fraction of micron-sized and larger grains in the interstellar medium stem from circumstellar disks [23].

References: [1] Weissman P. R. (1984) *Science, 224,* 987-989. [2] Beust H. et al. (1989) *AAp, 223,* 304-312. [3] Backman D. and Paresce F. (1993) *in Protostar and Planets III, 224,* 1253-1304. [4] Dominik C. and Decin G. (2003) *ApJ, 598,* 626-635. [5] Krivov A. V. et al. (2005) *Icarus, 174, 105-134.* [6] Grün E. et al. (1985) *Icarus, 62,* 244-272. [7] Krivov A. V. et al. (2000) *AAp, 362,* 1127-1137. [8] Burns, J. A. et al. (1979) *Icarus, 40,* 1-48. [9] Krivov A. V. and Loehne T. (2005) *in prep.* [10] Krivova N. A. et al. (2000) *ApJ, 539,* 424-434. [11] Artymowicz P. (1997) *AREPS, 25,* 175-219. [12] Brandeker A. et al. (2004) *AAp, 413,* 681-691. [13] Mouillet D. et al. (1997) *MNRAS, 292,* 896-904. [14] Kuchner M. J. and Holman M. J. (2003) *ApJ, 588,* 1110-1120. [15] Scholl,, H. et al. (1993) *Cel. Mech., 56,* 381—393. [16] Liou J.-C. and Zook H. A. (1999) *AJ, 118,* 580-590. [17] Quillen, A. C. and Thorndike S. (2002) *ApJ, 578,* L149-L152. [18] Holland W. S. et al. (2002) *ApJ, 582,* 1141-1146. [19] Lecavelier des Etangs A. et al. (1996) *Icarus, 123,* 168-179. [20] Baggaley, W. J. (2000) *JGR, 105,* 10,353-10,362. [21] Krivov A. V. et al. (2004) *AAp, 417,* 341-352. [22] Dorschner J. (1967) *Astron. N., 290,* 171-181. [23] Grün E. and Landgraf M. (2000) *JGR, 105,* 10,291-10,297.

Dust Stream Measurements from Ulysses' Distant Jupiter Encounter

H. Krüger[1,2], G. Linkert[2], D. Linkert[2], B. Anweiler[2], E. Grün[2,3] and the Ulysses dust science team

1) Max-Planck-Institut für Sonnensystemforschung, D-37191 Katlenburg-Lindau
2) Max-Planck-Institut für Kernphysik, Postfach 103980, D-69029 Heidelberg,
3) HIGP, University of Hawaii, Honolulu, HI 96822, USA

In 1992 the impact ionisation dust detector on board the Ulysses spacecraft discovered periodic burst-like streams of dust particles within 2 AU from Jupiter. The streams occurred at approximately monthly intervals (28 ± 3 days) and the maximum impact rates exceeded, by three orders of magnitude, the rates typically measured in interplanetary space [3]. These fluctuations were a complete surprise because no periodic phenomenon for small dust particles in interplanetary space was known before. The dust streams gave a completely new picture of interplanetary dust because they showed for the first time that dust originating from the environment of a planet can reach interplanetary space. The particles arrived at Ulysses in collimated streams radiating from close to the line of sight to Jupiter, suggesting a jovian origin. The 28-day periodicity was explained by the particle interaction with the interplanetary magnetic field [4]. Derived particle sizes were ~ 10 nm and the particle speeds exceeded 200 km s^{-1} [6]. With such high speeds, the jovian system turned out to be a source for interplanetary and even interstellar dust. Later Galileo measurements showed strong particle interaction with Jupiter's magnetosphere [5, 2] and Io was identified as the grain source [1].

12 years after its initial Jupiter flyby Ulysses approached the planet a second time in February 2004 with a closest approach distance of 0.8 AU. The first dust stream was detected in November 2002 at a distance of 3.3 AU from Jupiter which was the most distant stream detected so far. The maximum impact rates, measured around equatorial plane crossing of Jupiter, were three times larger than in 1992 (Figure 1). At least 17 dust streams were detected by December 2004, confirming grain properties recognised during the first flyby. The measured impact directions are consistent with a grain origin from the jovian system. The streams occur at about 26 day intervals closely matching the solar rotation period. Close to the equatorial plane the streams occur at a 13 day period, in agreement with theoretical predictions [4]. The impact direction of the streams is correlated with the polarity and strength of the interplanetary magnetic field. Taken all dust stream measurements since 1992 collected with three spacecraft together (Ulysses, Galileo, Cassini) the streams were detected over a large latitude range from the equator to the polar regions of Jupiter ($-35°$ to $+75°$ jovigraphic latitude).

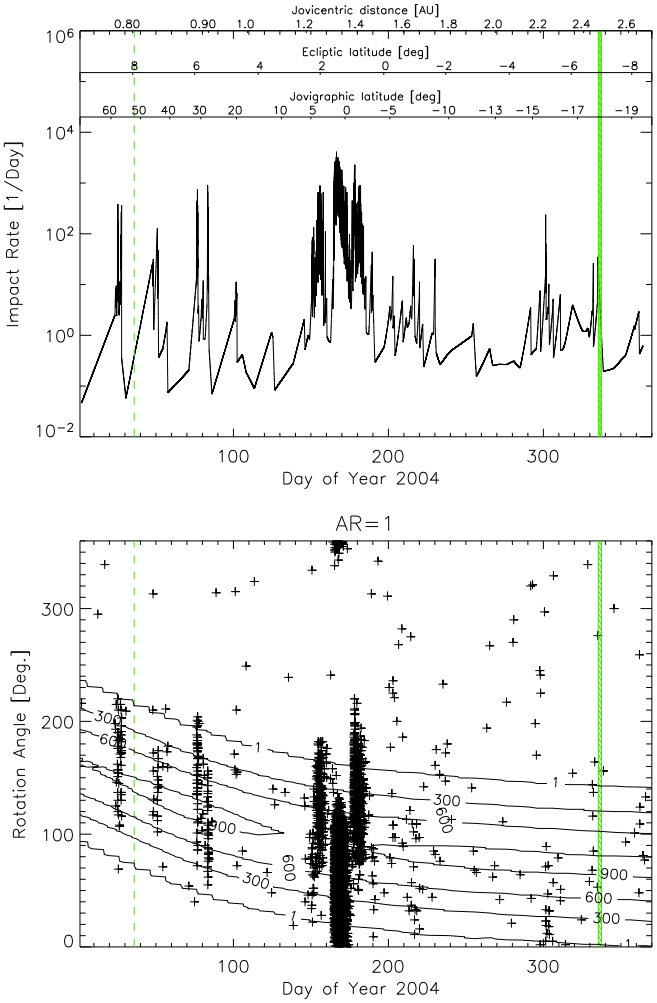

Figure 1: Ulysses dust stream measurements of 2004. *Top:* Impact rate. *Bottom:* Impact direction (spacecraft rotation angle at dust impact; ecliptic north is at 0°). Contour lines show the effective sensor area for particles approaching from the line-of-sight direction to Jupiter. A vertical dashed line shows Jupiter closest approch in February and the shaded area indicates a short period in late November 2004 when the dust instrument was switched off. The distance from Jupiter, ecliptic latitude and latitude with respect to Jupiter are shown at the top.

References

[1] A. L. Graps et al. Io as a source of the Jovian dust streams. *Nature*, 405:48–50, 2000.

[2] E. Grün et al. Galileo observes electromagnetically coupled dust in the Jovian magnetosphere. *Journal of Geophysical Research*, 103:20011–20022, 1998.

[3] E. Grün, et al. Discovery of Jovian dust streams and interstellar grains by the Ulysses spacecraft. *Nature*, 362:428–430, 1993.

[4] D. P. Hamilton and J. A. Burns. Ejection of dust from Jupiter's gossamer ring. *Nature*, 364:695–699, 1993.

[5] M. Horányi, E. Grün, and A. Heck. Modeling the Galileo dust measurements at Jupiter. *Geophysical Research Letters*, 24:2175–2178, 1997.

[6] H. A. Zook, et al. Solar wind magnetic field bending of Jovian dust trajectories. *Science*, 274:1501–1503, 1996.

Galileo In-Situ Dust Measurements in Jupiter's Gossamer Rings

H. Krüger[1,2], R. Moissl[1,2], D. P. Hamilton[3] E. Grün[2,4]

1) Max-Planck-Institut für Sonnensystemforschung, D-37191 Katlenburg-Lindau
2) Max-Planck-Institut für Kernphysik, Postfach 103980, D-69029 Heidelberg,
3) Department of Astronomy, University of Maryland, College Park, MD 20742-2 421, USA
4) HIGP, University of Hawaii, Honolulu, HI 96822, USA

Jupiter's ring system – the archetype of ethereal planetary ring systems – consists of at least three components: the main ring, the vertically extended halo and the gossamer ring(s). The small moonlets Thebe and Amalthea orbit Jupiter within the gossamer ring region, and structure in the intensity obtained from imaging observations indicates that these moons are the dominant sources of the gossamer ring material. Typical grain radii derived from imaging are a few microns. The current picture implies that particles ejected from a source moon evolve inward under Poynting-Robertson drag [1]. Beyond Thebe's orbit, a very faint outward extension of the gossamer ring was also observed which is not yet explained.

The Galileo spacecraft traversed the gossamer rings in November 2002 and September 2003, and the in-situ dust detector on board [3] collected dust measurements during both ring passages. These are the first in-situ measurements in a 'dusty' planetary ring which was also studied with imaging techniques. In-situ dust measurements provide information about the physical properties of the dust environment not accessible with imaging techniques. In particular, they provide dust spatial densities along the spacecraft trajectory as well as grain sizes and impact speeds.

Several thousand dust impacts were recorded during both ring traverses. The measurements reveal a gap in the dust spatial density between Amalthea's and Thebe's orbits (Figure 1) which is a previously unrecognised structure in the gossamer rings. The impact rate strongly increases in the Amalthea gossamer ring, consistent with imaging results. The measured size distribution of the grains ranges from 0.2 to 3 μm [6], extending by an order of magnitude the size distribution towards smaller particles is than accessible with optical techniques.

A shadow resonance, first investigated by [5], naturally explains gaps of material interior to Thebe's orbits and also explains the outward extension of the ring beyond the orbit of that satellite [4]. When a dust grain enters Jupiter's shadow, photoelectric charging by solar radiation switches off, and the grain's electric potential decreases. This changes the electromagnetic force acting on the particle and results in coupled oscillations of the orbital eccentricity and semimajor axis. These oscillations cause the rings to extend significantly outward, but only slightly inward, of their source moons while preserving their vertical thicknesses. This is exactly what is observed for the Thebe ring extension. The model leads to longitudinally asymmetric gossamer rings offset away from the Sun for positive grain charges. If most ring material is reabsorbed by the satellites before drag forces can draw it inward, this would create the gap interior to Thebe that is visible in the rate plot in Figure 1.

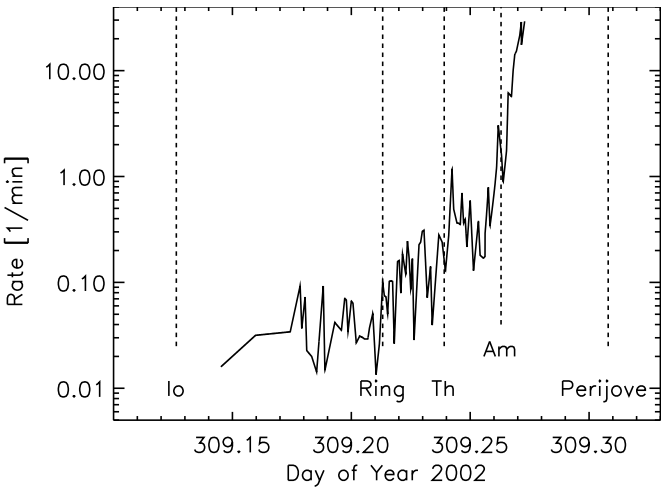

Figure 1: Impact rate of the smallest (sub-micron) dust particles (impact charges $Q_I < 10^{-13}$ C) at Galileo's gossamer ring passage in November 2002 (A34). Dotted vertical lines indicate the locations of the edge of the outer extension of the ring beyond Thebe's orbit seen on ring images at 3.75 R_J (Ring, Jupiter radius R_J = 71492 km), Thebe's orbit (Th, 3.11 R_J), and Amalthea's orbit (Am, 2.54 R_J). The spatial resolution is about 1100 km in radial direction. Note the strong dip between Thebe's and Amalthea's orbits. A similar dip also appears on ring images [2] but remains controversial .

References

[1] J. A. Burns et al. The formation of Jupiter's faint rings. *Science*, 284:1146–1150, 1999.

[2] I. De Pater et al. Keck Infrared Observations of Jupiter's Ring System near Earth's 1997 Ring Plane Crossing. *Icarus*, 138:214–223, 1999.

[3] E. Grün et al. The Galileo dust detector. *Space Science Reviews*, 60:317–340, 1992.

[4] D. P. Hamilton. Jupiter's Gossamer Rings Explained. *Bulletin of the American Astronomical Society*, 2003. Abstract presented at the DPS conference 2003.

[5] M. Horányi and J. A. Burns. Charged dust dynamics - Orbital resonance due to planetary shadows. *Journal of Geophysical Research*, 96:19283–19289, 1991.

[6] H. Krüger. *Jupiter's Dust Disc, An Astrophysical Laboratory*. Shaker Verlag Aachen, ISBN 3-8322-2224-3, 2003. Habilitation Thesis Ruprecht-Karls-Universität Heidelberg.

CASSINI RPWS OBSERVATIONS OF DUST IMPACTS IN SATURN'S E-RING. W. S. Kurth[1], T. F. Averkamp[1], D. A. Gurnett[1], and Z. Z. Wang[1], [1]Dept. of Physics & Astronomy, The University of Iowa, Iowa City, IA 52242; William-kurth@uiowa.edu.

Introduction: The Cassini radio and plasma wave science (RPWS) instrument observes signatures of micron-sized particles impacting the spacecraft which can provide information on spatial variations of the number density of dust particles in Saturn's E-ring and estimates of their masses. Preliminary results show that there is a local maximum of the number density of dust particles near the orbit of Enceladus with a thickness of about 5000 km (full width at half-maximum count rate). Preliminary estimates of the sizes of the impacting particles are a few microns.

Technique: The RPWS observes a voltage pulse at the input to its electric preamplifier that is due to a small dust particle impacting the spacecraft at speeds of order 10 km/s [1]. The impacting particle has sufficient kinetic energy to vaporize both itself and a small portion of the target material, resulting in a gas with temperatures of order 10^5 K. This temperature is high enough to ionize a significant fraction of the vapor, resulting in a rapidly-escaping electron cloud and a resulting time-variable electric field. If the impact rate is very high, the electric field spectrum will have an f^{-4} dependence. This was the case during crossings through the gap between the F- and G-rings before and after Saturn orbit insertion [1, 2] with impact rates of ~ 1000 s^{-1}. This f^{-4} spectrum allows an estimate of the rms mass of the impacting particles [2,3]. In the E-ring, however, the impact rate is only a few 10's s^{-1}, and shot noise (due to electrons moving past the antennas) dominates the high-frequency spectrum [3]. Here, we must rely on individual detections of the impacts using wideband waveforms that show the voltage pulses.

The individual impacts are found by analyzing temporal variations of the antenna potential appearing similar to those shown in Figure 1. This is best done on the ground, but requires that large data volumes be transmitted to the ground, as the wideband data is generated at rates of 10's of kbps or more, hence, the amount of time for which these data can be acquired is limited. The RPWS also has an on-board algorithm designed to detect the signature of dust impacts from the same waveform data, but the algorithm is limited by its simplicity and has a large effective threshold, limiting it to the largest particles and impact rates of only a few s^{-1}.

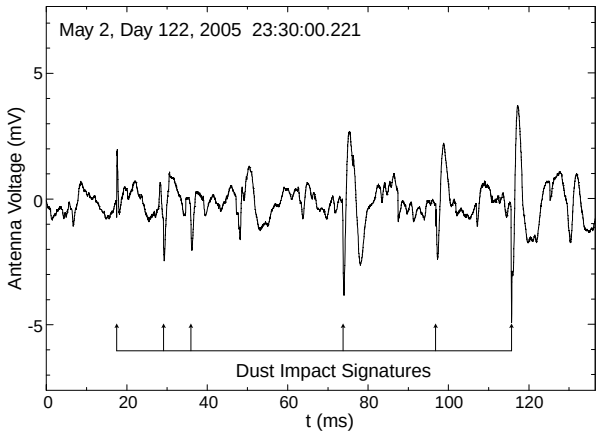

Figure 1: Examples of dust impact signatures.

Preliminary Results: In equatorial passes, impact rates peak near the orbit of Enceladus, suggesting a local source for E-ring particles at this location. Non-equatorial passes through the equator near the orbit of Enceladus allow for a measurement of the thickness of the E-ring at this location. Figure 2 shows the impact rate profile for one such pass on Cassini's 7th orbit of Saturn. The peak impact rate is about 50 s^{-1}. While there is some structure in the profile near its peak which is not currently understood, the remaining portion of the profile is well fit by a Gaussian distribution with a scale height of 2800 km. This translates to a full width at half-maximum of the order of 5000 km.

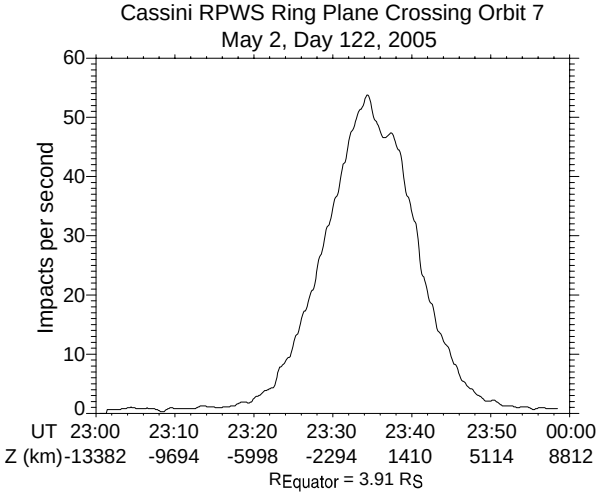

Figure 2: Impact rate profile for Orbit 7 ring plane crossing near the orbit of Enceladus

Knowing the relative impact speed v and an estimate for the cross-sectional area A of the spacecraft, we can calculate a number density n for the detected particles from the impact rate R using $n = R/vA$. The true cross-sectional area of relevance to this problem is likely a complicated function of the projected areas of different materials (which have different yields when impacted by a high velocity particle). For simplicity, we take the area of the 4-m diameter high gain antenna 12.6 m^2 for A. For the Orbit 7 ring plane crossing, the relative speed between the spacecraft and dust v (assuming circular Keplarian orbits) is 8 km/s. So, using the peak impact rate of 50 s^{-1}, the peak number density is approximately 5 x 10^{-4} m^{-3}.

While it is almost certainly true that the amplitude of the voltage pulse measured for a given impact is proportional to the mass of the impacting particle, there are numerous complicating factors that make it difficult to accurately determine the mass. For this work, we utilize the results of Wang et al. [2] who have used the method of Aubier et al. [3] to determine the root mean square mass m of particles detected during two crossings of the ring plane in the gap between the F- and G-rings near the time of Cassini's orbit insertion. The voltage V produced by an impact is $V = km v^{\beta}$ where k is a constant. The value for β is determined experimentally and is somewhat uncertain, but we use 3.2 given by Adams and Smith [4]. The impact speed for the measurements between the F- and G-rings is approximately 16 km/s, or a factor of two larger than for the Orbit 7 E-ring crossing. Simply taking the ratio of the expressions for the rms voltages determined by Wang et al. and those determined here for the E-ring and using the Wang et al. rms mass of ~ 5 x 10^{-11} g, we estimate the E-ring rms mass to be approximately 2 x 10^{-10} g. This corresponds to ice spheres of radius of a few microns. This estimate is larger than those determined for the E-ring in general of 1 micron [cf. 5]. We emphasize that the preliminary nature of our size estimate and the large uncertainties in the analysis of the impacts leading to this size. However, it may also be the case that these particles which we see preferentially near the orbit of Enceladus are actually larger and represent parent bodies for the E-ring population.

We are currently attempting to cross-calibrate these mass determinations with measurements by the Cosmic Dust Analyzer on Cassini. However, it is too soon to know whether or by how much the mass determined by the above impact analysis will change.

References: [1] Gurnett, D. A. et al. (2005) *Science, 307,* 1255–1259. [2] Wang, Z. Z. et al. (2005) *Planet. Space Sci.,* in preparation. [3] Aubier, M. G., Meyer-Vernet, N., and Pedersen, B. M. (1983) *GRL, 10,* 5-8. [4] Adams, N. G., and Smith, D. (1971) *Planet. Space Sci*., *19*, 195-204. [5] Showalter, M. R., Cuzzi, J. N., and Larson, S. M., (1991) *Icarus*, *94*, 451-473.

HYDROGEN ISOTOPIC FRACTIONATION AND THE ROLE OF DUST DURING SUBLIMATION FROM COMETARY ICE. D. S. Lauretta R. H. Brown, B. Schmidt, and J. Moores, Lunar and Planetary Laboratory, University of Arizona. Tucson, AZ 85721, USA. lauretta@lpl.arizona.edu

Introduction: The isotopic compositional variations in solar system materials are important indicators of the origin and evolution of the sun, the planets and the small bodies of the solar system. The deuterium-to-hydrogen ratio (D/H) is particularly important in this regard. Primordial deuterium was synthesized in the first few minutes of the Big Bang [1]. Since then nucleosynthesis in stellar interiors has converted a large fraction of the primordial D to ^{3}He. D has the lowest binding energy per nucleon of all the stable isotopes and can only be formed in extreme environments. There is no way to produce significant amounts of D during the chemical evolution of the galaxy [2].

Cosmochemical and geochemical processes are capable of significantly fractionating D from H. At low temperatures sizeable differences in the zero-point energies of a deuterated molecule and its H-bearing counterpart lead to strong fractionation effects in kinetically controlled chemical reactions [3]. Thus, the D/H ratio could provide a detailed record of temperatures during processing of materials in the interstellar medium and the solar nebula.

Comets are remnant icy and rocky material from the earliest stages of solar system evolution. Long-period comets were likely icy planetesimals that originally formed in the outer solar system and were ejected into the Oort cloud by encounters with the gas giant planets. Short-period comets formed in the Kuiper Belt, outside the orbits of Uranus and Neptune [5]. Because of its potential for constraining the source material and formation mechanisms of comets, the D/H ratio in comet ice has been the subject of intense interest over the past two decades.

The recent apparition of two exceptionally bright comets provided the first opportunity for ground-based detections of cometary D. [6] announced the first positive detection of HDO in Comet C/1996 B2 (Hyakutake) and an upper limit of 0.01 for $(D/H)_{HCN}$. One year later [7] reported on the double-detection of HDO and DCN in Comet C/1995 O1 (Hale-Bopp). These results, combined with water measurements from available IR, UV, and radio measurements made with other instruments, provide constraints on the bulk D/H ratio in water vapor in the cometary comae.

Two independent mass spectrometers aboard the Giotto spacecraft recorded mass-resolved ion spectra of H_3O^+ with a dynamic range large enough to detect the rare isotopes at masses 20^+ and 21^+. From these data the $(D/H)_{H2O}$ ratios for Comet 1P/Halley have been constrained. Measurements of D/H in the coma of these three Oort cloud comets show a D/H ratio that is roughly a factor of 2 higher than the value for standard mean ocean water (VSMOW), and an order of magnitude higher than the protosolar value [8]. These results place fundamental constraints on models large-scale mixing of the solar nebula [9] and the amount of cometary material accreted by the Earth [10].

Discussion: Though these measurements are ground-breaking and important, we urge caution in their interpretation. To obtain an accurate D/H ratio in water using telescopic techniques, one would ideally want to compare HDO with an optically thin line of the rare isotopic molecules $H_2{}^{18}O$ or $H_2{}^{17}O$ using the same instrument; however, all of the stronger transitions of these were inaccessible for the equipment used to detect HDO in both Hale-Bopp and Hyakutake. Hence, observations of HDO abundances in the comae of these comets had to be compared with production rates measured elsewhere at about the same time. For Hale-Bopp, follow-up measurements of HDO indicated that the absolute calibration of the receiver was not fully reliable at the time of the HDO experiment and the temperature scale had to be adjusted to account for this discrepancy [7].

We have noted some inconsistencies in the analysis of the *Giotto* data of the composition of the coma of Halley. The composition of the coma was determined using ion currents measured by the Neutral Mass Spectrometer in the 17.5 amu/e to 21.5 amu/e mass range. The $^{18}O/^{16}O$ ratio in the coma was determined using the intensities recorded at masses 19^+ and 21^+ assuming that there was no contribution from F^+, HF^+, or H_2F^+ and that no Ne was present [11]. Using these assumptions the $^{18}O/^{16}O$ ratio in the coma of comet Halley was determined to be 2130 +/- 180 ppm. While [11] claim that this value is "identical to the average terrestrial value", it in fact deviates from the $^{18}O/^{16}O$ of VSMOW by 82 ‰. This observation is important for calculating the D/H ratio in Halley's coma.

Determination of the D/H ratio in the coma of comet Halley relies on several factors including the measured ion densities at masses 18^+, 20^+, and 21^+, the relative contribution of the H_2O^+ ion to mass 18^+, and the $^{18}O/^{16}O$ and $^{17}O/^{16}O$ ratios. When calculating the D/H ratio, [11] used terrestrial values for both $^{18}O/^{16}O$ and $^{17}O/^{16}O$, despite having directly measured the $^{18}O/^{16}O$ at various positions within the coma. We have recalculated the D/H ratio using the same technique as [11] with two exceptions. We used the individual values for $^{18}O/^{16}O$ determined at each position in the

coma. Furthermore, we assumed that $^{17}O/^{16}O$ is related to $^{18}O/^{16}O$ via the equation, $\delta^{17}O = 0.52 * \delta^{18}O$, which is true if the isotopes are separated via a mass-dependent fractionation process. This treatment not only decreases the calculated D/H ratio (from 255 down to 212 ppm) but also reveals a gradient in the D/H ratio with distance from the nucleus. If this gradient is real, it raises the question: what processes are capable of fractionating the isotopes of H during this process?

Our entire knowledge about the chemical composition in cometary nuclei is tied to studies of the coma composition. In the past the question has been raised, whether, and how closely, observed D fractionations in the coma actually represent the conditions in the nucleus. In the absence of surface probes, it has generally been assumed that the D/H ratio measured spectroscopically in the comet coma is identical to that in the comet ice. [12] developed a simple model of sublimation from a cometary surface. Their results provide a strong indication that significant isotopic fractionation may occur during cometary sublimation in the inner solar system. If so, any inferred consequences for solar nebula models and the origin of terrestrial volatiles must be viewed with caution.

Experimental Study: In light of the importance in understanding the bulk D/H ratio in cometary ices and the questions raised as to the relationship between this value and the HDO/H_2O ratio in cometary coma, we performed an experimental study of ice sublimation under conditions relevant to the surface of a comet in the inner solar system. Our experimental results strongly suggest that the interpretations of measurements of the HDO/H_2O ratio in the coma are oversimplified. In addition, we have discovered some important, fundamental aspects of the mechanism of water ice sublimation in a vacuum.

We have observed a systematic increase in the D/H ratio of the vapor relative to the bulk composition for experiments using pure ice with small ice grain sizes. In these samples deuterated water molecules are able to diffuse relatively rapidly downward into the sample as the result of the many grain boundaries present. We have also performed experiments in which the D/H ratio of the vapor oscillates around the bulk composition. In these experiments, the ice was frozen slowly to produce large crystals and minimal grain boundaries. Finally, in experiments that contain a significant dust component, arguably the most realistic simulation of a comet surface, the D/H ratio in the vapor phase is depleted by as much as 70% relative to the bulk starting composition. Thus, depending on the experimental parameters, the vapor liberated from the icy surface can be enriched, depleted or equivalent in D/H relative to the bulk starting composition. Therefore, we consider it highly unlikely that the D/H ratio observed as HDO/H_2O in cometary nuclei is representative of the bulk D/H ratio in the nucleus.

The second major result of our study is that we have discovered a previously unreported and fundamental characteristic about the sublimation behavior of ice into a vacuum. In particular, we have observed the development of significant outbursts of vapor from a system which occur quasi-periodically. These bursts are accompanied by a significant (~10 degree) drop in the surface temperature of the sample. The decrease in temperature is consistent with transfer of energy to compensate for the latent heat of sublimation. The most D-enriched vapors are liberated during these pressure bursts.

Based on re-analysis of the Halley data and our experimental results we conclude that the reported D/H ratios in cometary comae are not robust. This is due in part to the fact that HDO and H_2O not measured simultaneously in ground-based observations. In addition, analyses of data from the NMS on Giotto are subject to questionable models and assumptions. Our experiments show that, depending on environmental conditions, vapor liberated from a sublimating cometary nucleus can be enriched, depleted or equivalent in D/H relative to bulk composition. Therefore, it is highly unlikely that the D/H ratio observed in a cometary coma is representative of the bulk D/H ratio in the nucleus. In every experiment performed, large pressure bursts were observed that correlate with a large decrease in the surface temperature of the sample. This phenomena is a fundamental characteristic of ice sublimation and is likely the cause of the massive outbursts observed from cometary nuclei.

References: [1] Wagoner, R. V. et al. (1967). *Astrophysical Journal* **148**, 3-49. [2] Epstein, R. I. et al. (1976). *Nature* **263,** 198-202. [3] Criss, R. E. (1999) *Principles of Stable Isotope Distribution*. Oxford University Press [4] Geiss, J. and H. Reeves (1981). *Astronomy and Astrophysics* **93,** 189-199. [5] Duncan, M. (1987) *Astronomical Journal* **94,** 1330-1338. [6] Bockelee-Morvan, D. et al. (1998) *Icarus* **133,** 147-162. [7] Meier, R. et al. (1998). *Science* **279,** 842-844. [8] Geiss J. and Gloecker G. (1998) *Space Science Reviews* **84**, 239-250. [9] Drouart, A. et al. (1999). *Icarus* **140,** 129-155. [10] Laufer, D. et al. (1999) *Icarus* **140**, 446-450. [11] Eberhardt, P. et al. (1995) *Astronomy and Astrophysics* **302**, 301-316. [12] Podolak, M. et al. (2002) *Icarus* **160**, 208-211.

Approaching Interplanetary Dust Physical Properties, from Light Scattering and Thermal Observations and Simulations. A.C. Levasseur-Regourd[1] and J. Lasue[1], [1]Université Paris VI and Aéronomie CNRS-IPSL, BP3, 91371 Verrières, France, aclr@aerov.jussieu.fr.

Introduction: Interplanetary dust particles physical properties (morphology, porosity, size distribution, albedo) are a clue to their origin and evolution. They are approached through (a few) in situ data, and through observations of the solar light they scatter (specially its polarization) and of their thermal emission.

Polarization and Temperature: We will first summarize results on the polarization and temperature of interplanetary dust particles (in the ecliptic and for solar distances below 1.5 AU), and compare them to our present understanding of the interstellar, cometary and asteroidal dust particles properties. As confirmed by recent in-situ missions (to comets and asteroids) and remote observations, cometary particles are likely to be fragile and porous aggregates of interstellar dust grains, while asteroidal particles could be more compact

Numerical Simulations: We will then present new numerical simulations providing the temperature and the polarization (obtained through Mie, T-matrix, DDA and ray tracing routines) for core-mantle grains, aggregates thereof and prolate spheroids. The results, obtained for silicates and spheroids, agree with the laboratory simulations performed on deposited and levitating particles.

Origin of the Dust Particles: These simulations are used to build a model of interplanetary dust particles of cometary (and interstellar) and asteroidal origin, which fits the observed thermal and polarimetric properties, and the expected size distribution of the dust particles. The constraints of the model on the relative contributions of cometary and asteroidal particles, as well as its significance for the origin and evolution of the dust particles will be discussed.

Polycyclic Aromatic Hydrocarbon Molecules in Protoplanetary and Debris Disks

Aigen Li

University of Missouri-Columbia

The polycyclic aromatic hydrocarbon (PAH) emission features at 3.3, 6.2, 7.7, 8.6, and 11.3 μm (previously also known as the "Unidentified Infrared" [UIR] features) are widely seen in protoplanetary disks around Herbig Ae/Be (hereafter HAeBe) stars. From an analysis of the space-borne and ground-based spectra of 41 HAeBe stars in the 3 μm region, Brooke et al. (1993) reported a firm detection of the 3.3 μm PAH feature in $\sim 20\%$ of these objects. Very recently, Acke & van den Ancker (2004) found that the PAH features have been detected in $\sim 57\%$ of the 46 HAeBe stars for which the ISO spectroscopic data is available. The PAH emission features have also been seen in debris disks around Vega-type stars, although not as often as seen in protoplanetary disks around HAeBe stars.

The PAH emission in dust disks is interesting because –

- It allows us to probe the disk structure. There exists evidence that most of the protoplanetary disks in which the PAH emission features have been detected have a flaring disk geometry (Meeus et al. 2001; Acke & van den Ancker 2004). A common interpretation for this is that flared disks intercept more stellar radiation than flat ones, especially at large distances from the central star; the PAH emission originates in the surface layers of a flared disk, where the dust is directly exposed to starlight (Chiang & Goldreich 1997; Meeus et al. 2001; Acke & van den Ancker 2004; Habart, Natta, & Krügel 2004).
- It allows us to obtain a better understanding of the physical conditions of the disk (e.g. electron density n_e, gas temperature $T_{\rm gas}$, and starlight intensity U). This is because the PAH band ratios are sensitive to its charge state which is determined by $U\sqrt{T}/n_e$ (see Weingartner & Draine 2001).
- The PAHs play an important role in the thermal budget and chemistry of the gas, by providing photoelectrons (for heating the gas) and large surface areas.

In this talk I will summarize our recent modeling efforts in understanding the origin, excitation and destruction of PAHs in dust disks and their implications for disk geometry and their physical and chemical conditions.

CHARACTERIZING THE NEAR-EARTH COSMIC DUST AND ORBITAL DEBRIS ENVIRONMENT WITH LAD-C. J.-C. Liou[1], F. Giovane[2], R. Corsaro[2], P. Tsou[3], and E. Stansbery[4], [1]ESCG/ERC, 2224 Bay Area Blvd., Houston, TX 77058, USA, jer-chyi.liou1@jsc.nasa.gov, [2]NRL, [3]NASA JPL, [4]NASA JSC

Introduction: A 10 m^2 aerogel and acoustic sensor system is being developed by the US Naval Research Laboratory (NRL) with main collaboration from NASA Jet Propulsion Laboratory and the NASA Orbital Debris Program Office at Johnson Space Center. This Large Area Debris Collector (LAD-C) is tentatively scheduled to be deployed by the US Department of Defense (DoD) Space Test Program (STP) on the International Space Station (ISS) in 2007. The system will be retrieved after one year. In addition to cosmic dust and orbital debris sample return, the acoustic sensors will measure important impact characteristics for potential orbit determination of the collected samples. The LAD-C science return will benefit orbital debris, cosmic dust, and satellite safety communities. This paper outlines the need for a large-area cosmic dust and orbital debris *in situ* experiment such as LAD-C, and the expected dust/debris impacts on LAD-C during the mission.

Background: Cosmic dust particles, or micrometeoroids, are known to exist throughout the Solar System. The main sources of micrometer-to-centimeter sized dust in the inner Solar System are asteroids and comets (both long-period and short-period). The Earth's accretion rate of cosmic dust is estimated to be about 15,000 to 40,000 tons per year [1, 2]. In addition to cosmic dust, man-made orbital debris, from micrometer-sized solid rocket motor exhaust and satellite breakup fragments to meter-sized retired spacecraft and rocket bodies, also occupy the near-Earth space from about 100 km altitude up to the geosynchronous orbit region [3].

Justification: It is a well-known fact that meteoroid and orbital debris impacts represent a threat to space instruments, vehicles, and extravehicular activities. On average, two Space Shuttle windows are replaced per mission due to damage caused by meteoroid and orbital debris impacts. Of particular significance are particles about 50 μm and larger. Particles smaller than 50 μm are generally too small to be of concern to satellite operations. To have reliable impact risk assessments for critical space assets, a well-defined cosmic dust/orbital debris environment is needed.

The near-Earth cosmic dust flux does not vary significantly over time. On the other hand, the orbital debris populations in the 50 μm to 1 mm size regime are highly dynamic both in time and in altitude. However, there is a lack of well-designed, large surface area *in situ* measurements to better characterize the cosmic dust environment and to monitor the fast-changing small orbital debris populations since the return of the Long Duration Exposure Facility (LDEF) in 1990. There is a need for an updated mission.

Analyzing the chemical composition of the collected cosmic dust can provide clues to the origin and formation of the Solar System. The information also leads to a better understanding of the on-going physical processes (collisions, etc.) that their parents are going through. Many cosmic dust particles have been collected from the stratosphere and analyzed for their compositions [4]. However, a reliable dynamical link has not been established for any collected sample. The combined LAD-C acoustic sensors [5] and aerogel collectors [6] are designed to measure impact parameters (impact time, location, speed, direction) for large particles. With the information, the orbits of some of the collected samples can be determined for possible source identification.

What to expect: The expected number of cosmic dust and orbital debris impacts on LAD-C depends on the location of the system on ISS and the orientation of the detection surface. Both the location and orientation are limited by engineering constraints and the requirement to avoid significant ISS waste contamination. To maximize the science return for cosmic dust and orbital debris, careful planning is needed. Preliminary analysis indicates that a starboard/port-facing orientation will yield the most debris impacts while maintaining a high-level of cosmic dust impacts. In addition, a significant portion of orbital debris impacts on a starboard/port-facing surface will have impact speeds less than 7 km/sec, where the impact characteristics are better understood and the tracks embedded in aerogel are better preserved.

References:

[1] Grün et al. (1985) Icarus, 62, 244-272. [2] Love S. G. and Brownlee D.E. (1993) Science, 262, 550-553. [3] Technical Report on Space Debris (1999), Scientific and Technical Subcommittee of the United Nations, United Nations Publication No. E.99.I.17. [4] Analysis of Interplanetary Dust (1994), AIP Conference Proceedings 310 (Eds. Zolensky et al). [5] Corsaro, R. et al. (2004) NASA Orbital Debris Quarterly News, Vol 8, Issue 3, 6-7. [6] Tsou, P. et al., (2003) JGR, 108, 10.1029.

Deep Impact and Comet 9P/Tempel 1 : From Evolved Surface to Interior Primeval Dust

C. M. Lisse Johns Hopkins University Applied Physics Lab, Laurel MD 20723
(carey.lisse@jhuapl.edu)

The Spitzer Space Telescope, the NASA/IRTF 3m and the Gemini 8m on Mauna Kea, and the Deep Impact HRI-IR used infrared imaging and spectroscopy to observe the rendezvous and impact of the NASA Deep Impact spacecraft before, during, and after the DI impactor hit the comet on July 4, 2005.

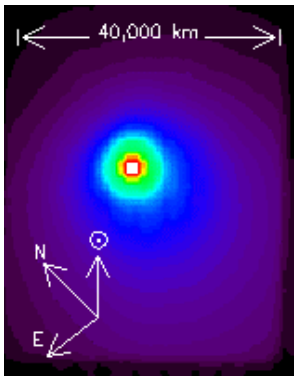

Mid-infrared (16 um) images of the comet before the impact using the Spitzer IRS peakup camera showed a normally active comet streaming dust from its nucleus into interplanetary space. (Figure 1). The size of this mid-infrared image of the heat radiation emitted by the outflowing dust is 40,000 km wide by 60,000 tall. The kind of dust seemed typical, about the size of fine sand, and its flow into space typical, first in all directions, then pushed back by the pressure of the Sun's light backwards into the comet's tail. IR images from the ground showed a similar morphology. HRI-

Figure 1 mapping of the comet from the spacecraft detected a low level of dust emission.

At impact, things changed dramatically (Figure 2). From the spacecraft, a huge fog of fine particles with high optical depth was seen. The particles completely obscured the impact site. From Spitzer, in the first 10 hours, two different streams of material were seen to flow out of the nucleus region and into space, in the SW direction. The first outburst coincides with the fast plume of hot gas and dust that was created when the DI impactor hit the comet and vaporized, then blew back out the hole it bored in the surface of the comet. The second, slower outburst is due to the larger solid material excavated by the shockwave of the impact.

Figure 2

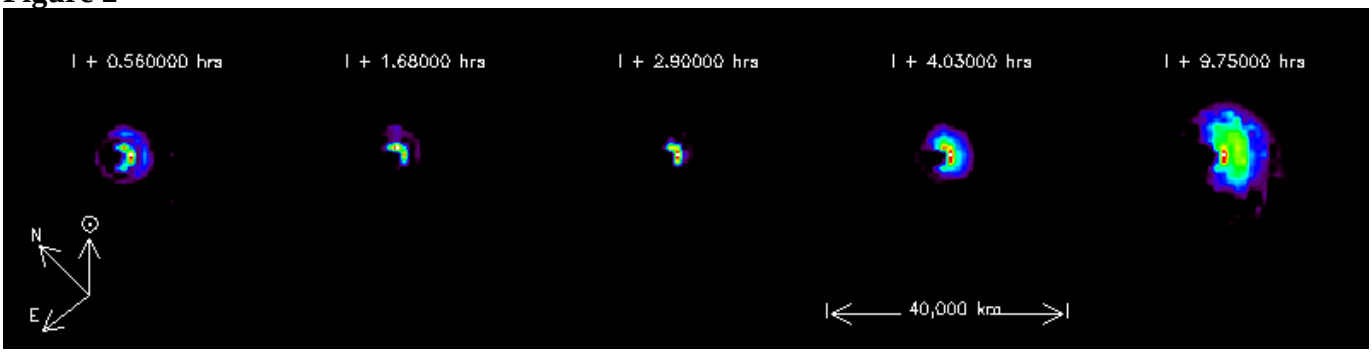

From the ground, a sharp rise in the IR flux was seen at the time of impact, with multiple inflection points due to the flash, plume, and ejecta.

Preliminary spectroscopic chemical analysis of the ejected material at 23 hours before impact and 0.6 hours after impact shows a remarkable change in the outflowing material, with chemical signatures as pronounced as was seen in the spectrum of the extraordinarily active comet Hale-Bopp by the European Infrared Space Observatory in 1996. Before impact, the outflowing dust appears to be typical of other low activity, near-Sun comets, with temperature about 240 Kelvin and the faint signature of the presence of large, amorphous pieces of silicate materials, materials that form rocks on Earth. After impact, there is a new, strong signature of highly crystalline silicates, due to dust particles with the extremely fine consistency of talcum powder, signifying that the DI experiment has released material from the comet similar to the dust found between stars in our galaxy. There is also the signature of water ice, gaseous water, and carbonate solids, like limestone, which can be formed in materials with water, silicates, and carbon dioxide. Evidence for solid CO2 ice and solid organic grains (PAHs) is surprisingly weak, although a large amount of CO2 gas and organic material was seen by the DI spectrometer at the comet, and these species may be obscured from detection by the extremely strong silicate signature. There are also some new, unidentified features which may be new to mid-IR spectroscopy of comets.

The overall temperature of the outflowing material appears to be very mild for such a violent event, about 325 degrees Kelvin from the Spizter continuum, a finding corroborated by the 1-5 um DI spectrometer at the comet and high time resolution NASA/IRTF 3m 0.8 - 2.5 um observations from Mauna Kea. Assuming that the dust has not had time to cool since the impact of the DI spacecraft, this slightly elevated temperature (LTE = 230 K) temperature is too low to alter the dusty materials seen in the ejecta from amorphous to crystalline– temperatures of ~1000K are required for many hours. If the dust was also not shock processed, as seems likely from Deep Impact models of crater excavation on the comet, then remote observations are directly measuring pristine cometary material from inside the comet, material that has been locked away since the beginnings of the solar system, and which holds clues to how the planets formed.

NEW OBSERVATIONS OF THE KINEMATICS OF THE ZODIACAL DUST CLOUD. G. J. Madsen[1], R. J. Reynolds[2], S.I. Ipatov[3], A. S. Kutyrev[4], J.C. Mather[4], and S.H. Moseley[4], [1]Anglo-Australian Observatory, P.O. Box 296, Epping, NSW 1710, Australia, *madsen@aao.gov.au*, [2]Univ. of Wisconsin – Madison, Madison, WI, 53711, [3]Univ. of Maryland, College Park, MD 20740, [4]NASA/GSFC, Greenbelt, MD, 20771.

Introduction: The motion of interplanetary dust particles contains important information about the origin, distribution, and evolution of the cloud in which they move. At optical wavelengths, dust with radii ~10-100μm that lie within ~3 AU of the Sun scatters the incident solar radiation to produce zodiacal light, and the relative motion of the dust modifies the location and shape of solar spectral lines [1-2]. The fraction of zodiacal dust with cometary or asteroidal origin is not well constrained at present [3], and the kinematics of these two components may shift the velocity and widths of the spectral features in unique ways.

However, the low surface brightness of zodiacal light has, until recently, limited the observability of this effect, requiring a combination of high sensitivity and high spectral resolution. Here, we report on new measurements of scattered solar Mg I λ5184 absorption line in zodiacal light with the Wisconsin H-Alpha Mapper (WHAM), and compare the observations with predictions from dynamical models of the zodiacal dust cloud.

Observations: WHAM consists of a 15cm, dual-etalon Fabry-Perot spectrograph coupled to a 0.6m siderostat, and produces an average spectrum over a 1° circular field of view with a 12 km/s resolution within a 200 km/s spectral window. It is specifically designed to detect faint, diffuse optical light [4]. We have recorded spectra centered on the Mg I line at 5183.6Å toward 49 directions along the ecliptic equator, with two directions at high ecliptic latitude [5]. We identified and removed several weak atmospheric emission lines that probably affected the results of previous investigations [6-7]. The line centroid, width, and area were measured for each spectrum. Figure 1 shows the change in velocity centroid with solar elongation for directions along the ecliptic equator. Figure 2 compares an average of several spectra taken toward the north ecliptic pole with an unperturbed twilight spectrum, demonstrating the high resolution and sensitivity of the observations. We see that the width of the line near the pole is broadened by 15-20 km/s relative to the solar line, suggesting that a significant number of particles follow orbits with inclinations up to 40° [5]. Somewhat less, but still significant, broadening is also observed along the ecliptic equator, including the antisolar direction. This implies particles with non-circular orbits [5].

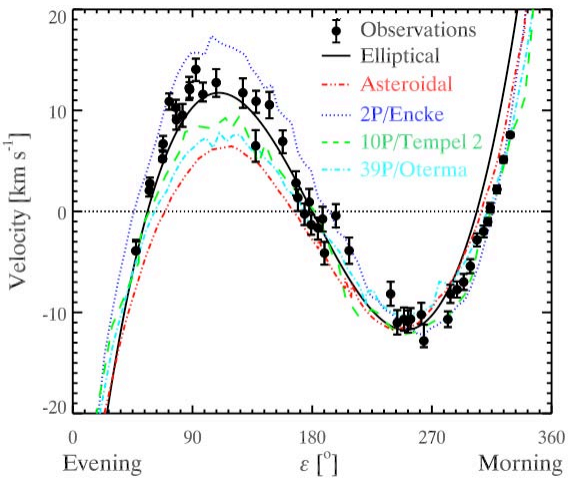

Figure 1: Velocity centroid of the scattered solar Mg I line as a function of solar elongation, with several models overlaid.

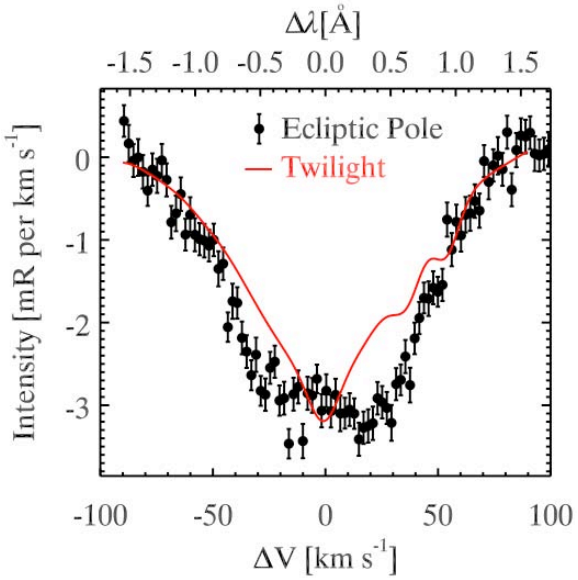

Figure 2: Spectrum of the twilight sky (red) and the zodiacal light toward the north ecliptic pole (circles), centered near the Mg I λ5184 line. The abscissa is in mill-Rayleighs per km/s.

Comparison to Models: The shape of the observed line profiles is determined by the population of dust particles of varying size, radial distance, scattering function, and relative motion along the line of sight. We compare our observations with

dynamical models of the zodiacal dust cloud in order to constrain the orbital properties of the particles which comprise the cloud. We consider a number of published models that make specific observable predictions, particularly for the change in velocity centroid with elongation angle.

Some of the models that compare favorably to the data are shown in Figure 1. The solid black line is a fit to a model from Hirschi & Beard [8]. This model describes particles on prograde, elliptical orbits with eccentricities uniformly distributed between 0 and 1, with randomly distributed perihelions. Their model did not include the influence of radiation pressure, and the particles were confined to the ecliptic plane. The model fits the centroid data well, but strongly overestimates the width of the lines. The inclusion of radiation pressure and/or inclined orbits could provide a better match to the observations [5,9].

The colored lines in Figure 1 are models from Ipatov et al. [10-11], which trace the motion of different populations of dust particles subject to gravity, radiation pressure, and drag forces. The individual lines represent particles with asteroidal and various cometary trajectories, with a ratio of radiation pressure to gravitational force of 0.002. We find that a better match is provided by the cometary particles on inclined, eccentric orbits compared to the asteroidal particles. We note that none of the models with trans-Neptunian particles match the data and are omitted for clarity.

Summary and Future Work: Observations of scattered solar absorption lines in the zodiacal light are a powerful technique for exploring the kinematics of the zodiacal dust cloud. Our data are fit well by models that contain particles on elliptical orbits that are inclined to the ecliptic plane. This suggests that most of the dust in the zodiacal cloud has a cometary origin [3].

Higher signal-to-noise observations covering a larger fraction of the ecliptic sky, that include other, more intrinsically narrow, absorption lines will provide a more complete picture of the kinematics of the zodiacal dust cloud. New dynamical models that explore a wider range of dust parameters can provide strong, quantifiable constraints on the nature of the zodiacal dust cloud when compared to the observations.

References:

[1] Grün E. et al. (2004) in *Astrophysics of Dust, ASP Conf. Series, 309*, 245-264. [2] Clarke D. et al. (1996), *Astronomy & Astrophys., 308*, 273. [3] Dermott S.F. et al. (1996) in *Physics, Chemistry, and Dynamics of Interplanetary Dust, ASP Conf. Series 104*, 143-153. [4] Reynolds R.J. et al (1998), *Pub. Astr. Soc. Of Australia*, 15, 14-18. [5] Reynolds R. J., Madsen G. J. and Moseley, S. H. (2004), *Astrophys. J., 612*, 1206-1213. [6] Fried J.W. (1978), *Astronomy & Astrophys.*, 68, 259. [7] East I. R. and Reay N. K. (1984), *Astronomy & Astrophys.*, 139, 512. [8] Hirschi D.C. and Beard D. B. (1987), *Planet. Space Sci., 35*, 1021. [9] Rodriguez G. L. and Magro C. S. (1978), *Astronomy & Astrophys., 64*, 161. [10] Ipatov S. I. et al. (2005a), *LPS XXXV*, Abstract #1266. [11] Ipatov S. I. et al. (2005b), *BAAS, 206*, Abstract #449.

DYNAMICS OF THE DUST GRAINS IN THE SATURN'S RINGS

E. Martínez-Gómez, H. Durand-Manterola, and H. Pérez de Tejada
Department of Space Physics, National University of Mexico, C.P. 04510, Mexico City
e-mail: affabeca@avantel.net , fax: (525) 550 24 86

Saturn's magnetosphere contains numerous sources of neutral gas. The neutral gas can become ionized and contribute to the thermal plasma and radiation belt particle populations. In particular, sputtering by charged particle and meteoroid bombardment of material from the rings and the surfaces of Saturn's icy moons is believed to create an extensive neutral cloud of water molecules and water dissociation products in the inner magnetosphere that seeds it with water product ions.

In order to explain the dynamics of the dust grains in the Saturn's rings as a source of particles for the magnetosphere we developed a model which considers that the gravitational field (for neutral dust grains) and the electric field (for charged dust grains) have a stochastic behavior simulated by a Monte Carlo Method.

Our results show that the neutral dust grain located in the E-Ring, gains approximately 1% of its initial energy. In the Cassini Division the energy remains unchanged. In the B-Ring, the neutral dust grain losses ~90% of its initial energy. The charged dust grains are accelerated to reach higher velocities.

ADVENTURES IN GRAVITATIONAL FOCUSING. M. J. Matney, NASA Johnson Space Center, 2101 NASA Parkway, Mail Code KX, Houston, TX, USA, 77058, mark.matney-1@nasa.gov

Abstract: The forces of gravity near a planet can have a profound effect on the flux, speed, and directionality of meteoroids in space. This gravitational focusing effect selectively intensifies low-velocity meteoroid fluxes relative to high-velocity ones. This effect can lead to biases when using fluxes measured within a planet's gravitational field to understand the meteoroid sources away from the planet in interplanetary space. However, this effect can also be used creatively to extend and enhance the capability of orbiting sensors. In this paper, I review the Liouville method for computing gravitational focusing originally outlined in Matney, 2002 [1]. Then, I present examples of how planetary gravity affects meteoroid fluxes on spacecraft. I conclude with ideas and examples on how spacecraft experiments can be designed to use a planet's gravity as a giant "lens" to aid in the detection and identification of meteoroid sources.

References: [1] Matney, M. J. (2002) *Dust in the Solar System and Other Planetary Systems*, COSPAR Colloquia Series Vol. 15, 359-362.

OXYGEN ISOTOPE MEASUREMENTS OF BULK UNMELTED ANTARCTIC MICROMETEORITES. G. Matrajt, *Department of Astronomy, University of Washington, Seattle WA, 98195 (matrajt@astro.washington.edu)*, Y. Guan, L. Leshin, *Department of Geological Sciences, Arizona State University, Tempe AZ, 85287*, S. Taylor, *U.S. Army Cold Regions Research and Engineering Laboratory, Hanover, NH, 03766*, M. Genge, *Department of Earth Sciences and Engneering, Imperial College London, London UK*, D. Joswiak, D. Brownlee, *Department of Astronomy, University of Washington, Seattle WA, 98195*.

Introduction:
Studies of oxygen isotopic compositions of meteorites including lunar and Mars meteorites, have provided critical insights into the processes that formed the early Solar System (for a review see [1]). The isotopic composition of small particles (micrometeorites and IDPs) should also provide insight into these processes. However, few studies exist of oxygen isotopic compositions of micrometeorites. Most studies have analyzed melted micrometeorites (also known as cosmic spheres) from the deep sea [2,3] or Antarctic ice [4, 5, 6]. Only individual phases of unmelted micrometeorites, such as silicates [7,8] and refractory grains [9] have been analyzed for oxygen isotopes. In this study we measured the oxygen isotopic composition of 28 unmelted Antarctic micrometeorites studied as whole particles and compared their ratios to the values measured in melted micrometeorites as well as in CIs chondrites. We use the comparison to discuss the possible origin of these micrometeorites.

Samples and Methods:
The micrometeorites were collected in the South Pole water well [10]. For this study we selected unmelted micrometeorites from the 150-250 μm size fraction. All the black particles with irregular shapes were mounted in *crystalbond*. After sectioning and polishing, the mounts were surveyed using a scanning electron microscope (SEM) and Energy-Dispersive X-ray (EDX) analyzer. The SEM micrographs were used to classify the micrometeorites and the EDX data were used to identify chondritic particles.
In preparation for the isotopic measurements, the micrometeorites were removed from the *crystalbond* using acetone. Each micrometeorite was then pressed between two tungsten carbide plates to make it as homogeneous and flat as possible. The particles were then pressed into gold. The samples were analysed for their oxygen isotopic compositions using the Secondary Ion Mass Spectrometry (SIMS) technique, with a CAMECA IMS 6f ion microprobe at Arizona State University. Analytical spots of about 20 μm in diameter, producing craters of about 1-2 μm in depth, were randomly made on the particle's surface. The analytical uncertaintity obtained during this study is less than 3 ‰. Chunks of San Carlos olivine were used as a standard for the calibration of the analytical instrument.

Results:
The micrometeorites were classified as fine-grained, scoriaceous, coarse-grained and composite (a mix of two other classes) and particles of each type were selected for ion microprobe analyses. In figure 1 we plot the average oxygen isotope values for each particle. The measured oxygen isotope values range from δ^{18}O= 3 to 60 ‰ and δ^{17}O= -1 to 32 ‰, and fall, within 2σ error, along the terrestrial fractionation line (TFL) of slope 0.52. Individual oxygen isotope measurements vary both among the micrometeorites and within a single micrometeorite (from -1.2 to 34.6 ‰) suggesting that these micrometeorites are isotopically heterogeneous.

Figure 1: Oxygen three-isotope plot of the averaged values obtained during two runs and over several spots. The points have been plotted according to the type of particle. Squares: coarse-grained; diamonds: fine-grained; triangles: scoriaceous and circles: composite particles. The cross represents 2σ error, the uncertainty due to instrumental mass fractionation.

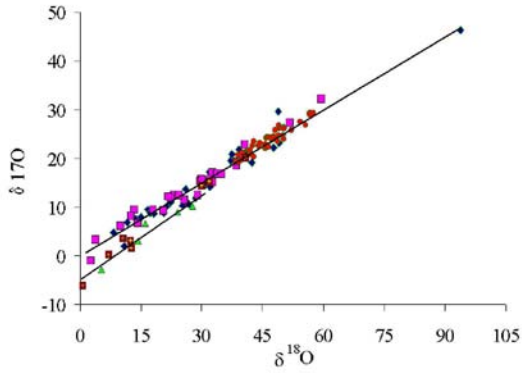

Figure 2: Oxygen three-isotope plot of the values obtained during this study, compared to the data from other studies on melted micrometeorites. Pink squares: this study; blue diamonds: silicate spheres [6]; red circles: deep sea iron spheres [3]; green triangles: deep sea stony spheres [3]; brown squares: stony spheres [5].

In general, the lightest isotope values are associated with the coarse-grained micrometeorites ($\delta^{18}O \leq 25‰$) whereas most of the fine-grained and scoriaceous mi-

crometeorites have $\delta^{18}O \geq 18‰$ (Fig. 1). This suggests that the matrix in MMs is isotopically heavier than the anhydrous silicate phases. Studies of olivine and pyroxene phenocrysts in MMs show that they have $\delta^{18}O$ values ranging from -9.9 to 8.0 ‰ [7]. Fine-grained micrometeorites that plot among the coarse-grained micrometeorites may contain a higher proportion of anhydrous silicates. The scoriaceous ($\delta^{18}O \geq 29‰$) and some fine-grained micrometeorites ($\delta^{18}O \geq 32‰$) have overlapping oxygen isotope ranges suggesting that the phases that vaporize to form the vesicles do not have a large isotopic effect on the isotopic composition of the micrometeorite. In Fig 2 is shown a comparison of our data to the data on melted micrometeorites. Our measurements are similar to the values found for melted micrometeorites. Both melted and unmelted micrometeorites studied as whole particles fall along the TFL with $\delta^{18}O$ values in the range 5 to 90 ‰ [3, 5, 6]. This suggests that there was not significant change in the oxygen isotope ratios of micrometeorites during their atmospheric entry because if oxygen exchange was taking place during the atmospheric entry, then cosmic spherules (completely melted micrometeorites) would have the highest $\delta^{18}O$ values.

Discussion:
Given that the values of $\delta^{18}O$ presented here are among the highest reported to date, we needed to address processes that could have altered the isotopic composition of the micrometeorites. We identified four such processes and discuss them in turn: a) isotopic exchange with Antarctic water, b) isotopic exchange with the oxygen in the atmosphere during atmospheric entry, c) atmospheric entry heating or d) instrument error.
Isotopic exchange with Antarctic ice or meltwater would drive the $\delta^{18}O$ to lighter isotopic values because the average $\delta^{18}O$ of Antarctic water is $\sim -50‰$ [11]. Our data show that the micrometeorites are enriched in ^{18}O indicating no significant effect from the water on the oxygen ratios measured in these MMs.
Additionally, the oxygen isotope values do not cluster near the value for air ($\delta^{18}O$= 23.5 ‰ [12]), but rather spread along the TF line (see Fig. 1). This suggests that the oxygen isotope values are not the result of simple mixing and/or replacement with atmospheric oxygen. Also, the lack of a ^{18}O rich oxygen source in the high atmosphere [12, 13] argues against atmospheric oxygen exchange with our micrometeorites.
Isotopic fractionation due to entry heating (evaporation) is observed only in a small subset of melted micrometeorites [4, 5]. The textures of the micrometeorites analyzed here indicate that they were not melted. In addition, our particles are chondritic and any loss of oxygen due to vaporization would be accompanied by evaporation of iron, magnesium and silicon [14, 15], rendering them non-chondritic in composition.
Finally, to ensure that the instrument was working properly we re-analyzed all the micrometeorites. The replicate measurements were, within analytical uncertainties, similar to the former measurements despite an upgrade of the sample stage and slightly different analysis conditions between the two analysis sessions.
We therefore conclude that the $\delta^{18}O$ values presented here accurately represent the isotopic compositions of the micrometeorites before they entered the Earth's atmosphere. If so, the parent body(ies) of these MMs has/have a high $\delta^{18}O$ compared to other planetary materials.
The extremely heavy values observed here have not been reported in previous analyses of chondrite matrix material. Furthermore, the isotopic values found in these micrometeorites show a wide range. These observations suggest that micrometeorites (unmelted + cosmic spheres) are a new type of Solar System object not present in the meteorite collections. A similar conclusion was reached during a detailed study of the mineralogy of unmelted micrometeorites by [16].
It is worth noting that some of our MMs have oxygen isotope values laying along the TFL in the same region where the CI carbonaceous chondrites values are found. This suggests that these particles could be sampling CI-like parent bodies. This idea is further supported by the founding of 9 unmelted micrometeorites that have a mineralogy almost identical to that of CI chondrites [16]. However, our knowledge of the level of microscale isotopic heterogeneity of C chondrite matrices is very limited and thus it is not yet possible to compare directly the data presented here with carbonaceous chondrite compositions.

Conclusions:
The oxygen isotope data suggest that micrometeorites are a type of Solar System material not otherwise represented in our meteorite collections to date. Their parent body was probably a very friable asteroid (or family of asteroids) that does not produce rocks upon collision with other bodies, but rather small particles that are then captured by the Earth penetrating its atmosphere in the form of dust.

References: [1] Clayton, R.N. (2003) *Space Sci. Rev.*, **106**, 19-32. [2] Clayton, R.N. et al. (1986) *Earth Planet. Sci. Lett.* **79**, 235-240. [3] Engrand, C. et al (1998) *LPSC*, **Abs**, 1473. [4] Alexander, C. et al. (2002) *GCA*, **66**, 173-183. [5] Taylor, S. et al. (2005) *GCA*, in press. [6] Yada, T. et al (2003) *LPSC*, **Abs**, 1587. [7] Engrand, C. et al (1999) *GCA*, **63**, 2623-2636. [8] Yada. T. et al (2002) *M&PS*, **37**, A152. [9] Greshake, A. et al (1996) *M&PS* **31**, 739-748. [10] Taylor, S. et al (1998) *Nature* **392**, 899-903. [11] Smith, B. et al (2002) *Ann. Glaciology* **35**, 107-110. [12] Thiemens, M. et al (1995) *Science* **270**, 969-972. [13] Thiemens, M. (1999) *Science* **283**, 341-345. [14] Davis, A.M. et al (1990) *Nature* **347**, 655-658. [15] Davis, A.M. et al (1991) *LPSC*, 281-282. [16] Noguchi, T. et al (2002) *M&PS*, **37**, A111.

CASSINI COSMIC DUST ANALYSER: COMPOSITION OF DUST AT SATURN. N. McBride[1], J. K. Hillier[1], S. F Green[1], J. P. Schwanethal[1], J. A. M. McDonnell[1], R. Srama[2], S. Kempf[2], F. Postberg[2] and E. Grün[2,3], [1]Planetary and Space Sciences Research Institute, The Open University, Milton Keynes, MK7 6AA, UK, n.m.mcbride@open.ac.uk, [2]MPI für Kernphysik, Saupfercheckweg 1, 69117 Heidelberg, Germany. [3]Hawaii Institute of Geophysics and Planetology, University of Hawaii, 1680 East West Road, POST 512c, Honolulu, Hawaii, HI 96822, USA.

The Cosmic Dust Analyser (CDA) aboard the Cassini spacecraft has been sampling dust within the Saturnian system since orbit insertion in July 2004. CDA consists of two primary subsystems: the Dust Analyser subsystem, with instruments capable of measuring charge, velocity, mass, low-rate flux and composition of dust particles, and the High-Rate Detector (HRD) which measures high-rate fluxes of impacting particles using a PVDF impact sensing system. The Dust Analyser uses the characteristics of the plasma generated by an impact of a dust particle on a metal target to determine (approximately) particle mass and speed. A crucial subsystem of CDA is the Chemical Analyser, which uses a discrete central rhodium target section within the Dust Analyser. This target is held at 1 kV with respect to a mesh grid 3 mm in front of it, producing a strong electric field that accelerates impact-generated ions towards an electron multiplier, so delivering positive ion time-of-flight mass spectra (TOFMS) of impacting particles.

The Chemical Analyser is now returning thousands of spectra from the Saturnian system. For example, during a single ring plane crossing (the descending ring plane crossing in October 2004), it produced nearly 300 TOFMS of E-ring dust particles at a distance of ~8 R_S from Saturn. Interpreting these TOFMS can be complicated. In principle the arrival time at the multiplier, of an initially stationary ion, is governed by the relation $t = b + a\sqrt{m}$, where m is the ion mass, b is a zero point time offset, and a is a 'stretch' parameter related to the instrument geometry and field strength. However, this behaviour is complicated by the initial velocity distribution of the ions, plasma shielding effects, differing geometries within the instrument, and unknown zero-point offsets attributable to triggering time differences. In cases where the ion species corresponding to at least two peaks can be identified unambiguously, the a and b parameters can be determined with reasonable accuracy (enabling spectra to be converted from time to mass space). However the aforementioned effects mean that a given ion species (a single m value) will give rise to spectral peaks which can vary from very narrow to extremely broad. Furthermore, the peak width and overall peak shape is likely to depend also on the impact velocity, mass and composition of the dust particle.

Identification of mass species within the TOFMS can be made easier by understanding the ion dynamics within the instrument as a whole. This paper presents an overview of the Chemical Analyser and discusses the effects of the ion dynamics within the instrument and how it affects the peak shapes and position. This is demonstrated by use of an in-house ion dynamics code developed specifically for the CDA instrument (see also Hillier et al., this abstract volume). We then present TOFMS obtained within the Saturnian system, with interpretation of the impacting particles' composition. For example, during the E-ring plane crossing during October 2004, we found that the particles predominantly consisted of water ice (manifesting itself in the TOFMS as hydronium ions, with varying numbers of water molecules attached) and minor silicate impurities. Results obtained up to September 2005 will be discussed.

THE NATURE AND HISTORIES OF PRESOLAR DUST GRAINS. S. Messenger, NASA Johnson Space Center, Astromaterials Research & Exploration Science Division, Robert M Walker Laboratory for Space Science, Houston TX 77058. scott.r.messenger@nasa.gov

Introduction: Meteorites and interplanetary dust particles (IDPs) are repositories for the least altered remnants of the building blocks of the Solar System, including pre-solar system stardust grains and organic compounds that likely formed in a cold molecular cloud [1,2]. Stardust identified to date includes grains of diamond, Si_3N_4, SiC, graphite, TiC, Al_2O_3, TiO_2, hibonite, spinel, forsterite, and amorphous silicates [3,4]. With the exception of nanodiamonds, these grains are large enough (>200 nm) to have their isotopic compositions measured by secondary ion mass spectrometry. Grains of extrasolar origin are identified by isotopic compositions in major and minor elements that differ from solar isotopic ratios in some cases by orders of magnitude.

These grains originated from a diversity of stellar sources, including red giant and asymptotic giant branch stars, novae, and supernovae. Their isotopic compositions show that their parent stars had a wide range in mass and chemical composition, requiring contributions from dozens of stars. No single stellar source appears to dominate.

Silicates are the most abundant type of presolar grains, but they were only discovered recently because of their small size (0.1 – 1.0 μm) and the difficulty in locating them among the overwhelming background of solar system silicates. The abundances of silicate stardust and other presolar grain types varies considerably among different classes of primitive meteorite, generally following the extent of parent-body metamorphism [4]. Silicate stardust is more abundant in anhydrous interplanetary dust particles (450 – 5,500 ppm; 5,6), than in meteorites (<180 ppm; 7). The greater survival of presolar grains in anhydrous IDPs shows that these are the least altered remnants of the early solar system, and lends support to the view that these particles derive from short period comets [8].

Presolar silicates: Of the few presolar silicates whose mineralogy has been definitively identified by TEM, 4 are amorphous silicates including GEMS grains, and 2 are olivine grains. The mineralogy of presolar silicates is distinctly different from interstellar silicates, that are inferred to be dominantly amorphous (>99%) based on the shape of the 10 μm silicate spectral feature [9]. Possible resolutions to this discrepancy are that: (1) the abundances of interstellar amorphous and crystalline silicates have been improperly derived from the ~10 μm feature [10], (2) most of the mass of interstellar silicate grains have been recycled through repetitive sputtering and recondensation in the ISM, rendering them isotopically homogeneous (~solar; 11).

The uncertainties in the natures and histories of interstellar silicates are major unsolved problems that bridge wide-ranging fields in astrophysics. However, the processing of grains in the interstellar medium and the solar nebula have distinct and observable consequences. Because the extremely low density of the diffuse ISM, grains are unlikely to condense directly, but gradual atom mixing between grains, as proposed in [11] is possible. If this is the case, the average chemical compositions of all interstellar grains are expected to become homogenized. Secondly, the isotopic compositions of individual homogenized interstellar grains will become less distinct.

Because the isotopic composition of typical grains from evolved stars are originally extremely exotic, interstellar grains polluted by extensive ion-mixing may retain detectable isotopic signatures [12]. The future challenge of identifying grains that largely formed in the interstellar medium from remnants of earlier generations of stardust will require measuring the major and minor chemical compositions and precise isotopic abundances on the scale of individual submicrometer grains.

References: [1] *Astrophysical Implications of the Laboratory Study of Presolar Materials*, T. J Bernatowicz and E. Zinner, Eds. (AIP Conf. Proc. **402**, American Inst. of Phys. Woodbury, NY, 1998). [2] Messenger S. (2000) *Nature* 404, 968. [3] Zinner E. , in *Treatise on Geochemistry*, K. K. Turekian, H. D. Holland, v. e. A. M Davis, Eds. (Elsevier, 2004), vol. 1, pp. 17-39 [4] Huss G. & Lewis R. S. (1995) *Geochim. Cosmochim. Acta* **59**, 115-160 [5]. Messenger S. et al. (2005) *Science*, 300, 105. [6] Floss C. & Stadermann F. J. (2004) *Lunar Planet. Sci.* 35, Abstract #1281. [7] Nguyen A. & Zinner E. (2004), *Science* **303**, 1496. [8] Bradley J. P., Sandford S. A. & Walker R. M. (1988), in *Meteorites and the Early Solar System*, J. Kerridge and M.S. Matthews, Eds. (Univ. Arizona Press, Tucson, AZ), pp. 861-895 [9] Kemper F., Vriend W. & Tielens A. G. G. M. (2004), *Astrophys. J.* **609**, 826. [10] Bowey J. E. and Adamson A. J. (2002) *Mon. Not. R. Astron. Soc.* **334**, 94-106 [11] Bradley J. P. and Dai Z. R. (2005) *Astrophys. J.* **617**, 650-655 [12] Keller L.P. & Messenger S. (2005) Proc. Chondrites and the Protoplanetary Disk.

A CCD SEARCH FOR THE DUST TRAIL OF DRACONID PARENT COMET 21P/GIACOBINI-ZINNER.

Naoya MIURA[1], Masateru ISHIGURO[2], Yuki SARUGAKU, Fumihiko USUI, Munetaka UENO. [1]Graduate School of Arts and Sciences, University of Tokyo, Tokyo 153-8902, Japan, miura@zodi.c.u-tokyo.ac.jp, [2]Institute of Space and Astronomical Science, 3-1-1 Yoshidamachi, Sagamihara, Kanagawa 229-8510, Japan, ishiguro@planeta.sci.isas.jaxa.jp

Introduction: Meteor streams occur when the Earth happen to enter a small portion of cometary dust trails. Hence we had rare chance to investigate the cometary dust trails during the meteoric streams. Infrared Astronomical Satellite (IRAS) discovered the thermal radiation from the particles in the dust trails, and it provided the unique way to obtain a synoptic view of wide-spread cometary debris [1]. Using the infrared images, it is possible to establish the intimate dynamical model of dust trails [2]. State-of-the-art technologies of data analysis and observing system have opened up the new opportunities to investigate the dust trails from the ground; Ishiguro et al. succeeded to detect the scattered sunlight by the dust trail particles of 22P/Kopff using the ground-based telescope with optical CCD camera [3]. The time comes to study the dust trails at any time with inexpensive astronomical instruments.

The Draconids show periodic activities, and they produced twice spectacular meteor storms in 1933 and 1946. Their parent comet is 21P/Giacobini-Zinner, which is thought to be unusual in the chemical composition [4]. It belongs to the group of "depleted" comets characterized by low abundances of carbon in the gas phase. It is likely that organics may be in the dust phase.

Observations: We searched a faint scattered light from meteoroids of 21P/Giacobini-Zinner using UH 2.24-m telescope and Kiso 1.05-m Schmidt telescope. The instruments consist of 8kCCD camera with R-band filter (UH88 run) and 2K CCD camera with R-filter (Kiso run). Observations were carried out at UH88 on 2004 May 23 and at Kiso between 2005 May 2 and 14. The perihelion passage of this comet is on 2005 July 2. Both UH88 and Kiso data were obtained under the photometric condition.

Results: Size of the dust particles can be identified by beta, the ratio of solar radiation pressure to gravity. No significant enhancement of the brightness on the line of beta<10^{-3} (assuming the spherical particles with mass density of 1.0 g/cc, the diameter is larger than 1mm grains). In this presentation we discuss the reasons of our negative results.

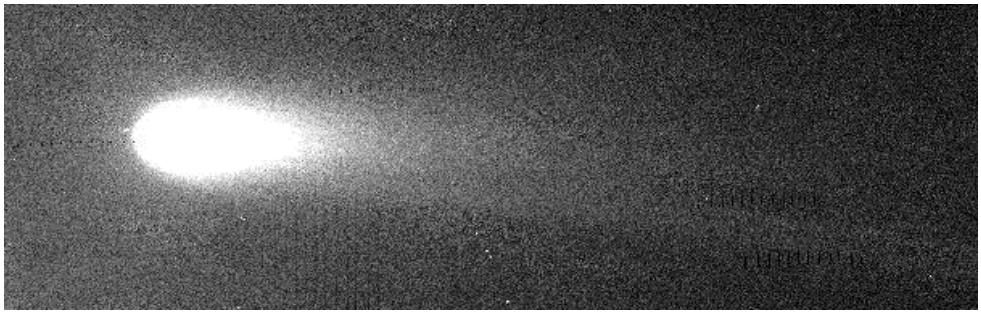

Obtained image of 21P/Giacobini-Zinner taken by 2K CCD camera attached to Kiso Schmidt

References: [1] Sykes M.V. and Walker R.G.(1992), *Icarus*, *95*, 180–210. [2 Reach et al. (2000), *Icarus*, *148*, 80-94. [3] Ishiguro et al. (2002), *ApJ,572*, 117-120. [4] A'Hearn et al. (1995) , *Icarus*, *118*, 223-227.

TOF spectrometry of hyper-velocity dust impacts and laser ionization.
A. Mocker (amocker@galileo.mpi-hd.mpg.de)

Dust detectors onboard interplanetary space missions are often based on impact ionization of hyper-velocity dust impacts. In order to calibrate those instruments the ion formation of the impact plasma is investigated. The plasma parameters and the ion yield are measured using a linear time-of-flight mass spectrometer.

To cover a sufficiently wide energy range for the simulation of dust particle impacts the impact experiments at the Heidelberg dust accelerator should be supplemented with a laser ionization experiment. Therefore it is necessary to investigate the properties of dust impact properties and laser ablation with respect to their comparability, and, if there is one, to determine which laser beam properties (i.e. energy) correspond to those of special dust particles.

For this purpose measurements with a wide variety of target materials, like rhodium, silver and various silicates, have been done for both dust impacts and laser ablation with the very same experimental set up.

The characteristics of both by the impact and the laser ablation generated plasma, such as the

- ion yield
- estimated ion temperature
- energy distribution of the ions
- appearance of individual species of ions in the time-of-flight mass spectra
- shifting of the time-of-flight mass spectra

and i.e. their dependence on the impact or laser energy, the densities and crystal properties of the target are investigated.

Afterwards the results of these investigation are compared with the predictions of models for impact ionisation and laser ablation to get a better understanding of this processes.

Generated dust impact charge measurements by Cassini's Dust Instrument, CDA

G. Moragas-Klostermeyer[1], R. Srama[1], S. Kempf[1], S. Helfert[1],
M. Roy[2], M. Burton[2], N. Altobelli[2], V. Dikarev[1], H. Krüger[3], E. Grün[1,3]

[1]MPI for Nuclear Physics, Heidelberg, Germany; [2]JPL , Passenda/California, USA;
[3]MPI for Solar System Research, Katlenburg-Lindau, Germany; [4]HIGP - University of Hawaii, Honolulu, USA

Abstract

After Cassini's Saturn Orbit Insertion on the first of July 2004 CDA [Srama et al., 2004a] - the Cosmic Dust Analyzer instrument onboard the Cassini spacecraft - has recorded many ten thousand dust impacts. Especially during the Saturn's E-ring plane crossings (29 until now) the majority of the impacts occured. The considered region is inside Titan's Orbit at 20 Saturn's Radii and has a height variation (Figure 1) of several Saturn Radii around the saturnian ring plane. CDA is an impact ionization detector that measures the charge released from a hypervelocity impact of typically micron sized dust particles. The instrument has an impact target of $0.1m^2$ sensitive area and a wide field-of-view. The dust impact charge released range from 10^{-15} C to 10^{-08} C.

The impact rates range from 10^{-3} to $\gg 1$ impacts per second during the E-ring crossings. Due to the roll of the Cassini spacecraft during some crossings CDA scans a wide range of impact directions. Additionally the instrument and measurement configuration in terms of threshold levels, shrinking and spacecraft pointing was taken into account. Both the impact charge amplitude distribution and the impact rate is determined at various positions in the E-ring and at different pointing directions.

Different moments of the impact charge distribution like the cumulative number of charges or rates should help to provide informations for a possible cross-calibration with other instruments on Cassini. One instrument is the Radio and Plasma Wave Science Instrument (RPWS) which records charges released by dust impacts on the Cassini surface as like the PRA Instrument did this on Voyager I and II [Meyer-Vernet et al., 1996 & 1998; Gurnett et al., 1983].

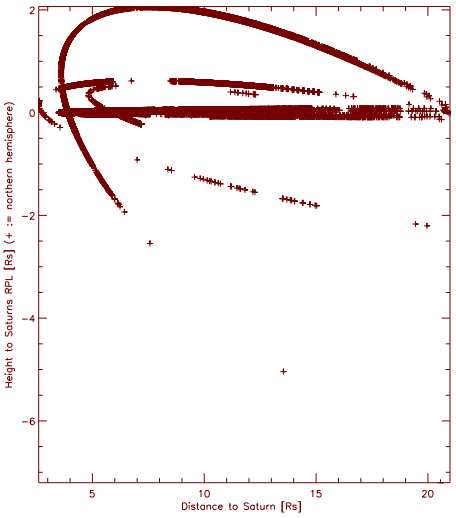

Figure 1: CDA dust impacts - Height above ring plane against radial distance to Saturn's Masscenter

References

[Gurnett et al., 1983] D.A. Gurnett, E. Grün, D. Gallagher, W.S. Kurth, F. L. Scarf, Micron-Sized Particles Detected near Saturn by the Voyager Plasma Wave Instrument, *Icarus* 53, 236-254 (1983)

[Meyer-Vernet et al., 1996] Nicole Meyer-Vernet, Alain Lecacheux, Bent M. Pedersen, Constraints on Saturn's E Ring from the Voyager 1 Radio Astronomy Instrument, *Icarus* 123, 113-128 (1996)

[Srama et al., 2004a] R. Srama et al., The Cassini Cosmic Dust Analyzer, *Space Sci. Rev.*, 114, 1-4, 465-518, 2004a

SIGNATURES OF PLANETS IN DEBRIS DISKS. A. Moro-Martín[1], R. Malhotra[2] and S. Wolf [3], [1] Department of Astrophysical Sciences, Peyton Hall, Princeton University, NJ 08544, US; amaya@astro.princeton.edu; [2]Department of Planetary Sciences, University of Arizona, 1629 East University Boulevard, Tucson, AZ 85721, US; [3]Max-Planck-Institute fur Astronomie, Konigstuhl 17, 69117, Heidelberg, Germany.

Abstract: Main sequence stars are commonly surrounded by debris disks, formed by cold far-IR-emitting dust that is thought to be continuously replenished by a reservoir of undetected dust-producing planetesimals. This indicates that plantesimal formation is a common by-product of the star formation process. In a planetary system with a belt of planetesimals (like the Solar System's Kuiper Belt) and one or more interior giant planets, as the particles spiral inward due to Poynting-Robertson drag they can get trapped in the mean motion resonances with the planets. This process can create structure in the dust disk, as the particles accumulate at certain semimajor axes. Sufficiently massive planets may also scatter and eject dust particles out of a planetary system, creating a dust depleted region inside the orbit of the planet, a feature that is commonly found in many of the spatially resolved debris disks observed so far. We have studied the efficiency of particle ejection and the resulting dust density contrast inside and outside the orbit of the planet, as a function of the planet's mass and orbital elements and the particle size. We discuss its implications for exo-planetary debris disks and for the interpretation of in-situ dust detection experiments on space probes traveling in the outer solar system.

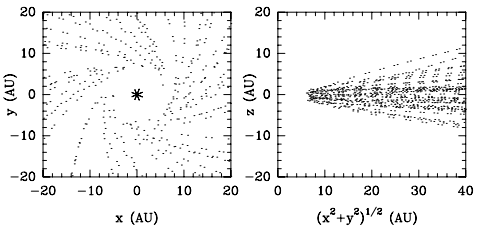

Figure 1: Trajectories of KB dust particles after scattering by Jupiter.

Because the debris disk structure is sensitive to long period planets, complementing a parameter space not covered by radial velocity and transit surveys, its study can help us learn about the diversity of planetary systems. In anticipation of future high-resolution high-sensitivity observations of spatially resolved debris disks with e.g. *ALMA, LBT, SAFIR, TPF* and *JWST*, we numerically calculate the 3-D equilibrium spatial density distributions of dust disks originated by a belt of planetesimals similar to the Kuiper Belt in the presence of interior giant planets in different planetary configurations (with planet masses ranging from 1-10 M_{Jup} in circular orbits with semimajor axis between 1-30 AU). For each of these modeled disks we use a radiative transfer code to obtain their brightness density distributions at different wavelengths that will help us interpret future observations of these dusty ``fingerprints'' in terms of planetary architecture.

Presently, the *Spitzer Space Telescope* is carrying out observations of debris disks most of which are spatially unresolved. It is interesting therefore to study how the structure carved by planets affects the shape of the disk's spectral energy distribution (SED), and consequently if the SED can be used to infer the presence of planets. Using the same numerical models mentioned above we have calculated the SEDs of dust disks originated by a belt of planetesimals in the presence of interior giant planets in different planetary configurations, and for a representative sample of chemical compositions. We discuss what types of planetary systems can be distinguishable from one another and the main parameter degeneracies in the model SEDs.

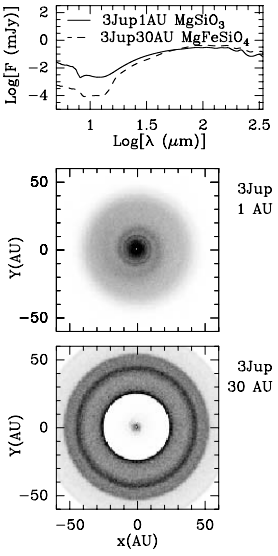

Figure 2: Possible degeneracy between the grain chemical composition and the location of the planet clearing the gap. High resolution images are needed to resolve the degeneracy.

OPTICAL PROPERTIES OF LARGE AGGREGATES. T. Mukai[1] and Y. Okada[1], [1]Graduate School of Science and Technology, Kobe University, Nada, Kobe 657-8501, Japan (mukai@kobe-u.ac.jp and dat0107@kobe-u.ac.jp).

Introduction: It is widely accepted that the comets supply large (about mm-size) grains, as seen in cometary dust trails (see, e.g. [1]). Furthermore, the existence of such large grains in circumstellar dust disk has been reported [2], i.e. the centimeter-size grains in TW Hydra observed at a wavelength of 3.5 cm.

Since it is natural to assume that the dust grains in space are irregularly shaped aggregates, the studies of optical properties of these aggregate become important scientific subject. Discrete Dipole Approximation (DDA) is a popular numerical method to calculate the optical properties of aggregates [3], as well as Mie theory associated with Maxwell-Garnett mixing rule (MG-Mie) [4]. However, it is known that DDA is not applicable for large aggregate because the number of monomers is beyond the limitation of computer resource. That is, the aggregate with an equivalent volume of 2 mm sphere consists of $8x10^{12}$ monomers of a radius of 0.1 micron.

In this paper, we will show our trial to study the optical properties of large aggregate with size larger than mm. The light absorption cross section Cabs of such large aggregate and its resulting temperature in the interplanetary space will be discussed.

Numerical Simulation: For the form of aggregate, we use the fractal aggregate called as BPCA (ballistic particle-cluster aggregate). We keep the structure of BPCA consisting of 2048 monomers, but increase the monomer radius to treat a large aggregate.

For small monomer, DDA has been applied to calculate the value of Cabs. On the other hand, the geometrical optics (GO) has been used to calculate Cabs of BPCA aggregate based on the ray tracing of incident light where each monomer has a size larger than a wavelength (0.6 micron) of incident light (see Fig. 1 and [5]). In the middle size region of monomer radius, MG-Mie has been applied.

As shown in Fig.2, the computed values of Cabs derived by different methods show good agreement in the over-lapping region of monomer radius. Therefore, we assume that GO method will provide the reasonable value of Cabs for large aggregate consisting of large monomers.

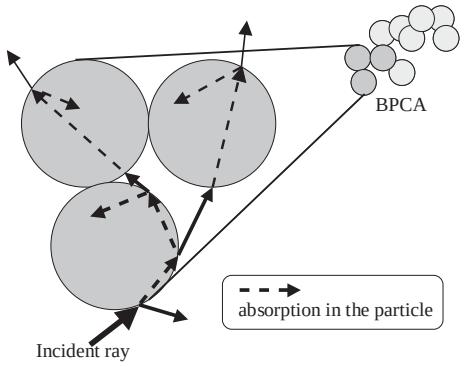

Fig.1 Ray tracing of incident light based on the geometrical optics for BPCA consisting of larger monomer compared with the wavelength of incident light.

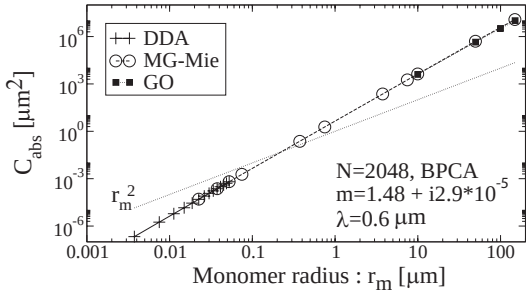

Fig.2. The computed results of light absorption cross section Cabs of BPCA aggregate consisting of 2048 monomers with different monomer radius.

Results: Referring to the derived values of Cabs at wavelengths from 0.2 micron to 300 micron, we have calculated the temperature of 2 mm silicate aggregate consisting of 2048 monomers with monomer radius of 155 micron. Its value becomes 206K at 1 AU, which is significantly lower than 280K for the black body. Other optical properties of large aggregate will be reported in the meeting.

References:

[1] Ishiguro M. et al. (2003) *ApJL.*, *589*, L101-L104. [2] Wilner D.J. et al. (2005) *ApJL.*, *626*, L109-L112. [3] Draine B.T. (1988) *ApJ.*, *333*, 848-872. [4] Mukai T. et al. (1992) *A & A*, *262*, 315-320. [5] Muinonen K. et al. (1996) *JQSRT*, *55*, 577-601.

MID-INFRARED OBSERVATION OF THE COLLISION BETWEEN DEEP IMPACT PROJECTILE AND COMET 9P/TEMPEL 1 WITH SUBARU/COMICS. T. Ootsubo[1], S. Sugita[2], T. Kadono[3], M. Honda[4], T. Miyata[5], S. Sako[5], I. Sakon[6], H. Fujiwara[6], T. Fujiyoshi[7], T. Yamashita[7], N. Takato[7], T. Fuse[7], and SUBARU/COMICS Deep Impact team, [1]Division of Particle and Astrophysical Sciences, Nagoya University, Nagoya 464-8602, Japan (ootsubo@u.phys.nagoya-u.ac.jp), [2]Department of Complexity Science and Engineering, University of Tokyo, [3]JAMSTEC/IFREE, [4]JAXA/ISAS, [5]Institute of Astronomy, University of Tokyo, [6]Department of Astronomy, University of Tokyo, [7]NAOJ/Subaru

Introduction: NASA's Deep Impact (DI) mission generated a hypervelocity collision between its 370kg cooper-based projectile and Comet 9P/Tempel 1 on July 4, 2005 (UT). This collision is expected to excavate fresh cometary material underneath a presumable refractory crust on the surface. Observation of such fresh material rich in pristine volatiles is highly valuable for studying comets and the origin of the Solar System. In order for this study, the information on both cratering process and chemical composition of excavated material is essential. Thus ejecta observation is expected to be extremely important. However, the spectral coverage of the spectrometer on the DI spacecraft is limited to the range between 1.05 and 4.8 μm. Since equilibrium thermal radiation from the comet has its peak around 10 μm, continuous observation of mid-IR radiation will be complementary and hence highly valuable. It is also expected that the use of infrared wavelengths is essential because the coma of 9P/Tempel 1 is optically thick at visible wavelength [1].

Observation: This DI event was observed with the Cooled Mid-Infrared Camera and Spectrometer (COMICS), which is mounted on the 8.2 m Subaru Telescope on Mauna Kea [2,3]. Imaging observations of the pre- and post-impact were done in the 8.8 μm, 10.5 μm, 12.4 μm, 17.7 μm, 18.8 μm, 20.5 μm (and 24.5 μm) bands. N-band low-resolution (R~250) spectroscopic observations were also made from July 3 to 5 (UT). The objective of this observation is to measure accurately the time evolution of the mid-infrared luminosity and spectrum of Comet 9P/Tempel 1 induced by collision.

Results: Subaru/COMICS successfully captured rapidly changing phenomenon occurred around the surface of the comet 9P/Tempel 1. The impact ejecta extending to sizes larger than 2 arcseconds to the south-west direction from the nucleus, which seems like fan-shaped, was detected 2 hours after impact (Fig. 1) in addition to the increased brightness (factor of 4-5) from the baseline measurements of the pre-impact. From both the imaging and spectroscopic observations, it can be concluded that most of the ejected grains are small silicates including the crystalline materials. We will report the preliminary results of analysis about the grain size distribution, composition of the dust minerals, and total mass of the impact ejecta. Information on ejecta grain size will help us infer the strength of the cometary surface and possibly the style of cratering [4]. Such information will be very valuable in considering both cometary surface strength and the effective depth of material excavated by the DI impact. The data of 10 μm spectral feature tells us whether the silicate dust is crystalline or amorphous [e.g. 5]. If most of the ejecta came from only near the cometary surface, it is expected that the information on the silicate dust will show the thermal property of the impact event. On the other hand, if the dust has also been released from inside the nucleus, the crystallinity of the silicate dust may also provide further insight into the origin of comets.

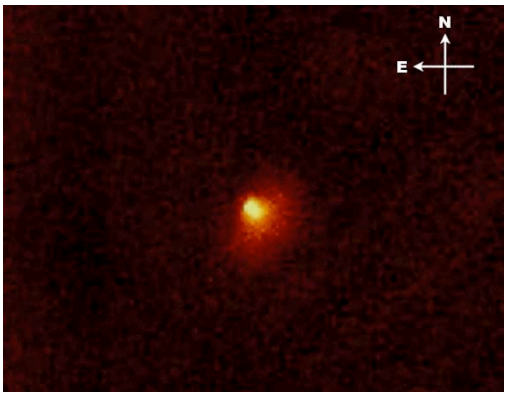

Figure 1. The 10.5 μm image of Comet 9P/Tempel 1 observed by COMICS 2 hours after impact.

References: [1] Fernandez Y. R. et al., (2003) *ICARUS, 164,* 481. [2] Kataza H. et al. (2000) *SPIE, 4008,* 1144. [3] Okamoto Y. J. et al. (2003) *SPIE, 4841,* 169. [4] Kadono and Arakawa (2002) *Phys. Rev. E., 65,* 5107. [5] Honda M. et al. (2004) *ApJ, 601,* 577.

COMETARY DEBRIS TRAILS: RELICS OF THE DISINTEGRATION OF SHORT-PERIOD COMETS.
William T. Reach (Spitzer Science Center, Caltech, MS 100-22, Pasadena, CA 91125, USA)

The imaging capabilities of the *Spitzer Space Telescope* [1] enable observations at unprecedented sensitivity of the extended distribution of debris around comets. Debris trails were serendipitously discovered along the orbits of 8 periodic comets using IRAS [2]. We have now imaged 31 periodic comets over fields of view large enough to clearly separate mm-sized debris from smaller grains produced in the present perihelion. Of these, 21 comets were found to a narrow trail of infrared emission closely following the projected path of the comet's orbit. An additional 7 may have trails but were exceptionally active and have not yet been separated from their small-grain tails. Three comets did not have (detectable) debris trails.

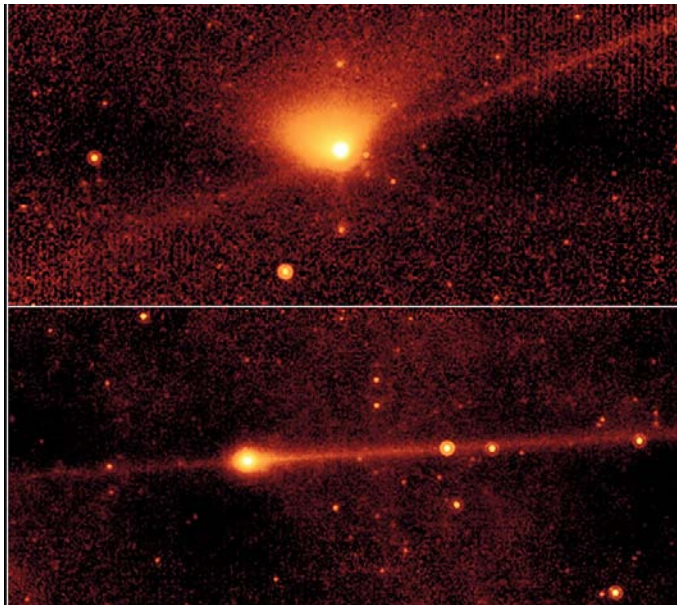

Two examples are shown in the Figure: 48P/Johnson *(top)* and 129P/Shoemaker-Levy 3 *(bottom)*. The large fan-shaped coma of 48P is due to small particles ($1>\beta>0.01$) from the present perihelion. The excellent viewing geometry (the Sun is to the lower right, and the comet's orbital motion is to the left) allows for clear segregation of particles by size. The situation is similar to that for the only high-quality large-scale image that had been previously made, 2P/Encke with the *Infrared Space Observatory* [3]. The debris trail can be seen both leading (toward lower-left) and trailing (toward upper-right) the nucleus. 138P was seen at greater heliocentric distance so its small-particle production is lower; the debris trail is distinct, both leading and trailing the nucleus.

In this talk, we discuss the systematics of cometary debris trails based on the infrared imaging survey, including dynamical simulations, and spectrophotometry (3.6-24 μm), and infrared spectroscopy (5-38 μm) for some of the survey comets.

References: [1] Werner, M. W. (2004), ApJS 154, 1. [2] Sykes, M. W., and Walker, R. G. (1992) Icarus, 95, 180. [3] Reach, W. T., Sykes, M. V. Lien, D., and Davies, J. K. (2000) Icarus, 148, 80

Acknowledgments: This work is based in part on observations made with the Spitzer Space Telescope, which is operated by the Jet Propulsion Laboratory, California Institute of Technology under NASA contract 1407. Support for this work was provided by NASA through an award issued by JPL/Caltech.

THE CASSINI SPACECRAFT AT SATURN: AN OVERVIEW OF SCIENCE AND SCIENCE OPERATIONS

Mou Roy[1], Marcia Burton[2], Georg Moragas Klostermeyer[3], Ralf Srama[4], Sascha Kempf[5] and Stefan Helfert[6].
[1]Jet Propulsion Laboratory, 4800 Oak Grove Drive, Pasadena, CA 91101, USA; Mou.Roy@jpl.nasa.gov,
[2]Jet Propulsion Laboratory, 4800 Oak Grove Drive, Pasadena, CA 91101, USA,
Marcia.Burton@jpl.nasa.gov, [3]MPIK, Saupfercheckweg 1, 69117 Heidelberg, Germany;
Georg.Moragas@mpi-hd.mpg.de, [4]MPIK, Saupfercheckweg 1, 69117 Heidelberg, Germany;
Ralf.Srama@mpi-hd.mpg.de, [5]MPIK, Saupfercheckweg 1, 69117 Heidelberg, Germany;
Sascha.Kempf@mpi-hd.mpg.de, [6]MPIK, Saupfercheckweg 1, 69117 Heidelberg, Germany;
Stefan.Helfert@mpi-hd.mpg.de

With the successful insertion of the Cassini-Huygens spacecraft into orbit about Saturn in July, 2004, followed by deployment and landing of the Huygens probe on Titan in January, 2005, the science discoveries made in the Saturnian system have been phenomenal. The spacecraft is highly sophisticated and complex with twelve instruments on the orbiter and six on the Huygens probe. The instrument payload consists of a suite of optical remote sensing instruments, RADAR, and a fields and particles payload making in-situ measurements of the magnetic field and plasma environment. The Cosmic Dust Analyzer (CDA) instrument on-board Cassini has been successfully making measurements of the dust environment in the Saturnian system. Operations and planning for science observations on such a complicated spacecraft with a diverse payload are necessarily complex. We take a look back at more than a year of science discoveries and highlight the successful tour operations that have made these discoveries possible. We will place special emphasis on activities that contribute to accurately characterizing the Saturnian dust environment.

OPTICAL OBSERVATIONS OF THE COMET 2P/ENCKE DUST TRAIL. Yuki Sarugaku[1,2], Masateru Ishiguro[2], Naoya Miura[3], Fumihiko Usui[2], and Munetaka Ueno[3], [1]The Univ. of Tokyo, 7-3-1, Hongo, Bunkyo-ku, Tokyo, 113-0033, JAPAN. sarugaku@planeta.sci.isas.jaxa.jp, [2]ISAS/JAXA, 3-1-1, Yoshinodai, Sagamihara, Kanagawa, 229-8510, JAPAN, [3]The Univ. of Tokyo, 3-8-1, Komaba, Meguro-ku, Tokyo, 153-8902, JAPAN.

Introduction: Cometary dust trails were first detected by the Infrared Astronomical Satellite [1], [2]. They are composed of large dark particles, which are ejected at low velocities from the nuclei and extend along the orbits of the parent bodies. It is recently that trails were detected in visible wavelength [3], [4]. The scattered light is a basic but a new tool to study dust trails.

Observations: Comet 2P/Encke is a good target to study dust trails for following reasons: (1) the existence of the 2P/Encke trail was clearly identified by the previous studies [5], [6]; (2) it is possible to observe 2P/Encke in wide range of phase angle because the orbit crosses the Earth orbit (perihelion distance is 0.34 AU, aphelion distance is 4.10 AU).

We observed 2P/Encke 15 nights from 2002 September to 2004 September (perihelion passege of 2P/Encke was on 29 December 2003.). The observations were carried out using Kiso 1.05-m telescope (13 nights) and University of Hawaii 2.24-m telescope (2 nights). During these observations 2P/Encke was at heliocentric distance R of 0.70-3.98 AU, geocentric distance Δ of 0.26-2.97 AU, and phase angle α of 1-135°. When 2P/Encke closed to the Earth (Δ = 0.26-0.35 AU), the trail was not detected. On the contrary we could detect it when 2P/Encke was near aphelion (R = 3.98 AU, Δ = 2.97 AU).

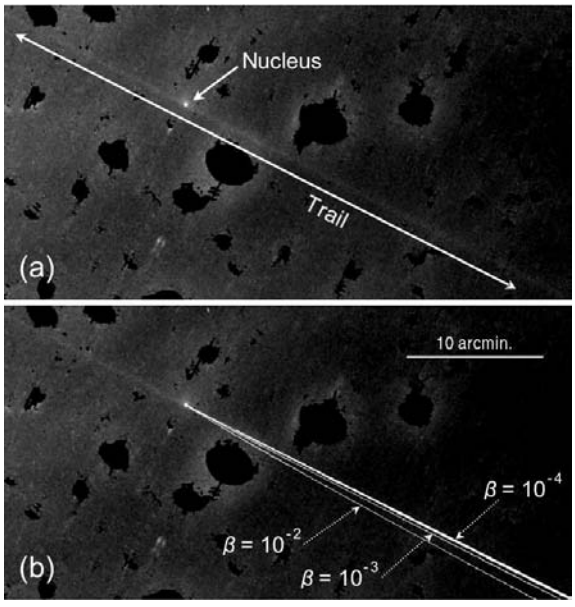

Figure 1: (a) Composite image of the 2P/Encke trail observed on 22 September 2003. Black spots have no value, which are made in the process of our data reduction to reduce contamination of stars. (b) Syndyne curves of $\beta = 10^{-2}, 10^{-3}$, and 10^{-4} are overlaid on fig. 1(a). The 2P/Encke trail agrees with syndyne curve of $\beta < 10^{-4}$.

Results: The 2P/Encke trail was detected at 5 different epochs. The range of R, Δ, and α of 2P/Encke, where the trail was detected, are 1.78-3.98 AU, 0.94-2.97 AU, and 1-26°, respectively (Table 1). According to fitting of the syndyne curves, we found that the trail is composed of particles whose size is larger than approximately 1 cm ($\beta < 10^{-4}$), which is consistent with the previous studies. In addition, it is likely that the intensity of scattered light increases at low phase angle by comparison of the data obtained at different phase angles.

Table 1: Observational summary. All observations were carried out with R band filter. Symbol ◯ shows that 2P/Encke trail was detected.

DATE (UT)	R (AU)	Δ (AU)	α (°)	TEL.	EXP. (min.)	TRAIL
2002/09/09	3.98	2.97	1	Kiso	72	◯
2003/09/22	1.78	0.94	24	Kiso	65	◯
2003/11/14	1.05	0.26	69	Kiso	86	–
2003/11/16	1.02	0.26	76	Kiso	40	–
2003/11/17	1.00	0.26	79	Kiso	67	–
2003/11/18	0.99	0.26	83	Kiso	73	–
2003/11/21	0.94	0.27	93	Kiso	58	–
2003/11/22	0.92	0.27	97	Kiso	67	–
2003/11/23	0.90	0.27	100	Kiso	53	–
2003/11/26	0.85	0.29	110	Kiso	48	–
2003/12/02	0.74	0.33	129	Kiso	26	–
2003/12/04	0.70	0.35	135	Kiso	16	–
2004/05/23	2.28	2.12	26	UH88	50	◯
2004/08/13	2.94	1.93	2	Kiso	55	◯
2004/09/09	3.12	2.25	11	UH88	42	◯

References: [1] Davies, J. K. et al. (1984) *Nature*, 309, 315-319. [2] Sykes, M. V. et al. (1986) *Science*, 232, 1115-1117. [3] Ishiguro, M. et al. (2002) *ApJ*, 572, L117-120. [4] Lowry, S. C. et al. (2003) *LPS XXXIV*, Abstract #2056, [5] Sykes, M. V. and Walker, R. G. (1992) *Icarus*, 95, 180-210, [6] Reach, W. T. et al. (2000) *Icarus*, 148, 80-94.

SUMMARY OF OBSERVATION OF INTERPLANETARY AND INTERSTELLAR DUST BY MARS DUST COUNTER ON BOARD NOZOMI. S. Sasaki[1], E. Igenbergs[2], H. Ohashi[3], R. Münzenmayer[2$], W. Naumann[2#], R. Senger[2], F. Fischer[4], A. Fujiwara[5], E. Grün[6], K. Nogami[7], I. Mann[8], H. Svedhem[9], [1] Mizusawa Astrogeodynamic Observatory, National Astronomical Observatory of Japan, 2-12 Hoshigaoka, Mizusawa, 023-0861, Japan (sho@miz.nao.ac.jp), [2] LRT, TU-München, 85748 Garching, Germany, [3] Tokyo University of Marine Science and Technology, Tokyo 108-0075, Japan, [4] RTSG, TU-München, 80333 München, Germany, [5] ISAS/JAXA, Sagamihara, 229-8510, Japan, [6] MPI-Kernphysik, 69117 Heidelberg, Germany, [7] Dokkyo University School of Medicine, Tochigi 312-0207, Japan, [8] Institut für Planetologie, Westfälische Wilhelms-Univ., 48149 Münster, Germany, [9] ESA-ESTEC, PO Box 299, 2200 AG Noordwijk, The Netherlands, [$] Now at Astrium Space, Postfach 1420, 88039 Friedrichshafen, Germany, [#] Now at Kayser-Threde GmbH, 81379 München, Germany.

Introduction:

Mars Dust Counter (MDC) is a dust detector of impact ionization type on board Japanese Mars mission NOZOMI. Although its weight is only 730g, MDC can determine mass, velocity, and direction of a dust particle using rise time of impact-induced charge signals [1]. The main objective of MDC is to discover the predicted martian dust ring or torus [2]. Dust abundance detectable by NOZOMI-MDC was predicted under the self-sustaining mechanism, where satellite-dust collisions are the main dust source [3].

Due to a problem at the powered fly-by with the Earth on December 1998, NOZOMI orbital plan was changed. From December 1998 to December 2002, NOZOMI takes an eccentric orbit whose perihelion and aphelion are at the Earth's orbit and at the Mars' orbit, respectively. Then, after two flybys with the Earth in December 2002 and June 2003, NOZOMI approached Mars in December 2003. NOZOMI would have observed circummartian environment by highly elliptic orbits around Mars from 2004. However, NOZOMI did not recover from electronic trouble which occurred in April 2002. Insertion into circummartian orbit was finally given up in December 2003. MDC continued observation of interplanetary (and interstellar) dust by April 2002. Here we summarize dust observation of MDC.

Dust detection:

After the launch on 4th, NOZOMI took eccentric parking orbits around the Earth for five months performing two fly-bys with the moon. MDC has detected more than 20 impact during the circumterrestiral orbit. During encounter with Leonids meteor stream, MDC detected a couple of high-velocity dust particles but their direction differed from meteor stream dust. From 1999, NOZOMI entered the cruising phase. Particles with impact velocities smaller than 4km/s have not been detected in the cruising phase. On the contrary, high velocity particles (v>40km/s) are detected only during the cruising phase, especially in 1999.

Impact data in the cruising phase are shown in Figs. 1 nd 2. Impact events in 1999 are shown in Figs. 1. Most of dust particles are Keplerian dust particles moving around the sun. There are several high velocity particles which are apparently different from such Keplerian particles, although there is direction ambiguity of ±several tens degree because of the large aperture of MDC sensor. In Fig. 1 (b), direction of two dust particles (**b**, **e**) corresponds to that of typical interstellar particles, which should correspond to the direction of the solar system moving against the surrounding interstellar gas cloud with a relative velocity 26km/s [4]. Particle **a** has a large vertical component. Other high-velocity particles **c**, **d** would have different origin but the component with this direction has not been reported in the interstellar dust source [5].

In 2000-2001 season, MDC detected similar number of dust particles but fewer high velocity particles (Fig. 2(a)) compared with those in 1999. Figure 2(b) shows that there is only one candidate **f** of interstellar dust. Most of particles are typical interplanetary dust particles moving around the sun. The difference between 1999 data and 2000-2001 data does not necessarily mean the change of interstellar dust flow. It could be rather explained by the change of dust detection efficiency according to NOZOMI spin axis direction.

In summary, MDC detected more than 100 dust particles in space. Not only Keplerian dust particles but also interstellar dust particle candidates were detected by MDC.

References: [1] Igenbergs, E., Sasaki, S., et al., *Earth Planets Space* **50**, 241-245, 1998. [2] Sasaki, S., *Adv. in Space Res.* **23**, 1907-1910, 1999. [3] Sasaki, S., *In Physics, Chemistry, and Dynamics of Interplanetary Dust*, ASP Conf. Ser. **104**, 187-190, 1996. [4] Grün, E.,et al., *Astron. Astrophys.* **286**, 915-924, 1994. [5] Taylor, A. et al., *Nature* **380**, 323-325, 1996.

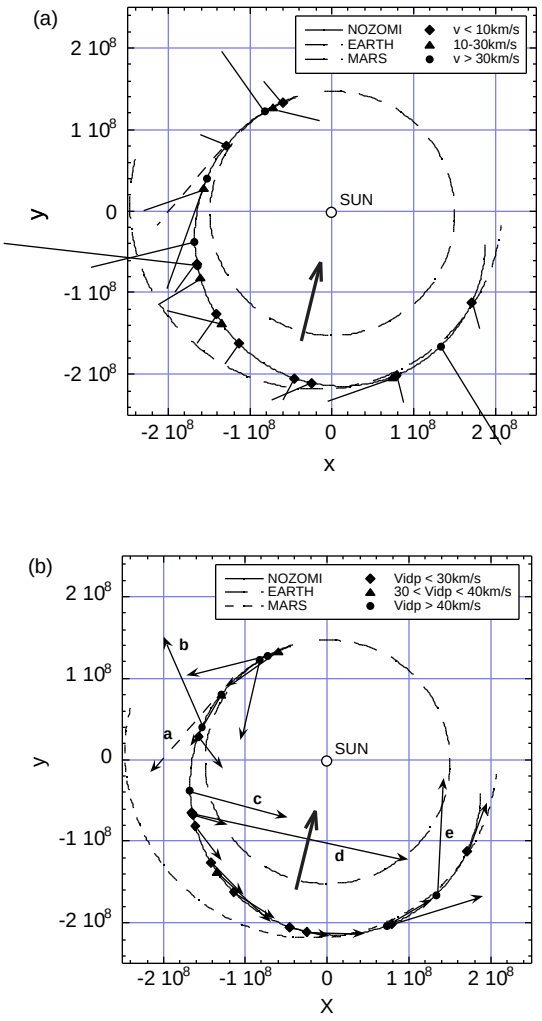

Fig. 1 Dust particle impacts detected by MDC in 1999. Orbits of NOZOMI, the Earth, and Mars are shown in the ecliptic plane. The +x direction is the direction of the Sun at vernal equinox. An arrow toward the sun denotes the direction of interstellar gas flow into the solar system. (a) Direction of MDC sensor aperture and impact velocity (i.e. relative velocity between NOZOMI and a dust particle). For each impact, direction is expressed by a line from the impact mark. The length of each line corresponds to velocity of the impacted particle. One event with a broken line denotes a fast impact with a large vertical velocity component. (b) Velocity of dust in the interplanetary space calculated from impact velocity and orbital velocity. Dust particles with high velocity (>40km/s) are denoted by attached characters (**a**, **b**, **c**, **d**, **e**).

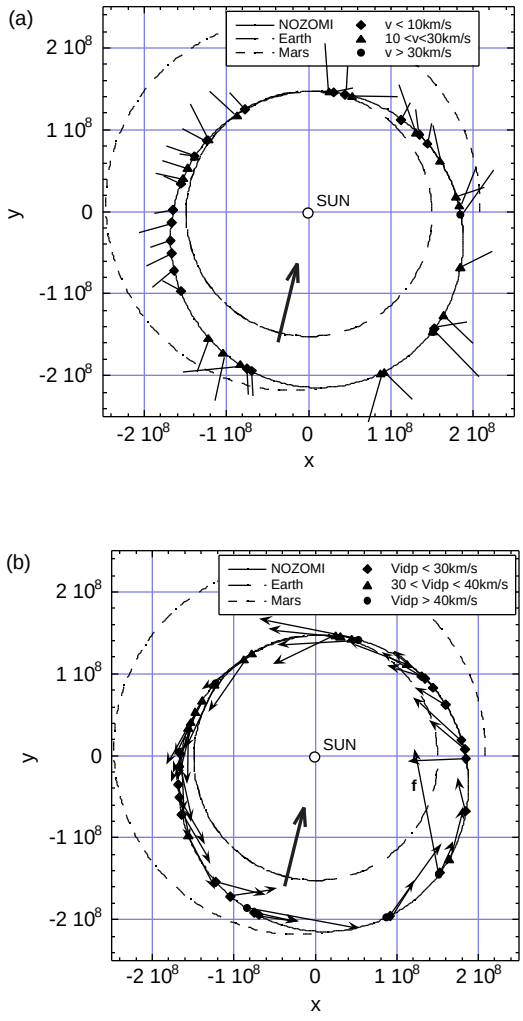

Fig. 2 Dust particle impacts detected by MDC in 2000 and 2001. Legends and figure formats are the same as Fig.2. (a) Direction of MDC sensor aperture and impact velocity. (b) Velocity of dust in the interplanetary space calculated from impact velocity and orbital velocity. A dust particle with high velocity is denoted by attached characters (**f**).

UPDATES ON THE DUSTY RINGS OF JUPITER, URANUS AND NEPTUNE. M. R. Showalter[1], J. A. Burns[2], I. de Pater[3], D. P. Hamilton[4], J. J. Lissauer[5], and G. Verbanac[6], [1]SETI Institute (515 Whisman Road, Mountain View, CA 94043, mshowalter@seti.org), [2]Cornell University (328 Space Sciences Bldg., Ithaca, NY 14853, jab16@cornell.edu), [3]U. C. Berkeley (601 Campbell Hall, Berkeley, CA 94720, imke@astron.berkeley.edu) [4]U. Maryland (Dept. of Astronomy, College Park MD 20742, hamilton@astro.umd .edu), [5]NASA Ames Research Center (M.S. 245-3, Moffett Field, CA 94035-1000, jlissauer@mail.arc.nasa.gov), [5]Geophysical Institute "Andrija Mohorovicic" (Horvatovac bb, 10000 Zagreb, Croatia, verbanac@irb.hr).

Introduction: We present recent results from observing the ring systems of Jupiter, Uranus and Neptune, using the Hubble Space Telescope (HST) in the visual and the 10-meter W. M. Keck Telescope in the infrared. Using Earth's most powerful telescopes, we find that all three ring systems are revealing new and unexpected properties.

Neptune: HST images taken November 2004 to June 2005 have revealed the ring-arcs of Neptune in visual light for the first time since the Voyager flyby of 1989 (Fig. 1). By operating at wavelengths similar to that of Voyager's cameras, we determine that the trailing arcs Egalité and Fraternité show no significant absolute change in brightness over the last 16 years, contradicting earlier suggestions. However the leading arcs Courage and Liberté have nearly vanished, confirming the continuation of trends noted in recent Earth-based infrared detections. The inner Leverrier ring is also detectable in the new HST data. Initial analysis indicates that it is several times brighter than in the Voyager images; this preliminary result requires further investigation.

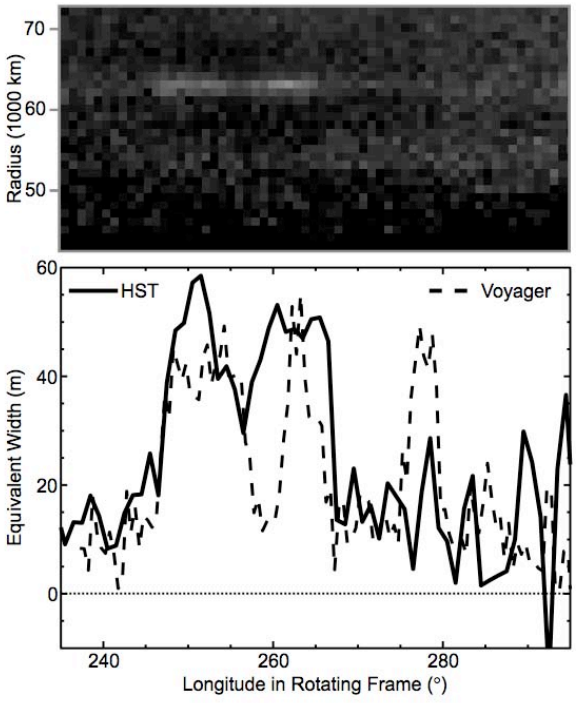

Fig. 1. Arc image and profile compared to Voyager.

This same data set has also recovered all the inner moons of Neptune except tiny Naiad; our data should be sufficiently sensitive to detect Naiad and we attribute its non-detection so far to the large uncertainty in this moon's ephemeris.

Jupiter: Our studies of the three components of Jupiter's ring system incorporate a reanalysis of Galileo and Voyager data in addition to the newer Earth-based data sets.

Gossamer Rings. This system consists of two overlapping rings, one bounded by Amalthea and the other by Thebe. The rings are superficially consistent with the model of Burns et al. [1], in which dust is ejected from each moon and evolves inward under Poynting-Robertson (PR) drag. We confirm that the ring thicknesses vary in proportion to radius, as one would expect if orbital inclinations are conserved. However both rings, and especially the Thebe ring, show signs that inclinations get somewhat randomized about their mean values during the dust's journey inward. Both rings also show a distinct peak in density just inward from their source moons, followed by a more uniform density downward to the main ring. The uniform regions are consistent with the PR drag model, but the peaks require a different explanation. The peak in Amalthea's ring is associated with material trapped in the plane of Amalthea's inclined orbit, indicating a population of dust whose nodes are locked. How Amalthea maintains this population is unclear. It is possible that the outer peak in Thebe's ring shows a similar morphology; the data are insufficient to say for certain.

We have performed detailed photometry of the Amalthea ring for the first time. Observations from HST, Keck, Galileo and Voyager are all consistent with a relatively flat power law size distribution of dust, of the form $n(r) \sim r^{-q}$, where q = 2–2.5. This is very similar to the size distribution in the main ring and is consistent with collisional ejecta evolving inward under a drag force. The ring's phase curve in backscatter is nearly flat, requiring that the dust grains be highly non-spherical.

Main Ring. In backscattered light, the ring shows a sharp increase in brightness between the orbits of Metis and Adrastea. This peak is not present in high-phase Galileo images, suggesting that this region contains a large population of macroscopic bodies bounded by the two moons. These macroscopic bodies, in addition to the two moons, are likely to serve as the primary parent bodies for the ring's prominent dust. Interior to the orbit of Metis the ring's profile in forward- and backscattered light appears similar, suggesting that dust is the primary component of this region.

One set of high-phase images from Galileo shows a series of vertical "ripples" in the ring (Fig. 2). The vertical amplitude is of order 1 km and the radial wavelength is irregular but typically ~ 1000 km. A density wave cannot be sustained in this low-mass ring; we propose that the vertical distortions may arise from an unseen population of smaller moons on slightly inclined orbits.

Halo. The inner halo is observed both in Galileo images at high phase and in Keck images at low phase. Both consistently show an inner limit of 100,000 km, a sharp concentration within a few thousand km of the ring plane, but with faint material still visible tens of thousands of km above and below.

Two competing models have been invoked to explain the halo. Schaffer and Burns [2] propose that PR drag draws dust inward from the source region, where it encounters Lorentz resonances that produce the large increases in thickness. Horanyi and Cravens [3] propose that grains evolve under "gyrophase drift" (GD), in which electric charges on the dust grains vary with orbital radius, causing the grains to spiral inward rapidly. In this scenario, Lorentz resonances play no explicit role.

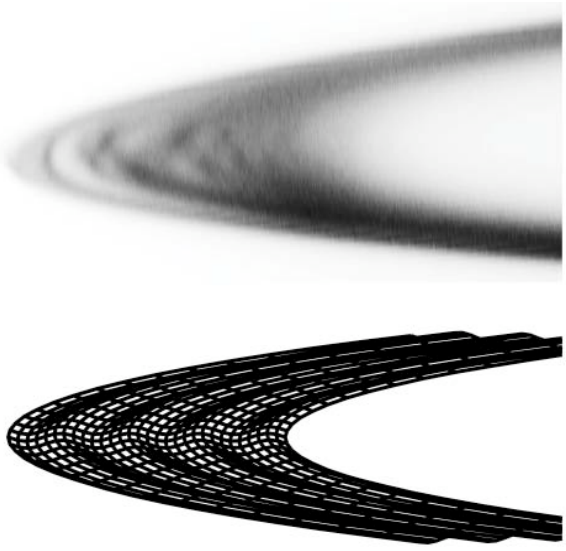

Fig. 2. A contrast-enhance negative of Galileo image 3689741.39 shows brightness variations across the ring ansa. A simple wire-frame diagram illustrates how these variations can be caused by vertical distortions of the ring plane.

Images of the main ring and halo pose a serious challenge to the GD model. This process admits a constant of the motion, the Jacobi integral, which involves only the orbital semimajor axis a and eccentricity e. As particles drift inward their eccentricities must grow, yielding a net increase in their apocenter radii. If the halo's sources lie in the main ring, then this process should be visible as an outward extension beyond the main ring's tip. Close examination of the finest-resolution images from Galileo, HST and Keck *exclude* the existence of this outward extension. The only material outside the main ring is from the gossamer rings; additional equatorial material cannot be brighter than ~ 1% of the main ring, which is incompatible with the much larger amount of material in the halo.

Uranus: Ongoing HST observations of Uranus span July 2003 to June 2006, during which the ring opening angle decreases from 18° to 3°. We have obtained repeated images spanning phase angles 0–3° and wavelengths 0.33 to 0.82 μm. All 9 of the brightest rings are resolved except the close inner set of Rings 6, 5 and 4. This data set has already yielded the discovery of two moons [4] too small to have been imaged by Voyager. We also detect longitudinally variable structures in several rings, most of which are related to known resonant perturbations and modes. We are employing photometric modeling to better define the dust content of these rings. We will also report on our attempts to detect the faint, dusty Ring λ. This work complements recent reports of secular changes in the Uranian dusty rings by de Pater et al. [5], based on Keck data in the infrared.

References: [1] Burns J. A. et al. (1999) *Science 284*, 1146–1150. [2] Schaffer L. and Burns J. A. (1996) *Icarus 96*, 65–84. [3] Horanyi M. and Cravens T. E. (1996) *Nature 381*, 293–295. [4] Showalter M. R. and Lissauer J. J. (2003) IAU Circular #8209. [5] de Pater, I. et al. (2005) *Icarus*, in press.

Acknowledgments: Partial support for this work was provided by NASA through grants GO-09823 and GO-10398 from the Space Telescope Science Institute, which is operated by the Association of Universities for Research in Astronomy, Inc., under NASA contract NAS5-26555.

E RING SOURCES — CASSINI FLYBYS WITH ENCELADUS

F. Spahn[1], N. Albers, V. Dikarev, T. Economu, E. Gruen, M. Hoerning, S. Kempf, A. V. Krivov, M. Makuch, J. Schmidt, M. Seiss, R. Srama, M. Sremcevic
[1]Institute of Physics, University Potsdam, D-14469 Potdam, Germany
(fspahn@agnld.uni-potdam.de)

Abstract

The satellite Enceladus is considered to be the main source of Saturn's E ring. Impactor-ejecta mechanisms are very likely the major processes to lift off particles from its surface. Nevertheless, it is still not clear what is the main impactor family causing the dust ejecta and whether other bodies in the E ring serve as additional sources. In order to distinguish the dust ejecta originating from potential sources (Enceladus and Tethys) from the bulk of the E ring we perform numerical particle experiments in order to simulate the fate of grains just ejected from Enceladus and Tethys. In this way we model the E ring configuration where the A ring, Enceladus and Tethys act as sinks and where Enceladus and Tethys are the only source. We found striking differences in the dust fluxes coming from the source satellites compared to the E ring background in the vicinity of the sources – this concerns both, the size distribution and also the impact rate expected at a dust detector. These can possibly be measured with the cosmic dust analyzer (CDA) or high rate detector (HRD) aboard the Cassini spacecraft. We compare these theoretical predictions with the HRD-data for certain Cassini flybys (E3, E4 and E11) with Enceladus and try to distinguish the freshly ejected material from the E ring background. Especially the E11 encounter provides the unique chance to measure the dust "cloud" around Enceladus – another strong hint for the impactor-ejecta mechanism as a dust generating process. We further found that Tethys contributes a considerable amount (30of the Enceladus contribution, depending on the impactor family) of dust to the E ring – a dust supply necessary to explain the large extent of that ring and also the additional density hump near the Tethys orbit seen in ground based observations (I. dePater).

CASSINI SATURN DUST MEASUREMENTS. R. Srama[1], M. Burton[4], S. Helfert[1,3], S. Kempf[1], G. Moragas-Klostermeyer[1], A. Mocker[1], F. Postberg[1], M. Roy[4], the CDA science team and E. Grün[1,2], [1]Max Planck Institute Nuclear Physics, Heidelberg, Germany, [2]HIGP, Univ. of Hawaii, Honolulu, Hawaii, USA, [3]Helfert Informatik, Mannheim, Germany, [4]JPL, Pasadena, USA.

Abstract The Cassini spacecraft is in orbit around Saturn since July 2004. During the first year, amazing discoveries of the dust environment at Saturn were achieved by the dust instrument onboard Cassini, the Cosmic Dust Analyzer (CDA)[1]. Here, an overview is given about the discoveries and achievements of CDA.

The approach to Saturn showed sporadic increases of the dust rate caused by tiny (few nano meter) and fast (>100 km s^{-1})particles ("nano-dust") which reached Cassini 100 million km away from Saturn. This discovery of Saturn's dust streams was further investigated by CDA during the first orbits and a detailed analysis has shown, that Saturn's A ring is partly responsible for this type of stream particles [2, 3].

In the saturnian system many grains carrying an electrical charge were detected by CDA. CDA has measured for the first time both, negative and positive charges of dust particles which are correlated to the distance to Saturn and to the local magnetosphere properties (compare [4]).

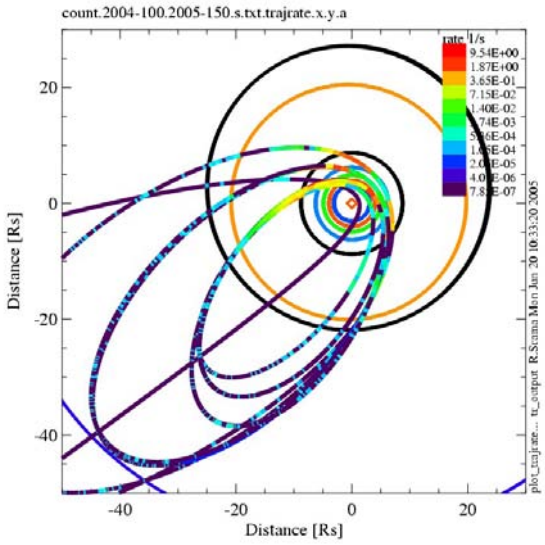

Fig. 1: The trajectory of Cassini, the orbit of the moons (from the outside to the inside: Hyperion, Titan, Rhea, Dione, Tethys, Enceladus), and the CDA dust event rate (color coded on the Cassini trajectory). The measured event rate is highly fragmented due to Cassini's pointing changes.

Saturn is surrounded by its optically faint E ring. CDA performed outstanding measurements of dust densities, particle size distributions and even particle compositions. This was possible due to the fact that an in-situ dust instrument like CDA is a factor of 1000 more sensitive to detect dust densities than an optical instrument. CDA confirmed that the particles are composed of micron sized, almost pure water ice particles.

Furthermore, it was shown, that Saturn's E ring is much more extended in both, the radial and the vertical dimensions (Fig. 1). Significant dust densities were detected as far as 16 Saturn radii away from Saturn.

A significant source of the E ring particles is the surface of the icy moon Enceladus, which is continuously bombarded by ring and interplanetary particles. The flyby of Cassini at Enceladus and crossings of the orbit of Enceladus lead to a strong increase of the particle density. In addition, the High Rate Detector (HRD) detected a clear population of dust particles bigger than 2 µm. Cassinis' flyby at Enceladus on day 195 in 2005 will shed light on the fundamental question, if Enceladus is the major source of the E ring particles [5].

References

[1] Srama R. et al. (2004) *SSR*, 114, 1-4, 465-518
[2] Kempf S. et al. (2005) *Nature*, 433, 7023, 289-291
[3] Kempf S. et al. (2005) *Science*, 307, 5713, 1274-1276
[4] Kempf S. et al. (2004) *Icarus*, 171, 317-335
[5] Spahn F. et al. (1999) *JGR*, 104, 2411-24120

Acknowledgements The Cosmic Dust Analyzer project is supported under the DLR grant 50OH0304.

A NEW LARGE AREA TOF MASS SPECTROMETER. R. Srama[1], M. Rachev[1], S. Helfert[1,3], S. Kempf[1], G. Moragas-Klostermeyer[1], A. Mocker[1], F. Postberg[1] and E. Grün[1,2], [1]Max Planck Institute Nuclear Physics, Heidelberg, Germany, [2]HIGP, Univ. of Hawaii, Honolulu, Hawaii, USA, [3]Helfert Informatik, Mannheim, Germany.

Abstract Based on experience with current space dust instruments on-board interplanetary missions, a novel Dust Telescope is being developed. A dust telescope is a combination of a dust trajectory sensor and a mass analyzer. The trajectory sensor is used to determine the speed, mass and trajectory of interplanetary and interstellar dust grains. In contrast, the mass analyzer provides the elemental composition of individual grains. Here, we report about the successful tests of the large area mass analyzer (LAMA) at the dust accelerator of the Max Planck Institute for Nuclear Physics in Heidelberg.

Instrument The flux of interplanetary and interstellar dust in the vicinity of the Earth can be as low as $1x10^{-5}$ s^{-1} m^{-2}. For this reason we developed a time-of-flight mass spectrometer with a sensitive area as big as 0.1 m^2. The lower limit for the required mass resolution was supposed to be 100. The result of the design study using the SIMION modeling package is a an instrument with a plane ring shaped target, an acceleration grid, a field free drift zone and a one-stage reflectron. The reflectron uses parabolic shaped grids in order to focus the ions, generated by the hyper-velocity impact of a micro meteoroid, onto a large ion detector (multi channel plate) (Fig. 1). The calculated mass resolution is above 150 for all impact positions and for a large variety of initial ion energies and ion emission angles in front of the target. The instrument employs an acceleration voltage of +5000 V.

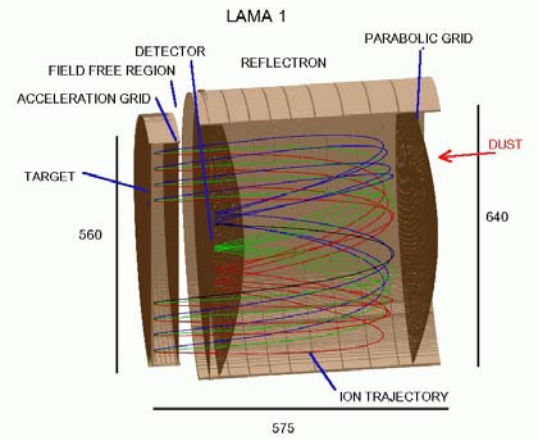

Fig. 1: Schematics of the Large Area Mass Analyzer. The dimensions are given in mm. The colored curves represent ion trajectories of different impact locations.

Measurements Initial test were performed with the laboratory model of LAMA at the dust accelerator facility in Heidelberg. Micron sized grains of iron and latex with impact speeds between 5 and 20 km s^{-1} were used to study the mass resolution of the instrument. Fig. 2 shows a typical spectrum achieved with iron projectiles and Fig. 3 shows a mass spectrum of a latex particle impact. Both spectra show very clearly the separation of adjacent mass lines even in the mass range above 100. A preliminary analysis revealed mass resolutions of up to 300. The first results therefore confirm the predicted mass resolutions of the SIMION calculations. The instrument concept was proven and is ready for a Cosmic DUNE mission.

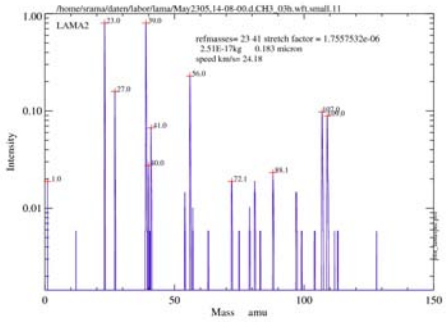

Fig. 2: Time-of-flight mass spectrum measured by LAMA. An iron particle with a speed of 24 km/s was shot onto the silver target.

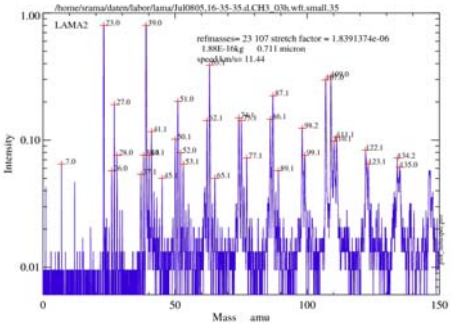

Fig. 3: LAMA mass spectrum of a latex particle with an impact speed of 11 km/s and a size of 0.7 µm. The target was silver. The impact process forms a variety of hydrocarbons which are well resolved by the spectrometer. The silver isotopes appears at 107 amu and 109 amu and are clearly separated.

Acknowledgments This research is supported by DLR grant 50OO0201.

TRAJECTORY SENSOR FOR SUB-MICRON SIZED DUST. R. Srama[1], A. Srowig[1,2], S. Helfert[1], S. Kempf[1], G. Moragas-Klostermeyer[1], S. Auer[3], D. Harris[4], E. Grün[1,4], [1]MPI-K, Heidelberg, Germany, [2]ASIC Lab. Univ. Heidelberg, Germany, [3]A&M Assoc., Basye, USA, [4]HIGP, Honolulu, USA.

Dust particles' trajectories are determined from the charges induced in sensor electrodes by charged dust grains. Based on experience with current space dust instruments [1] a novel Dust Trajectory Sensor has been developed. The Dust Trajectory Sensor will provide a ten times increased sensitivity of charge detection over Cassini's Dust Analyzer sensitivity [2] such that even in interplanetary space statistically significant numbers of dust trajectories can be obtained. The sensor measures dust charges $\geq 10^{-16}$ C and allows us to determine trajectories of submicron-sized grains with accuracies of ~1° in direction, and ~1% in speed.

A trajectory sensor has been set-up (Fig. 1) for dust accelerator tests. It consists of four sensor grids mounted between two electrical shielding grids [2]. Each sensor grid consists of 15 parallel wire electrodes (wires separated by 20 mm), each electrode being connected to a separate charge-sensitive amplifier (CSA). The wire directions of adjacent sensor grids are orthogonal. The distance between grid planes is 40 mm. Each pair of adjacent wire electrodes within a sensor grid acts as a one-dimensional position-sensitive detector: The wire that senses the highest induced charge is closest to the dust particle's trajectory. Neighboring wires sense lower charges. The ratios of charge amplitudes yield the exact coordinate of the grain's location of passage through that grid plane [3]. Accuracies of 0.1° in direction and 0.1% in speed have been demonstrated with dust particles from the Heidelberg dust accelerator facility [4].

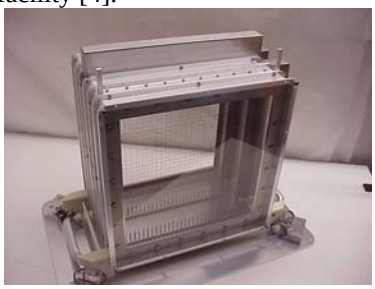

Fig. 1 Lab set-up of the dust trajectory sensor

Key elements of the trajectory sensor are the charge-sensitive amplifier (CSA) and the transient recorder. An Application Specific Integrated Circuit (ASIC) version (Fig. 2) was developed in cooperation with the Kirchhoff Institute for Physics of the Heidelberg University. It consist of two individual chips [5]. The front-end chip contains the CSA and a logarithmic amplifier for the compression of the dynamic range from 10^{-16} C to 10^{-13} C. Its rms noise performance is 1.5 10^{-17} C (100 electrons), in a bandwidth from 10 kHz to 10 MHz. The transient recorder chip has 32 channels of analog-digital converters with an accuracy of 10 bits at a 20 MHz sampling rate and 32 digital pipelines. A pipeline is a synchronous SRAM ring-buffer for 50 ms trigger latency. An external trigger signal (e.g. derived from the dust impact onto an impact detector placed behind the trajectory sensor) stops the recording and all data is serially readout.

First dust accelerator tests at the Max-Planck-Institute for Nuclear Physics have been performed with the described set-up. A network of 30 front end microchips and one transient recorder chip were integrated with the sensor. The tests were performed with iron particles with speeds up to 30 km/s (0.1 to 1 µm grain size) which demonstrate the expected performance.

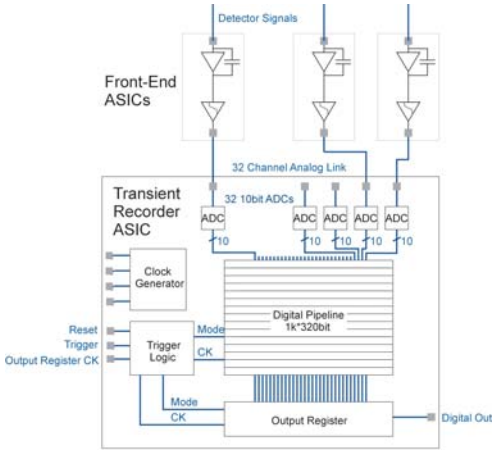

Fig.2 Block diagram of both the front-end and transient recorder ASICs

[1] Kempf, S., et al., 2004, Icarus, 171, 317-335. [2] Srama, R., et al., 2004b, ESA-SP 543, 73-78. [3] Auer S. and von Bun, F., 1994, in: Workshop on Particle Capture, Recovery, and Velocity/Trajectory Measurement Technologies (Zolensky M.E., ed.), LPI Tech. Rept. 94-05, Lunar and Planetary Institute, Houston, Texas, pp. 21-25. [4] Auer S., 1996, in: Physics, Chemistry, and Dynamics of Interplanetary Dust, ASP Conference Series, vol. 104, IAU Colloquium no. 150, Aug. 14-18, 1995, Gainesville, FL, pp. 251-254. [5] Srowig, A., 2004, PhD thesis, Heidelberg

Acknowledgements: This research is supported by NASA grant NAG5-11782 and by DLR grant 50OO0201.

TOF-SIMS ANALYSIS OF RESIDUES FROM ALLENDE PROJECTILES SHOT ONTO ALUMINUM FOIL – A STARDUST DRESS REHEARSAL. T. Stephan[1], J. Leitner[1], and F. Hörz[2], [1]Institut für Planetologie, Wilhelm-Klemm-Str. 10, 48149 Münster, Germany (stephan@uni.muenster.de), [2]NASA Johnson Space Center, Houston, Texas 77058, USA.

Introduction: Samples from the ongoing *Stardust* mission will offer the first opportunity to analyze cometary material that has been collected under controlled conditions at comet *81P/Wild 2* as well as contemporary interstellar dust [1, 2]. Furthermore, *Stardust* is the first sample return mission ever that will return material from a known object other than the Moon.

After return of the comet samples to Earth in January 2006, the primary goal will be to determine the elemental, isotopic, mineralogical, and organic composition of the dust and hence the properties of the cometary nucleus itself.

The *Stardust* mission will provide two different types of capture media containing cometary samples [2]. The primary sampling material is silica aerogel with density gradients varying from 5 to 50 mg/cm^3. It is used to decelerate impinging cometary grains with the least possible shock pressure during impact. In addition to 1039 cm^2 surface area of exposed aerogel, some 153 cm^2 of aluminum foils (Al 1100; >99 % pure) were exposed. These foils were primarily used to fix the aerogel cuboids and to facilitate their removal from the sample tray assembly.

Although even small cometary grains impacting on a metal foil at a velocity of 6.12 km/s are not expected to survive this process unaltered, the Al foil represents a valuable sampling material that might be the primary target material for small (sub-micrometer) or fluffy particles that disintegrate during penetration of the aerogel and that cannot be extracted easily from this highly porous and friable capture medium.

In this study, we used time-of-flight secondary ion mass spectrometry (TOF-SIMS) for the analysis of crater residues on Al foil from impact experiments using material from the Allende meteorite. The major goal of this study is to determine how well the chemical composition of Allende can be reproduced.

TOF-SIMS: The TOF-SIMS technique has been used for the analysis of extraterrestrial matter for more than a decade [3] including the analysis of impact residues from *LDEF* [4] and the *Hubble Space Telescope* solar array [5].

For the *Stardust* samples, TOF-SIMS has the unique opportunity to allow a comprehensive analysis with high lateral resolution and minute sample consumption [6]. During a typical analysis, less than one atomic monolayer is consumed while the sample is rastered with a ~0.2 µm Ga^+ primary ion beam. All secondary ions with a single polarity are detected quasi simultaneously after their passage through the time-of-flight spectrometer. Both polarities can be measured in two consecutive analyses. Elemental, isotopic, and molecular compositions are determined in parallel. Further analytical details are given in the literature [3].

Samples and Experimental Procedures: Powdered bulk material of 38–43 µm grain size of the CV3 chondrite Allende was shot onto Al foil at a velocity of 5.9 km/s. Based on the nominal projectile size, crater diameters as large as 180 µm are to be expected [7]. However, many individual grains fragmented during launch, resulting in a wide range of crater sizes.

In this study, four craters (#1–4) were selected for TOF-SIMS analysis. In the vicinity of crater #1, another crater (#1.1) and a Si-rich deposit without crater (#1.2) were chosen for further investigation. In the direct neighborhood of crater #4 also an additional crater (#4.1) was found that was treated separately. The following table comprises all samples investigated in this study.

sample	#1	#1.1	#1.2	#2	#3	#4	#4.1
size [µm]	120	7	9×5	100	40	18	4

All sample regions were analyzed after sputter cleaning by Ar ion bombardment. This cleaning became necessary since the entire Al foil was covered with a thin layer of mainly organic contaminants from the vaporized projectile sabot, which inhibited a proper analysis in the first place.

From the distribution of Mg, Si, Ca, and Fe, regions of interest were selected, and complete mass spectra were generated for these regions. After correction for Al foil blank, bulk element ratios were calculated using relative SIMS sensitivity factors obtained from glass standards that are usually used for quantitative TOF-SIMS analysis of silicates [3].

Results: Crater #1 does not show any residual material for a proper impactor characterization. However, all other sample regions exhibit enough material for quantitative analysis. Figure 1 shows lateral element distributions in the area of craters #4 and #4.1.

Quantitative results for all samples are summarized in Fig. 2: Element ratios normalized to Si show huge variations. Deposit #1.2 is clearly non-chondritic. Its Mg/Si-ratio is below 0.012×CV and also other major elements are more than a factor of 10 depleted compared to CV. Therefore, sample #1.2 was omitted for the calculation of average values. These average val-

ues are for most elements close to CV element ratios. Only three elements show deviations larger than a factor of two: Ca is enriched, Fe and Ni are depleted. However, a general element fractionation generated by the impact process cannot be deduced from the present data set.

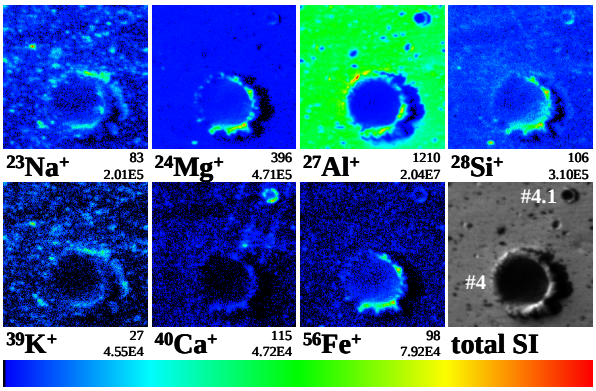

Fig. 1: TOF-SIMS secondary ion images showing two craters (#4 and #4.1) in Al foil. Field of view is 47×47 μm². All images use the same linear color scale normalized to the most intense pixel. Below each image, numbers for maximum and integrated intensities are given. A total positive secondary ion image is given in the lower left.

Since sputter cleaning was necessary prior to TOF-SIMS analysis, no useful information on organic constituents of the projectiles could be obtained. Usually organic compounds fragment during Ar bombardment. Typical silicone oil fragments as well as polycyclic aromatic hydrocarbons observed only before sputtering cannot be connected with the impact craters.

Contamination of the Al foil with Li, Be, B, C, and O prevents a quantitative analysis of these elements. Contamination with Na, Si, K, Sc, and V is responsible for some of the large error bars in Fig. 2, since blank subtraction had a major effect here. It is presently unknown, if this contamination is indigenous to the Al foil or if it results from the conditions during the impact experiments. Ar sputtering was not sufficient to remove this contamination completely.

Discussion: Although variations in element ratios from crater to crater are rather large, the average composition of all analyzed samples resembles remarkably well the expected element pattern. If compared with element ratios of different chondrite types [8], the TOF-SIMS data yield correlation coefficients above 0.95 for CV and CK, and below 0.95 for other carbonaceous chondrite classes. For L and LL ordinary chondrites, also correlation coefficients above 0.95 were found, mainly due to their low Fe and Ni concentrations. However, from the available data set, an unequivocal assignment to a specific chondrite class could not be made. Except for CH and EH chondrites, correlation coefficients are above 0.9 for all chondrite classes. For an unambiguous classification, data for light elements, especially C, would be crucial. It is hoped that the *Stardust* Al targets will be less contaminated with those elements.

The present results clearly indicate that chondritic projectiles impinging on Al foil at ~6 km/s can be identified by subsequent TOF-SIMS analysis of their residues. Further analyses will clarify, if deviations for Ca, Fe, and Ni are due to fractionation effects during impact or simply represent statistical variations in the inhomogeneous projectile material.

References: [1] Brownlee D. E. et al. (2003) *JGR, 108*, E8111. [2] Tsou P. et al. (2003) *JGR, 108*, E8113. [3] Stephan T. (2001) *Planet. Space Sci., 49*, 859–906. [4] Stephan T. et al. (1992) *LPS XXIII*, 1357–1358. [5] Stephan T. et al. (1995) *ESTEC Workshop on Space Debris on HST*, 25 pp. [6] Stephan T. (2003) *Workshop on Cometary Dust in Astrophysics, LPI Contrib. 1182*, 71. [7] Bernhard R. P. et al. (1994) *LPS XXV*, 107–108. [8] Lodders K. and Fegley B., Jr. (1998) *The Planetary Scientist's Companion.* Oxford University Press. 371 pp.

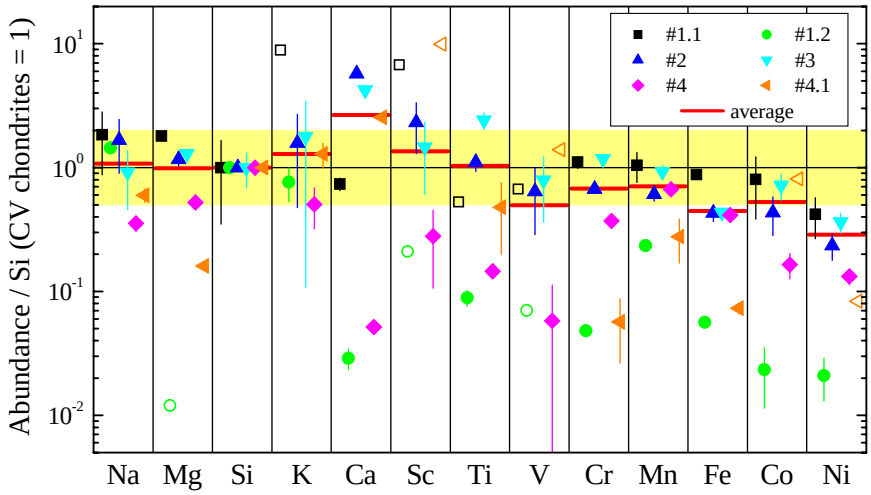

Fig. 2: Element ratios normalized to Si and CV chondrites show huge variations. Open symbols represent upper limits. Average values were calculated using all samples except #1.2, which is clearly non-chondritic. Most element ratios are within a factor of two (yellow area) CV-chondritic.

DEVELOPMENT OF THE LARGE AREA MASS ANALYZER. Z. Sternovsky[1], M. Horanyi[1], K. Amyx[1], S. Robertson[1], G. Bano[1], E. Gruen[2,3], R. Srama[2], S. Auer[4], [1]Laboratory for Atmospheric and Space Physics, University of Colorado, Boulder, CO, 80309 (Zoltan.Sternovsky@colorado.edu), [2] MPI-K, Heidelberg, Germany, [3] HIGP, Honolulu, USA, [4] A&M Assoc., Basye, USA

An instrument to analyze the chemical composition of dust particles in space is under development. Compared to similar previous instruments, such as the Galileo/Ulysses or Cassini dust detectors [1,2], this new instrument has a larger target area that makes it suitable for detecting interstellar dust particles. The device is a reflectron type time-of-flight mass spectrometer that measures the ions from the impact generated plasma due to hypervelocity dust impacts on solid surfaces. The mass spectrometer consists of the target, a single-stage reflectron potential configuration and an ion detector. The SIMION ion optics software package has been used to investigate different potential field configurations and optimize the mass resolution and focusing of the ions. The final configuration selected uses a set of six ring electrodes on the side and six annular electrodes at the top biased to different potentials to create the potential distribution of the reflectron. The annular target is of effective area approximately 0.2 m^2 and the mass resolution is m/dm ≈ 150. The target is biased to 5 kV and a grounded grid in front of the target is used to accelerate the ions. A microchannel plate is used as an ion detector. The laboratory model of the instrument has been fabricated and is undergoing preliminary testing. Dust impacts are simulated by using a frequency doubled (532 nm) Nd:YAG laser with ~8 ns pulse length. The laser can deliver up to 10 mJ of energy per pulse and its beam is focused to a ~ 15 micron spot size. The instrument will be calibrated at the Heidelberg dust acceleration facility.

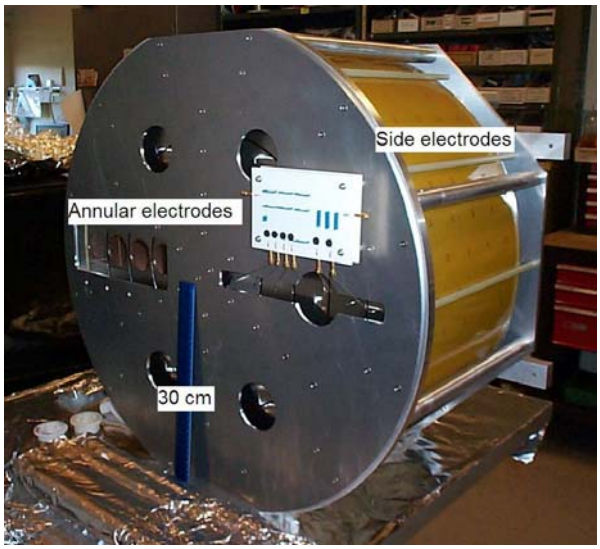

[1] Göller J. R. and Grün E. (1989) *Planet. Space Sci., 37*,1179-1206.

[2] Srama R., Ahrens T. J., Altobelli N., et al. (2004) *Space Sci. Rev. 114*, 465-518.

LUNAR SURFACE CHARGING: A GLOBAL PERSPECTIVE USING LUNAR PROSPECTOR DATA.

T. J. Stubbs[1], J. S. Halekas[2], W. M. Farrell[1], and R. R. Vondrak[1], [1]NASA Goddard Space Flight Center, Greenbelt, MD 20771, USA, [2]University of California, Berkeley, CA 94720, USA. Timothy.J.Stubbs.1@gsfc.nasa.gov.

Introduction: Our aim here is to use moments of the electron distribution function derived from Lunar Prospector Electron Reflectometer (LP/ER) data [1], together with basic probe equations [2], to determine the global variation in lunar surface electrostatic potentials for the different plasma environments encountered by the Moon. This will be a first step in better understanding and predicting global lunar surface charging under various conditions. This work will also include some simple estimates of the horizontal electric fields near the lunar terminator.

The surface of the Moon, like any object in a plasma, charges to an electrostatic potential that minimizes the total incident current [3]. The charging currents come from four sources: photoemission of electrons (J_{ph}), plasma electrons (J_e), plasma ions (J_i), and secondary electrons (J_{sec}). (J_{sec} arises primarily from surface ionization by plasma electrons.) The Moon is exposed to a variety of plasma environments during its orbit such that incident currents span several orders of magnitude. For about three-quarters of the time, the Moon is in the solar wind flow; otherwise, it is either in the tenuous plasma of the magnetospheric tail lobes, or the turbulent and energetic plasmas encountered in the geomagnetic plasma sheet and magnetosheath.

The lunar dayside typically charges positive, since J_{ph} usually dominates (see Fig. 1). As a result a "photoelectron sheath" forms above the surface, which in the solar wind extends ~1m, and effectively shields the charged surface from the surrounding plasma [4]. On the nightside, the lunar surface usually charges negative since J_e typically dominates. In this case a "Debye sheath" shields the surface potential [5] and can extend from meters to possibly ~1km [6]. There are significant uncertainties in current estimates of lunar surface potentials and almost nothing is known about their spatial distribution and temporal variation.

Implications: Surface charging processes are thought to drive the transport of lunar dust grains with radii <10μm, particularly near the terminator. The Surveyor landers observed ≈5μm grains levitating ~10cm above the surface [7,8]. During the Apollo missions 0.1μm-scale dust in the lunar exosphere was observed up to ~100km altitude [9,10,11]. The most viable mechanisms proposed to explain these observations have been based on the principle that the like-charged surface and dust grains act to repel each other such that dust is ejected from the surface. Under certain conditions, the heavier grains are predicted to electrostatically levitate near the surface [5,12], while the smaller grains are electrostically "lofted" to ~10km in altitude [13,14]. These phenomena could present a significant hazard to future robotic and human exploration of the Moon [15,16].

Spacecraft and Instrumentation: The LP spacecraft was in a rapidly precessing polar orbit about the Moon (period ~2 hours), which gave full coverage of the lunar surface twice every lunation. LP collected data for 18 months, with its altitude varying between 20 and 115 km, thus providing good coverage under most conditions. ER data is used to calculate electron concentrations (n_e) and temperatures (T_e) from kappa fits to the electron distribution functions [1]. As there is no ion data from LP we assume that the plasma near the Moon is quasi-neutral and the electrons and ions have the same temperature, i.e., $n_i = n_e$ and $T_i = T_e$.

Surface Charging Model: We calculate the electrostatic surface potential, ϕ_S, using the method and equations given in [2]. We solve numerically to find ϕ_S such that the net incident current is approximately zero, i.e., $J_e + J_i + J_{ph} \approx 0$. ($J_{sec}$ is not included here since on the dayside and near the terminator it is expected to be

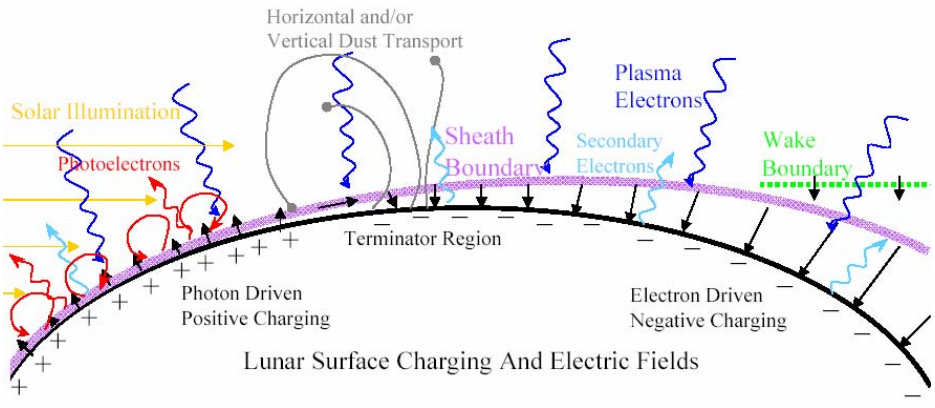

Fig. 1. Schematic of lunar electrostatic environment, showing charging current sources, surface charge, and electric fields (not to scale).

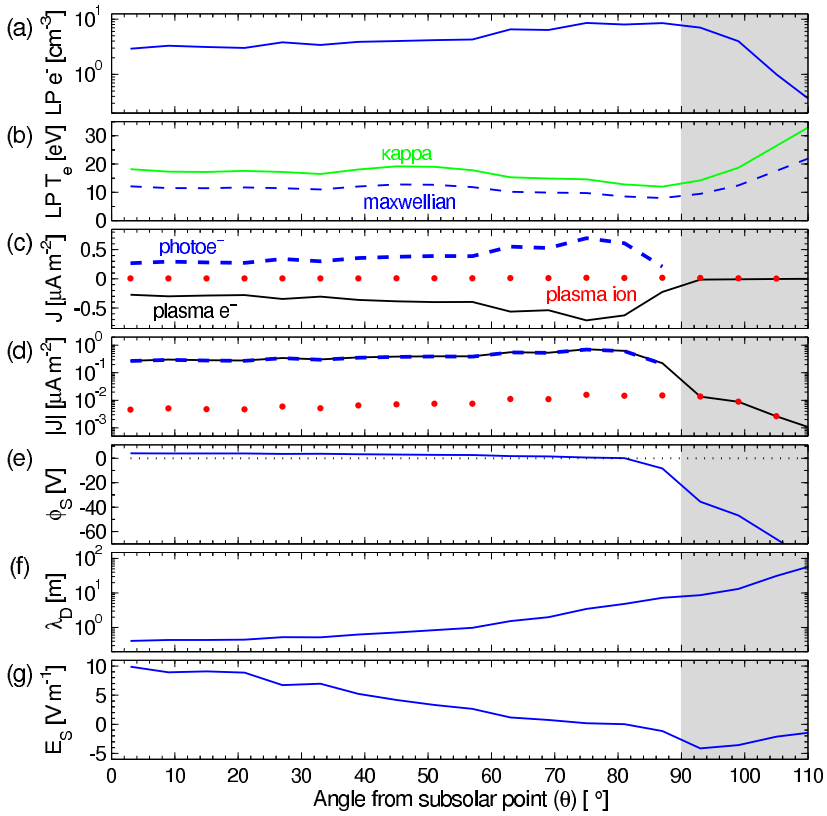

Fig. 2. Lunar surface charging predictions under typical solar wind conditions plotted as a function of angle from the subsolar point (θ). Input data: LP/ER derived electron (a) concentrations and (b) kappa (solid line) and maxwellian (broken line) temperatures. Current contributions from J_e (broken line), J_i (dots) and J_{ph} (solid line) shown on (c) linear and (d) log scales. (e) Lunar surface potential, ϕ_S, (f) Debye length of attracted species, λ_D, and (g) Surface electric field, E_S.

less significant than either J_e, J_i or J_{ph}.) The current density equations are different for positive ($\phi_S > 0$) and negative ($\phi_S < 0$) surface potentials [14]. Photocurrent density from normally incident sunlight is assumed to be 4.0×10^{-6} A m^{-2} [17] (given a surface photoelectron efficiency of 0.1). J_{ph} varies with the angle from the subsolar point, θ, and so is highest at the equator at local noon ($\theta = 0°$) and drops off to zero at the terminator ($\theta = 90°$). The Debye lengths used in this model are for the species attracted to the surface (e.g., where $\phi_S > 0$ we use the electron Debye length). It is important to note that the dominant source of electrons on the lunar dayside is from photoemission (at ~500 cm^{-3} this is ~100 times greater than in the solar wind). Assuming 1-D Debye shielding above a plane, the lunar surface electric field is given by $E_S = \phi_S / \lambda_D$.

Initial Predictions: Fig. 2 shows predictions for lunar surface charging given typical solar wind conditions. As expected the dayside is photo-driven ($\phi_S > 0$) and the nightside is electron-driven ($\phi_S < 0$). Due to the lower plasma concentrations, the nightside currents are much weaker.

In Fig. 2 we have only considered the vertical component of E_S. Horizontal electric fields will form between regions of different potential, and we would expect this to be most significant near the transition from $\phi_S > 0$ to $\phi_S < 0$ (i.e., near the terminator). We will make zeroth order estimates of horizontal E_S using a similar method to that described above. This could explain the enhancement in horizontal dust transport observed in-situ by the Apollo 17 LEAM experiment near the terminators [18,19].

References: [1] Halekas, J.S., et al. (2002) Geophys. Res. Lett., 2001GL014428. [2] Manka, R.H. (1973) Photon & Particle Interactions with Surfaces in Space, 347. [3] Whipple, E.C. (1977) J. Geophys. Res., 1525. [4] Singer, S.F. and Walker, E.H. (1962) Icarus, 1, 7. [5] Nitter, T. et al. (1998) J. Geophys. Res., 6605. [6] Halekas, J.S., et al. (2003) Geophys. Res. Lett., 2003GL018421. [7] Criswell, D.R. (1973) Photon & Particle Interactions with Surfaces in Space, 545. [8] Rennilson, J.J. and Criswell, D.R. (1974) The Moon, 10, 121. [9] McCoy, J.E. and Criswell, D.R. (1974) Proc. Lunar Sci. Conf. 5th, 2991. [10] McCoy, J.E. (1976) Proc. Lunar Sci. Conf. 7th, 1087. [11] Zook, H.A. and McCoy, J.E. (1991) Geophys. Res. Lett., 18, 2117. [12] Sickafoose, A.A. et al. (2002) J. Geophys. Res. 2002JA009347. [13] Stubbs, T.J., et al. (2005) Adv. Space Res., in press. [14] Stubbs, T.J., et al. (2005) Lunar Planet. Sci. Conf. 36th, 1899. [15] NASA Robotic and Human Lunar Exploration Strategic Roadmap (2005). [16] Stubbs, T.J., et al. (2005) Lunar Planet. Sci. Conf. 36th, 2277. [17] Goertz, C.K. (1989) Rev. Geophys., 27, 271. [18] Berg, O.E., et al. (1976) Interplanetary Dust and Zodiacal Light, 233. [19] Berg, O.E. (1978) Earth Planet. Sci. Lett., 39, 377.

IMPACT OF LUNAR DUST ON SPACE EXPLORATION. T. J. Stubbs, R. R. Vondrak and W. M. Farrell, NASA Goddard Space Flight Center, Greenbelt, MD 20771, USA, Timothy.J.Stubbs@gsfc.nasa.gov.

Introduction: From the Apollo era it is known that dust on the Moon can cause serious problems for exploration activities. Such problems include adhering to clothing and equipment, reducing external visibility on landings, and causing difficulty to breathing and vision within the spacecraft [e.g. 1,2]. An important step in dealing with dust-related problems is to understand how dust grains behave in the lunar environment.

Past Experiences. All astronauts who walked on the Moon reported difficulties with lunar dust. Eugene Cernan, commander of Apollo 17, stated that "… one of the most aggravating, restricting facets of lunar surface exploration is the dust and its adherence to everything no matter what kind of material, whether it be skin, suit material, metal, no matter what it be and it's restrictive friction-like action to everything it gets on" [1].

Highest Future Priority. NASA's Requirements for Lunar Exploration Program (RLEP) Document (ESMD-RQ-0014) states that the RLEP shall investigate the potential biological impacts of the lunar environment, including the micrometeoroid and dust environments (RLEP-M20 and RLEP-T20) [3]. Dust has also been highlighted as a priority by the Mars Exploration Program Assessment Group (MEPAG): "1A. Characterize both aeolian dust and particulates that would be kicked up from the martian regolith by surface operations of a human mission with fidelity sufficient to establish credible engineering simulation labs and/or software codes on Earth."

We shall briefly describe the properties of lunar dust and its impact on the Apollo astronauts, and then summarize three main problems areas for understanding its behavior: (1) Dust Adhesion and Abrasion, (2) Surface Electric Fields and (3) Dust Transport. These issues are all inter-related and must be well understood in order to minimize the impact of dust on future robotic and human exploration of the Moon.

Properties of Lunar Dust: Lunar dust was found to be similar to fine-grained slag or terrestrial volcanic ash [3].

Grain Size. With an average grain radius of ≈70μm, most dust is too fine to see with the human eye. 10–20% of dust has a radius <20μm [3].

Grain Shape. Dust grain shapes are highly variable and can range from spherical to extremely angular. Although, in general, grains are somewhat elongated [4].

Grain Conductivity. Lunar dust has low conductivity, and so can hold charge. However, conductivity can increase with: surface temperature; Infra-red (IR) light by ~10; and Ultra-violet (UV) light by ~10^6 [4].

Dust Impact on Astronauts:

Reduced Visibility. Exterior to the Lunar Module (LM) dust was kicked-up during landings which significantly reduced visibility [2]. Interior to the LM, dust would be brought in after moonwalks. It was reported by Alan Bean on Apollo 12 that "After lunar liftoff … a great quantity of dust floated free within the cabin. This made breathing without a helmet difficult, and enough particles were present in the cabin atmosphere to affect our vision" [2].

Respiratory. As mentioned, dust can make breathing difficult. It is very possible that chronic respiratory problems could arise in astronauts due to micro-scopic particulates in the lungs, especially after prolonged periods on the lunar surface [5].

Dust Adhesion and Abrasion:

Dust on Spacesuits. Alan Bean also noted that "… dust tends to rub deeper into the garment than to brush off" [2]. Dust adhered to spacesuits both mechanically and electrostatically. Mechanical adhesion was due to the barbed shapes of the dust grains, which allowed them to work into the fabric. Electrostatic adhesion was caused by charging of objects by the solar wind plasma and photo-ionization (see below). The abrasive effect of adhered dust can wear through the fabric of a spacesuit, drastically reducing its useful lifetime [1,2].

Dust on Lunar Surface Apparatus. Problems were experienced during Lunar Roving Vehicle (LRV) excursions, with much dust being kicked-up and covering exposed areas [1,4], leading to increased friction at mechanical surfaces. The resulting abrasive effect of dust increased wear and tear, which limited the lifetime of surface equipment.

From the recovery and examination of parts from Surveyor 3 during Apollo 12, it was found that dust accumulation and adhesion were heavier than anticipated [4] on both aluminum and painted surfaces.

Surface Electric Fields:

Lunar Surface Charging. Probe equations can be used to determine incident electric current densities on the Moon's surface, which can be used to find the surface electrostatic potential [6]. Using this approach it can be shown that the lunar dayside charges positive, as photo-electron currents dominate; and the lunar nightside charges negative, since plasma electron currents dominate. It is also possible for the transition from positive to negative surface potential to occur dayside of terminator [7].

Inclusion of Wake Physics. A wake or "void" forms downstream of the Moon when it is immersed in the solar wind flow [8]. This complicated interaction creates large electric potentials in the wake which leads to the formation of ion beams [9], and large electric fields at the terminators [8], amongst other phenomena.

Lunar Dust Transport:

In-situ Evidence for Transport of Charged Dust. Data from the Apollo 17 Lunar Ejecta and Micrometeoroids (LEAM) experiment was dominated by low energy impacts from electrostatically charged dust [10]. The peaks in the counts registered occurred around the terminators.

Evidence for Dust Above the Lunar Surface. Horizon glow (HG) and "streamers" from forward scattered sunlight were observed above the terminator by both surface landers and astronauts [e.g., 11,12]. It was suggested that near-surface HG (<1m) was caused by scattering from levitating dust grains with radii of ~5μm. This was due to electrostatic charging of the lunar surface and dust grains by the solar wind plasma and photo-ionization by solar UV and X-rays [6], which caused the dust to be repelled from the like-charged surface [e.g., 11,12,13]. Note that HG was ~10^7 too bright to be explained by micrometeoroid-generated ejecta [12,13].

There was also evidence for 0.1μm-scale lunar dust present sporadically at much higher-altitudes (~ 100km) [14]. The scale height for this dust population was determined to be ~10 km, which is too short to be caused by Na or K gas in the lunar exosphere [15]. Also, observations of these gases have been too dim to be seen by the unaided human eye [15].

It has been suggested that dust observed at high-altitudes is electrostatically "lofted" by the "dynamic dust fountain" effect [7], as opposed to static levitation mechanism used to explain heavier grains nearer the surface [12,13]. In the dynamic dust fountain model charged dust grains follow ballistic trajectories, subsequent to being accelerated upwards through a narrow sheath region by the surface electric field. These dust grains could affect the optical quality of the lunar environment for astronomical observations and interfere with exploration activities [e.g., 16].

References: [1] Goodwin R. (2002) Apollo 17 – The NASA Mission Reports: Vol. 1. [2] Bean, A.L. et al. (1970) Apollo 12 Preliminary Science Report, 29, NASA SP-235. [3] Robotic and Human Lunar Exploration Strategic Roadmap (2005). [4] Heiken, G.H., et al. (1991), Lunar Sourcebook a User's Guide to the Moon. [5] Biological Effect of Lunar Dust Workshop, NASA/ARC, March 29-31 (2005). [6] Manka, R.H. (1973) Photon & Particle Interactions with Surfaces in Space, 347. [7] Stubbs, T.J., et al. (2005) Adv. Space Res., in press. [8] Farrell, W.M. et al. (1998) Geophys. Res. Lett., 103, 23,653. [9] Ogilvie, K.W. et al. (1996) Geophys. Res. Lett., 23, 1255. [10] Berg, O.E., et al. (1976) Interplanetary Dust and Zodiacal Light, 233. [11] McCoy, J.E. (1976) Proc. Lunar Sci. Conf. 7th, 1087. [12] Rennilson, J.J. and Criswell, D.R. (1974) The Moon, 10, 121. [13] Criswell, D.R. (1973) Photon & Particle Interactions with Surfaces in Space, 545. [14] McCoy, J.E. and Criswell, D.R. (1974) Proc. Lunar Sci. Conf. 5th, 2991. [15] Zook, H.A. and McCoy, J.E. (1991) Geophys. Res. Lett., 18, 11, 2117. [16] Murphy, D.L. and Vondrak, R.R. (1993) Proc. Lunar Planet. Sci. Conf. 24th, 1033.

Lunar Exploration Issues	→ Connection →	Space Science Expertise
Dust Adhesion	Determining how charged particulates in a plasma interact with a surface.	Surface physics Plasma surface interactions, e.g. sputtering
Surface Electric Fields	Understanding how large objects charge in a plasma and under UV & X-rays.	Spacecraft charging Probe physics Wake physics
Dust Transport	Understanding how particulates immersed in a plasma interact with it. Knowing how the dust and plasma are modified by this interaction.	Dusty plasma physics Planetary Rings
Surface Composition	Understanding the source and composition of sputtered ions.	Pick-up ions, e.g. from comets.

***Spitzer's* View on Resolved Debris Disks – Vega, Fomalhaut and β Pictoris** K. Y. L. Su[1], G. H. Rieke[1], J. A. Stansberry[1], K. R. Stapelfeldt[2], M. W. Werner[2], D. E. Trilling[1], D. C. Hines[3] , M. Marengo[4], S. T. Megeath[4], G. G. Fazio[4], J. Van Cleve[5], [1]Steward Observatory, University of Arizona (933 N Cherry Ave, Tucson, AZ 85721, ksu@as.arizona.edu), [2]JPL/Caltech (4800 Oak Grove Dr, Pasadena, CA), [3]Space Science Institute (4750 Walnut St., Suite 205, Boulder, CO), [4]Harvard-Smithsonian Center for Astrophysics (60 Garden St., Cambridge, MA), [5]Ball Aerospace Corporation (1600 Commerce Str, Boulder, CO).

Introduction: One of the highlights of the *IRAS* mission was the discovery of a large infrared excess around normal stars attributed to dust particles collisionally replenished by asteroids and comets. Debris disks are the most visible signposts of other planetary systems, representing evidence of planetary system formation. *Spitzer* brings new levels of sensitivity and spatial resolution to debris studies in the thermal infrared [1]. Early results from *Spitzer* studies of debris disks around A type stars demonstrate that debris disks come in a huge variety, indicating both a large range in initial planetary system structures and also that individual disks may be dominated by debris created in individual events [2]. The characteristics found in A-star debris disks are analogous to our ideas of the early evolution of the solar system [3]. Here we present the first high spatial resolution far-infrared observations of resolved debris disks: Vega, Fomalhaut and β Pictoris, obtained with the Multiband Imaging Photometer for *Spitzer* (MIPS) [4]. We discuss the results as a whole set and try to understand the diversity of the debris phenomenon. These data provide a foundation for understanding other unresolved debris disks.

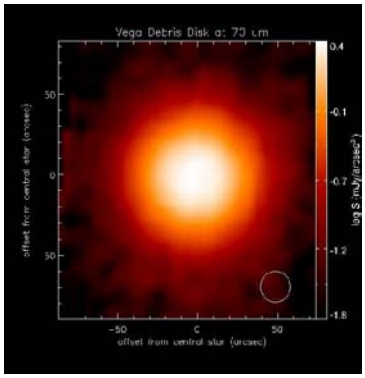

Figure 1 - Vega Disk image at 70 μm. The white circle on the lower left corner indicates the beam size at 70 μm. N is up and E is toward the left.

Vega: The disk around Vega was resolved as face-on disk with a radius of ~22" by *IRAS* [5] and *ISO* [6] at 60 μm. The 850 μm map obtained by Holland et al. [7] with SCUBA on JCMT shows an extended, roughly circular structure with an elongated bright central region oriented NE-SW. Observations at 1.3 mm by Koerner et al. [8] and by Wilner et al. [9] resolved dust emission peaks offset from the star by 8" to 14" that appear to be associated with a ring of emission at a radius of 60 to 95 AU.

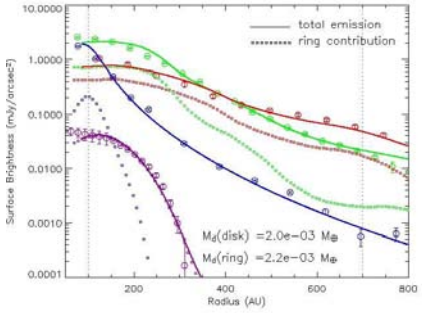

Figure 2 - Radial Surface brightness profiles at 24 (blue), 70 (green) and 160 (red) μm. The open circles are the observed data, and the solid lines are model profiles (see text). SCUBA 850 um is plotted in purple.

Figure 1 shows the disk image (after photosphere subtraction) of Vega at 70 μm. The disk appears very circular, smooth and without clumpiness. The disk angular size is much larger than found previously (at least, ~100" in radius) [10]. Assuming an amalgam of amorphous silicate and carbonaceous grains, the disk can be modeled as an axially symmetric and geometrically think disk, viewed face-on, with the surface particle number density following an inverse radial power law. The disk radiometric properties at 24, 70 and 160 μm are consistent with a range of models using grains of sizes ~1 to ~50 μm. A handful of grain models are consistent with the observed radial surface brightness distributions, but all these models require an 1/*r* surface number density law and a total mass of ~$3x10^{-3}$ earth mass in grains to explain the MIPS observations. A ring, containing grains larger than 180 μm and at radii of 86-200 AU from the star, can reproduce the observed 850 μm flux. The best model fit radial surface profile is shown in Figure 2. This ring could be associated with a population of larger astreroidal bodies analogous to our own Kuiper Belt. Cascades of collisions starting with encounters among these large bodies in the ring produce the small debris that is

blown outward by radiation pressure to much larger distances where we detect its thermal emission. The relatively short lifetime (<1000 years) of these small grains and the observed total mass, set a lower limit on the dust production rate, ~10^{15} g/s. This rate would require a very massive asteroidal reservoir for the dust to be produced in a steady state throughout Vega's life (~350 Myr). Instead, we suggest that the disk we imaged is the aftermath of a large and relatively recent collisional event, and subsequent collisional cascades.

Fomalhaut: A member of the Caster moving group like Vega, Fomalhaut and Vega have similar age, mass and distance. The disk around Fomalhaut was also first found by *IRAS*, and latter inferred as a donut-like disk with ~18" in radius and inclined ~20° from edge-on [11]. Submillimeter maps obtained by Holland et al. [12] and Marsh et al. [13] revealed a ring brightness asymmetry that has been interpreted as a dense clump between the ring ansae, and which might represent the dust particles dynamically trapped in resonance with a perturbing object [14].

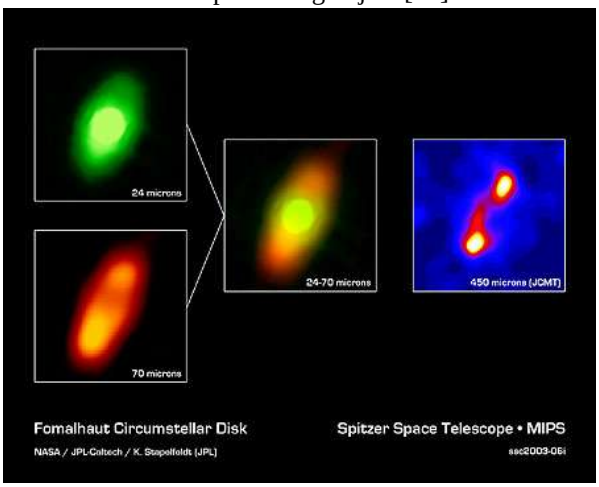

Figure 3 - MIPS images of Fomalhaut debris disk compared to the submillimeter map.

The disk images (after photosphere removal) are shown in Figure 3. While the disk orientation and outer radius are comparable to values measured in the submillimeter (unlike Vega), the disk inner radius cannot be precisely defined: the central hole in the submillimeter ring is at least partially filled with emission from warm dust [15]. The disk surface brightness becomes increasingly asymmetric toward shorter wavelengths, with the S-SE ansa always brighter than the N-NW one. The dusty ansae represent the result of collisional cascades in the asteroidal belt around Fomalhaut seen in submillimeter. The color in the mid-infrared range (20-30 μm) is consistent with an 1/*r* radial density distribution and the inward drift of grains from the outer ring. The new MIPS images suggest that the dust production in Fomalhaut is in a quiescent state, no major dust production event (like the one in Vega) in the past millions years. The dust particles last longer and slow drifting inward under P-R drag before destructed by collisions into smaller particles that are subject to radiation blowout.

β Pictoris: Unlike Vega and Fomalhaut, β Pictoris is a much younger system (~20 Myr) [16]. The amount of dust and gas in this nearly edge-on disk is more abundant than the one in Vega and Fomalhaut. Although the exact gas content in the disk is still in debate. The dust particles in the disk are primarily dominated by small grains that are subject to radiation blowout [17,18,19]. The disk is resolved in *Spitzer* IRS blue (15 μm) and red(22 μm) peakup images as well as MIPS 24, 70 and 160 μm images. Figure 4 shows the disk image at 70 μm with a radius of ~1000 AU. Detail analysis on the resolved multi-color images will be presented in the meeting.

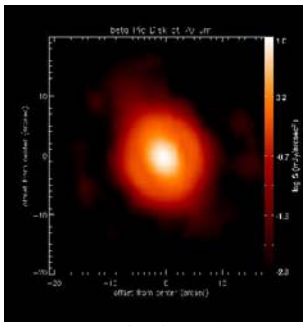

Figure 4 - MIPS 70 μm image of β Pictoris disk.

References: [1] Werner, M. W. et al. 2004, ApJS, 154, 1. [2] Rieke, G. H., et al. 2005 ApJ, 620, 1010. [3] Chambers, J. E. 2004, Earth & Plan. Sci. Letters, 223, 241. [4] Kenyon, S. J., & Bromley, B. D. 2004, ApJL, 602, L133. [5] Aumann, H. H. et al. 1984, ApJL, 278, 23. [6] Heinrichsen, I. Et al. 1998, MNRAS, 293, L78. [7] Holland et al. 1998, Nature, 392, 788. [8] Korener et al. 2001, ApJL, 580, 181. [9] Wilner et al. 2002, ApJL, 569, 115. [10] Su et al. 2005, ApJ, 628, in press. [11] Dent et al. 2000, MNRAS, 314, 702. [12] Holland, W. S. et al. 2003, ApJ, 582, 1141. [13] Marsh, K. A. et al. 2005, ApJL, 620, 47. [14] Wyatt & Dent 2002, MNRAS, 334, 589. [15] Stapelfeldt, K. R. S. et al. 2004, ApJS, 154, 458. [16] Barrado y Navascues, D. et al. 1999, ApJL, 520, 123. [17] Backman, D. & Paresce, F., Protostars & Planets III, p1253. [18] Okamoto, Y. K. et al. 2004, 431, 660. [19] Telesco, C. M. et al. 2005, 433, 133.

CONSTRUCTING THE ZODIACAL CLOUD

M. V. Sykes, Planetary Science Institute (sykes@psi.edu)

Modeling the interplanetary dust cloud has long involved inversion techniques on zodiacal light measurements to determine parametric model components. This contemplates the cloud as something relatively homogeneous, but provided important insights into its distribution and the properties of some of its smallest components scattering visible light. Since the discovery of actual dust production sources by the Infrared Astronomical Satellite, their subsequent observations by other spacebased infrared telescopes, increasingly sensitive and extensive in-situ measurements and sophisticated modeling of the dynamical evolution of dust, the zodiacal cloud can be viewed as the superposition of a number of components of different origins and processes, each of which is subject to focused investigation. These include dust production from the recent collisional disruption of asteroids, the emission of large refractory particles from comets, material arising from collisional processes in the Kuiper Belt and the interloping particles from outside the solar system. This does not necessarily provide a complete picture - there may be evidence of as yet unidentified dust production processes as these components are put back together in an attempt to explain observations of the whole. The study of the modern production of dust in our own solar system provides insight into a variety of evolutionary processes, as well as provides models for the production of dust around other stars.

SIZE DISTRIBUTION OF ANTARCTIC MICROMETEORITES.

S. Taylor[1], G. Matrajt[2], J.H. Lever[1], D.J. Joswiak[2], and D. E. Brownlee[2], [1]Cold Regions Research and Engineering Laboratory, 72 Lyme Rd., Hanover NH 03755, [2] Department of Astronomy, University of Washington, Seattle WA 98195.
Susan.Taylor@erdc.usace.army.mil

Introduction:

Micrometeorites are terrestrially collected extraterrestrial dust particles smaller than about a millimeter. The accretion rate, size distribution and composition of micrometeorites bears on numerous studies including: deducing the compositions of parent bodies; calibrating terrestrial sedimentation rates; interpreting the isotopic record of seawater; linking influx to global climate change; and assessing the role of ET materials in life processes.

In 1995 Taylor et al. [1] retrieved ~ 200g of material from the bottom of the South Pole water well (SPWW) of which about 0.1% were cosmic spherules (melted micrometeorites). Using the particle size distribution, area suctioned and age of ice melted (1100–1500 AD) they computed a terrestrial accretion rate for cosmic spherules 50–700 µm in diameter of 1600 ± 300 tons/yr [1] or 4 ± 2 percent of the flux measured above the atmosphere [2].

We are repeating this analysis using samples collected in 2000 from the SPWW. Compared with 1995 collection, the 2000 samples have less iron-oxide contamination allowing us to find unmelted micrometeorites. We are analyzing the deployment dedicated to the central plateau. Because this area was vacuumed in 1995 the 2000 sample should contain only those particles derived from the older, 700–1100 AD, ice [3] and allow us to calculate a flux for a second time period.

We have found and mounted 3272 micrometeorites from the central plateau sample. We present a preliminary size distribution (as not all micrometeorites have yet been measured) and an estimate of unmelted to melted ratio for the different size fractions.

Methods:

The samples studied were collected in 2000 from the SPWW, a 4,000-m^3 reservoir melting pre-industrial ice. The well's central plateau was vacuumed and yielded ~ 10 g of material. We sieved this sample into >425, 250–425, 150–250, 106–150 and 53–106µm size fractions. Using a binocular microscope we sorted 100% of the >150-µm fractions, 29% of the106-150 fraction and 9% of the 53–106-µm fraction and removed all potential ET grains. We mounted and sectioned over 4000 particles. Using a SEM/EDAX we checked each particle for composition and found that 3272 of particles mounted were micrometeorites. Optical microscopy was used to size the particles and to classify them based on their cross-sectional textures.

Results:

The size distributions for the 1995 and for the 2000 plateau samples are shown in Figure 1. For the 2000 collection we show individual data points for micrometeorites >250µm, as these have all been sized, and plot the cumulative number of micrometeorites for the three smallest size fractions. The numbers of micrometeorites in the smallest two size fractions have been increased to account for the fact that only a portion of each size fraction was sorted. The best-fit line to the tail of the 2000 plateau sample has a slope of -4.5 slightly less steep than the -5.2 tail-slope calculated for the 1995 plateau sample [2]. Nevertheless the two curves are quite similar indicating that the size distributions from the two collections are similar.

The 2000 collection has more micrometeorites than the 1995 collection. The addition of the unmelted component cannot explain the increased number as the unmelted micrometeorites would predominantly change the number of micrometeorites in the smaller size fractions. The fact that we found an order of magnitude more >250µm micrometeorites in the 2000 collection may be due to an increase in the plateau area as the well deepens or to an increase in the flux rate. Although we have not yet measured the plateau area our video records do not show an order of magnitude increase in the plateau area.

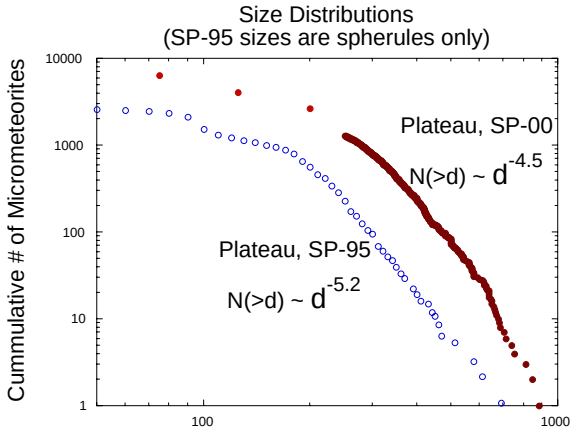

Figure 1. Cumulative size distributions for micrometeorites collected for two different time intervals from the bottom of the South Pole water well.

The numbers of melted and unmelted micrometeorites in each size fraction are given in Table 1. As expected, and noted by others [e.g. 4], the number of unmelted micrometeorites generally increases as the size fraction decreases. We found very few unmelted micrometeorites in the >250µm size fractions and similar number of melted and unmelted micrometeorites in the < 150µm size fractions.

We compare our results with those given for other collections (Table 1). From Greenland ice, Maurette et al. [4] found more un-melted than melted micrometeorites in the <100µm size fraction and about half the number of unmelted as melted in the 100-300µm range. From ice at Cap Prudhomme, Antarctica Maurette et al. [5] found 5 times as many unmelted micrometeorites in the <100µm size fraction and close to half as many unmelted to melted micrometeorites in the 100-400µm size range. Terada et al. [6] sampled ice of three different ages in Antarctica (16, 30 and 60 thousand years before present) and found a range in the unmelted to melted ratio from 0.5 to 4.5 for micrometeorites 40–238µm in diameter. Genge and Grady [7] extracted over 500 micrometeorites from Cap Prudhomme samples and found an

unmelted to melted ratio of ~3. For similarly sized particles, 53–250µm this study, 50–300µm [4] and 40–238µm [6] the unmelted to melted ratios are 0.2, 0.5 and 0.6 respectively. These preliminary results indicate that SPWW collection has a lower number of unmelted micrometeorites than the other two collections. Possible explanations include variations in the types of micrometeorites being deposited, destruction or masking of the unmelted micrometeorites in the SPWW samples and differences in the way micrometeorites are classified. There are many micrometeorites that are transitional between melted and unmelted (Figure 2). How these are tallied can change the unmelted to melted ratio. We intend to photograph all the micrometeorites from the plateau collections and to document how we classified each particle so that the third possibility can be assessed.

Reference	Size fraction (µm)	Number unmelted	Number melted	U/M
This study	>425	1	135	7.41E-03
	250-425	23	1138	2.02E-02
	150-250	134	1288	1.04E-01
	106-150	169	174	9.71E-01
	53-106	70	135	5.19E-01
Maurette et al. 1987	50-100	1500	1060	1.42E+00
	100-200	265	570	4.65E-01
	200-300	45	101	4.46E-01
Maurette et al. 1991	50-100			>5
	100-400			~0.3
Terada et al. 2001	40-238	101	78	1.29E+00
	40-238	134	138	9.71E-01
	40-238	172	84	2.05E+00
	40-238	18	4	4.50E+00
	40-238	30	53	5.66E-01
Genge & Grady 2002	50-400	412	138	2.99E+00

Conclusions:

We expect to calculate a flux for the 700–1100 AD time interval and to complete the particle size distribution for the 2000 SPWW collection this year. Next year we hope to image and classify all the micrometeorites. When complete this collection-level analysis will allow us to place an individual micrometeorite in context and determine how a micrometeorite relates to the population of micrometeorites as a whole.

Acknowledgements: We thank NSF (Dr. Julie Palais program manager) for funding the collection of micrometeorites from the South Pole water well and NASA (Dr. David Lindstrom program manager) for funding the analysis of the 2000 collection. We also thank Sarah (Sally) Elliott for imaging several hundred of these micrometeorites and Dr. Charles Daghlian for use of Dartmouth College's SEM.

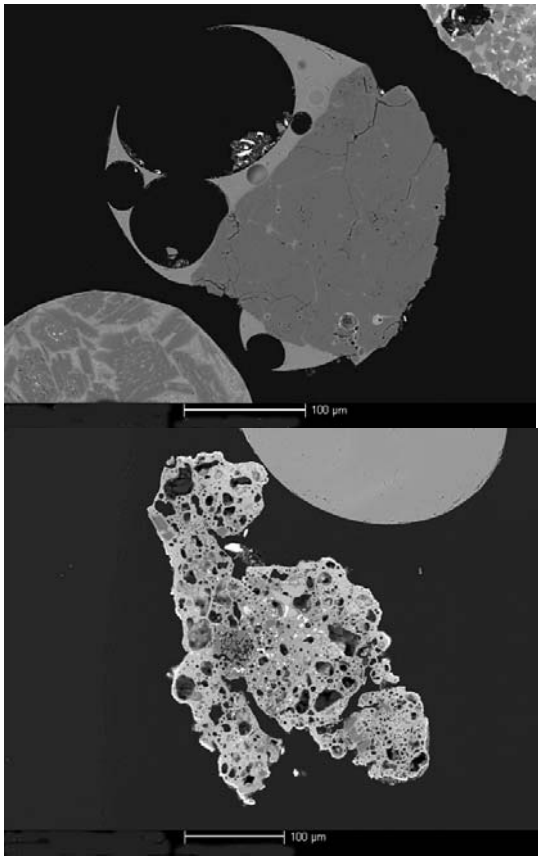

Figure 2. Transitional forms: Relic grain bearing and scoriaceous micrometeorites.

References:

[1] Taylor S, Lever J. H., and Harvey R.P. (1998) Accretion rate of cosmic spherules measured at the South Pole. *Nature* **392**, 899-903. [2] Love S.G. and D.E. Brownlee (1993) A Direct measurement of the terrestrial mass accretion rate of Cosmic dust, *Science* **262**, 550-553. [3] Kuivinen K.C., Koci, B.R., Holdsworth, G.W. and Gow A.J. (1982) South Pole ice core drilling, 1981-1982. Antarctic Journal of the United States XVII, 89-91. [4] Maurette M., Olinger C., Christophe, M., Kurat G., Pourchet, M., Brandstatter, F., and Bourot-Denise, M. (1991) A collection of diverse micrometeorites recovered from 100 tonnes of Antarctic blue ice, *Nature* **351**, 44-47. [5] Maurette M., Hammer C., Brownlee D.E., Reeh N. and Thomsen H.H. (1986) Placers of cosmic dust in the blue ice lakes of Greenland, *Science*, **233**, 869-872. [6] Terada K and 23 others (2001) General characterization of Antarctic micrometeorites collected by the 39th Japanese Research Expedition: Consortium studied of JARE AMMs (III), *Anatarct. Meteorite Res*. **14**, 89-107. [7] Genge M.J. and M.M. Grady (2002) The Distribution of Asteroids: Evidence from Antarctic Micrometeorites, LPSC XXXIII, 1010.pdf.

FE-NI-OXIDE SPHERULES WITH NI-FE-RICH AND FE-AL-RICH SILICATE CORES AND A CHONDRITIC AGGRIGATE SPHERULE FROM DEEP-SEA SEDIMENTS. Y. Tazawa[1] and T. Fukuoka[2], [1]Department of Physics, Graduate School of Science, Kyoto University, Kyoto 606-8502, Japan (tazawa@cr.scphys.kyoto-u.ac.jp), [2]Department of Environmental Systems, Faculty of Geo-Environmental Science, Rissho University, Kumagaya 360-0194, Japan.

Introduction: Deep sea floor is an environment with extremely low rates of sedimentation of terrigeneous particles (*e.g.*, apploxately several mm/10^3 yr for the Pacific Ocean red clay), where is chemically inactive compared to the ground in some cases. Therefore, microparticles of extraterrestrial origin fallen on the Earth extended over 10^4~10^5 years has been preserved in less than a meter-thick of the red clay, though it had been more or less affected by Atmospheric frictional heating, leaching by sea water, biological activity of benthos, *etc.* Spherical microparticles in deep-sea floor (Deep-Sea Spherules, DSSs) which have composition similar to chondrite and/or rich in siderophile elements (SPEs: *e.g.*, Ni, Ir, Os, Au, *etc*.) are thought to be of "cosmic" origin because the shapes seem to be ablation droplets formed during the Atmospheric entry of meteoroids [*e.g.*, 1] in addition to the composition above. They are classified into three groups, typical of them are: (a) iron (metallic, magnetic) spherules (ISs) consist of nickeliferous magnetite and wüstite with or without Fe-Ni metallic cores, (b) stony (silicate) ones (SSs) consist of olivine, magnetite, and glass with chemical composition similar to chondrite, and (c) glassy ones (GSs) consist of glass with the chondritic composition [*e.g.*, 2]. Thermal history and alteration scenario of the spherule formation have been also discussed based on the chemical and mineralogical simulation and observation of internal features [e.g, 3, 4, 5]. DSSs are the important samples thought to be microscopic analogues of meteoroidal and cometary bodies, even though nowadays mass collection of fresh, primitive, and unaltered cosmic particles have been obtained from the Stratosphere and Polar region.

Samples and Experimental: Six DSSs are investigated, which were extracted by sieves and an electromagnet from water-diluted sediments dredged from the 4700 m deep floor at the Central Pacific Ocean (9°30'N, 174°18'W ~ 9°31'N, 174°17'W) by the R/V Hakurei-maru II, Metal Mining Agency of Japan in 1979 and provided for studies on the extraterrestrial matter. Each of them was observed and weighed by using a stereo-zoom microscope and an electro microbalance prior to the analyses.

INAA: They were investigated firstly by instrumental neutron activation analysis (INAA). The procedures were applied basically after [6] and as follows: Four kinds of standards and references were used: (1) glass chips made from JB-1 (GSJ standard rock, basalt, [7]) for the lithophile elements (LPEs), (2) synthetic Ni-platinoid alloy for SPEs [6], (3) ultra-pure synthetic qualtz for references of ^{28}Si (n,p)^{28}Al reaction, and (4) Canyon Diablo iron meteorite (C.D., [8]) for references of SPEs, respectively.

INAA for short-lived nuclides were firstly carried out. The samples were activated individually in sequence with thermal neutron for 5 min at ~2x10^{13} neutrons/cm^2/sec in the pneumatic pipe PN-3 of the reactor JRR-3, the Japan Atomic Energy Research Institute (JAERI), and counted for 400 sec after 2 ~10 min cooling using a gamma-ray counting facility at JRR-3. They were secondly counted for 1000 sec at 1 ~ 6 hr after the first counts at the Inter-University Laboratory for the Joint Use of JAERI Facilities, Research Center for Nuclear Science and Technology (RCNST), University of Tokyo.

INAA for long-lived nuclides were done after those the above. The samples were irradiated together again with thermal neutron for 98 hours at 1x10^{14} neutrons/cm^2/sec in a hydraulic rabbit irradiation facility HR-1 of JRR-3. They were also counted repeatedly in accordance with their half-lives and activities using gamma-ray counting facilities of Aoyama Gakuin University and Gakushuin University.

EPMA: After the INAA study, three ISs and a SS were embedded individually in P-resin. They were sectioned by polishing and coated with carbon to observe textures and distribution of major elements. Each section was photomicrographed with secondary and back scatter electron images (SEI/BEI), and analyzed quantitatively for major and minor chemical composition at several points by a SEM/EDX at Department of Geology and Mineralogy, Kyoto University. Then, it was slightly polished and coated again, and investigated for elemental mapping and point analyses of major elements in the new section by an EPMA at National Institute for Polar Research (NIPR), Tokyo. Both analyzers were operated with an accelerating voltage at 15 KV and probe currents at 14 nA for point analyses and 200 nA for elemental mapping, respectively.

Results and Discussion: Weghts, sizes, and specific gravities (estimated from the weights and sizes) are listed together with the INAA results in Table 1.

Spherules A, B, and C have black shining or metallic luster, and higher specific gravities (4.5 ~ 5.3 g/cm^3), while the D, E, and F have dullish black or dark brown color, or partially translucent blobs, and the lower specific gravities (2.3 ~ 3.1 g/cm^3). These features are usually seen in DSSs. The Spherule D is fragile so that it has partially got out of shape at the time of polishing. CI normalized abundance patterns revealed by INAA and BEIs of the polished sections are shown in Fig 1 and 2.

The B, whose bulk composition assayed by INAA is Fe 67.6%, Ni 4.50%, Co 0.18%, and Ir 2.34ppm, has a mantle of Ni, Co rich Fe oxide, *i.e.*, Fe 69.6%, Ni 4.06%, Co 0.35%, and O 25.3%, and an eccentric spherical core of Ni, Fe rich silicate, *i.e.*, SiO_2 35.2%, NiO 31.8%, FeO 19.1%, Al_2O_3 6.6%, and MnO 3.2%. The C, whose bulk composition is Fe 67.0%, Ni 1.59%, Co 0.24%, and Ir 0.41ppm, has also a mantle of Ni, Co rich Fe oxide, *i.e.*, Fe 71.1%, Ni 1.46%, Co 0.40%, and O 25.6%, and an "amoeboidal (or a walnut-shape)" silicate (glassy?) core consists of Si, Fe, Al, Mg, and K, *i.e.*, SiO_2 64.9%, FeO 17.4%, Al_2O_3 10.9%, MgO 3.68%, and K_2O 2.14%. These kinds of silicate cores have never been observed in IS. One of SS, the D, is a fragile porous aggregate of μ-sized grains of mafic silicates, oxides, and sulphides, whose bulk composition is, *i.e.*, Mg 20.3%, Fe 20.1%, Ni 1.27%, Al 0.46%, Cr 0.20%, Mn 0.10%, Co 484ppm, V 89ppm, Sc 4.91ppm, Os 1.9ppm, Ir 0.51ppm, and Au 0.42ppm, quite similar to CI, except for high Os, Au, and Mg (approx. 4, 3, and 2 times of CI, respectively), and low Al and Mn (approx. a half of CI) contents. Two other SS also have a composition similar to the above SS except for the depletion of SPE.

Acknowledgment: We thank late Prof. K. Yamakoshi, and also K. Nogami for providing the DSSs studied in this work. We thank Y. Ito, H. Sawahata and M. Kawate, RCSNT, University of Tokyo, H. Nagasawa, Gakushuin University, Y. Yokota, Aoyama Gakuin University, M. Kitamura and N. Shimobayashi, Kyoto University, and H. Kojima and N. Imae, NIPR, for making analyzing installations available to us. This work was supported partly by the Inter-University's Program for the Joint Use of JAERI Facilities.

References:[1] Blanchard M. B. et al. (1980) *EPSL, 46,* 178-190. [2] Brownlee D. E. (1985) *Ann. Rev. Earth Planet. Sci., 13,* 147-173. [3] Brownlee D. E. et al. (1984) *Nature, 309,* 693-695. [4] Love S. G. and Brownlee. D. E. (1991) *Icarus, 89,* 26-43. [5] Yada T. et al. (1996) *Proc. NIPR Symp. Antarctic Met., 9,* 218-236. [6] Fukuoka T. and Tazawa Y. (1996) *Abst. 1996 Fall Meeting Jap. Soc. Planet. Sci.*, pp-16. [7] Nagasawa H. et al. (1979) *GCA, 43,* 267-272. [8] Nogami K. et al. (1980) *Geochem. J., 14,* 11-18. [9] Anders E. and Grevesse N. (1989) *GCA,53,* 197-214. [10] Ando A. and Terashima S. (1985) *Abst. Ann. Meeting Geochim. Soc. Jap.* [11] Vdobykin G. P. (1973) *Space Sci. Rev., 14,* 758.

Table 1. INAA Results of Deep Sea Spherules

Sample		A	B	C	D	E	F
Wt[1]	μg	152.1	18.9	12.1	8.9	90.7	17.1
D[2]	μm	400	190	163	195	410	220
SG[3]	g/cm^3	4.5	5.3	5.3	2.3	2.5	3.1
Element							
Al	%	0.253	0.034	0.29	0.46	0.705	0.64
Fe	%	66.0	67.6	67.0	20.1	9.84	25.0
Mg	%	-	-	-	20.3	22.9	23.5
Mn	%	-	0.15	-	0.10	0.326	0.18
Cr	%	0.122	0.202	0.0052	0.202	0.180	0.197
V	ppm	55	96	15	89	77	96
Sc	ppm	1.98	-	1.77	4.91	6.61	6.15
Co	ppm	1810	1820	2360	484	27.5	257
Ni	%	5.16	4.5	1.59	1.27	0.05	0.38
Os	ppm	1.1	-	-	1.9	0.30	-
Ir	ppm	3.97	2.34	0.41	0.51	0.017	0.032
Au	ppm	-	-	-	0.42	0.010	-

Sample		JB-1	Alloy	C.D.	Error(%)	CI	[C.D.]
Wt[1]	μg	31.5	39.8	158.6			
Element							
Al	%	**8.07**	4.11	-	1 - 12	0.868	
Fe	%	**6.3**	-	90.3	1 - 1.5	19.04	92.3
Mg	%	**4.67**	-	-	3 - 13	9.89	
Mn	%	**0.116**	-	-	2 - 10	0.199	
Cr	%	**0.0414**	-	-	1 - 9	0.266	
V	ppm	**207**	-	-	3 - 50	56.5	
Sc	ppm	**28.9**	-	-	1 - 5	5.82	
Co	ppm	**39.1**	23.8	3990	2 - 13	502	4900
Ni	%	-	**82.6**	11.2	3 - 40	1.10	7.25
Os	ppm	-	**52000**	4.7	10 - 50	0.486	3.6
Ir	ppm	-	**1920**	3.62	1 - 28	0.481	2.10
Au	ppm	-	**7410**	2.43	2 - 20	0.14	1.26

Note: 1) Weight in μ g. 2) Diameter. 3) Spacific Gravity. Values bold-faced and underlined are the standard values for the determination, JB-1[10] Alloy [6]. C.D.: Canyon Diablo Iron Meteorite (this work). Error (%): Range of % errors of determination. CI [9]. [C.D.] [11].

Figure 1. CI normalized Abundances of Deep Sea Spherules

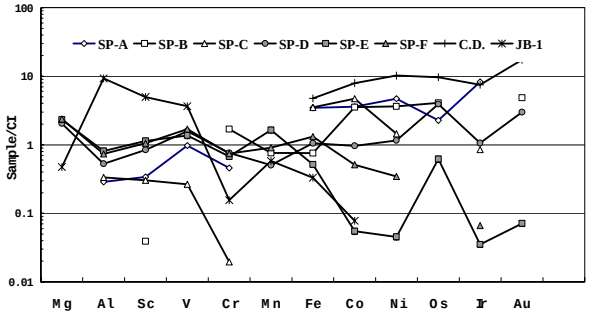

Figure 2. BEIs of Fe-Ni-oxide Spheres with Silicate Cores

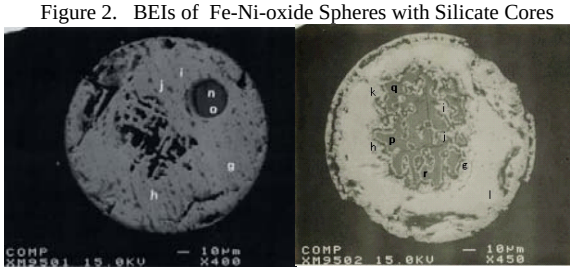

Spherule B Spherule C

INAA RESULTS OF INDIVIDUAL ANTARCTIC MICROMETEORITES AND THEIR TYPES. Y. Tazawa[1], T. Fukuoka[2], Y. Fukushi[2,7], Y. Saito[3], H. Sakurai[4], Y. Suzuki[4], T. Noguchi[5] and T. Yada[6], [1]Department of Physics, Graduate School of Science, Kyoto University, Kyoto 606-8502, Japan (tazawa@cr.scphys.kyoto-u.ac.jp), [2]Department of Environmental Systems, Faculty of Geo-Environmental Science, Rissho University, Kumagaya 360-0914, Japan, [3]Radio Isotope Laboratory, College of Science and Engineering, Aoyama Gakuin University, Sagamihara 229-8551, Japan, [4]Department of Physics, Faculty of Science, Yamagata University, Yamagata 990-8560, Japan, [5]Department of Materials and Biological Science, Ibaraki University, Mito 310-8512, Japan, [6]Department of Earth and Planetary Science, University of Tokyo, Tokyo 113-0033, Japan, [7](Present Address) Department of Earth and Planetary Sciences, Tokyo Institute of Technology, Tokyo 152-8551, Japan.

Introduction: Micro particles thought to be of cosmic origin and collected from the Earth's environments have survived from the heating and the weathering during their Atmospheric entry and their residence on the Earth. Most of them have lost their inherent features and have altered into fully molten droplets, *e.g*., "Cosmic Spherules (CSs)"[1]. Since three decades, a large number of scarcely altered extraterrestrial particles have been collected from the Stratosphere [2, 3] and the Polar Regions [4, 5]. Typical of them are fragile aggregates of chondritic constituents; *i.e*., "Interplanetary Dust Particles (IDPs)" thought to be of cometary origin [2] and "Antarctic Micrometeorites (AMMs), especially, unmelted ones (UMMs)"[4]. AMMs have been collected and investigated widely in recent years [6,7,8,9,10] because it may be found among them that unique samples of primitive Solar System materials have never been known in neither IDPs nor tiny constituents of conventional meteorites.

We report here characteristics of individual AMMs so far investigated by Instrumental Neutron Activation Analyses (INAA)[11,12,13] and their types classified by abundance patterns of LPEs, SPEs and REEs.

Samples: AMMs studied are thirty-one MMs provided by National Institute for Polar Research (NIPR), Tokyo, which were collected from deposits in a storage tank of melting snow for daily life at Dome Fuji Station (DF: 77°19'S, 39°42'E, JARE-37/38)[6], melting and microfiltering bare ice near the Kuwagata Nunatak (KN: 72°06'S, 35°15'E) and south of Minami-Yamato Nunataks (MY: 72°26'S, 35°20'E) at Yamato Mountains (JARE-39)[8], and also melting and microfiltering bare ice near Tottuki Point on the Soya Coast (TP: 68°55'S, 39°51'E, JARE-41)[9]. They are an I-type spherule, fourteen S-type spheres or spheroids, and sixteen S-type UMMs (irregular shape). Three other MMs were also provided but lost during sample preparations for long term neutron irradiations. Assortments and preliminary investigations of the AMMs have been also performed by the AMM initial examination team organized by NIPR [6].

INAA: INAA were performed on the individual MMs and tiny (< 1mm in size) chips of standard materials; *i.e*., glass made from Japanese Standard Rock (basalt) JB-1 (GSJ) for lithophile elements (LPEs), and metal wire Al-Au (0.1%: IRMM-530) and Pt (SRM-680a) for siderophile elements (SPEs). Each of the samples was weighed by an electro-microbalance prior to INAA. We could not use plural gamma-ray counting systems at the same time, so that total numbers of the samples which should be analyzed in a series of INAA including standards and references were to be no more than fifteen or so. Therefore, the MMs were divided into four groups, and four sets of INAA were carried out: *i.e.*, two times of neutron irradiations and consecutive gamma-ray countings should be done in each set. The procedures were applied after [14] and seen in [11,12,13], and as follows:

INAA for short-lived nuclides (SL series). Each of the MMs and the standards was heat-sealed in each small (ca. 2x2 mm^2) bag made with ultra pure polyethylene sheet and irradiated by thermal neutron for 10 min at 20 MW ($1.5x10^{13}$ neutrons/cm^2/sec) in the pneumatic pipe (PN-3) of the reactor JRR-3M, Japan Atomic Energy Research Institute (JAERI). The first counts were done for 400 sec, after 2 ~10 min cooling using a gamma-ray counting facility at PN-3. The second counts were also done for 1000 sec, 1 ~ 6 hr after the end of irradiation, using a facility at the Inter-University Laboratory for the Joint Use of JAERI Facilities, Research Center for Nuclear Science and Technology (RCNST, Tokai br.), University of Tokyo.

INAA for long-lived nuclides (LL series). After the SL series, the samples were picked out from the polyethylene bags and encased again individually in ultra-pure synthetic quartz vials. Then they were activated again all together for 100 hr at 20 MW ($1x10^{14}$ neutrons/cm^2/sec) in the hydraulic rabbit irradiation facility HR-1 of the JRR-3M. They were counted repeatedly in accordance with their half-lives and activities, using gamma-ray counting facilities of Institute for Cosmic-Ray Research, University of Tokyo, and Aoyama Gakuin University. Counting durations and cooling times were about for 2~12 hr after 4~8 days, for 6~24 hr after 2~3 weeks, 1day ~1 week after more than 1 month, respectively.

Results: As shown partly in Table and Figures, results are as follows; *i.e.*, (a) Abundance patterns of LPEs (Al, Ti, Ca, Mg, Cr, Mn, and Na) normalized to CI and Mg, and those of SPEs (Ir, Cr, Mn, Fe, Co, Au) normalized to CI and Fe of the MMs illustrate their features similar to chondrites (except Na, Ir, Au are more or less depleted in two thirds of them) rather than achondrites. (b) As for the LPEs abundances mormalized to CI and Mg (except for those of the I-type MYIB007), Na show the range from 2.2×10^{-3} to 1.6, while Al show that from 2.6×10^{-2} to 12. The ratios Al/Na also range from 5.5×10^{-1} to 3.8×10^{2}. (c) In contrast to Deep Sea Spherules (DSSs), AMMs do not so much deplete volatile elements; *e.g.*, Na and Au, but fully deplete K. Enrichment of refractory elements do not also show so much (< 11). (d) REE (La, Sm, Yb, Lu) abundances also show those of unfractionated similar to chondrite (eleven MMs), a little fractionated (seven MMs), fractionated (six MMs), and fairly fractionated or not detected (seven MMs). (e) SPEs (Ir,Cr, Mn, Fe, Co, Au) abundances normalized to CI and Fe show those unfractionated (four MMs), unfractionate but with only Ir severely depleted (0.004~0.03 times of Fe, ten MMs), those with Ir and Au depleted (six MMs), those with additionaly rich in Mn (3~6 times of Fe, six MMs) and others (four S-type and an I-type). (f) AMMs studied are classified into six types (five S-types and an I-type) based on the abundance patterns mentioned above.

Acknowledgements: This study was supported partly by the Inter-University's Program for the Joint Use of JAERI Facilities, RCNST, University of Tokyo, the Cooperative Research Program of Institute for Cosmic Ray research (ICRR), University of Tokyo, and also the Cooperative Research Program of NIPR.

References:[1] Murry J. and Reneard A. F. (1883) *Proc. Roy. Soc. Edinburgh, 12,* 474–495. [2] Brownlee D. E. et al. (1976) *NASA Tech. Mem., TMX-73152,* 1-42. [3] CDPET (1981-1997) *Cosmic Dust Catalog, NASA/JSC, Vol. 1-15.* [4] Maurette M. et al. (1986) *Science, 233,* 869–872. [5] Maurette M. et al. (1991) *Nature, 351,* 44–47. [6] Nakamura T. et al. (1999) *AMR, 12,* 183–198. [7] Fukuoka T. et al. (1999) *Ant. Met. XXIV,* 24-25. [8] Yada T. and Kojima H. (2000) *AMR, 13,* 9-18. [9] Iwata N. and Imae N. (2002) *AMR, 15,* 25-37. [10] Noguchi T. et al. (2000) *AMR, 13,* 270-284. [11] Fukuoka T. et al. (2000) *Ant. Met. XXV,* 10-11. [12] Tazawa Y. et al. (2003) *Internatl. Symp. Evolution of Solar System Materials, NIPR,* 138-139. [13] Fukushi Y. et al. (2004) *Ant. Met. XXVIII,* 12-13. [14] Fukuoka T. and Tazawa Y. (1996) *Ant. Met. XXI,* 33-34.

Partial INAA results of AMMs

Sample	F96CB003	F96CB004	F96CB019	F97AG008	MYIB004	MYIB005	MYIB007
wt µg	3.1	3.0	10.7	1.9	3.3	5.8	9.4
Na %	0.07	0.32	0.017	0.77	0.42	0.005	0.002
Mg %	9.5	7.63	20.6	15.0	11.2	11.5	-
Al %	9.84	1.2	0.87	1.52	1.64	1.64	0.037
Ca %	4.08	0.46	0.68	1.70	1.01	2.30	-
Ti %	0.38	-	0.54	-	0.20	0.26	-
Sc ppm	25.8	7.12	5.28	15.1	7.78	8.64	0.17
V ppm	60	48	46	86	68	80	2.4
Cr ppm	3800	2140	149	4370	4980	3800	2800
Mn %	0.12	0.19	0.72	0.28	0.43	0.20	0.01
Fe %	11.3	22.4	11.7	26.2	26.4	27.4	8.86
Co ppm	138	620	57.0	531	435	255	150
La ppm	2.5	0.39	0.21	-	0.25	0.22	-
Sm ppm	-	0.08	0.143	0.320	0.20	0.20	-
Yb ppm	-	0.35	0.31	0.15	0.26	0.32	-
Lu ppm	0.42	0.12	0.09	0.048	0.07	0.03	-
Au ppb	-	3.33	2.64	80	2.02	1.5	3.3
Ir ppb	295	775	107	3.79	640	308	34
Type	IVb	I	IVa	IIa	I	IIIb	VI(Iron)
LPEs	L2a	L1b	L4b	L1b	L1a	L3b	L5
REEs	R4a	R3a	R2b	R1b	R2a	R1a	R5
SPEs	S1	S1	S5	S2a	S1	S3	S6

Sample	K5100030	K5100031	K5100033	K5100041	TPND7	TPNJ5	TPNR6
wt µg	3.8	6.8	4.8	1.2	20.5	4.7	13.3
Na %	0.42	0.45	1.22	0.77	0.03	0.03	-
Mg %	15.3	7.6	15.4	11.2	18.5	15.0	30.6
Al %	0.92	1.96	1.16	2.04	1.34	1.75	0.415
Ca %	0.49	0.78	0.97	-	1.41	-	0.458
Ti %	0.27	0.23	-	-	0.10	-	-
Sc ppm	14.0	31.8	8.64	16.4	11.2	11.6	13.9
V ppm	126	62.1	72.4	118	93.1	115	164
Cr ppm	6480	3710	3410	4060	3540	3900	726
Mn %	0.36	0.20	0.36	0.11	0.510	0.217	0.134
Fe %	10.9	26.8	16.9	42.4	13.00	19.60	3.13
Co ppm	15.3	162	107	336	245	127	40.9
La ppm	-	0.59	0.33	2.2	0.28	0.62	0.13
Sm ppm	-	0.689	0.156	0.386	0.199	0.332	0.065
Yb ppm	-	0.38	0.13	0.29	0.256	0.269	0.154
Lu ppm	0.032	0.113	0.030	0.063	0.038	0.052	0.036
Au ppb	-	1.10	4.9	1.80	1.98	2.2	-
Ir ppb	21.7	15.5	1.73	6.87	7.04	13.6	2.73
Type	V	IIb	IIa	IIb	IIIa	IIIb	IVa
LPEs	L2a	L2a	L1b	L2b	L3a	L3a	L4b
REEs	R4b	R2b	R1a	R3b	R1a	R2a	R3a
SPEs	S4	S2a	S2b	S2b	S4	S3	S4

Abundances normalized to CI, Mg (LPS) and Fe (SPE)

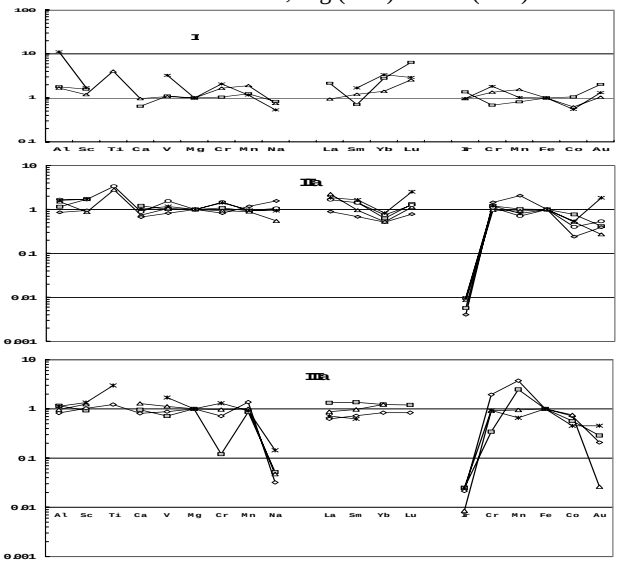

EXPERIMENTAL CONDENSATION OF SILICATE GASES: APPLICATION TO THE FORMATION OF DUST IN CIRCUMSTELLAR ENVIRONMENTS. A. Toppani[1,2*], F. Robert[2], G. Libourel[1,3], P. de Donato[4], O. Barrès[4], L. d'Hendecourt[5], J. Ghanbaja[6], [1]Centre de Recherches Pétrographiques et Géochimiques, Nancy, France, [2]Muséum National d'Histoire Naturelle, Paris, France, [3]Ecole Nationale Supérieure de Géologie, Nancy, [4]Laboratoire Environnement et Minéralurgie (LEM), Nancy, [5]Institut d'Astrophysique Spatiale (IAS), Orsay, France, [6]Université Henri Poincaré (UHP), Nancy, *current address: IGPP, Lawrence Livermore National Laboratory, Livermore, USA, toppani2@llnl.gov.

Introduction: Condensation processes play a major role in the cycle of dust in the galaxy from the formation of interstellar dust to that of the building blocks of our planetary system. However, they are mostly understood via models predicting the chemical composition of the grains condensed at equilibrium in nebular or stellar conditions (e.g. [1]). In order to better understand condensation processes and to evaluate the role of kinetics on the nature of the condensed matter, a new apparatus was developed to perform condensation experiments of multi-elemental refractory gases at various temperatures (25 to 1350°C) and under different pressures (10^{-6} to 1 bar). Here, we present results of condensation experiments performed under thermal non-equilibrium and equilibrium conditions that show the large range of products that can be formed by condensation.

Experimental: Our design [2] consists of a reaction chamber linked to a high-vacuum metal line in which different mixtures of gases can flow. In the reaction chamber, the multi-elemental refractory gas to be condensed is produced by laser ablation (Nd-Yag laser) of a glass target of known composition. We previously showed [2] that the produced gas is not fractionated relative to the target. The ablated glasses were close to "solar" composition [3] for calcium, aluminum, magnesium and silicon (MgO, SiO_2, Al_2O_3, CaO: 36.1, 56.9, 4, 3 wt%), or of Ca-Al rich composition (MgO, SiO_2, Al_2O_3, CaO: 9.3, 48.6, 18.7, 23.4 wt%). Experiments were performed in static mode.

Condensation in non-equilibrium conditions: The non-equilibrium condensation of these refractory gases occurred directly above the target as the hot laser-ablated gas expanding in the cold ambient gas is rapidly supersaturated due to the relatively high pressure in the reaction chamber [4]. This condensation was performed at different total pressures (1 to 30 mbar) of different mixtures of gases (Ar, CO_2, H_2O+CO_2). Temperatures of these ambient gases, i.e. condensation temperatures and durations ranged from 25°C and ~150°C, and from ~40 to 464 min, respectively. The condensed material was collected on a horizontal steel plate 2 to 10 cm above the target. Condensed material collected during these experiments consist of fluffy aggregates of ~10 nm size particles. Their observation by transmission electron microscopy has shown that they are not chemically fractionated (25°C, ±20%) relative to the gas composition and that they are amorphous in almost all explored conditions.

The infrared signatures of the condensed material depend on the nature of the ambient gas. The mid-infrared spectra of products condensed in "dry" CO_2 or Ar gas from Ca-Al-rich or "solar" gas show that only amorphous silicates are present. At the opposite, spectra of material condensed in "wet" CO_2 gas (H_2O + CO_2) show, in addition to the Si-O-Si stretching vibrations feature, three features indicative of the presence of highly bonded water, trapped free water and doubly degenerate asymmetric stretching ν_3 carbonate. The IR characteristics and these features suggest that the carbonate is a complex hydrated carbonate. The far-infrared spectrum of Ca-Al-rich material condensed in "wet" CO_2 shows the bands characteristics of the calcite lattice vibrations [5]. Mid and far infrared spectra of Ca-Al-rich and "solar" condensate indicate thus that the non-equilibrium condensation of the silicate gases in wet CO_2 yields formation of calcium-rich carbonates within a amorphous silicate matrix.

Different tests experiments revealed that carbonates formed directly during the non-equilibrium condensation of the silicate nanoparticles, by a kinetically controlled chemical reaction involving CO_2(g), H_2O(g) and the silicate gas, with P_{H2O} being the limiting parameter. We propose that the reaction proceeds in two steps: (1) hydration in the gas phase of molecular clusters of Ca- or Mg-rich silicate and (2) reaction of these complexes with CO_2(g).

Ca-rich carbonates have been recently detected [5, 6, 7] in planetary nebulae (PN) NGC 6302, NGC 6537 and in several low and intermediate-mass protostars. The main dust component observed in circumstellar envelopes is amorphous silicate [8] thought to have formed by non-equilibrium condensation [8]. Based on our experimental results, we propose that the "astrophysical" carbonates form by chemical reaction between a "hot" silicate gas, and a 300-500K H_2O-CO_2 rich gas during a condensation process far from thermal equilibrium in H_2O(g)-CO_2(g)-rich, high-temperature and high-density regions such as evolved star winds [10] or those

induced by grain sputtering upon shocks in protostellar outflows [11]. Our experiments suggest thus that non-equilibrium vapour phase condensation may be an important mechanism of dust formation in astrophysical environments.

Condensation in equilibrium conditions: In these experiments, a platinum furnace with a positive temperature gradient from bottom to top was located about 2 cm above the target. The fluffy nanoparticles, condensed out of equilibrium above the target, were vaporized at the entrance of the furnace producing a non-fractionnated gas relative the target composition. Because of the temperature gradient inside the furnace, this gas condensed inside the platinum furnace at a controlled temperature (± 20°C). Condensates were deposited directly on a Pt-grid welded to the end of a Pt-Rh10 thermocouple entering the furnace. These Pt-grids were observed by TEM at UHP (Nancy).

The condensation of the "solar" or Ca-Al-rich gas under a total pressure of 10^{-3} bar at temperatures from 1000°C to 1300°C and for run times of 4 to 60 minutes yields direct formation of crystals, oxides or silicates (corundum, spinel, anorthite, melilite, Al-diopside, forsterite and enstatite). The condensed crystals are mainly euhedral to spherical. Crystals show various sizes (50 nm up to 4 µm), with the largest condensed at the highest experimental temperatures and/or the longest run times. They show various textures, from single mineral to aggregates of crystals of similar composition.

The mineralogy of the condensates, close to that predicted at equilibrium, varies with the duration of condensation experiments, with the attainment of a steady state in less than one hour. The mineralogy of the condensates vary also with the temperature of condensation. For instance, the condensation of the solar gas yields the formation of Mg, Si-rich silicates at low-temperature (e.g. enstatite and forsterite at 1045°C) and that of only Al-rich oxides at high-temperature (1280°C). Spinel and corundum occured at all temperatures. The condensation results thus in a chemical fractionation of the gas, i.e. a depletion of the gas in refractory elements at high temperature. However, this study shows also that phases, such as spinel, have favoured kinetics of condensation.

Our experimental results confirm that refractory inclusions in primitive meteorites [12] could have formed by condensation from a hot nebular gas. Similarly, we confirm that crystalline grains can be formed in the outflows of evolved stars by high-temperature condensation. In both cases, our results indicate that kinetic processes certainly influence their mineralogy.

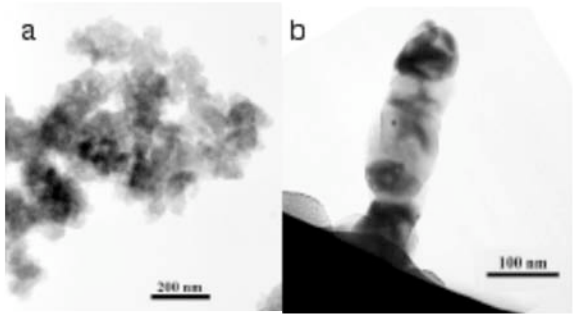

Figure 1: Dust particle formed (a) by non-equilibrium condensation at 25°C in dry CO_2 and (b) by equilibrium condensation at high temperature.

Conclusion: Our experiments show that non-equilibrium low-temperature condensation yields formation of chemically non-fractionated amorphous nanoparticles. In the presence of water vapor, amorphous carbonates can be formed. At the opposite, high-temperature equilibrium condensation does not yield formation of metastable amorphous particles with stochastic composition but of crystalline condensates whose composition is controlled by temperature-time conditions of condensation.

Undifferentiated objects such as comets, asteroids or interplanetary dust. formed, 4,5 Ga year ago, through the aggregation of both interstellar dust formed in the evolved stars and solar dust condensed from the hot nebular gas. Because we successfully reproduced meteoritic or astronomical observations, our experimentally condensed dust particles are valuable analogs of primitive condensates. Our study provide thus information about the physico-chemical environments of formation of these primitive solar system solids.

References: [1] Grossman L. (1969) *Geochim. Cosmochim. Acta, 36*, 597-619. [2] Toppani, A. *et al.* (2004) *Lunar Planet. Sci. Conf.* **XXXV**, #1726. [33] Anders, E., Grevesse, N. (1989) *Geochim. Cosmochim. Acta* **53**, 197-214. [4] Chen, L.-C. (1994) in *Pulsed Laser Deposition of Thin Films*, ed. Chrisey & Hubler, 167-198. [5] Kemper, F. *et al.* (2002) *Nature* **415**, 295-297. [6] Ceccarelli, C. et al. (2002) *Astron. Astrophys.* **395**, L29-L33. [7] Chiavassa, A. et al. (2005) *Astron. Astrophys.* **432**, 547-557. [8] Tielens, A.G.G.M. *et al.* (1998) *Astrophys. Space Sci.* **255**, 415-426. [9] Gail, H.-P. *et al.* (1999) *Astron. Astrophys.* **347**, 594-616. [10] Ferrarotti, A.S. and Gail, H.-P. (2005) *Astron. Astrophys.* **430**, 959-965. [11] Van Dishoeck, E.F. (2004) *Annu..Rev.Astron.Astrophysics* **42**, 119-167 [12] Christophe M.l. (1968) *Bull. Soc. Fr. Minéral. Cristallogr.*, **91** , 212-214.

DUST SAMPLES FROM COMET WILD 2 AND INTERSTELLAR STREAM. P. Tsou[1], D.E. Brownlee[2], F. Hörz[3], G. Flynn[4], L. Keller[3], K. McKeegan[5], S. A. Sandford[6], M. E. Zolensky[3], [1]Jet Propulsion Laboratory, California Institute of Technology, (peter.tsou@jpl.nasa.gov), [2]Astronomy Department, University of Washington, [3]NASA Johnson Space Center, [4]State University New York-Plattsburgh, [5]University of Californa, Los Angeles, [6]NASA Ames Research Center

Introduction: STARDUST is the first mission designed to bring samples back to Earth from a known comet and also the first to bring back contemporary, free interstellar particles[1]. On January 2, 2004, for about five minutes about 19:21:32 UTC, STARDUST captured dust grains from comet 81P/Wild 2 at 236.4 ± 1 km from the nucleus [2]. On the reverse side of the Wild 2 sample collector tray, there are equal number of aerogel capture cells optimized to capture dust from the contemporary interstellar stream in the 2 AU range [3]. Interstellar dust collection began on February 16, 2000 through May 20, 2000 and again from July 27, 2002 through December 9, 2002, a total of 246 days.

Uniqueness of Samples: Wild 2 is a unique comet for coma sample return since it was relatively "fresh". Our sample collection was only the fifth perihelion passage. In 1974, the comet had a close encounter with Jupiter that dramatically changed its orbit [4]. The comet now has a perihelion distance of 1.58 AU and an aphelion near Jupiter's orbit at 5.2 AU. The outer layers of Wild 2 have only been subjected to moderate solar heating allowing our samples to be more representative of the nucleus composition. Wild 2 samples represent well-preserved relics of the outer regions of our solar nebula and fundamental building blocks of our planetary system.

Interstellar grains are the main repositories of condensable elements, which permeate the galaxy. On the average, interstellar grains are expected to be considerably smaller than Wild 2 particles, mostly in the submicron size range, although interstellar particles as large as 10 μm are distinctly possibility [5]. It is most advantageous to capture these particles when the spacecraft's orbit carries it in the same direction as the interstellar dust stream's velocity vector to reduce the capture speed by the amount of the spacecraft speed. For STARDUST, this occurred as the spacecraft was on the inbound portion of the orbit.

The unique opportunity for STARDUST is to study the interstellar grains accreted in Wild 2 at the formation of the comet which can now be compared with dust captured from the contemporary interstellar stream, possibly billions of years apart.

Sample Instrument: These solid samples are captured in two back-to-back sample collection trays occupied by newly developed smooth-gradient-density silica aerogel. There are 132 silica aerogel capture cells of 3 cm and 1 cm thickness for the cometary and the interstellar sides, respectively. The aerogel capture cells were wedged into the sample collection trays and wrapped on all four sides with 101.6 μm thick 1100 aluminum foil to facilitate aerogel capture cell removal as well as serving as a small grain capture medium. The total exposed Wild 2 aerogel surface area is 1039 cm^2 and 153 cm^2 of aluminum foil.

Preliminary Examination: On January 15, 2006, these samples will be returned to Earth in a direct reentry capsule at the Utah Test and Training Range. There are about 150 sample analysts in six disciplines (optical, composition, mineralogy/petrology, isotopes, organics and cratering) who will participate in the Preliminary Examination of the Wild 2 samples. Preliminary results for Wild 2 will be reported by September 2006 and the interstellar samples results a year later.

References:

[1] Brownlee, D. E. et al. (2003) *JGR, 90,* 1151–1154. [2] Tsou P. et al. (2003) *JGR, 32,* A74. [3] Tsou P. (2004) *JGR,*. [4] Sekanena S.. (2003) *JGR*. [5] Grün et al., (1993) *Nature*.

A LARGE AREA COSMIC DUST COLLECTOR ON THE INTERNATIONAL SPACE STATION. P. Tsou[1], F. Giovane[2], R. Corsaro[2], J. C. Liou[3], [1]Jet Propulsion Laboratory, California Institute of Technology (peter.tsou@jpl.nasa.gov), [2]Naval Research Laboratory, [3]ESCG/ERC at NASA Johnson Space Center.

Introduction: The Large Area Dust Collector (LAD-C), ten-square meter (10 m^2) of instrumented silica aerogel mounted externally on the International Space Station (ISS) [1], will capture and return large dust particles intercepted in Earth orbit. The uniqueness of LAD-C is that it carries a self-contained acoustic impact recording and locationing system to offer the opportunity to determine the particles' trajectories nondestructively. With which LAD-C can provide, for the first time, an opportunity to ascertain the particles' parent sources.

Another uniquness of LAD-C is that the flight cost for space deployment, integration and Earth return will be provided by the Department of Defense (DoD) Space Test Program (STP). The cost of the flight instrument itself is furthered shared among science and space debris participants.

Technologies: LAD-C makes use of matured silica aerogel capture medium developed at Jet Propulsion Laboratory (JPL) for Space Shuttle Get Away Special Sample Return Experiment, the Mir Sample Return Experiment and the STARDUST mission, the 4th Discovery Program. The self-contained capture time acoustic recording system, originally concieved and developed at the JPL [1], offers nondestructive particle trajectory determination. The acoustic system was subsequently further developed and demonstrated under a NASA Planetary Instrument Definition and Development (PIDD) Program in a joint effort between JPL, JSC and the US Air Force Academy, led by the Naval Research Laboratory (NRL).

Consortium: A highly leveraged consortium of technologies and resources has been organized for LAD-C: DoD provids the flight through an agreement with NASA, NRL provides experiment management and the acoustic system, NASA Orbital Debris Program Office provides debris and dust dynamics and modeling, the US Naval Academy provides and adjunct uplink/downlink system for real-time examination, and JPL provides the experiment concept and capture medium. Other participants are under discussion, each contributing appropriate resources to accomplish this overall LAD-C experiment.

This LAD-C experiment serves both the cosmic dust science community in capturing rare large (~100 μm) extratresstrial dust particles from asteroids and comets and possible dust from interstellar sources. For the space debris community, LAD-C provides statistics for smaller (< 1mm) sized orbital debris [3]. The International Space Station offers a unique opportunity for a long term space platform from which larger sized particles from-large number of sources can be collected. For the dust community, LAD-C revives the desire for the Cosmic Dust Collection Facility that was cancelled as an External Attached Payload on the Space Station Freedom in 1988.

Science Return: LAD-C flight will provide: 1) statistical significant samples of ~thirty 100 μm large extraterrestrial particles for an one year exposure; 2) the potential of assigning the parent sources of the captured particles; 3) the retrieval of samples themselves for detailed Earth based laboratory analysis to determine the chemical and physical nature of the particles; 4) demonstration for a low-cost and long term sampling of a large number of solar system bodies on the space station, a NASA's goal to promote the external usage of the ISS.

References: [1] Corsaro, R. et al., (2004) Orbital Debris Quarterly News. [2] Tsou, P., (1988), LPI TR 88-01. [3] Liou, J.-C. et al., (2005) Proceedings of the 4th European Copnference on Space Debris.

WIZARD – A new observation system of the zodiacal light

Munetaka Ueno[1] (ueno@zodiacal-light.org), Masateru Ishiguro[2], Fumihiko Usui[2], Ryosuke Nakamura[3]
Takafumi Ootsubo[4], Naoya Miura[1], Yuki Sarugaku[2], Suk Minn Kwon[5], SeungSoo Hong[6], Tadashi Mukai[7]
[1] Department of Earth Science and Astronomy, University of Tokyo, 3-8-1 Komaba, Meguro, Tokyo 1538902 Japan
[2] Institute of Space and Astronautical Science, Japan Aerospace Exploration Agency
[3] National Institute of Advanced Industrial Science and Technology, [4] Nagoya University
[5] Kangwon National University, [6] Seoul National University, [7] Kobe University

Introduction: We developed a new observation system WIZARD; "***W****ide-field* ***I****mager of* ***Z****odiacal light with* ***Ar****ray* ***D****etector*" (Figure 1). Since the zodiacal light is faint and very extended all over the sky, WIZARD employs a sensitive CCD and a wide field optics with sufficient spatial resolution to measure the contribution of integrated flux of the individual stars. WIZARD is designed to measure the absolute brightness of the diffuse sky at visible wavelength and to have good stability of the system zero-level as well as low noise feature. The first light of WIZARD was performed in 2001 at Mauna Kea, Hawaii, and the first scientific image of the gegenschein was taken in 2002 under collaboration with SUBARU observatory. We have been promoting extended observations of the zodiacal light along the ecliptic plane, for three years at NASA/ IRTF's site. We present the design and the performance of WIZARD system, and also the preliminary results of our observations.

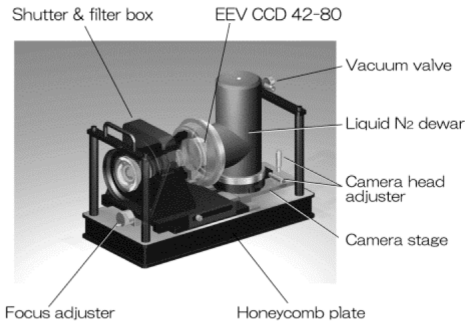

Figure 1 WIZARD system

WIZARD system: The stability of the CCD camera is very important issue to measure the absolute brightness of zodiacal light, because it extends even beyond the wide field of view of WIZARD, which means that it is still hard to assign the zero-level within the image. WIZARD employs a liquid-nitrogen cooled dewar to operate the CCD (EEV CCD 42-80) to minimize the temperature fluctuation of the CCD device, which causes unexpected uncertainty of the zero point of the photometry. The device has large imaging area, 27.6 x 55.3 mm^2 with 2048 x 4096 pixels, and quantum efficiency of 90 % at 460 nm. The optics is also designed very carefully to realize efficient observations, and has F-ratio 2.8 and focal length 32.5 mm (much shorter than the device size!), giving field-of-view of 49 x 98 square degree of arc and the plate scale of 86 arcsec./pixel. The lens system is designed and manufactured by Genesia Corporation in Japan. The band-pass filter is placed at a position of the optical pupil, and also specially developed to suppress the airglow emissions (Figure 2). The CCD, the shutter, and the mounting are controlled by COGITO-3, a multi CCD control system.

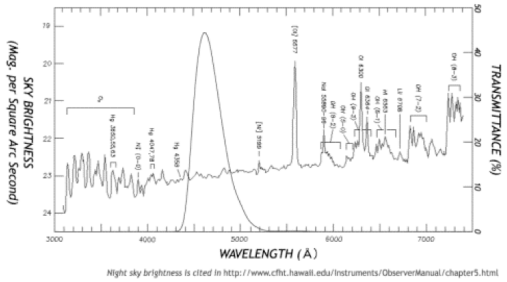

Figure 2, Transmittance of the filter and the airglow

Observations: The zodiacal light images taken by WIZARD are shown in Figure 3.

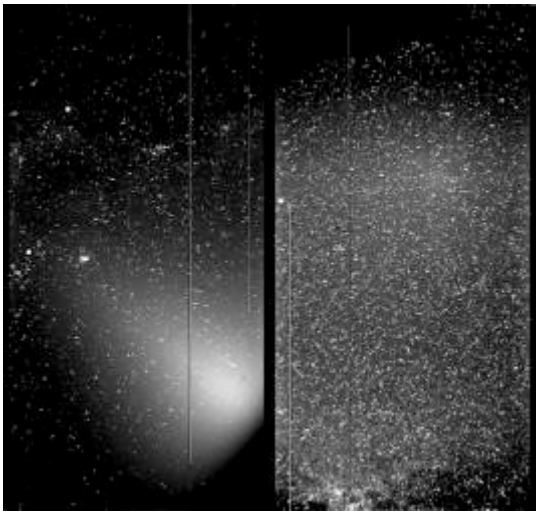

Figure 3. The evening zodiacal light (left) and the gegenschein (right), with the exposure time 180 sec. and 300 sec., respectively.

A DYNAMIC FOUNTAIN MODEL FOR DUST IN THE LUNAR EXOSPHERE.

R. R. Vondrak, T. J. Stubbs and W. M. Farrell, NASA Goddard Space Flight Center, Greenbelt, MD 20771, USA, Timothy.J.Stubbs@gsfc.nasa.gov.

Introduction: During the Apollo era of exploration it was discovered that sunlight was scattered at the terminators giving rise to "horizon glow" and "streamers" above the lunar surface [1,2]. This was observed from the dark side of the Moon during sunset and sunrise by both surface landers and astronauts in orbit (Fig.1). These observations had not been anticipated since the Moon was thought to have a negligible atmosphere or exosphere. Subsequent investigations have shown that the sunlight was most likely scattered by electrostatically charged dust grains originating from the surface [2,3,4,5,6]. This dust population could have serious implications for astronomical observations from the lunar surface [7] and future exploration [8].

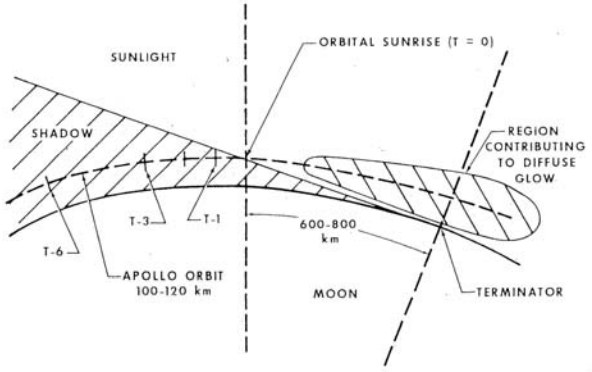

Fig. 1. Schematic showing a cross-section of the Moon in the plane of the Apollo orbit (dashed line). This depicts the physical situation consistent with Apollo 17 observations of "horizon glow" and "streamers" [1].

The lunar surface is electrostatically charged by the local plasma environment and the photoemission of electrons by solar UV and X-rays [8]. Under certain conditions, the like-charged surface and dust grains act to repel each other, such that the dust grains are ejected from the surface [2,3,4].

A dynamic "fountain" model has recently been proposed, as illustrated in Fig. 2b, to explain how submicron dust can reach altitudes of up to ~100km [10,11]. Previous static dust levitation models focused on heavier micron-sized grains near the surface, which did not explain the presence of much lighter grains at higher altitudes. By relaxing the static constraint, [10] showed that grains can be "lofted" to high altitudes under the action of dynamic forces. Here we aim to improve the dynamic fountain model by including more realistic electric field profiles [12] and new results relating to grain cohesion at the surface [13].

Apollo-era Observations: Horizon glow (HG) observed by the Surveyor-7 lander was most likely caused by electrostatically levitated ≈5μm dust grains at heights of ~10cm near the terminator [3]. HG observations were ~10^7 times too bright to be explained by secondary ejecta from micro-meteoroid impacts [2,3].

Astronaut observations of orbital sunrise revealed HG and streamers above the lunar surface (Fig. 1) varying on ~1–100s timescales. This indicated that they were produced by light scattering in the lunar vicinity by particles that were present sporadically [4]. The HG had a scale height of ~10km, so was unlikely to be caused by gases in the lunar exosphere [6].

The Lunar Eject and Meteorites (LEAM) experiment on the Moon detected the transport of electrostatically charged lunar dust [5]. The dust impacts were observed to peak around the terminator regions, thus indicating a relationship with the HG observations.

HG appeared as "excess" brightness in photographs taken from orbit of the solar corona above the lunar terminator. Excess brightness could not be accounted for by a co-orbiting cloud of spacecraft contaminants [1]. This evidence strongly suggested the presence of a variable lunar "atmosphere" of ~0.1μm dust extending to altitudes >100 km created by some electrostatic suspension mechanism [4,5].

Dynamic Dust Fountain Concept and Model: Fig. 2 shows a schematic comparing (a) the static levitation concept [1,2,3] with (b) the evolution of a dust grain in the dynamic fountain model [10]. In the levitation model the dust grain finds a point near the surface where the electrostatic (F_q) and gravitational (F_g) forces acting on it are about equal and opposite, and it is thus suspended. In the dynamic fountain model, once the dust grain has attained sufficient charge to leave the lunar surface (i.e., $F_q > F_g + F_c$), it is accelerated upward through a sheath region with a height ~λ_D (plasma Debye length). (Note: F_c is the force of grain cohesion at the surface.) The dust grains in question are so small that initially $F_q >> F_g$, such that the dust grains leave the sheath region with a large upward velocity (V_{exit}) and follow a near-parabolic trajectory back toward the lunar surface since the main force acting on them now is gravity.

Initial Results: Surface charging in the model is photo-driven on the dayside and plasma electron-driven on the nightside [8]. Fig. 3 shows the maximum height reached by a dust grain (Z_{MAX}) as a function of r_d and the angle from the subsolar point (θ) for typical solar wind conditions [10]. This suggests that dust can

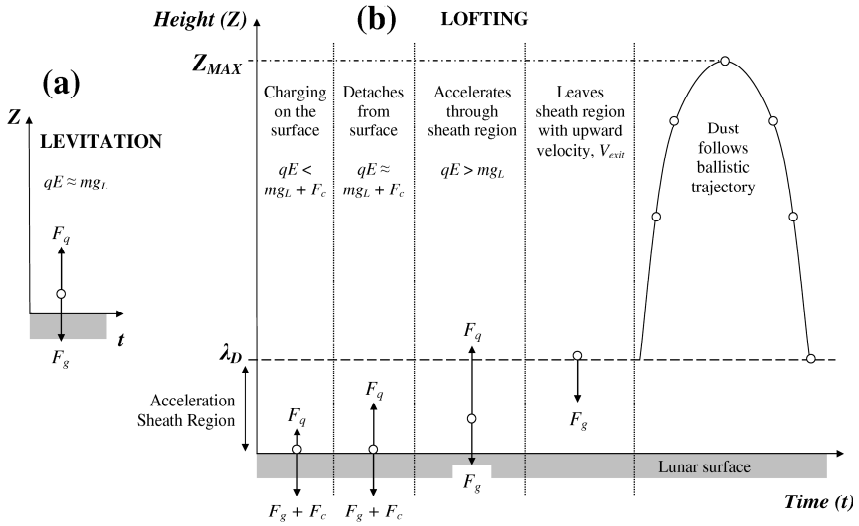

Fig.2. (left) Schematic comparing (a) the static levitation concept with (b) the evolution of a dust grain in our dynamic fountain model [10]. Forces on the grains: electrostatic (F_q), gravitational (F_g), and grain cohesion at the surface (F_c).

Fig. 3. (below) Spectrogram plot showing the maximum dust grain height reached (Z_{MAX}) as a function of angle from the subsolar point (θ) and dust grain radius (r_d) [10].

be lofted at most locations on the lunar surface, apart from in the region just sunward of the terminator labeled the "Dead Zone" ($\theta \approx 80°$), where the electrostatic surface potential $\phi_S \approx 0$. Fig. 3 also shows that at the terminator dust grains <0.1μm can be lofted to ~1–100km.

Discussion: In the model presented by [10] neglected effects included: (1) grain adhesion to the surface [14], (2) secondary electron currents [9,15,16], (3) realistic surface electric field profiles [12] and horizontal electric fields at the terminator [17], (4) the lunar wake electric fields near the terminator [18], (5) collective behavior on dust grain charging [16].

In order to improve the accuracy of this model we will include more realistic surface electric field profiles and grain cohesion at the surface. Inclusion of realistic surface electric field profiles [e.g., 12] is unlikely to affect the Z_{MAX} reached by the lightest grains; however, it will likely significantly increase the time-of-flight estimates. Grain cohesion at the surface is anticipated to limit dust transport for surface potentials <10V [13], although estimates of this effect still require significant refinement.

Conclusions: From a comparison with [7] it appears that sub-micron dust grains could contaminate astronomical observations of infra-red, visible and UV light over a significant portion of the lunar surface, and not just at the terminator. This one of many ways in which dust could interfere with science and exploration activities on the Moon [8], therefore a thorough understanding of lunar dust behavior is necessary in order to effectively tackle future problems.

Acknowledgements: T.J.S. funded by NRC. Thanks to J.S. Halekas for LP/ER data. Fig. 1 courtesy of J.E. McCoy.

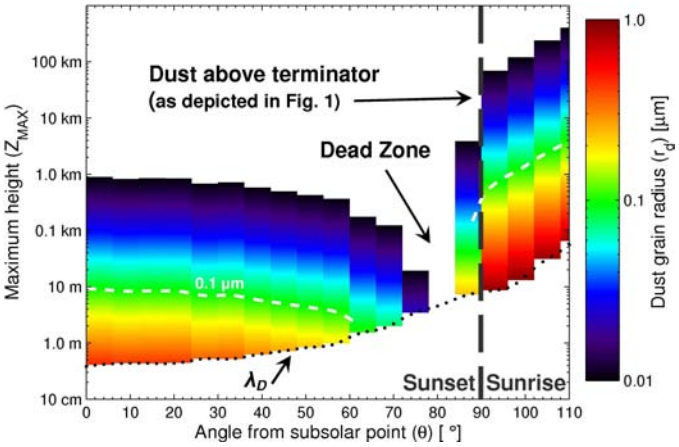

References: [1] McCoy, J.E. (1976) Proc. Lunar Sci. Conf. 7th, 1087. [2] Rennilson, J.J. and Criswell, D.R. (1974) The Moon, 10, 121. [3] Criswell, D.R. (1973) Photon & Particle Interactions with Surfaces in Space, 545. [4] McCoy, J.E. and Criswell, D.R. (1974) Proc. Lunar Sci. Conf. 5th, 2991. [5] Berg, O.E., et al. (1976) Interplanetary Dust and Zodiacal Light, 233. [6] Zook, H.A. and McCoy, J.E. (1991) Geophys. Res. Lett., 18, 2117. [7] Murphy, D.L. and Vondrak, R.R. (1993) Proc. Lunar Planet. Sci. Conf. 24th, 1033. [8] Stubbs, T.J., et al. (2005) Lunar Planet. Sci. Conf. 36th, 2277. [9] Manka, R.H. (1973) Photon & Particle Interactions with Surfaces in Space, 347. [10] Stubbs, T.J., et al. (2005) Adv. Space Res., in press. [11] Stubbs, T.J., et al. (2005) Lunar Planet. Sci. Conf. 36th, 1899. [12] Nitter, T. et al. (1998) J. Geophys. Res., 6605. [13] Starukhina, L.V. (2005) Lunar Planet. Sci. Conf. 36th, 1343. [14] Rhee, J.W. et al. (1977) COSPAR Space Res. 17th, 627. [15] Horányi, M. et al. (1998) Geophys. Res. Lett., 103, 8575. [16] Goertz, C.K. (1989) Rev. Geophys., 27, 271. [17] Berg, O.E. (1978) Earth Planet. Sci. Lett., 39, 377. [18] Farrell, W.M. et al. (1998) Geophys. Res. Lett., 103, 23,653.

CHARACTERISTICS OF DUST PARTICLES OBSERVED BY CASSINI AT SATURN'S RING PLANE CROSSINGS. Z. Z. Wang, D. A. Gurnett, T. F. Averkamp, A. M. Persoon, and W. S. Kurth (University of Iowa, Dept. of Physics and Astronomy, Iowa City, IA 52242,USA; zhenzhen-wang@uiowa.edu).

The Cassini spacecraft passed over the rings of Saturn on July 1, 2004. Figure 1 shows the trajectory of the Cassini spacecraft. The spacecraft passed northbound through the ring plane between the F and G rings on the inbound pass and southbound between the same two rings on the outbound pass. The inbound ring plane crossing occurred at 00:46:31 Universal Time (UT) at a radial distance of 2.634 R_S (R_S = 60,286 km). The outbound ring plane crossing occurred at 04:33:51 UT at a radial distance of 2.630 R_S. At both ring plane crossings very intense impulsive signals were detected by the Radio and Plasma Wave Science (RPWS) instrument on the spacecraft. The noise is attributed to small micron-sized dust particles striking the spacecraft.

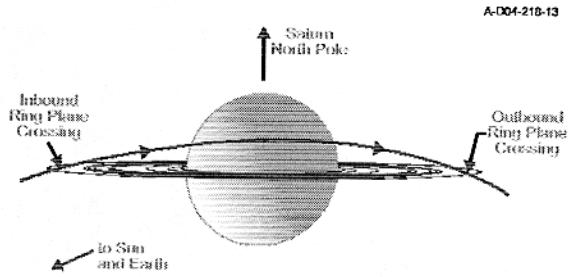

Figure 1. Cassini trajectory at Saturn encounter.

When a small high-velocity dust particle strikes the spacecraft, the kinetic energy is converted into heat which vaporizes both the particle and part of the spacecraft target, thereby producing a small partially ionized plasma cloud. The electrons in the plasma cloud expand from the impact site at high velocities, forming an electric field between the spacecraft body and the escaping plasma cloud. As the electric field sweeps outward, it induces a voltage in the antenna, which is a function of the charge released by the impact. Since laboratory measurements have shown that the charge released is proportional to the mass of the impacting particle [1], these measurements provide information on the mass and size distribution of the dust impacts. The dust impact rate is one of the most basic quantities that can be determined from the RPWS waveform data. Figures 2 and 3 illustrate the impact rate *R* as a function of time (UT) and distance above/below the equatorial plane (*z*) for the inbound and outbound ring plane crossings. In both cases the impact rate reaches a maximum value very close to the equator crossing. Making the assumption that the particle distribution depends only on the distance *z* from the equatorial plane, the impact rate can be fit to a combination of Gaussian curves using the function

$$R = R_0 + R_1 e^{-(z-h)^2/L_1^2} + R_2 e^{-(z-h)^2/L_2^2},$$

where *h* is the offset from the equatorial plane and L is a measure of the thickness of the respective Gaussian component. The fit parameters for the inbound ring plane crossing are listed in Figure 2. In this case the impact rate from the Gaussian fit reaches a maximum value of 1164/second.

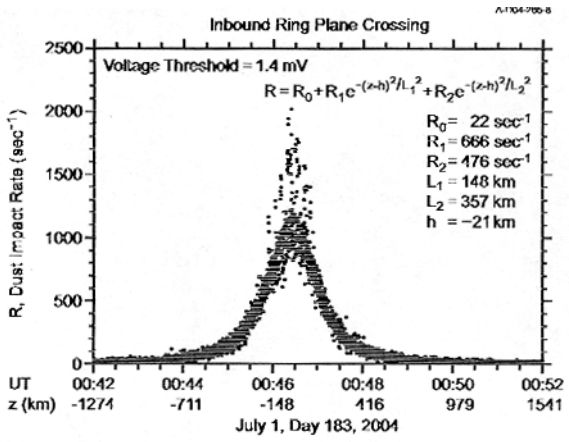

Figure 2. Dust impact rate on inbound ring plane crossing.

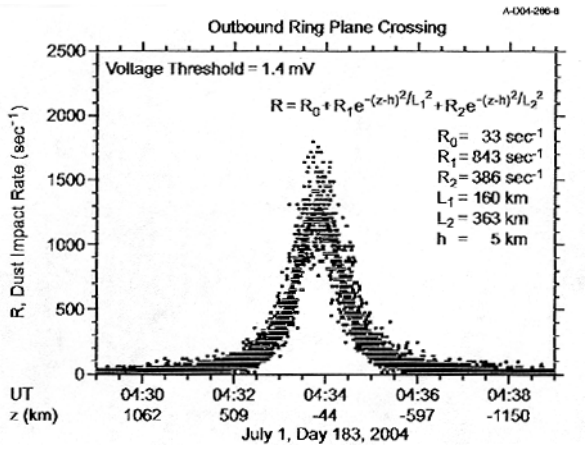

Figure 3. Dust impact rate on outbound ring plane crossing.

Figure 3 illustrates the impact rate and the best Gaussian fit (shown as a solid line) for the outbound ring plane crossing. The impact rate from the Gaussian fit reaches a maximum value of 1262/second, again very close to the equator. The fit parameters for the outbound crossing are listed in Figure 3.

The mass distribution depends on the distance from the ring plane and varies approximately as m^{-2} near the center of the ring plane at $z = 0 \pm 70$ km. The rms mass estimated from the voltage spectrum is about 8×10^{-11} grams, giving a corresponding size of 2.3 μm, on the order of a micron.

Reference:

[1] Grün, E. (1981) *ESA Rep., SP-155*, 81.

THE FUNDAMENTAL ROLE OF PHOTOPHORESIS FOR DUST IN PLANETARY SYSTEMS. G. Wurm[1] and O. Krauss[1], [1]Institute for Planetology, Wilhelm-Klemm-Str. 10, D-48149 Münster, Germany, e-mail: gwurm@uni-muenster.de.

Introduction: It is common knowledge that radiation pressure is important for the dynamics of dust in optical thin environments like the Solar System or debris disks. In very young systems like protoplanetary disks particles are embedded in a gaseous environment, and it is also common knowledge that this gas will drag particles along. However, if dust particles are embedded in a gaseous AND optical thin disk another effect emerges – photophoresis. Though this force is known since at least 1874 [1], it has been treated extremely stepmotherly. It almost completely escaped attention in space science and astrophysics so far, though this force can be extraordinarily strong, e.g. it can be orders of magnitude larger than radiation pressure, as nicely illustrated by "light mills".

Photophoresis in Space: There is little doubt that the conditions necessary for photophoresis to work exist in a more or less transitional stage from dense protoplanetary disks to debris disks. Solids and gas are separate components and evolve quite differently. While the dust aggregates to planetesimals, protoplanets, and planets on timescales of a few million years the gas stays for about ten million years [2][3][4]. With the dust getting depleted the disk turns optically thin. Small particles will quickly move outwards due to photophoresis then. Photophoresis will clear the inner disk of all small bodies and will concentrate particles in rings around a star. With typical parameters assumed (minimum mass Solar Nebula, low thermal conductivity of porous dust aggregates) a concentration will occur at regions of several tens of AU suggesting a link to the Kuiper belt [5]. For other systems like HR 4796A with the given star parameters and assuming a twice as massive gas disk, a concentration would occur at about 60 AU [6]. This is seen in Fig. 1 which shows the ratio of the photophoretic (and radiation pressure) force to residual gravity. The position can be perfectly matched with the inner edge of the observed dust ring [5][6].

While the gas might be dispersed at a certain time, the photophoretic concentration might have triggered the formation of Kuiper belt objects by then and provided the reservoir for the observed dust produced in collisions of larger bodies. In total, dust properties will not only depend on the reservoir that originally existed in the outer region but a significant fraction of solids might be a mixture of dust from the whole inner system transported outwards. Photophoresis is a very effective mechanism to transport solid particles outwards.

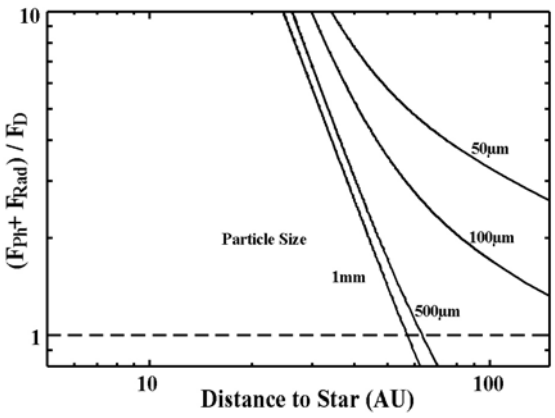

Fig. 1 Photophoretic force (+rad. pres.) to residual gravity. Rings would form at a ratio of 1. Below: HST image (inverted) of HR 4796A matched by this model.

Photophoresis will also concentrate *compact* particles like chondrules found in meteorites closer to the sun. Assuming "typical" parameters photophoresis would concentrate these particles in the asteroid belt region [7].

Certainly, photophoresis plays a limited role for the motion of a dust particle in the current, essentially gas-free Solar System. However, it might have been a major factor for – if not triggering the formation of the two most important dust reservoirs in the Solar System – comets from the Kuiper belt and the asteroids [5][7].

References: [1] Crookes W. (1874) *Proc. Phys. Soc. London, 1,* 35–51. [2] Haisch K. E., Lada E. A., and Lada C. J. (2001) *ApJ, 553,* L153–L156. [3] Greaves J. S. (2004) *MNRAS, 351,* L99–L104. [4] Takeuchi T. et al. (2005) *ApJ, 627,* 286–292. [5] Krauss O. and Wurm G. (2005) *ApJ,* (accepted). [6] Wahhaj Z. et al. (2005) *ApJ, 618,* 385–396 [7] Wurm G. and Krauss O. (2005) *Icarus,* (submitted).

LARGE SAMPLES OF CHONDRITIC INTERPLANETARY DUST PARTICLES IN CHONDRITIC METEORITES.

M.E. Zolensky. KT, NASA Johnson Space Center, Houston, TX 77058, USA (michael.e.zolensky@nasa.gov).

Introduction: We know that the parent asteroids of the bulk of the chondritic interplanetary dust particles (IDPs) are not represented by known meteorites [1-4]. However, we should expect to find samples of these materials within existing regolith breccias, and over the past several years we have identified two likely candidates.

Ningqiang Chondrite: Ningqiang is a unique carbonaceous chondrite, though with some similarities to the oxidized CV3s. We have published a report on a large (5mm) Ningqiang dark inclusion [5]. This Ningqiang dark inclusion appears to record the following processes: (1) formation (condensation and Fe-enrichment) of olivine crystals in the nebula with compositions of Fo_{42-62}, (2) irradiation resulting in amorphitization of the olivine to varying degrees, and pyrrhotite formation, (3) partial annealing resulting in fairly large, euhedral, olivine and pyroxene grains with remnant amorphous sharply-bounded rims, (4) in some cases prolonged annealing resulting in microcrystalline olivine or pyroxene rims - the annealing would have been a natural consequence of irradiation near the critical temperature for olivine, (5) mixture of the above materials with nebular clinopyroxene and olivine, which escaped nebular processing.

Many chondritic interplanetary dust particles (IDPs) also appear to preserve evidence of an irradiation event, in the form of nm-sized GEMS. The preservation of the fine glassy structures in the Ningqiang dark inclusion, caused by nebular radiation damage, suggests that it was added late into the Ningqiang chondrite, post-dating any parent alteration event. The fayalitic-enrichment of the olivine, and incomplete replacement of some magnetite by fayalitic olivine, and some fayalitic olivine by pyrrhotite must also have occurred in the nebula since it predates the radiation damage event. Survival of the amorphous ferromagnesian materials and carbon, *as well as their pre-irradiation precursor mineralogy*, requires that the entire subsequent history of the Ningqiang dark inclusion occurred under conditions of low temperature and low humidity. Thus, this material represents one of the most pristine nebular samples available for study in the lab today, more primitive than even the bulk of anhydrous chondritic IDPs.

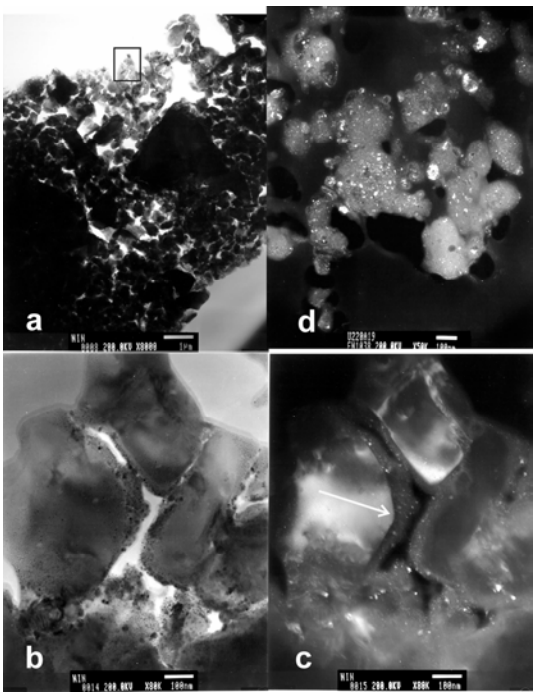

Figure 1: TEM images of Ningqiang dark inclusion (a-c) and a chondritic IDP (d). (a&b) Light-field and (c) dark-field TEM images of euhedral olivine crystals rimmed with amorphous mafic silicate material (dark and arrowed in the dark-field image) and embedded spinels and pyrrhotite (white spots in dark-field). Images (b) and (c) are from the outlined area in (a). (d) Dark field TEM image of GEMS in an anhydrous chondritic interplanetary dust particle. Compare the texture of the GEMS with the amorphous rims in (c), these images are at the same scale. Scale bars measure 100 nm. Image of IDP courtesy of J. Bradley.

NOTES

NOTES